Reproduced by
NATIONAL TECHNICAL
INFORMATION SERVICE
Springfield, Va. 22151

The contents of this report reflect the views of Wyle Laboratories which is responsible for the facts and the accuracy of the data presented herein. The contents do not necessarily reflect the official views or policy of the Department of Transportation. This report does not constitute a standard, specification, or regulation.

WHITE SECTION
BUFF SECTION
DISTRIBUTION/AVAILABILITY CODES
DIST. AVAIL. and/or SPECIAL
A

TECHNICAL REPORT STANDARD TITLE PAGE

1. Report No. FAA-RD-71-101, I	2. Government Accession No.	3. Recipient's Catalog No.
4. Title and Subtitle FAR FIELD NOISE GENERATION BY COAXIAL FLOW JET EXHAUSTS. VOLUME I - DETAILED DISCUSSION		5. Report Date November 1971
		6. Performing Organization Code
7. Author(s) Kenneth M. Eldred, et al		8. Performing Organization Report No.
9. Performing Organization Name and Address Wyle Laboratories - Research Staff, 128 Maryland Street, El Segundo, California 90245		10. Work Unit No. 550-001-05H
		11. Contract or Grant No. DOT FA68WA-1889
12. Sponsoring Agency Name and Address Federal Aviation Administration, Systems Research and Development Service, 800 Independence Avenue, S.W., Washington, D.C. 20590		13. Type of Report and Period Covered FINAL REPORT March 1968 - November 1971
		14. Sponsoring Agency Code
15. Supplementary Notes		

16. Abstract

Model scale air jets were used in an anechoic room to conduct a parametric study on the sound produced by coaxial circular jets. The following parameters were varied.

- Primary nozzle Mach numbers (from 0.85 to 1.47)
- Primary flow total temperature (60°F to 800°F)
- Ratio of secondary flow velocity to primary flow velocity (zero to sonic secondary velocity)
- Ratio of secondary nozzle area to primary nozzle area (zero to 10).
- Axial position of primary nozzle relative to secondary velocity (±11 primary nozzle diameters).

The results from these model tests were analyzed and scaled to give the overall sound power output, directivity indices and the sideline sound pressure spectra and perceived noise levels for engine thrusts ranging from 10,000 pounds to 80,000 pounds. The results were used to determine the reduction in overall sound power and maximum sideline perceived noise level as a function of the ratio of the secondary nozzle area to primary nozzle area and the ratio of secondary velocity to primary velocity. The maximum reduction was found to occur at a velocity ratio of approximately 0.5. The maximum reduction was 10 dB in overall power level and 11 PNdB in maximum perceived noise level on a 1500 foot sideline. These results were shown to be in accordance with a simple theoretical model of noise generation by coplanar coaxial jets. The noise reduction curves were also reinterpreted to indicate the flow characteristics required to produce an acoustically optimum, practical jet engine and to show the noise penalties that result due to deviations from this optimum configuration. Volume I is a detailed discussion and Volume II is a compilation of test results.

17. Key Words: Acoustics, Aircraft Noise, Coaxial Jets, Jet Noise, Minimum Noise, Noise Source Control, Noise Prediction		18. Distribution Statement: Availability is Unlimited. Document may be released to the Clearinghouse for Federal Scientific and Technical Information, Springfield, Virginia 22151, for sale to the public.

19. Security Classif. (of this report)	20. Security Classif. (of this page)	21. No. of Pages	22. Price
Unclassified	Unclassified	252	$3/pc $.95/mc

Form DOT F 1700.7 (8-69)

PREFACE

The author wishes to thank Mr. William Sperry of the Office of Noise Abatement, FAA, for his counsel and patience throughout this program, and for his most helpful detailed review of the final report and its findings.

In addition, sincere appreciation is due to several members of the Wyle Laboratories Research Staff who contributed significantly to the program, the report, or both. Victor Mason accomplished much of the original data analysis and interpretation; Elizabeth Cuadra and Richard Potter planned and directed the experimental and preliminary analysis phases; John Wilson conducted the detailed experiments. All of these contributed significant portions of the drafts of this report and its value owes much to their efforts.

TABLE OF CONTENTS

		Page
1.0	INTRODUCTION	1
2.0	NOISE GENERATION BY COAXIAL JET FLOWS	3
2.1	Noise Generation of Jets from Single Circular Nozzles	3
2.2	Noise Prediction for Jet Flows from Mixing Nozzles	13
2.3	Noise Prediction for Jet Flows from Coplanar Coaxial Nozzles	19
3.0	EXPERIMENTAL APPARATUS AND DATA ANALYSIS PROCEDURES	31
3.1	Jet Flow Parameters and Design of the Experiment	31
3.2	Test Hardware	33
3.2.1	Jet Rig	33
3.2.2	Jet Nozzles	36
3.2.3	Air Supply	39
3.2.4	Jet Traversing Mechanism	40
3.2.5	Anechoic Room	40
3.3	Instrumentation	41
3.3.1	Acoustical Data Acquisition System	41
3.3.2	Acoustical Data Analysis System	41
3.3.3	Thrust Measurement	46
3.3.4	Jet Profile Measurements	46
3.3.5	Discrete Tones and the Resulting Hardware Modifications	47
3.4	Analytical Basis for Data Reduction Computer Program	48
3.4.1	Flow Velocities and Thrust	50
3.4.2	Sound Pressure Levels	51
3.4.3	Sound Power Levels	51
3.4.4	Directivity Patterns	53
3.4.5	Acoustic Conversion Efficiency	53
3.4.6	Sideline Sound Pressure Levels for Full-Scale Engines	54
3.4.7	Perceived Noise Level	58
4.0	DESCRIPTION OF THE EXPERIMENTAL DATA	59
4.1	Computer Output Data	59
4.2	Some Experimental Anomalies	63

TABLE OF CONTENTS ... continued

	Page
5.0 DISCUSSION OF RESULTS AND THEIR APPLICATION TO FULL-SCALE ENGINES	71
5.1 Discussion of Principal Experimental Results	71
5.1.1 Noise of the Primary Nozzles	71
5.1.2 Reduction in Overall Sound Power Level Associated with Coaxial Jet Flows	75
5.1.3 Changes in Sound Power Spectra and Directivity	86
5.1.4 Change in Maximum Sideline Perceived Noise Level	89
5.2 Prediction of the Noise Characteristics of Full-Scale Coaxial Jets	97
5.3 Comparison of Noise Characteristics of Practical Coaxial Jet Engines with Optimum Single-Nozzle Engines	110
6.0 SUMMARY AND CONCLUSIONS	119
REFERENCES	123
APPENDIX A - DIRECTORY OF EXPERIMENTAL RUNS	A-1
APPENDIX B - JET FLOW PROFILE MEASUREMENTS	B-1
APPENDIX C - COMPUTER PROGRAM FOR DATA ANALYSIS	C-1
APPENDIX D - SUMMARY OF OVERALL SOUND POWER LEVEL DATA	D-1
APPENDIX E - SUMMARY OF MAXIMUM PERCEIVED NOISE LEVEL DATA	E-1
APPENDIX F - PRIMARY JET SOUND POWER SPECTRA AND DIRECTIVITY DATA	F-1
APPENDIX G - NOISE OF A SUPERSONIC NOZZLE OPERATING AT OFF-DESIGN PRESSURE RATIOS	G-1

LIST OF TABLES

Table		Page
1	Calculated Ideal Primary Flow Velocities for Various Temperatures and Pressure Ratios	32
2	Summary of Runs Completed	33
3	Primary Velocity Ratios (U_p/U_s) for a 3 dB and 6 dB Increase in Overall Power Level from Figure 64	109
4	Primary Velocity Ratios (U_p/U_s) for a 3 dB and 6 dB Increase in Sideline Perceived Noise Level from Figure 65	109
5	Secondary-Primary Velocity Ratio for Specified Increase in Overall Sound Power	120
6	Secondary-Primary Velocity Ratio for Specified Increase in Perceived Noise Level	121
	Appendix A	
A-1	Directory of Experimental Run Conditions	A-2
A-2	Experimental Run Conditions	A-3
	Appendix B	
B-1	Test Conditions for Flow Profile Data	B-2

LIST OF FIGURES

Figure		Page
1	Relationship Between Overall Sound Power Level, Normalized by Nozzle Size and Velocity for Jets from Circular Nozzles at Pressure Ratios Less Than 2.3.	4
2	Normalized Sound Power Spectrum Level for Hot and Cold Model Jets and Turbojet Engines.	5
3	Far-field Directional Characteristics of the Overall Sound Pressure Level for Four Types of Jet Flow.	4
4	Variation of the Predominant Propagation Angle for Various Frequencies from Measurements Along the 10-Degree Boundary of a J-57 Engine as a Function of a Non-dimensional Axial Frequency Parameter.	6
5	Comparison of Assumed Velocity Profile for Axisymmetric Constant Density Jet with Mach 0.7.	7
6	Examples of Flow for Constant Density Axisymmetric Single-Nozzle Jets.	9
7	Variation in Core Length (x_t) for Constant Density Axisymmetric Jet as a Function of Mach Number.	10
8	Calculated Increase in the Ratio of the Length of the Jet Core with Non-Zero External Velocity (U_∞) to its Length with Zero External Velocity for Constant Density Jets.	10
9	Source Strength Distribution Along Jet Axis.	11
10	Jet Source Normalized Sound Power Spectra.	12
11	Idealized Power Spectra of Non-Interfering Axisymmetric Jets Having a Thrust of 10,000 Lbs, Exit Total Temperature 1720°F, Together with Two Jets of Lower Temperature and Exit Velocity.	14
12	Sketch of Two Nozzles in the Plane Containing the Axis of a Simplified Axisymmetric Peripheral Tube Nozzle Illustrating Development of Final Mixed Jet and the Mixing of the Individual Jets.	15

LIST OF FIGURES ... continued

Figure		Page
13	Example of Flow Data and Comparison with Calculated Profiles for Three-Lobed Nozzle at Mach 0.3.	16
14	Comparison of Calculated Power Spectra with Power Spectra Derived from Measured Power Reduction for Two 12-Lobe Nozzles with J-57 Engine.	17
15	Computed Variation in Total Acoustic Power for Idealized Mixing Nozzle Relative to that of Baseline Single Circular Nozzle for $T_n/T_o = 3$, as a Function of the Ratio of the Envelope Diameter of the Mixing Nozzle to the Diameter of the Baseline Single Nozzle, with Tube Element Diameter as a Parameter.	18
16	Approximate Velocity Profiles at Various Downstream Stations for Constant Density Annular Coplanar Jet with $U_s/U_p = .5$ and $r_s/r_p = 1.5$.	19
17	Sketch of Equivalent Jet Flow Profile for Two Cases.	21
18	Calculated Regions of Complete and Incomplete Shrouding of the Primary Core as a Function of Area and Velocity Ratios.	23
19	Relationship Between Radius and Velocity of Equivalent Jet and the Parameters of a Constant Density Coplanar Coaxial Jet.	25
20	Estimated Contributions to and Total Reduction in Overall Sound Power Level with Velocity Ratio for Coaxial Jets with an Area Ratio of 10 and a Fixed Thrust.	28
21	Estimated Reduction in Overall Sound Power Level with Velocity Ratio for Coplanar Coaxial Jets of Fixed Thrust and Various Area Ratios.	29
22	The Jet Flow Assembly.	34
23	Photograph of Jet Flow Assembly.	34
24	Primary Nozzles and Nozzle Extention Pieces (Photograph).	37
25	The Four Secondary Nozzles (Photograph).	38

LIST OF FIGURES ... continued

Figure		Page
26	Inverse Square Law Measurements in the Anechoic Room Using Full Octave Bands of Random Noise.	42
27	Block Diagram of Acoustic Data Acquisition System.	43
28	Block Diagram of Acoustic Data Analysis System.	44
29	The Functional Flow Loop for the Computer Program.	49
30	Geometry for Obtaining Sideline Sound Pressure Levels from Measured Data.	55
31	Atmospheric Attenuation Utilized to Compute Sideline Sound Pressure Level.	56
32	Example of Computer Output for One Computer Run.	61
33	Variation in Overall Sound Power with Bypass Ratio for Thrusts Scaled to 20,000 Lbs.	62
34	Variation in Maximum Perceived Noise Level on a 1500-Foot Sideline with Bypass Ratio for Thrusts Scaled to 20,000 Lbs.	62
35	Power Spectra for Unity Velocity Ratio and Various Area Ratios for Coplanar Jet with Primary Nozzle Pressure Ratio of 1.6 and Temperature of 60°F.	64
36	Variation in Maximum Perceived Noise Level on a 1500-Foot Sideline with Bypass Ratio for Thrusts Scaled to 20,000 Lbs.	66
37	Directivity Pattern for Run 128 (Coplanar) Showing the Anomaly in the High Octave Bands.	67
38	One-Tenth Octave Band Analysis of Directivity Anomaly for Run 128 at 110 Degrees.	68
39	Variation in Measured Overall Sound Power Level with Velocity for the Model Scale Primary Nozzles Alone.	72

LIST OF FIGURES ... continued

Figure		Page
40	Variation in Overall Sound Power Level with Velocity for the Primary Nozzles Alone, Scaled to 20,000 Lbs Thrust.	73
41	Variation in Maximum 1500-Foot Sideline Perceived Noise Level for the Primary Nozzles Alone, Scaled to 20,000 Lbs Thrust.	74
42	Effect of Jet Thrust on Calculated Maximum Perceived Noise Level on 1500-Foot Sideline for the Primary Nozzles of Figure 41.	76
43	Change in Overall Sound Power Level with Velocity Ratio for Coplanar Coaxial Jets of 20,000 Lbs Thrust and Four Area Ratios.	77-78
44	Change in Overall Sound Power Level with Velocity Ratio for Coaxial Jets with a Nozzle Area Ratio of 1 and Thrust of 20,000 Lbs.	80
45	Change in Overall Sound Power Level with Velocity Ratio for Coaxial Jets with a Nozzle Area Ratio of 2 and Thrust of 20,000 Lbs.	81
46	Change in Overall Sound Power Level with Velocity Ratio for Coaxial Jets with a Nozzle Area Ratio of 5 and Thrust of 20,000 Lbs.	82
47	Change in Overall Sound Power Level with Velocity Ratio for Coaxial Jets with a Nozzle Area Ratio of 10 and Thrust of 20,000 Lbs.	83
48	Effect of Axial Position or the Primary Nozzle as Measured by the Change in Overall Sound Power Level Relative to the Level for Each Nozzle and Pressure Combination in the Coplanar Position.	85
49	Model Jet Sound Power Spectrum for Coplanar Nozzles (Primary Nozzle Pressure Ratio 1.6, Primary Nozzle Temperature 450°F, Area Ratio 10, Thrust Variable).	87
50	Model Jet Sound Power Spectrum for Fully Extended Primary Nozzle (Primary Nozzle Pressure Ratio 1.6, Primary Nozzle Temperature 450°F, Area Ratio 10, Thrust Variable).	88
51	Effect of Area Ratio of Shrouding of Model Primary Jet (Primary Nozzle Pressure Ratio 1.6, Primary Nozzle Temperature 450°F, Velocity Ratio 0.38, Thrust Variable).	90

LIST OF FIGURES ... continued

Figure		Page
52	Directivity Pattern for a Primary Nozzle Alone.	91
53	Directivity Pattern of Coplanar Nozzle with Velocity Ratio of 0.375.	92
54	Directivity Pattern for Coplanar Nozzle with Velocity Ratio of 0.731.	93
55	Directivity Pattern for Coplanar Nozzle with Velocity Ratio of 0.88.	94
56	Change in 1500-Foot Sideline Maximum Perceived Noise Level with Velocity Ratio for Coplanar Coaxial Jets of 20,000 Lbs Thrust and Four Area Ratios.	95-96
57	Change in 1500-Foot Sideline Maximum Perceived Noise Level with Velocity Ratio for Coaxial Jets with a Nozzle Area Ratio of 5 and Thrust of 20,000 Lbs.	98
58	Effect of Axial Position of the Primary Nozzle as Measured by the Change in Maximum Perceived Noise Level in the 1500-Foot Sideline Relative to the Level for Each Nozzle and Pressure Combination in the Coplanar Position.	99
59	Effect of Velocity Ratio of 1500-Foot Sideline Perceived Noise Level for Coplanar Nozzle (Primary Nozzle Pressure Ratio 1.6, Primary Nozzle Temperature 450°F, Area Ratio 10, Data Scaled to 20,000 Lbs Thrust).	100
60	Prediction of Overall Sound Power Level Based on Primary Nozzle Data in Figure 40 and Mean Curves of Experimental Variation in the Decrease in Overall Sound Power with Velocity Ratio for Jets with Coplanar Coaxial Nozzles and Fixed Thrust.	102
61	Prediction of 1500-Foot Sideline Perceived Noise Level Based on Primary Nozzle Data in Figures 41 and 42 and Mean Curves of Experimental Variation in the Decrease in 1500-Foot Sideline Maximum Perceived Noise Level for Jets with Coplanar Coaxial Nozzles and Fixed Thrust.	103

LIST OF FIGURES ... continued

Figure		Page
62	Variation of Minimum Sound Power as a Function of Area Ratio and Primary Velocity.	104
63	Variation of Minimum Value of the Maximum Perceived Noise Level on a 1500-Foot Sideline as a Function of Area Ratio and Primary Velocity.	105
64	Prediction of Sound Power Level for a Coaxial Jet Using Secondary Velocity for Reference.	107
65	Prediction of Maximum Perceived Noise Level on a 1500-Foot Sideline for a Coaxial Jet Using Secondary Velocity for Reference.	108
66	Sound Power Spectrum for Coplanar Nozzles, Primary Nozzle Pressure Ratio 1.6, Data Scaled to 20,000 Lbs Thrust.	111
67	Octave Band Sound Pressure Spectrum at Position of Maximum Perceived Noise Level on 1500-Foot Sideline. Primary Nozzle Pressure Ratio 1.6, Thrust 20,000 Lbs.	112
68	Directivity Pattern for Primary Nozzle Alone.	114
69	Directivity Pattern for Coplanar Nozzles with Area Ratio 5, Velocity Ratio 0.722.	115
70	Directivity Pattern for Coplanar Nozzles with Area Ratio 10, Velocity Ratio 0.731.	116
71	1500-Foot Sideline Perceived Noise Level for Three Configurations Scaled to 20,000 Lbs Thrust, Primary Nozzle Pressure Ratio 1.6.	117
72	Effect of Jet Thrust on 1500-Foot Sideline Perceived Noise Level for Near-Optimum Jet with 20,000 Lbs Thrust (Nozzle Pressure Ratio 1.6, Temperature 60°F, No Secondary Nozzle).	118

Appendix B

B-1	Typical Graphic Record of Total Pressure Profile for a Primary Nozzle with Pressure Ratio 1.6.	B-3

LIST OF FIGURES ... continued

Figure		Page
B-2	Effect of Temperature on Boundary Layer at the Exit of Primary Nozzle.	B-3
B-3	Typical Flow Velocity Profiles Through Exit Plane Boundary Layer for the Three Primary Nozzles.	B-4
B-4	Typical Profile of Total Pressure at Exit Plane of Supersonic Nozzle (Pressure Ratio 3.5) Operating at Off-Design Conditions.	B-4
B-5	Total Pressure Profiles at Exit Plane of Secondary Nozzle (Coaxial Nozzles with No Flow in Primary Nozzle).	B-6
B-6	Total Pressure and Temperature Profiles at Several Axial Positions for Coplanar Nozzles with Area Ratio 10. Primary Pressure Ratio 2.1, Secondary Pressure Ratio 1.5. (Primary Operating Below Design Pressure Ratio.)	B-7
B-7	Total Pressure and Temperature Profiles at Several Axial Positions for Pressure Ratio 3.5 Primary Nozzle Alone. (Operating Slightly Below Design Pressure.)	B-8
B-8	Total Pressure and Temperature Profiles at Exit Plane of Secondary Nozzle (Pressure Ratio 1.89, Area Ratio 10) with Primary Nozzle (Pressure Ratio 2.5, Total Temperature 790°F) Fully Retracted.	B-9
	Appendix C	
C-1	Basic Flow Diagram for Complete Data Reduction Computer Program.	C-2
	Appendix D	
D-1	Variation in Overall Sound Power with Bypass Ratio for Thrusts Scaled to 20,000 Lbs.	
	Experimental Run Numbers 102-117	D-2
	Experimental Run Numbers 119-130	D-2
	Experimental Run Numbers 132-143	D-3

LIST OF FIGURES ... continued

Figure		Page
D-1	continued ...	
	Experimental Run Numbers 145-156	D-3
	Experimental Run Numbers 158-165	D-4
	Experimental Run Numbers 167-174	D-4
	Experimental Run Numbers 176-187	D-5
	Experimental Run Numbers 189-196	D-5
	Experimental Run Numbers 198-205	D-6
	Experimental Run Numbers 215-230	D-6
	Experimental Run Numbers 231-242	D-7
	Experimental Run Numbers 243-254	D-7
	Experimental Run Numbers 255-266	D-8
	Experimental Run Numbers 267-274	D-8
	Experimental Run Numbers 275-282	D-9
	Experimental Run Numbers 283-292	D-9
	Experimental Run Numbers 311-326	D-10
	Experimental Run Numbers 327-338	D-10
	Experimental Run Numbers 339-350	D-11
	Experimental Run Numbers 407-422	D-11
	Experimental Run Numbers 423-434	D-12
	Experimental Run Numbers 435-446	D-12
	Experimental Run Numbers 447-458	D-13
	Experimental Run Numbers 459-466	D-13
	Experimental Run Numbers 467-474	D-14
	Experimental Run Numbers 503-516	D-14
	Experimental Run Numbers 519-530	D-15
	Experimental Run Numbers 531-542	D-15

LIST OF FIGURES ... continued

Figure		Page
	Appendix E	
E-1	Variation in Maximum Perceived Noise Level on a 1500-Foot Sideline with Bypass Ratio for Thrusts Scaled to 20,000 Lbs.	
	Experimental Run Numbers 102-117	E-2
	Experimental Run Numbers 119-130	E-2
	Experimental Run Numbers 132-143	E-3
	Experimental Run Numbers 145-156	E-3
	Experimental Run Numbers 158-165	E-4
	Experimental Run Numbers 167-174	E-4
	Experimental Run Numbers 176-187	E-5
	Experimental Run Numbers 189-196	E-5
	Experimental Run Numbers 198-205	E-6
	Experimental Run Numbers 215-230	E-6
	Experimental Run Numbers 231-242	E-7
	Experimental Run Numbers 243-254	E-7
	Experimental Run Numbers 255-266	E-8
	Experimental Run Numbers 267-274	E-8
	Experimental Run Numbers 275-282	E-9
	Experimental Run Numbers 283-292	E-9
	Experimental Run Numbers 311-326	E-10
	Experimental Run Numbers 327-338	E-10
	Experimental Run Numbers 339-350	E-11
	Experimental Run Numbers 407-422	E-11
	Experimental Run Numbers 423-434	E-12
	Experimental Run Numbers 435-446	E-12
	Experimental Run Numbers 447-458	E-13
	Experimental Run Numbers 459-466	E-13

LIST OF FIGURES ... continued

Figure		Page
E-1	continued ...	
	Experimental Run Numbers 467-474	E-14
	Experimental Run Numbers 503-516	E-14
	Experimental Run Numbers 519-530	E-15
	Experimental Run Numbers 531-542	E-15

Appendix F

F-1	Model Jet Sound Power Spectra for Primary Nozzles with Pressure Ratio 1.6.	F-2
F-2	Directivity Pattern for Run Number 101 (Pressure Ratio 1.6, Temperature 60°F).	F-3
F-3	Directivity Pattern for Run Number 144 (Pressure Ratio 1.6, Temperature 450°F).	F-4
F-4	Directivity Pattern for Run Number 175 (Pressure Ratio 1.6, Temperature 800°F).	F-5
F-5	Model Jet Sound Power Spectra for Primary Nozzles with Pressure Ratio 2.5.	F-6
F-6	Directivity Pattern for Run Number 118 (Pressure Ratio 2.5, Temperature 60°F).	F-7
F-7	Directivity Pattern for Run Number 157 (Pressure Ratio 2.5, Temperature 450°F).	F-8
F-8	Directivity Pattern for Run Number 188 (Pressure Ratio 2.5, Temperature 800°F).	F-9
F-9	Model Jet Sound Power Spectra for Primary Nozzles with Pressure Ratio 3.5.	F-10
F-10	Directivity Pattern for Run Number 131 (Pressure Ratio 3.5, Temperature 60°F).	F-11

LIST OF FIGURES ... concluded

Figure		Page
F-11	Directivity Pattern for Run Number 166 (Pressure Ratio 3.5, Temperature 450°F).	F-12
F-12	Directivity Pattern for Run Number 197 (Pressure Ratio 3.5, Temperature 800°F).	F-13

Appendix G

G-1	Directivity Index for Overall Sound Pressure Level for a Supersonic Nozzle Operating at Off-Design Pressure Ratios.	G-3
G-2	Octave Band Sound Pressure Spectra at 45 Degrees to Jet Axis for Supersonic Nozzle Operating at Off-Design Pressure Ratios.	G-4
G-3	Effect of Off-Design Operation of the Sound Power Generation by a Supersonic Jet Nozzle.	G-5
G-4	Effect of Off-Design Operation on the Maximum Perceived Noise Level on a 1500-Foot Sideline. Scaled to 20,000 Lbs Thrust.	G-6
G-5	Octave Band Sound Pressure Level at 110 Degrees, Showing Onset of the Third Anomaly Above 1200-ft/sec from Measured Raw Data.	G-7

LIST OF SYMBOLS

a	radius of jet core at downstream station x $(0 \leq a \leq r_n)$ in Equation (1) in feet
a	speed of sound in feet/sec
a_o	speed of sound for standard conditions (1120 feet/sec)
a^*	critical speed of sound in flow with velocity Mach Number of 1
A	area in square feet
A_i	incremental area on sound measurement sphere in square feet
A_p	area of primary nozzle in square feet
A_s	area of secondary nozzle in square feet
b	jet mixing width parameter in Equation (1) in feet
d	typical diameter or dimension of jet in feet
d_n	nozzle exit diameter in feet
d_s	secondary nozzle diameter in feet
d_2	envelope diameter of mixing nozzles
DI	directivity index in dB
E	mechanical power of jet in watts
f	frequency in Hertz
f_m	octave band center frequency for model jet in Hertz
f_S	octave band center frequency for full-scale jet in Hertz
F	thrust in pounds
F_e	thrust of equivalent jet (defined in Equation (4)) in pounds

F_m	thrust of model jet in pounds
F_n	thrust for a single-nozzle jet in pounds
F_p	thrust of primary jet in pounds
F_S	thrust of full-scale jet in pounds
g	acceleration of gravity 32.2 feet/sec
I	Sound intensity in watts/sq. cm.
k	constant in Equation (16)
L	propagation distance to sideline in feet
L_d	sideline distance in feet
m_p	mass flow of primary nozzle in pounds/sec
m_s	mass flow of mass flow of secondary nozzle in pounds/sec
M	flow Mach Number
M_c	eddy convection Mach Number
M_x	jet momentum flow rate across axial station x in pounds
p	sound pressure in dynes/sq. cm.
P_a	measured ambient pressure in inches of mercury
p_i	sound pressure in i^{th} incremental area
PNL	perceived noise level in PNdB
PNL_L	perceived noise level at sideline distance L_d in PNdB
PWL	sound power level in dB re 10^{-13} watts (overall is implied unless otherwise stated)

PWL_m	sound power level for model configuration in dB re 10^{-13} watts
PWL_s	sound power level for full-scale configuration in dB re 10^{-13} watts
PWL_{OA}	overall sound power level in dB re 10^{-13} watts
r	radius in feet
r_b	baseline jet radius as defined in Equation (13)
r_e	equivalent jet radius as defined in Equations (2) and (7)
r_n	jet nozzle radius in feet
r_p	primary nozzle radius in feet
r_s	secondary nozzle radius in feet
r_1	radius of separation boundary between primary and secondary momentum flows for coaxial jets in feet
R	total pressure ratio across nozzle
R_c	critical pressure ratio across nozzle which just produces sonic flow through throat ($R_c = 1.89$)
S	Strouhal number based on diameter used in Figure 2
S_x	Strouhal number based on axial distance from nozzle used in Figure 10
SPL	sound pressure level in dB re 0.0002 dynes/sq. cm.
SPL_m	sound pressure level measured for model in dB re 0.0002 dynes/sq. cm.
SPL_S	sound pressure level scaled from model to full-scale in dB re 0.0002 dynes/sq. cm.
T	jet nozzle flow temperature in degrees Rankine
T_a	measured ambient temperature in degrees Rankine

T_t	jet total temperature in degrees Rankine
T_o	temperature for standard conditions (519°R)
u	fluctuating turbulent velocity in feet/sec
U	flow velocity in feet/sec
U_c	jet centerline flow velocity in feet/sec
U_e	equivalent jet flow velocity as defined in Equations (2) and (8)
U_n	jet nozzle exit velocity in feet/sec
U_p	primary jet nozzle exit velocity (fully expanded flow) in feet/sec
U_p'	actual primary nozzle velocity when primary is retracted within secondary nozzle in feet/sec
U_r	jet velocity at radius r in feet/sec
U_s	secondary jet nozzle exit velocity (fully expanded flow) in feet/sec
U_∞	freestream velocity in feet/sec
W	total acoustic power in watts
W_b	total acoustic power of baseline jet which has same thrust as coaxial jet and same velocity as its primary, in watts
W_e	total acoustic power of equivalent jet which has the same thrust and downstream flow as does the coaxial jet, in watts
W_{po}	total acoustic power from unshrouded portion of primary jet mixing with ambient, in watts
W_{ps}	total acoustic power of primary jet mixing with secondary jet, in watts
W_{so}	total acoustic power of secondary jet mixing with ambient
W_t	total acoustic power of coaxial jet, in watts

x	downstream axial distance from nozzle plane, in feet
x_t	axial distance to tip of jet core, in feet

Greek

α	atmospheric attenuation coefficient in dB/1000 ft
$\alpha_o, \alpha_1, \alpha_2$	constants for atmospheric absorption, Equation (35)
β	ratio of area of secondary nozzle to area of primary nozzle (A_s/A_p)
δ	ratio of velocity of secondary jet to velocity of primary jet (U_s/U_p)
Δ_{DP}	decrease in 1500-foot sideline perceived noise level for coplanar coaxial jet (in Figure 61), in dB
Δ_{DW}	decrease in overall sound power level for coplanar coaxial jet (in Figure 60) in dB
Δ_{IP}	increase in 1500-foot sideline perceived noise level for coplanar coaxial jet (in Figure 65) in dB
Δ_{IW}	increase in overall sound power level for coplanar coaxial jet (in Figure 64) in dB
ΔL	ratio of core tip length with external flow to core tip length without external flow in Figure 8
ΔU	velocity difference across stated portion of jet
λ_o	sound wavelength for standard conditions
η	nondimensional jet radius parameters; $(r - a)/b$
η_1	nondimensional jet radius parameters for coaxial equivalent jet; $(r_1 - a)/b$
θ	angle from jet flow axis in degrees

ρ	density in slugs
ρ_e	density of equivalent jet in slugs
ρ_n	density of jet flow in plane of nozzle in slugs
ρ_p	density of primary jet flow (fully expanded flow) in slugs
ρ_s	density of secondary jet flow (fully expanded flow) in slugs

1.0 INTRODUCTION

The noise produced by jet engines comes from three sources – the intake compressor or fan, the internal engine components, and the jet flow of gases from the engine exhaust. This report is concerned solely with the latter source, which determines the jet noise level threshold of the engine after the first two sources have been sufficiently reduced.

Jet noise results from the mixing of the jet flow with the ambient air. This mixing process is turbulent in nature, consisting of velocity and aerodynamic pressure fluctuations in the mixing region which produce the noise audible in the acoustic far field. This far-field noise is reasonably well understood for a single circular jet and accurate prediction methods are available, although many details remain to be clarified.

However, modern jet engines are no longer pure jet engines but utilize the bypass principle. The exhaust from such an engine consists of a central jet of hot gas that has passed through the combustion chamber (termed the primary jet in this report) which is surrounded by the cooler, slower bypass flow (termed the secondary jet).

On some low bypass engines, the bypass flow does not completely surround the primary flow. This practice is being discontinued with increasing ratios, however, so that for all practical purposes the secondary bypass air can be considered to be coaxial with the primary flow and to completely surround it.

The mixing flow pattern from such a coaxial jet is much more complex than that from a single jet with the additional complication that there are many more variables to be considered. Consequently, accurate theoretical prediction of the noise is much more difficult. This difficulty in prediction motivated this experimental study to measure the noise from coaxial flows, covering the full range of physical and aerodynamic parameters to be expected from existing and future bypass jet engines. The parameters of interest include:

- Ratio of the secondary (bypass) mass flow to the primary mass flow
- Ratio of the secondary flow velocity to the primary flow velocity
- Ratio of the secondary flow area to the primary flow area
- Relative axial positions of the secondary and primary nozzles
- Primary nozzle pressure ratio
- Temperature of the primary jet

This report gives the results of an experimental study using model jets in which all the above parameters were examined. The study included a series of more than three hundred separate model jet tests. The data from these tests were then analyzed to determine sound power output and directivity patterns of the model jet configurations,

and were scaled to give the equivalent acoustic output for full sized engines. The full-scale data are presented in terms of the sound pressure spectrum and perceived noise level along two sidelines at 500 feet and 1500 feet from the jet axis.

The data were also used to determine the decrease in acoustic output that results from the use of a bypass flow configuration relative to the acoustic output of a single jet nozzle which has the same flow characteristics as the primary jet and the same thrust as that of the bypass flow configuration. The effects of area ratio, velocity ratio, and the relative axial position of the primary and secondary nozzles on this noise reduction were examined. Finally, these noise reduction data were reinterpreted to indicate the flow characteristics required to give a jet with minimum acoustic output for a given amount of gross thrust and the acoustic penalty that results if the actual flow characteristics depart from those optimal design conditions.

Section 2 reviews pertinent aspects of the noise generation of jets from circular and multiple nozzles, and develops a simple analytical model which describes the noise generation of coaxial jets. Section 3 details the experimental test hardware, instrumentation and the data analysis procedures. Section 4 presents the basic experimental data, and Section 5 contains a discussion of the results and the development of prediction techniques applicable to full-scale engines. The principal conclusions are given in Section 6.

Seven (7) appendices are included in this volume. They include a directory of experimental runs, the computer program for data analysis, some samples of measured jet flow profiles and a summary of the principal acoustic data obtained. The detailed flow and acoustic data are contained in Volume II.

2.0 NOISE GENERATION BY COAXIAL JET FLOWS

2.1 Noise Generation of Jets From Single Circular Nozzles

Jet flows generate sound by the turbulent mixing of the gas flow with the ambient atmosphere. This process was first properly documented by Lighthill (References 1 and 2), who recognized that the turbulent shear stresses resulting from the momentum exchange produced pressure fluctuations and a radiated sound field. The process of conversion of jet mechanical energy to acoustical energy is relatively inefficient. However, because of the high mechanical energy of a jet exhaust flow, the resulting noise is of great significance for the design of jet aircraft engines.

In the studies of the properties of jet noise generation, the importance of the velocity of the jet flow is easily identified. The overall sound power of single circular jet flows up to approximately 2000 fps is proportional to the eighth power of the velocity. Although the flow velocity is the most important parameter in the determination of the sound power output of a jet, the physical size and the temperature of the jet are also important. Lighthill showed that the sound output was directly proportional to the jet nozzle area. The flow velocity is a function of temperature; heating the flow will increase the velocity for a given nozzle pressure ratio, thus increasing the noise. Alternatively, if the velocity is maintained constant, the noise will decrease as temperature is increased because of a reduction in density. It is possible to reduce the noise slightly for fixed thrust by heating the gas while maintaining the same exit velocity, as documented by Plumblee et al (References 3 and 4).

The relationship between overall sound power level and jet flow parameters is given in Figure 1. The power spectrum can be normalized on the basis of a strouhal number (fd/U) modified by the ratio (a^*/a_o) of the critical velocity of sound in the flow to that in the surrounding ambient air (References 5 and 6). The results for typical jets are given in Figure 2. The sound field is directional, with a predominant sound radiation occurring at an acute angle to the jet flow direction, as illustrated in Figure 3. This directionality is believed to be the result of the convection of the disturbances within the flow and the refraction of the sound within the flow field, with the approximate relationships indicated in Figure 4 (References 5, 9, 10 and 11).

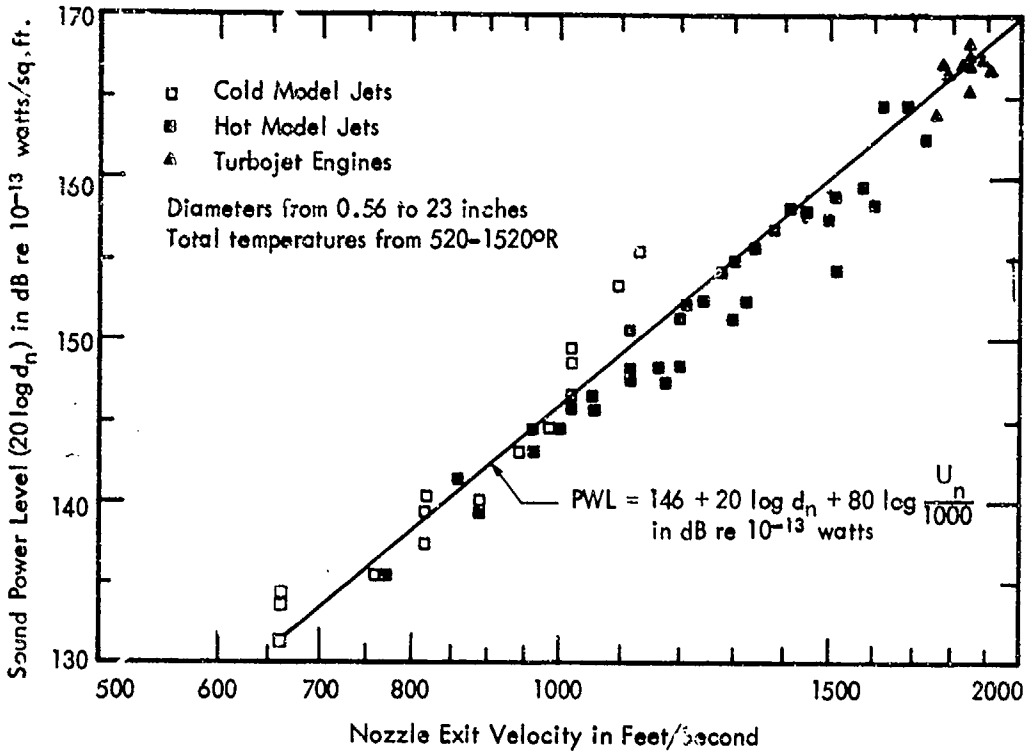

Figure 1. Relationship Between Overall Sound Power Level, Normalized by Nozzle Size and Velocity for Jets from Circular Nozzles at Pressure Ratios less than 2.3. Data from References 6 and 7.

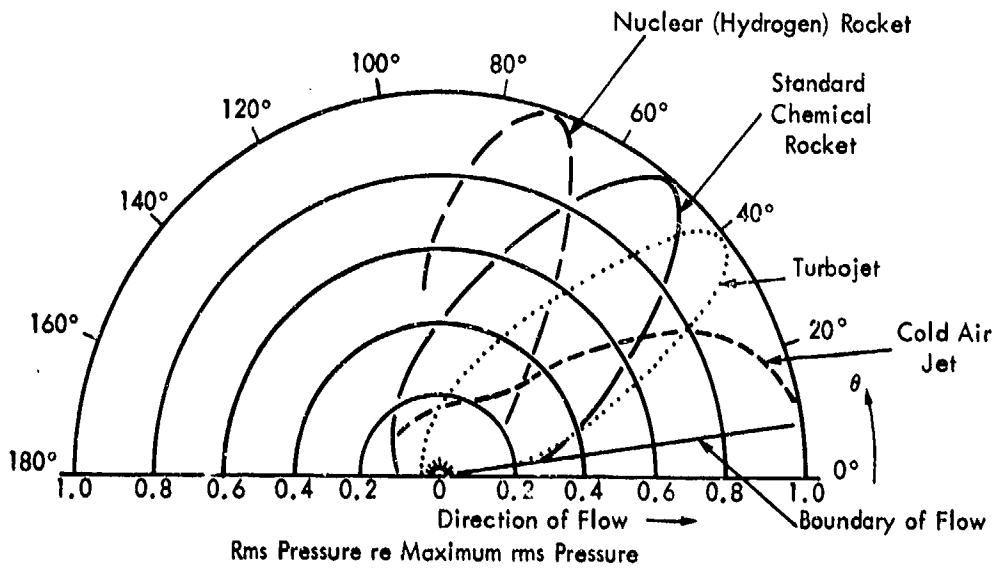

Figure 3. Far-field Directional Characteristics of the Overall Sound Pressure Level for Four Types of Jet Flow (from Reference 8).

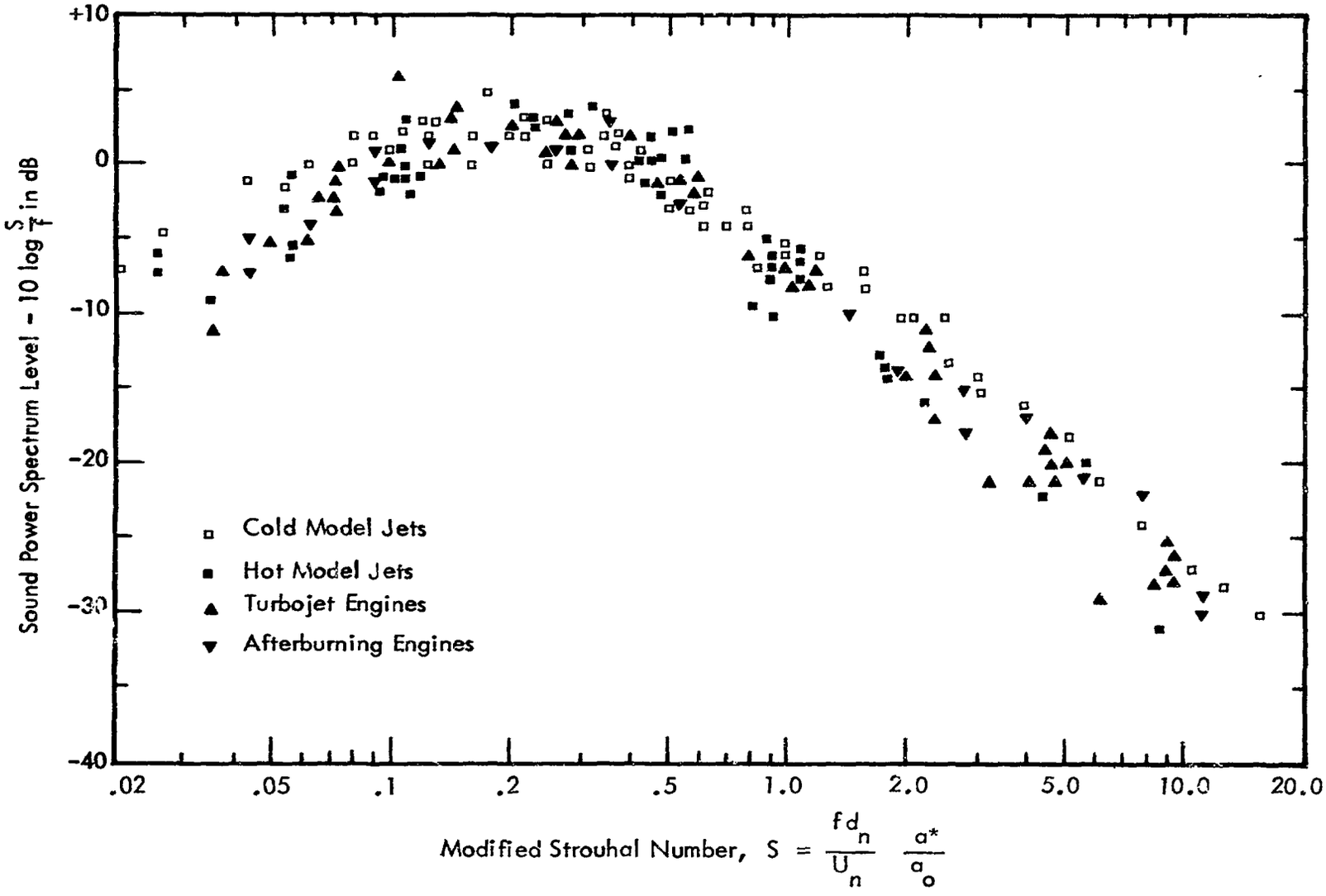

Figure 2. Normalized Sound Power Spectrum Level for Hot and Cold Model Jets and Turbojet Engines. (Data from Reference 6.)

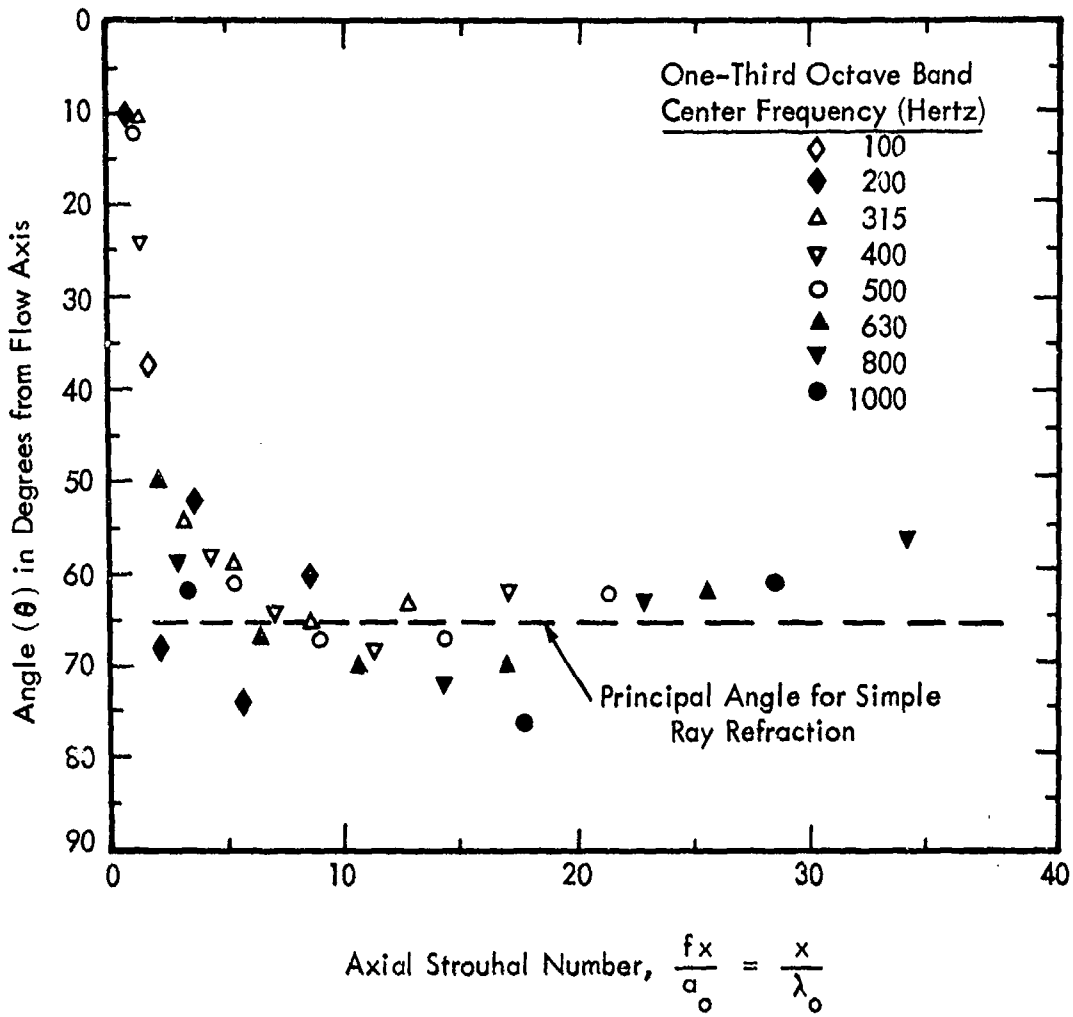

Figure 4. Variation of the Predominant Propagation Angle for Various Frequencies from Measurements Along the 10 Degree Boundary of a Jet from a J-57 Engine as a Function of a Non-dimensional Axial Frequency Parameter. Data from Howes, References 5 and 12.

The velocity profiles in the flow of a constant density circular jet can be approximated with the profile given in Figure 5. The flow momentum rate across any downstream station, which equals the net thrust of the jet, is given by:

$$M_x = F_n = \pi r_n^2 \rho_n U_n^2 = \pi \rho_n \left[a^2 U_n^2 + 2 \int_a^\infty U_c^2 e^{-\eta^2} r\,dr \right] \qquad (1)$$

where

M_x = jet momentum at downstream station x
F_n = jet thrust
r = radius
r_n = jet nozzle radius
ρ_n = density in plane of nozzle
a = radius of core at downstream station x ($0 \leq a \leq r_n$)
U_n = nozzle exit velocity
U_c = centerline velocity at station x ($0 \leq U_c \leq U_n$)
η = $(r - a)/b$
b = width parameter

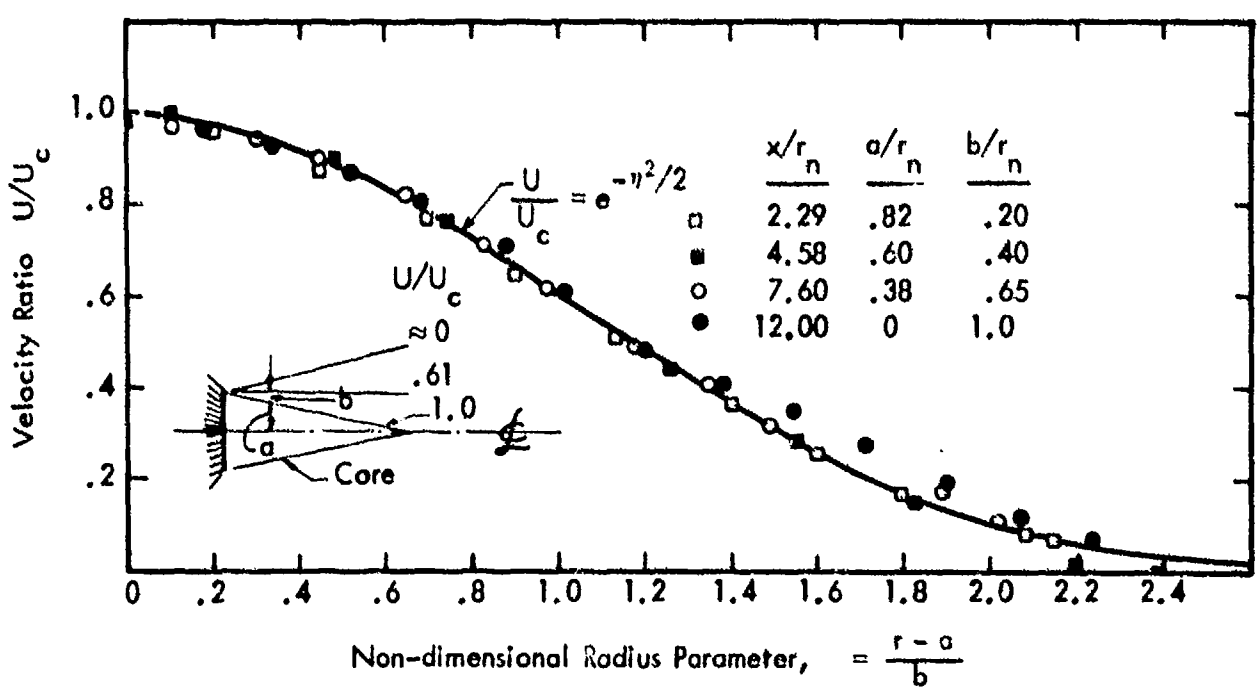

Figure 5. Comparison of Assumed Velocity Profile for Axisymmetric Constant Density Jet with Mach 0.7. Data from Laurence, Reference 13.

This relationship, together with the assumption of a constant coefficient of momentum exchange throughout the mixing process in the flow, permits an analytical solution of the constant density jet velocities throughout the entire flow, as illustrated in Figure 6. This solution was obtained in terms of the normalized axial distance (x_t/r_n) from the nozzle to the tip of the potential core. The length of the core is a function of Mach number, as shown by the empirical curve in Figure 7. When the jet is surrounded by a moving medium, as for an aircraft in flight, the mixing process is less rapid and the distance from the nozzle to the tip of the core lengthens, as illustrated in Figure 8.

The characteristics of the noise generated along the jet vary with axial position, as do the parameters of the flow. Theoretical examination of Lighthill's basic theory of aerodynamic noise generation resulted in identification of the initial mixing region as the prime noise source for a subsonic jet flow (References 17 and 18). These analyses indicated that there should be a uniform source strength along the length of the initial mixing region, where the potential core still exists and the velocity difference across the mixing region is constant. Further, theory indicates that the magnitude of the noise generation should decrease rapidly, following an x^{-7} law, in fully developed mixing regions downstream of the core tip. These results were obtained by applying similarity arguments to the mixing flow properties (mean velocity profile and turbulence intensity).

Experimental measurements shown in Figure 9 appear to validate theory in the initial mixing region. However, the noise generation does not fall as rapidly as predicted by theory downstream of the core tip, perhaps because the turbulent eddies developed in the initial mixing region decay less rapidly as they are convected downstream than do the mean flow velocities. This possible explanation is reinforced by observing the non-dimensional source noise spectra in Figure 10. In the initial mixing region, the frequency of maximum amplitude varies inversely with axial distance; in the downstream region, the spectrum appears almost independent of axial distance.

The basic similarity relationships between the total sound power spectrum and mean jet flow parameters, and between the local sound power spectra and the local flow relationships, provide a powerful tool for estimating the noise generation characteristics of jets with complex nozzles or non-standard initial flow profiles. The similarity laws between flow, turbulence and noise can enable solutions to the noise of a complex flow by analogy to the well known circular jet, once the velocity profiles of the complex flow are defined. This approach was used for the estimation of the noise characteristics of jet flows from mixing nozzles which have multiple tubes or corrugations (Reference 5) and is applied in this report to jet flows from coaxial nozzles, as discussed in the following two subsections.

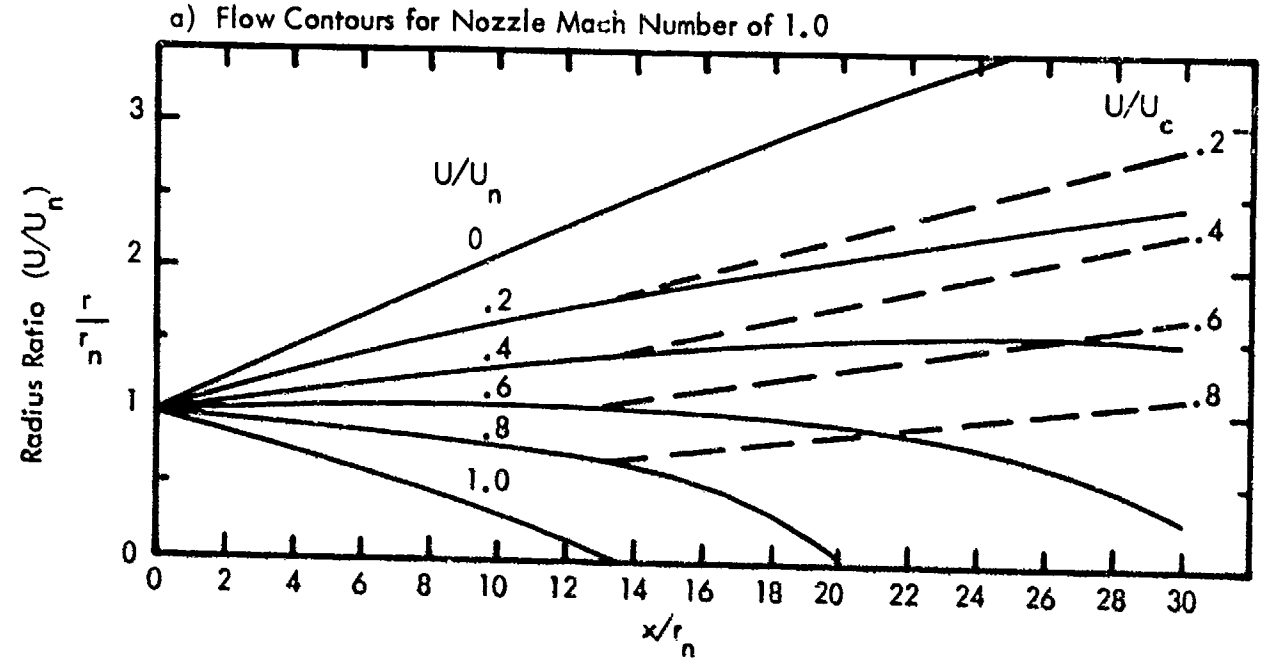

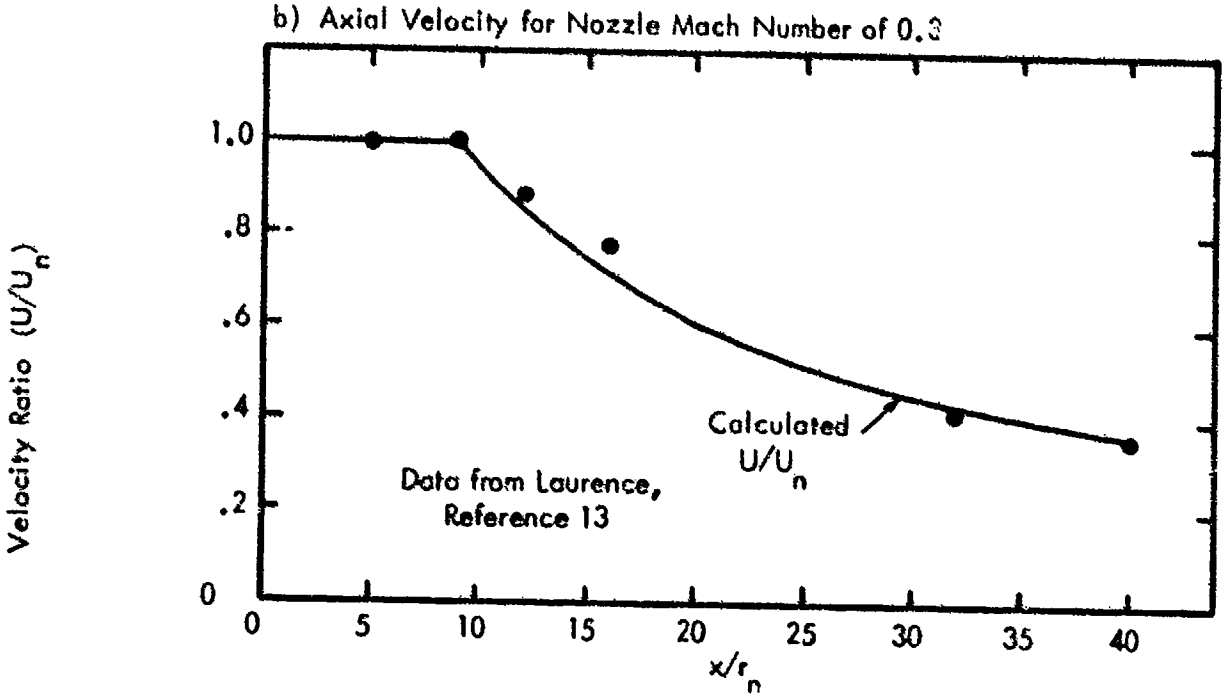

Figure 6. Examples of Flow for Constant Density Axisymmetric Single-Nozzle Jets. (From Reference 5.)

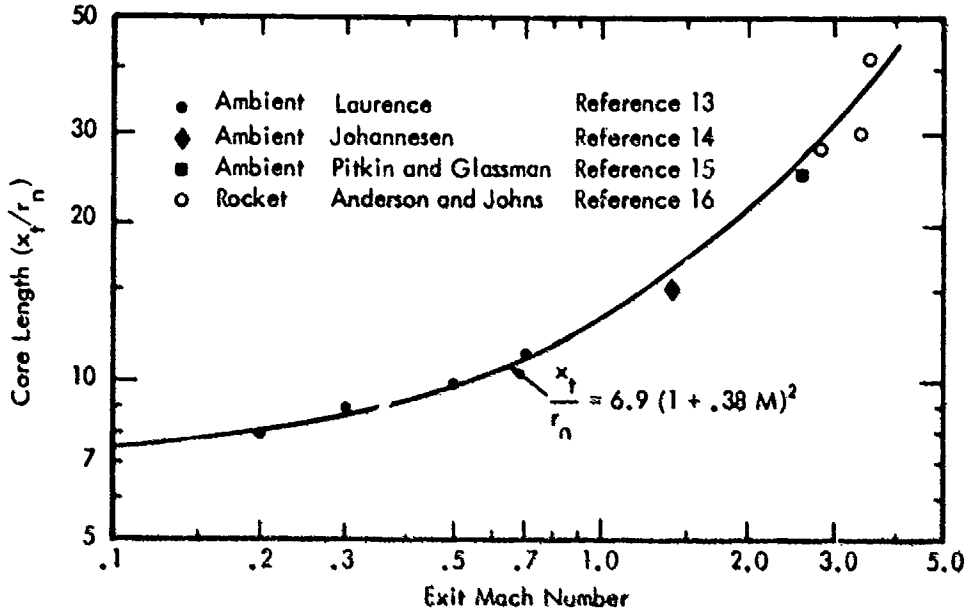

Figure 7. Variation in Core Length (x_f) for Constant Density Axisymmetric Jet as a Function of Mach Number. (From Reference 5.)

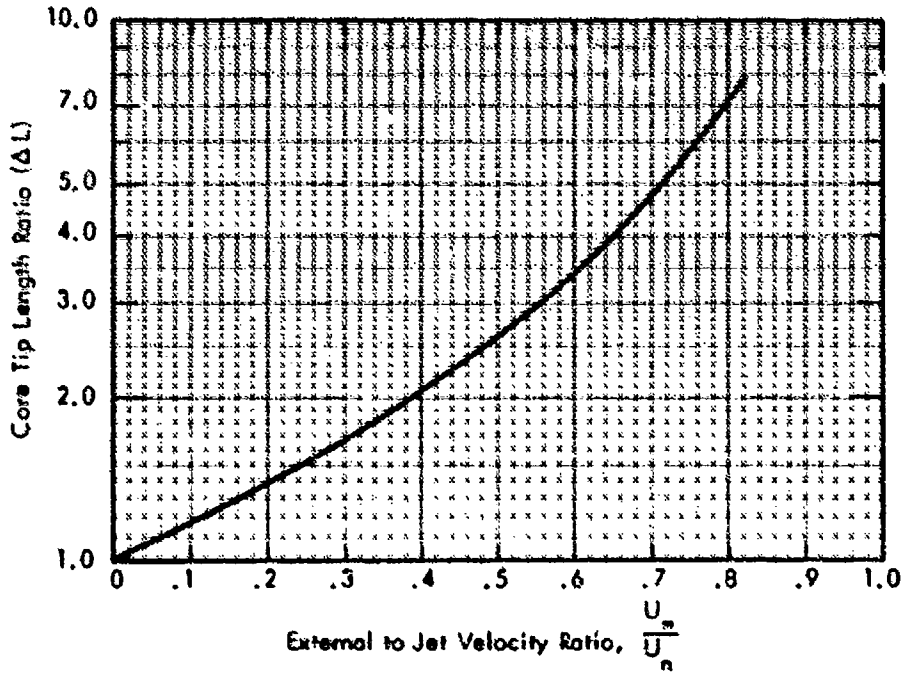

Figure 8. Calculated Increase in the Ratio of the Length of the Jet Core with Non-Zero External Velocity (U_∞) to its Length with Zero External Velocity for Constant Density Jets. (From Reference 5.)

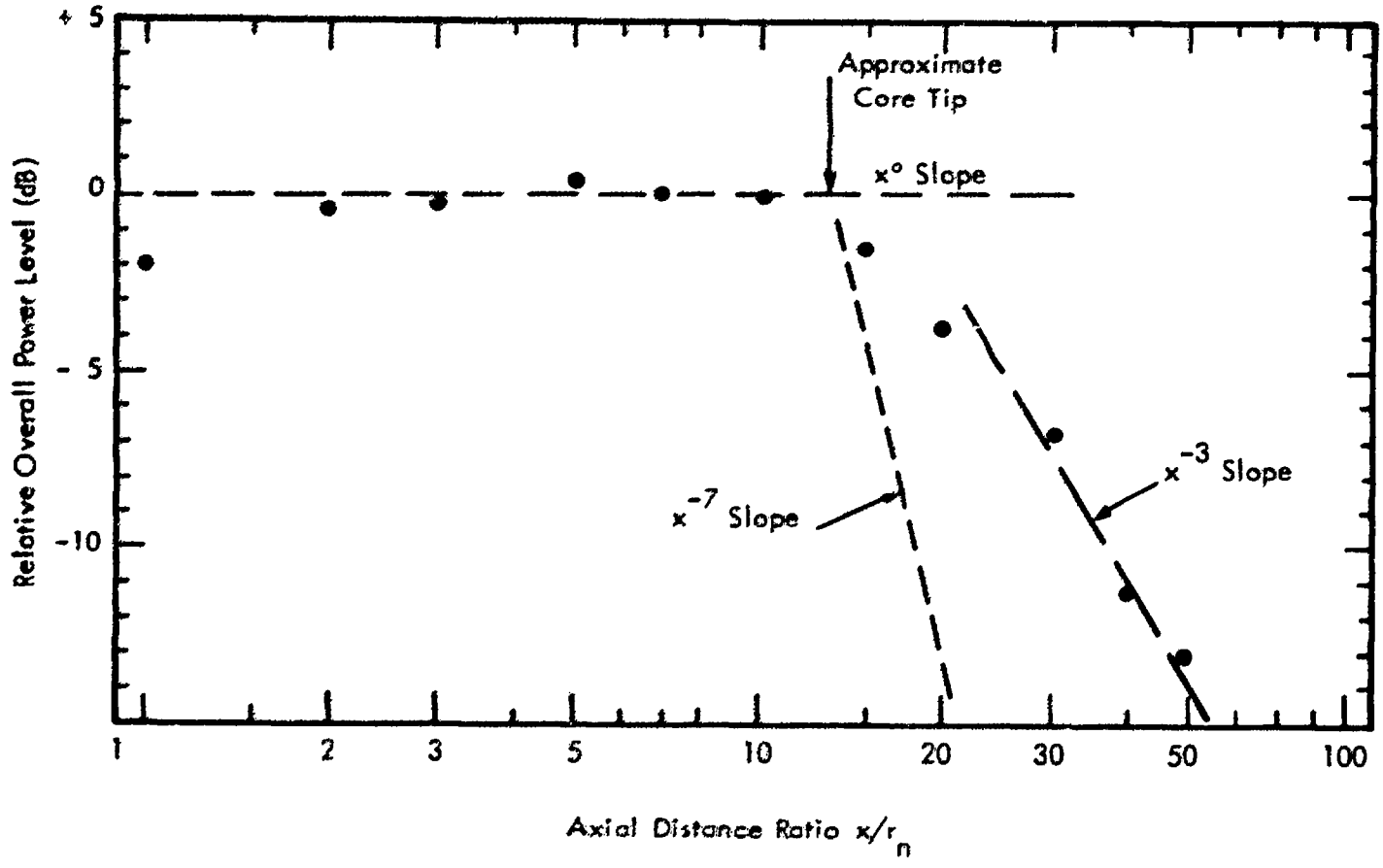

Figure 9. Source Strength Distribution along Jet Axis. Data from J-57, References 5 and 12.

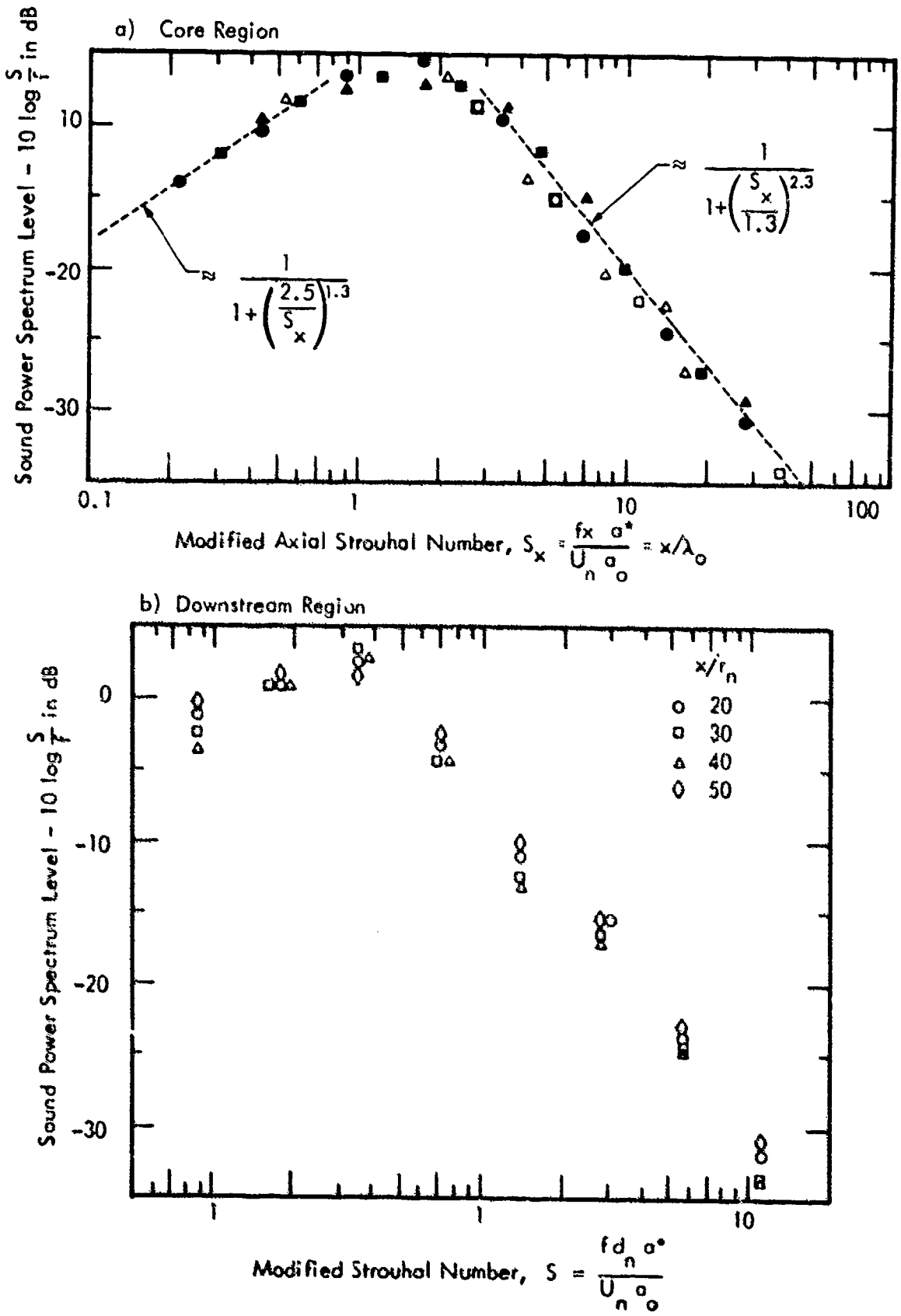

Figure 10. Jet Source Normalized Sound Power Spectra. Data from J-57, References 5 and 12.

2.2 Noise Prediction for Jet Flows from Mixing Nozzles

The possibility of modifying the noise of a single jet by changing the nozzle shape was first discovered by Westley and Lilley (Reference 19), when they observed a reduction in total noise as the result of inserting tooth-like projections into the nozzle. Initial full-scale application of this discovery was made by Greatrex of Rolls Royce and Callaghan, et al, of NASA (Lewis), (References 20 - 24). The concept was reduced to practice in this country in the 1950's with the use of 21- and 9-tube nozzle suppressors on the Boeing 707 series aircraft, corrugated nozzles on the Convair 880 aircraft and corrugated nozzles with ejectors on the Douglas DC-8 series aircraft. More recent developments include the multiple chutes proposed by General Electric for the U.S. supersonic transport engine.

These devices all act to subdivide the single jet into several smaller jets. If the smaller jets are spaced sufficiently far apart so that each jet mixes as a normal single jet, the length of the mixing region is reduced in proportion to the ratio of the diameter of one of the small jets to the diameter of a baseline circular single nozzle which has the same area as the total of the small jets. Similarly, the total acoustic power of each of the small jets relative to the baseline circular jet is reduced in proportion to the nozzle area ratio, with its characteristic frequency shifted up relative to the circular nozzle in inverse proportion to the diameter ratio. However, the acoustic power of the sum of all the smaller nozzles equals that of the baseline circular jet since the sum of the areas of the smaller nozzles equals that of the baseline nozzle.

The power spectrum levels for a variety of sizes of non-interfering tube nozzles for a 10,000 lb thrust jet is illustrated in Figure 11. Also included in the figure is the power spectrum for two cases where the exit velocity was reduced by lowering temperature while retaining total pressure and the baseline circular nozzle.

In general, it is impractical to space the smaller jets sufficiently far apart to enable them to mix normally without interference. Consequently, for most practical configurations, only the peripheral small jets mix rapidly, as would be expected for independent small jets. The inner jets tend to recombine, with the degree of recombination critically dependent upon the amount of ambient air which can be induced into the central portion of the flow.

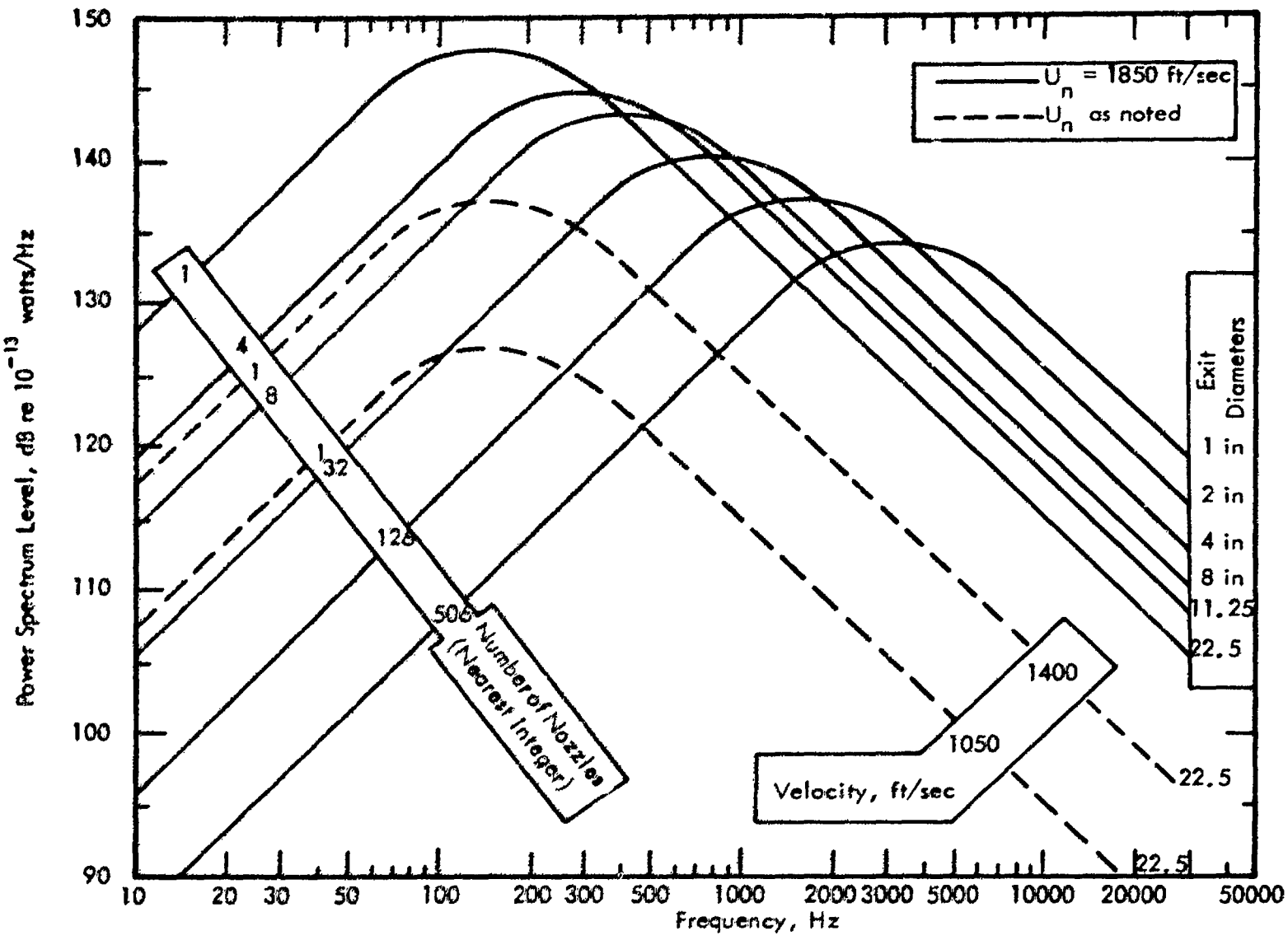

Figure 11. Idealized Power Spectra of Non-Interfering Axisymmetric Jets Having a Thrust of 10,000 lbs, Exit Total Temperature 1720°R, Together with Two Jets of Lower Temperature and Exit Velocity. (From Reference 5.)

A simplified sketch of the flow from a circular ring of tube nozzles is illustrated in Figure 12. Reference 5 gives approximate solutions for the flow from idealized nozzles of this type and compares the solution with data taken by Lawrence and Benninghoff (Reference 25), as shown in Figure 13.

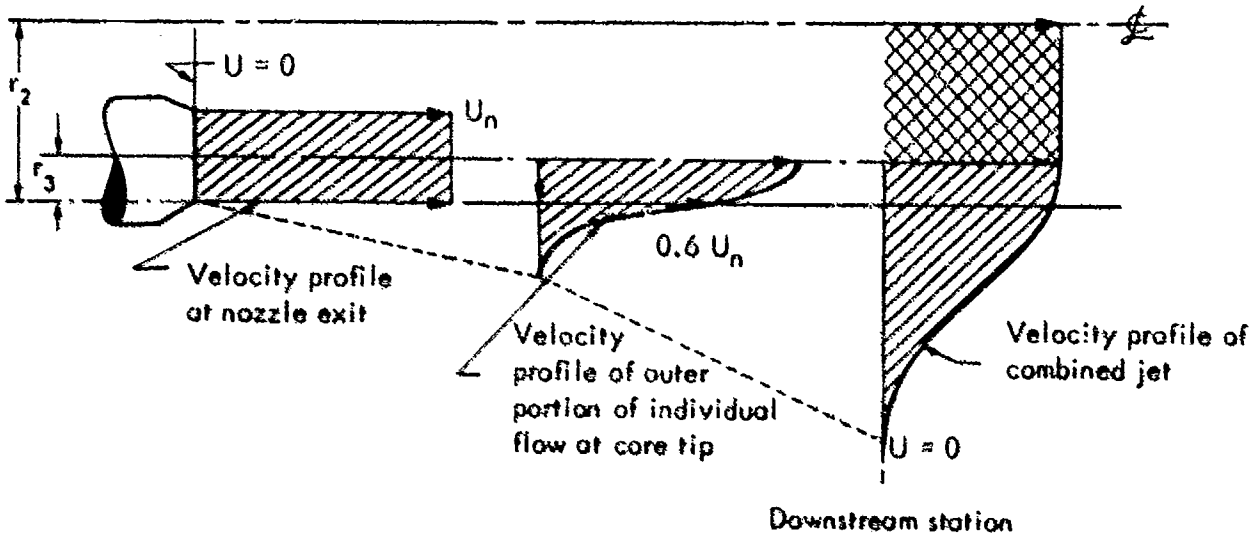

Figure 12. Sketch of Two Nozzles in the Plane Containing the Axis of a Simplified Axisymmetric Peripheral Tube Nozzle Illustrating Development of Final Mixed Jet and the Mixing of the Individual Jets. (From Reference 5.)

A method for computing the noise for ideal tube nozzles which were equally distributed within a circular envelope was developed in Reference 5. The method consisted of computing the sum of the total acoustic power for the peripheral small jets and the acoustic power for the slower, larger diameter, combined mixed jet. The velocity and size of the slower combined mixed jet were related to the nozzle exit velocity and the diameter (d_2) of the circle which envelopes the tube array.

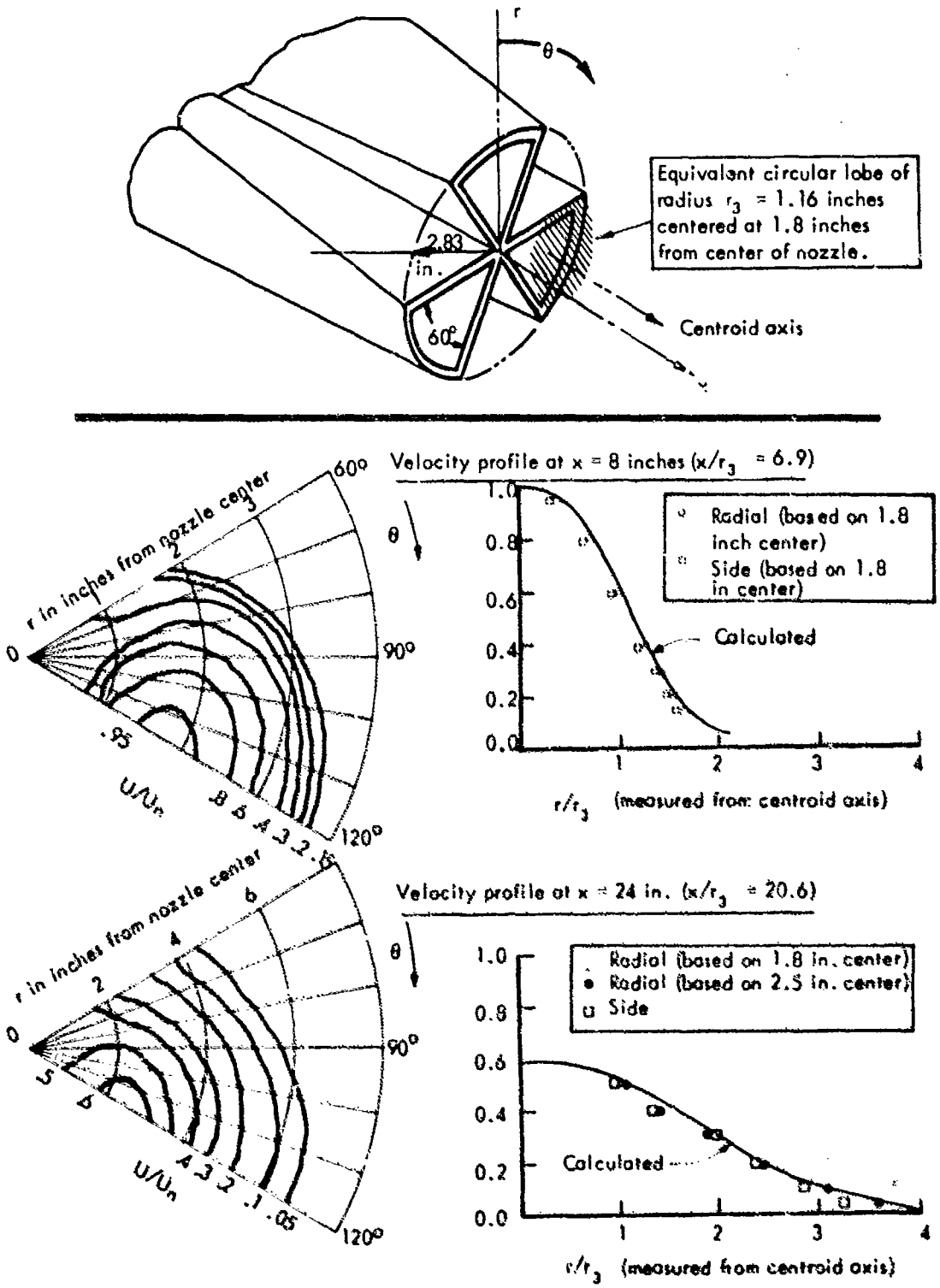

Figure 13. Example of Flow Data and Comparison with Calculated Profiles for Three-Lobed Nozzle at Mach 0.3. (Data from Laurence and Benninghoff, Reference 25.)

Figure 14 shows two examples of a comparison of the results from the Reference 5 method with data for two configurations of 12-lobe nozzles. The low frequency peak in the sound power spectrum results from the combined jet and is lower in magnitude for the configuration with the larger envelope diameter. The high frequency peak in the calculated sound power spectrum results from the flow from the 12 lobes; its characteristic frequency is associated with the typical peripheral dimension of the lobes.

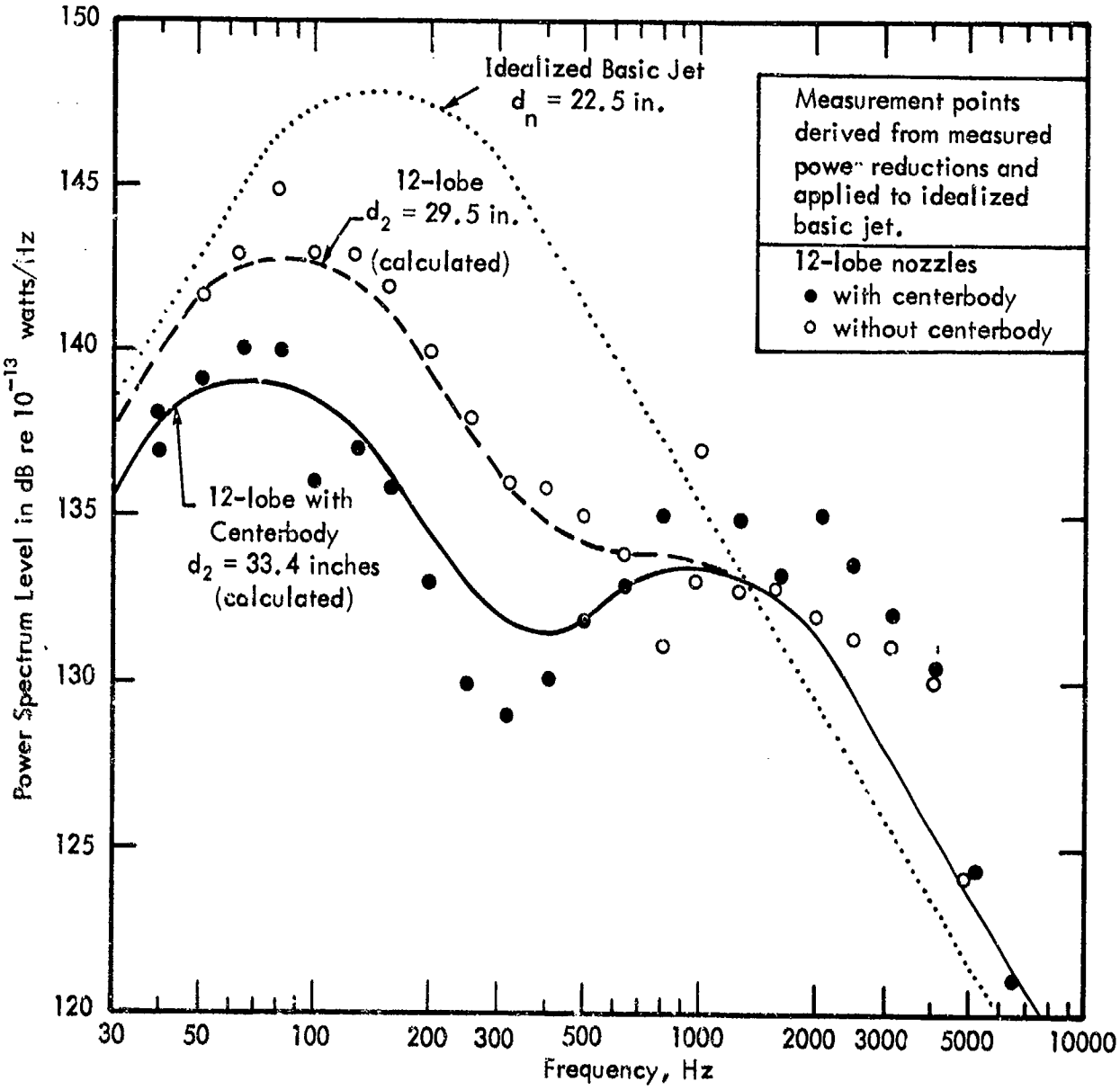

Figure 14. Comparison of Calculated Power Spectra with Power Spectra Derived from Measured Power Reduction for Two 12-Lobe Nozzles with J-57 Engine. (From References 5 and 26.)

An example of the variation in total acoustic power for a series of idealized circular arrays of uniformly distributed tube nozzles as a function of tube size, and the ratio of the envelope diameter to the diameter of a baseline single circular nozzle which has the same area as the sum of the areas of the tube nozzles, is shown in Figure 15. This method has not been generalized to the prediction of perceived noise level along the sideline, although recently it has been applied successfully in an individual case for the proposed supersonic transport (SST) engine, utilizing the appropriate directivity functions for the jet noise. Such generalization is required to determine optimum values for both the characteristic diameter of the tubes or corrugations and the envelope diameter for application to perceived noise level for aircraft operations near airports. It is expected that the optimum values for this case will differ from those indicated in Figure 15 which apply to overall power level.

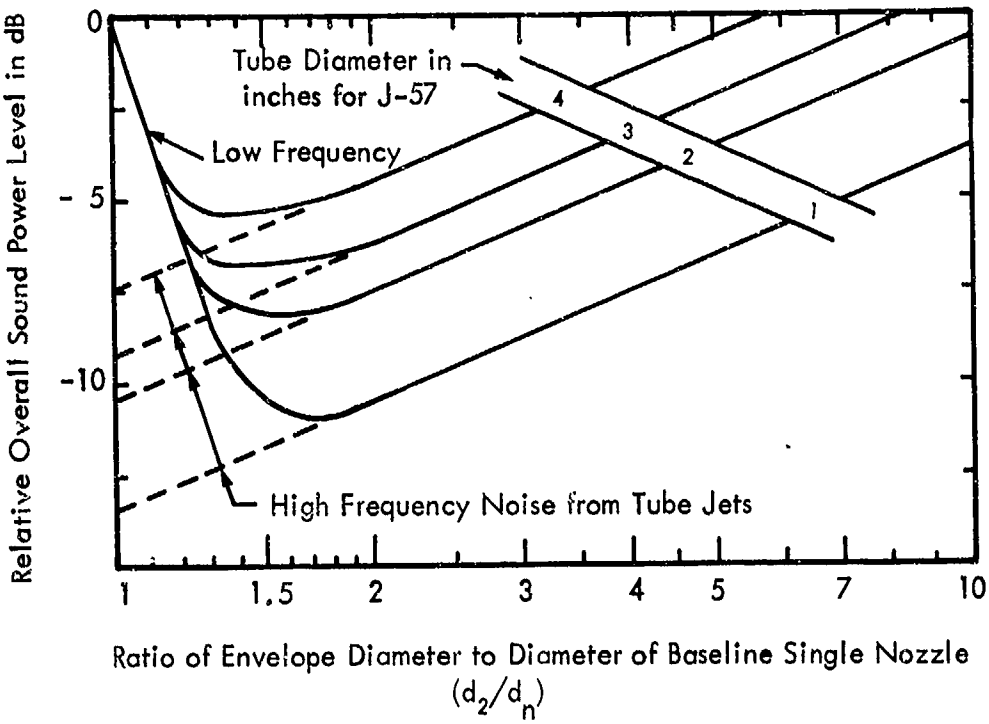

Figure 15. Computed Variation in Total Acoustic Power for Idealized Mixing Nozzle Relative to That of Baseline Single Circular Nozzle for $T/T_o = 3$, as a Function of the Ratio of the Envelope Diameter of the Mixing Nozzle to the Diameter of the Baseline Single Nozzle, with Tube Element Diameter as a Parameter. (From Reference 5.)

2.3 Noise Prediction for Jet Flows from Coplanar Coaxial Nozzles

The flow from a low bypass ratio coaxial jet nozzle is illustrated in Figure 16. It is characterized by two basic regions. In the upstream region, the secondary flow shrouds the primary flow. In the downstream region, the two flows have merged and behave as a single jet in accordance with the similarity parameters discussed in Section 2.1. The axial distance to the station separating these two regions is a function of both the area ratio (β) of the secondary to primary nozzles and their velocity ratio ($U_s/U_p = \delta$). When the secondary flow is large, relative to the primary, the flows will generally merge downstream of the tip of the primary core. However, as in Figure 16, when the secondary flow is small relative to the primary, the merger will occur upstream of the tip of the primary and only a small amount of the primary jet flow will be shrouded.

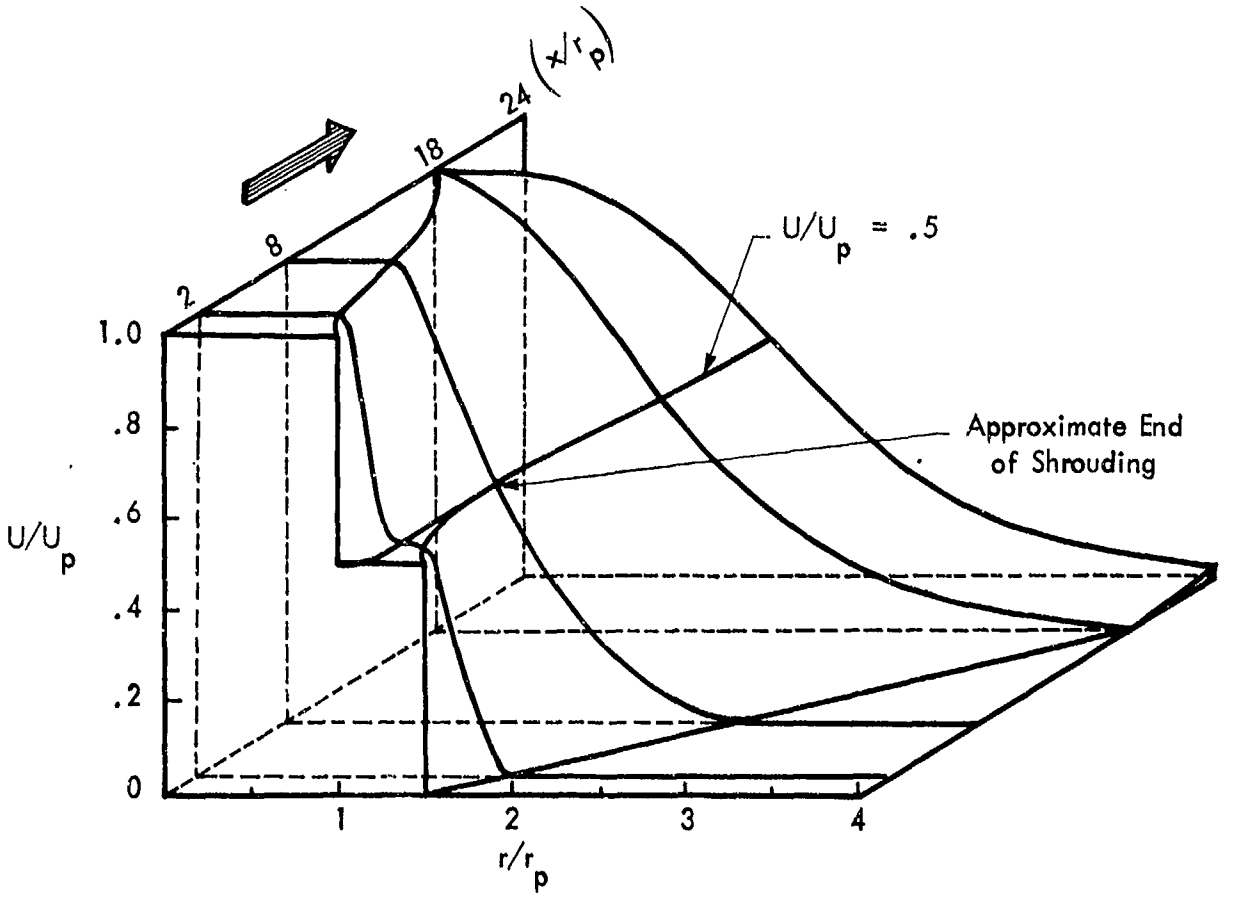

Figure 16. Approximate Velocity Profiles at Various Downstream Stations for Constant Density Annular Coplanar Jet with $U_s/U_p = .5$ and $r_s/r_p = 1.5$.

Greatrex (Reference 27) observed that the noise of a coaxial jet should be composed of three parts:

- Noise of the secondary jet mixing with the atmosphere (shrouded region)
- Noise of the primary jet mixing into the secondary (shrouded region)
- Noise of the large combined jet

Similar concepts were advanced in Reference 5 and approximate estimates were made of the reduction in acoustic power which could be obtained as a function of bypass ratio, for a velocity ratio of .5, considering only the noise produced by the combined jet.

In order to develop quantitative estimates of these three noise sources, it is necessary to define the extent of the shrouded region and the parameters of the combined jet. The velocity profiles in the combined jet could be duplicated by a portion of the flow from a single-nozzle jet which has the appropriate nozzle velocity and radius. Such a single-nozzle jet may be called an "equivalent jet," in both an aerodynamic and an acoustic sense.

The thrust of the equivalent jet must equal the thrust of the actual coaxial jet:

$$F_e = \pi \rho_e U_e^2 r_e^2 = \pi \rho_p U_p^2 r_p^2 + \pi \rho_s U_s^2 \left(r_s^2 - r_p^2 \right) \tag{2}$$

where the subscripts e, p and s denote equivalent, primary and secondary, respectively.

For a constant density jet, which will be considered here, this equality gives:

$$U_e^2 r_e^2 = U_p^2 r_p^2 + U_s^2 \left(r_s^2 - r_p^2 \right) \tag{3}$$

At the beginning of the combined jet from the coaxial nozzle, it is postulated that the flows have merged and obey the similarity profile for the single jet shown in Figure 5. Hence, at the most upstream or initial station at which this condition is fulfilled, the thrust for the combined jet is given by:

$$F_e = \pi \rho U_e^2 r_e^2 = \pi \rho \left[a^2 U_p^2 + 2 \int_a^\infty U_c^2 e^{-\eta^2} r\,dr \right] \tag{4}$$

If the flows merge upstream of the primary core tip, the first term in the brackets is non-zero and the equivalent jet velocity equals the primary velocity. If the merger occurs downstream of the primary core tip, the first term in the brackets is zero and the equivalent jet velocity equals the jet centerline velocity. These two cases are illustrated in Figure 17.

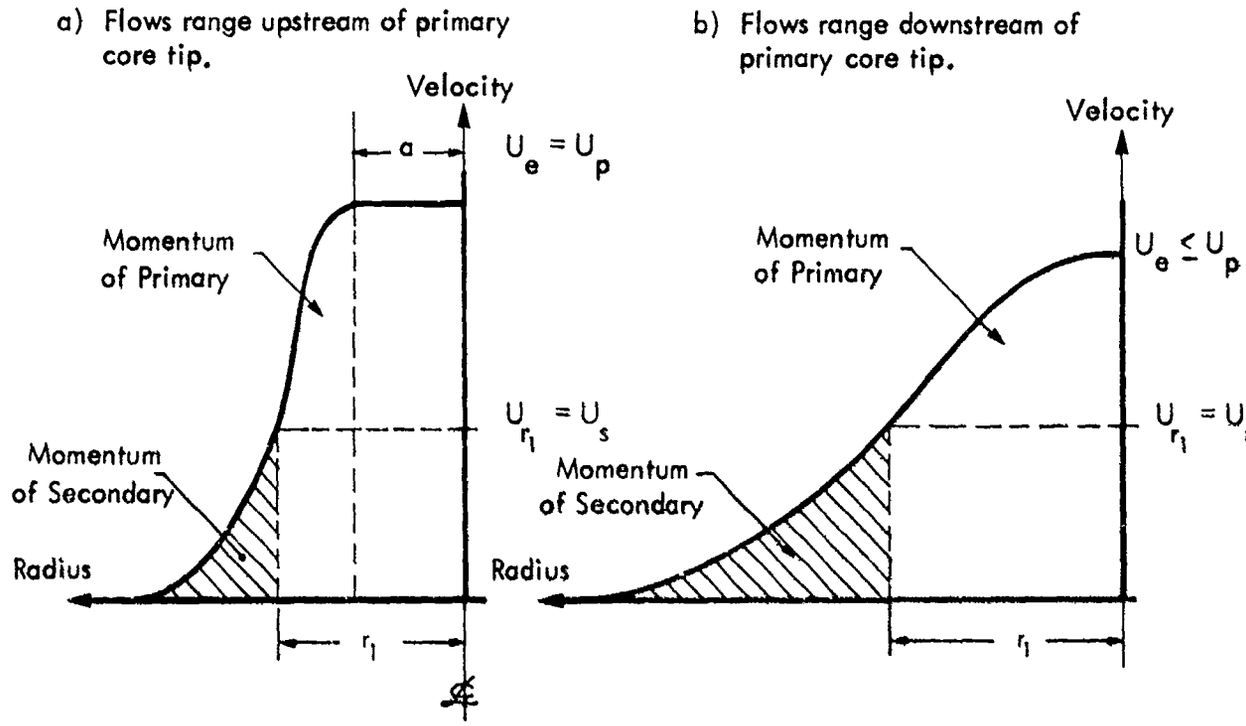

Figure 17. Sketch of Equivalent Jet Flow Profile for Two Cases.

The radius of the separation boundary between the inner momentum flow due to the primary, and the outer momentum flow due to the secondary, may be defined for any axial station. At the initial station, however, where the flows merge and initially obey the similarity profile for the combined jet, the velocity associated with the radius (r_1) is approximately equal to the secondary flow velocity. Hence, at the initial station:

$$U_{r_1} = U_s = U_c e^{-\frac{\eta_1^2}{2}} \tag{5}$$

For case (b) of Figure 17, the momentum of the outer flow at Station 1 may be written as:

$$\pi \rho U_s^2 \left(r_s^2 - r_p^2\right) = 2\pi\rho \int_{r_1}^{\infty} U_c^2 \, e^{-(r/b_1)^2} \, r\,dr$$

$$= \pi \rho b_1^2 U_c^2 \, e^{-(r_1/b_1)^2} \tag{6}$$

Substituting from Equation (5) and recognizing that the tip of the core of the equivalent jet $r_e = b_1$:

$$r_e^2 = r_s^2 - r_p^2, \quad \text{or} \quad \left(\frac{r_e}{r_p}\right)^2 = \beta \tag{7}$$

where β is the area ratio of the secondary to primary jets.

From Equations (3) and (7), the velocity is given by:

$$\left(\frac{U_e}{U_p}\right)^2 = \left(\frac{U_s}{U_p}\right)^2 + \frac{r_p^2}{r_s^2 - r_p^2},$$

$$\text{or} \quad \left(\frac{U_e}{U_p}\right)^2 = \delta^2 + \frac{1}{\beta} \tag{8}$$

where δ is the velocity ratio, U_s/U_p.

For case (a) of Figure 17, $U_e = U_p$ and the radius of the equivalent jet is given by:

$$r_e^2 = r_p^2 + \left(\frac{U_s}{U_p}\right)^2 \left(r_s^2 - r_p^2\right), \quad \text{or} \quad \left(\frac{r_e}{r_p}\right)^2 = 1 + \delta^2 \beta \tag{9}$$

This case of incomplete shrouding occurs whenever the combination of area ratio and velocity ratio are such that:

$$\left[\left(\frac{r_s}{r_p}\right)^2 - 1\right]\left[1 - \left(\frac{U_s}{U_p}\right)^2\right] \leq 1, \quad \text{or} \quad \beta(1 - \delta^2) \leq 1 \tag{10}$$

The effect of this relationship is shown in Figure 18.

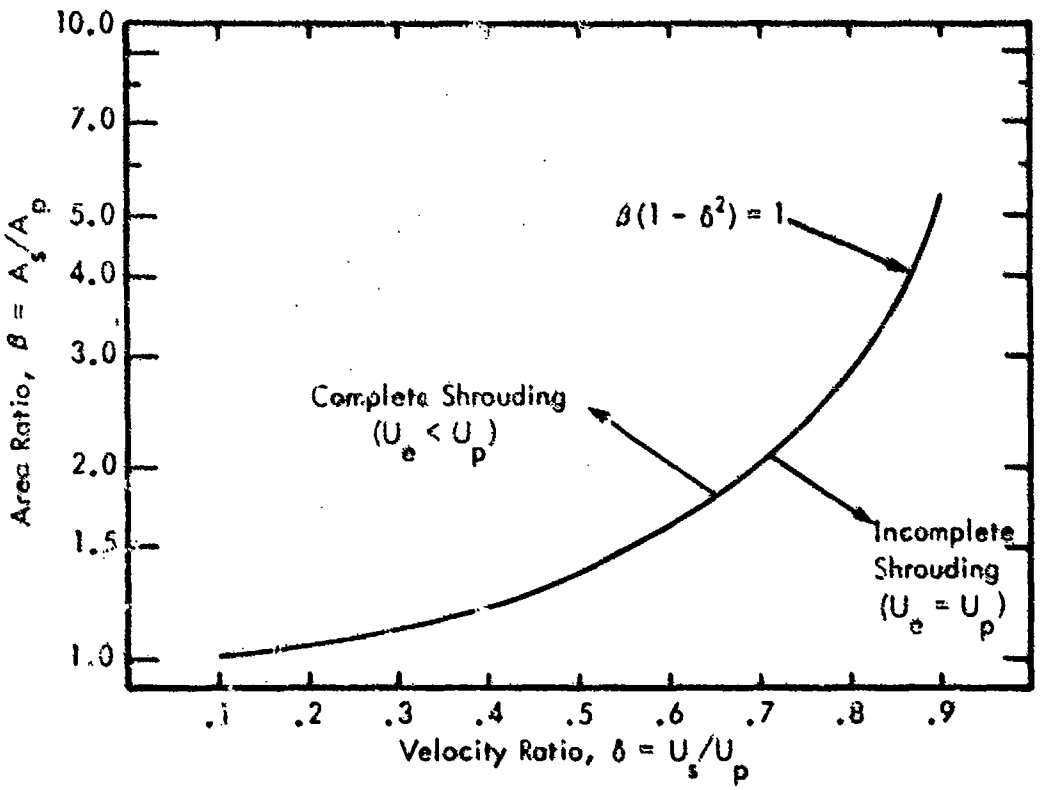

Figure 18. Calculated Regions of Complete and Incomplete Shrouding of the Primary Core as a Function of Area and Velocity Ratios.

The radius and velocity ratios for the equivalent jet from Equations (7), (8) and (9) are plotted in Figure 19 as a function of the area and velocity ratios of the coaxial jet. When the nozzle area ratio is less than 1, the equivalent jet velocity equals the primary velocity for all values of the secondary velocity. The minimum area ratio required to ensure complete shrouding of the primary jet core increases from 1 at low values of the velocity ratio to approximately 2 for $\delta = 0.7$ and to over 5 for $\delta = 0.9$. When the area ratio is less than the minimum required for complete shrouding, the equivalent jet radius is indicated by the dashed lines in the figure.

This information can be used to construct an approximate model of the entire flow-field and estimate the resulting acoustic power spectrum utilizing the general methods of Reference 5. However, the purpose of these experiments is to develop generalized curves of sideline perceived noise level, and the detailed computation of power spectra is not sufficient for this purpose. Rather, it is more relevant to examine the gross trends in overall acoustic power as a function of coaxial jet parameters to obtain guidance for understanding the experimental variations of perceived noise level.

For this discussion, the noise estimates for the coaxial jet flows will be compared to the noise of a baseline single-nozzle circular jet which has the same velocity as the primary nozzle of the coaxial jet and has the area required to make its thrust equal to that of the coaxial jet.

The acoustical power estimates are based on the Lowson and Pao relationships (References 28 and 29) which consider the total acoustic power (W) proportionality as:

$$W \sim \rho A u^4 M_c^4 \tag{11}$$

where u is the fluctuating turbulent velocity which is proportional to the velocity difference (ΔU) across a mixing layer, and M_c is the eddy convection Mach Number.

For a single jet, both u and M_c are proportional to the flow velocity U, so that Equation (11) is equal to the simple $\rho A U^8$ Lighthill relationship. For shrouded flows, however, u is proportional to the velocity difference, whereas M_c should be proportional to a typical value of the absolute velocity in the mixing flow. For this analysis, M_c will be considered proportional to the maximum velocity in the mixing layer.

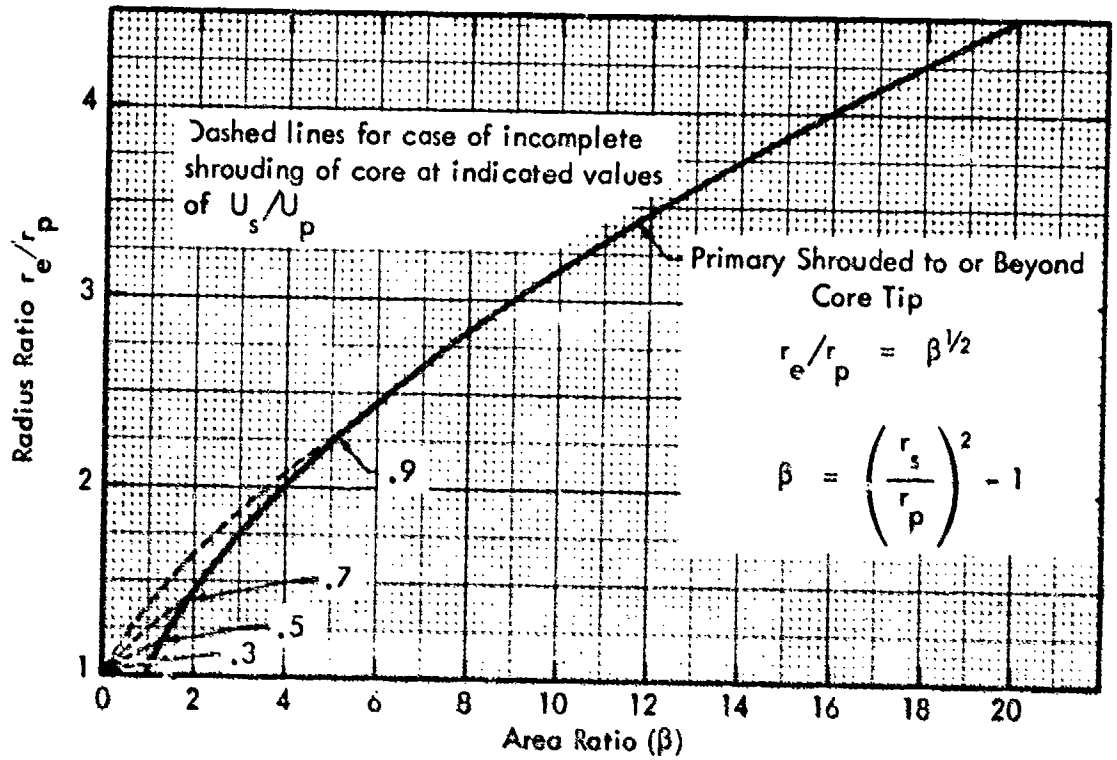

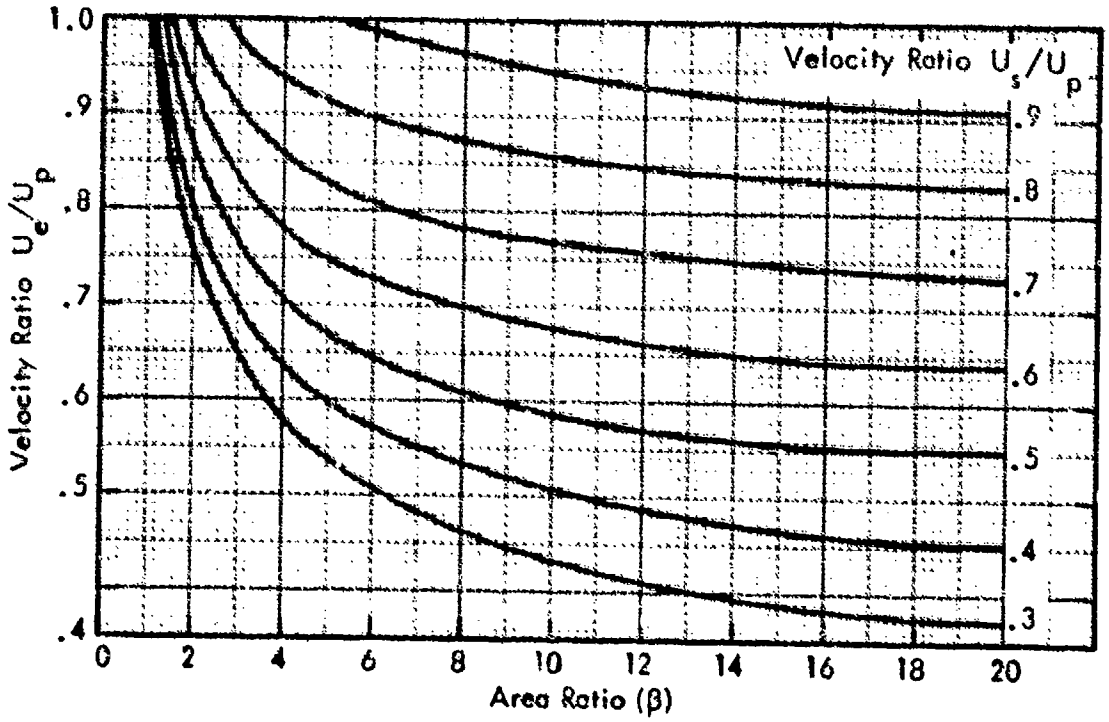

Figure 19. Relationship Between Radius and Velocity of Equivalent Jet and the Parameters of a Constant Density Coplanar Coaxial Jet.

The acoustic power for the three principal source regions can be approximated by:

$$\left.\begin{array}{ll} \text{Equivalent jet:} & W_e \sim r_e^2\, U_e^8 \\ \text{Primary mixing with secondary:} & W_{ps} \sim r_p^2\, (U_p - U_s)^4\, U_p^4\, \Delta L \\ \text{Secondary mixing with ambient:} & W_{so} \sim r_s^2\, U_s^8 \end{array}\right\} \qquad (12)$$

where ΔL is the factor accounting for the lengthening of the primary jet by the presence of an external flow, as shown in Figure 8.

The size of the baseline jet which has the same thrust as the coaxial jet and the same velocity as its primary nozzle flow can be determined from the momentum equation:

$$U_p^2\, r_b^2 = U_p^2\, r_p^2 + U_s^2 \left(r_s^2 - r_p^2\right), \quad \text{or} \quad \left(\frac{r_b}{r_p}\right)^2 = 1 + \delta^2 \beta \qquad (13)$$

Its acoustic power is proportional to:

$$W_b \sim r_b^2\, U_p^8 = r_p^2\, U_p^8\, (1 + \delta^2 \beta) \qquad (14)$$

The ratio of the power generated by the downstream flow of the equivalent jet (one-half its total power) to that of the baseline jet is from Equations (7), (8), (12) and (14):

$$\frac{W_e}{2W_b} = \frac{r_e^2\, U_e^8}{2 r_p^2\, U_p^8\, (1 + \delta^2 \beta)} = 1/2 \left(\frac{\delta^2 \beta + 1}{\beta}\right)^3 \qquad (15)$$

Similarly, the power ratio for the primary mixing with the secondary is:

$$\frac{W_{ps}}{kW_b} = \frac{(U_p - U_s)^4 U_p^4 \Delta L}{k U_p^8 (1 + \delta^2 \beta)} = \frac{(1 - \delta)^4 \Delta L}{k (1 + \delta^2 \beta)} \tag{16}$$

and for the secondary mixing with the ambient:

$$\frac{W_{so}}{2W_b} = \frac{r_s^2 U_s^8}{2 r_p^2 U_p^8 (1 + \delta^2 \beta)} = \frac{(\beta + 1) \delta^8}{2(1 + \delta^2 \beta)} \tag{17}$$

The constant k in Equation (16) has a value between 1 and 2, with the lower value appropriate when the significant noise-generating region of the primary flow is shrouded. The upper value should apply when the primary flow is shrouded only to the tip of its core. Between these two cases, intermediate values should apply. For the estimates in this report, $k = 2$ was used for the area ratio of 1, and $k = 1$ was used for the area ratios 2, 5 and 10.

A first approximation of the noise from the unshrouded portion of the primary can be obtained from:

$$\frac{W_{po}}{2W_b} = 1/2 \left[1 - \left(\frac{(\beta + 1)(1 - \delta^2)}{2 - \delta^2} \right)^{1/2} \right] \tag{18}$$

Figure 20 summarizes the estimates of the reduction in overall sound power level for a coaxial jet with an area ratio of 10 using Equations (15), (16) and (17). A maximum reduction occurs at a velocity ratio of approximately .55. Below that velocity, the noise output of the coaxial jet is dominated by the noise generated by the primary jet mixing into the secondary jet. Above a velocity ratio of .55, the noise output is dominated by the noise of the equivalent jet with a lesser contribution by the noise generated by the secondary mixing with the ambient.

Similar calculations have been made for area ratios of 1, 2 and 5, with the results summarized in Figure 21. The equivalent jet for an area ratio of 1 has a velocity equal to the primary velocity for all values of velocity ratio, as seen in Figures 18 and 19. Therefore, the noise of the equivalent jet is almost constant and the reduction is primarily controlled by the amount of the primary core which is shrouded.

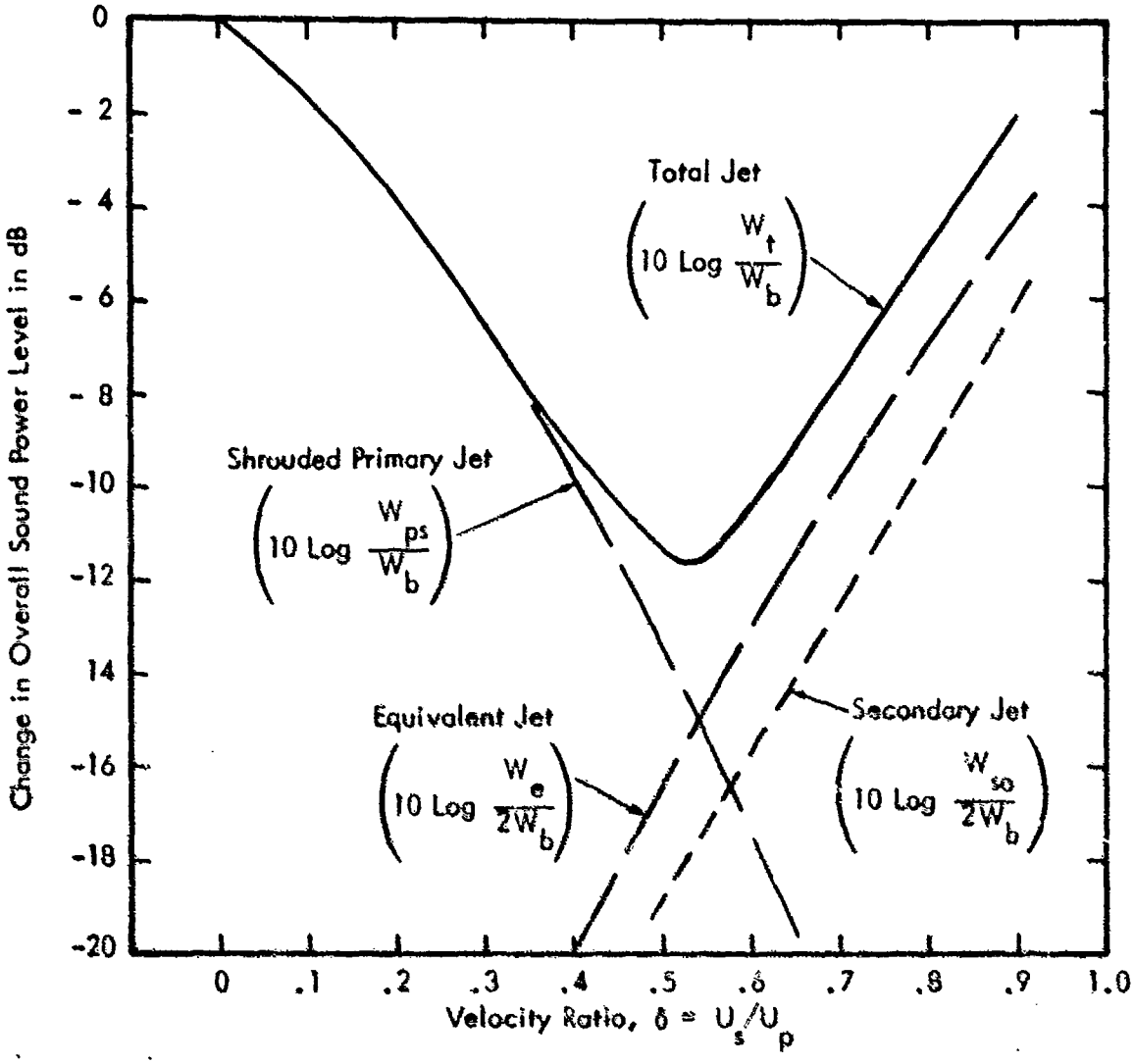

Figure 20. Estimated Contributions to and Total Reduction in Overall Sound Power Level with Velocity Ratio for Coaxial Jets with an Area Ratio of 10 and a Fixed Thrust. Reduction is Measured Relative to a Single-Nozzle Jet Which has Equal Thrust and a Velocity Equal to U_p.

Incomplete shrouding also affects the results for area ratio 2 for velocity ratios of .7 and above. However, for the remainder of the curves, the equivalent jet velocity is less than the primary and the maximum noise reduction occurs at a velocity ratio in the vicinity of .5. These simple theoretical estimates of sound power reduction are shown in Section 5 to be in general agreement with the experimental data, particularly for the higher values of area ratio.

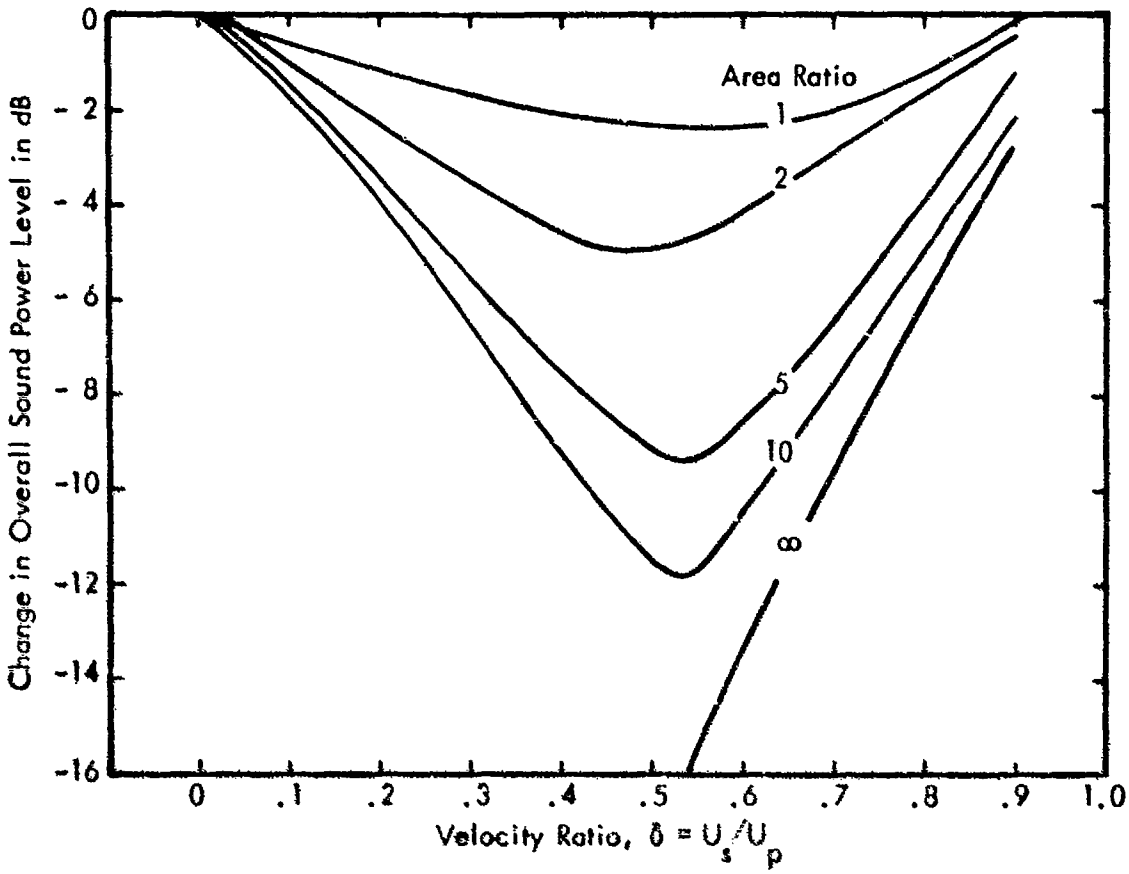

Figure 21. Estimated Reduction in Overall Sound Power Level with Velocity Ratio for Coplanar Coaxial Jets of Fixed Thrust and Various Area Ratios. Reduction is Measured Relative to a Single-Nozzle Jet Which has Equal Thrust and a Velocity Equal to U_p.

Intentionally Left Blank

3.0 EXPERIMENTAL APPARATUS AND DATA ANALYSIS PROCEDURES

The experimental program was conducted using model jets located in an anechoic room in order to provide free-field conditions. In this section, details are given of the experimental rig, supporting measurement equipment and the analytical basis for computer data analysis.

3.1 Jet Flow Parameters and Design of the Experiment

The following jet flow and nozzle configuration parameters must be considered in the design of the experimental program for determining the noise characteristics of coaxial jets:

- Secondary and primary flow velocities
- Temperature (density) of the flows
- Relative size of the secondary and primary nozzles
- Relative axial position of the secondary and primary nozzles
- Thrust

A range of values must be chosen for each of these which covers the range to be expected from existing and projected jet engines (Reference 30). In practice, an engine designer works with additional factors which are related to those listed above, such as pressure ratios, bypass ratios and Mach numbers, so these also must be considered. On this basis, the following variation in jet engine parameters was chosen for investigation in this experimental model study:

- Thrust

The thrust values of jet engines vary from less than 10,000 lbs for the smaller civil aircraft up to 30,000 to 40,000 lbs for large long-range commercial transport aircraft. Engines with even greater thrusts are under development. Four engine thrusts of 10,000 lbs, 20,000 lbs, 40,000 lbs and 80,000 lbs were therefore used in this program as the equivalent full-scale thrusts.

- Primary Nozzles

Three different configurations were chosen with pressure ratios of 1.6, 2.5 and 3.5. The first is subsonic, whereas the latter two are supersonic. The pressure ratio of 3.5 is higher than that currently used in jet engines or proposed for future engines, but was included to give a significant variation in primary nozzle exit velocities.

Preceding page blank

- Secondary Nozzles

Present indications are that engines with bypass ratios up to ten-to-one are being considered. In order to cover this range, the secondary nozzles were chosen to give secondary to primary area ratios of approximately unity, two, five and ten. All the secondary nozzles were simple convergent nozzles to be run at subsonic or just sonic conditions.

- Flow Temperature

On existing bypass jets, the bypass air is not used for combustion. For the purposes of this program, the secondary flow was therefore assumed to be at ambient temperature. For the primary jet, three different temperatures were used. These were ambient, 450°F and 800°F. The latter temperature was a limitation provided by the experimental facility and is slightly less than conditions necessary to cover the normal operating range of present jet engines.

- Flow Velocity

At design conditions, the calculated ideal primary flow velocities were as shown in Table 1.

Table 1

Calculated Ideal Primary Flow Velocities
for Various Temperatures and Pressure Ratios

	Total Temperature		
Pressure Ratio	60°F	450°F	800°F
1.6	889 ft/sec	1174 ft/sec	1437 ft/sec
2.5	1201 ft/sec	1590 ft/sec	1943 ft/sec
3.5	1375 ft/sec	1818 ft/sec	2223 ft/sec

- Axial Position

Most existing bypass engines have a primary nozzle that protrudes beyond the secondary (bypass) nozzle, but the tendency is to reduce the axial distance between the two nozzles in order to facilitate the incorporation of silencing devices. The experimental facility was therefore designed so that the secondary nozzle could be moved axially relative to the primary nozzle over a range of plus or minus eleven primary nozzle diameters. In the experiments, axial displacements of 11, 5.5, 0, -5.5 and -11 primary nozzle diameters were used.

The complete set of runs utilizing all possible combinations of the above parameters results in nearly five hundred (500) runs. In the actual experiments, approximately two-thirds of these possible runs were undertaken. Table 2 summarizes the runs for which experimental data was obtained and analyzed. Greater detail may be found in Appendix A.

Table 2

Summary of Runs Completed

	Primary Temperature		
	Ambient	450°F	800°F
Primary Fully Extended	All	All	1.6 Primaries 3.5 Only
Primary Half Extended	All	All	None
Coplanar	All	All	All
Primary Half Retracted	All	None	None
Primary Fully Retracted	All	None	None

All = { 3 Primary Nozzles, 4 Secondary Nozzles, 3 or 4 Secondary/Primary Velocities } = All Combinations

3.2 Test Hardware

3.2.1 Jet Rig.

Figures 22 and 23 show the configuration of the jet rig. It consisted of two coaxial pipes through which two separate air supplies were directed to demountable coaxial nozzles. Each air supply pipe contained flow straighteners at the inlet end, composed of bundles of thin wall tubes laid axially within the supply pipes. The construction of the assembly allowed a limited amount of longitudinal movement of the primary (inner) supply pipe within the secondary (outer) supply pipe. By this means, the relative positions of the primary and secondary nozzles could be adjusted. A means of locking the inlet ends of the coaxial pipes provided the longitudinal constraint for the primary supply pipe and nozzle. By supporting the forward end of the primary supply pipe on a three-point axial suspension system, relative longitudinal movement could occur between the coaxial pipes, as required to allow for differential expansion. Additional longitudinal adjustment of the relative positions of the primary and secondary nozzles was attained by the use of extension tubes on the primary nozzle supply.

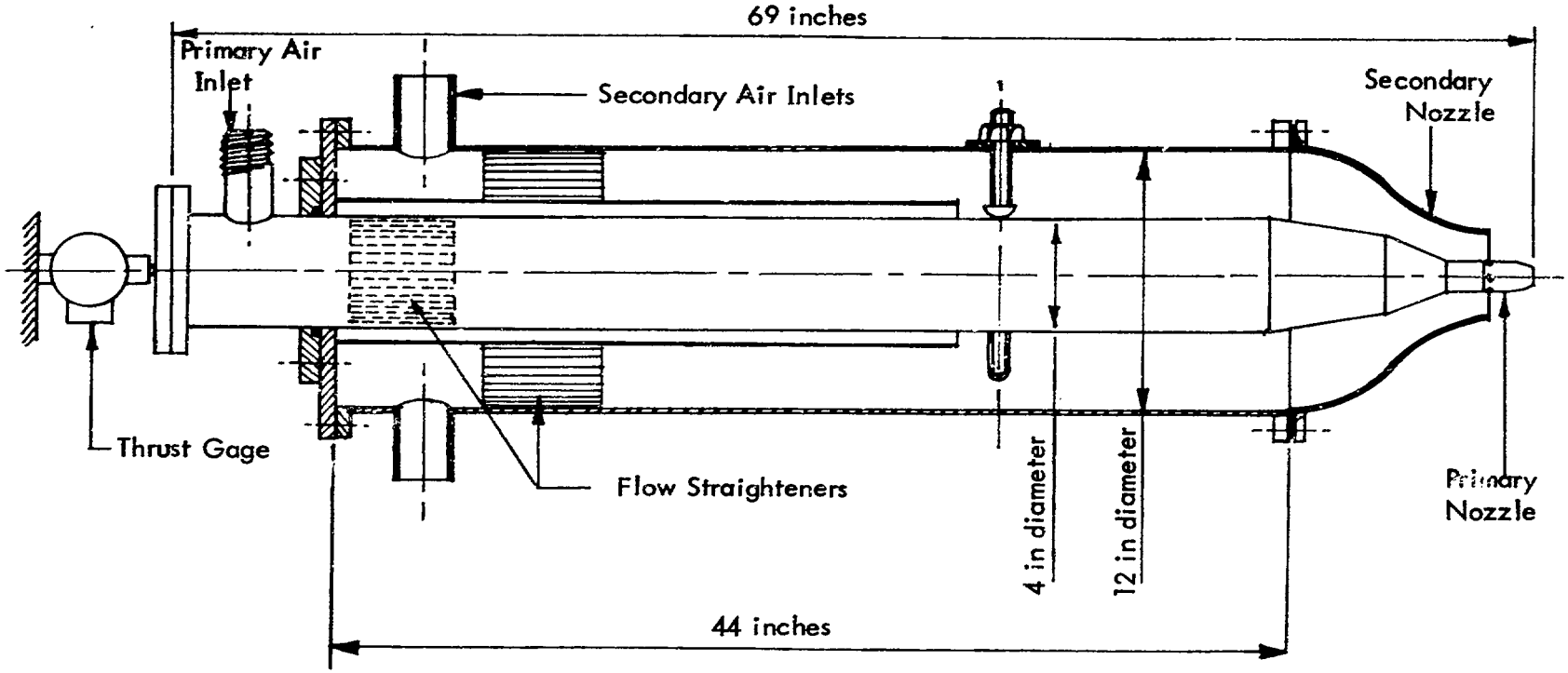

Figure 22. The Jet Flow Assembly.

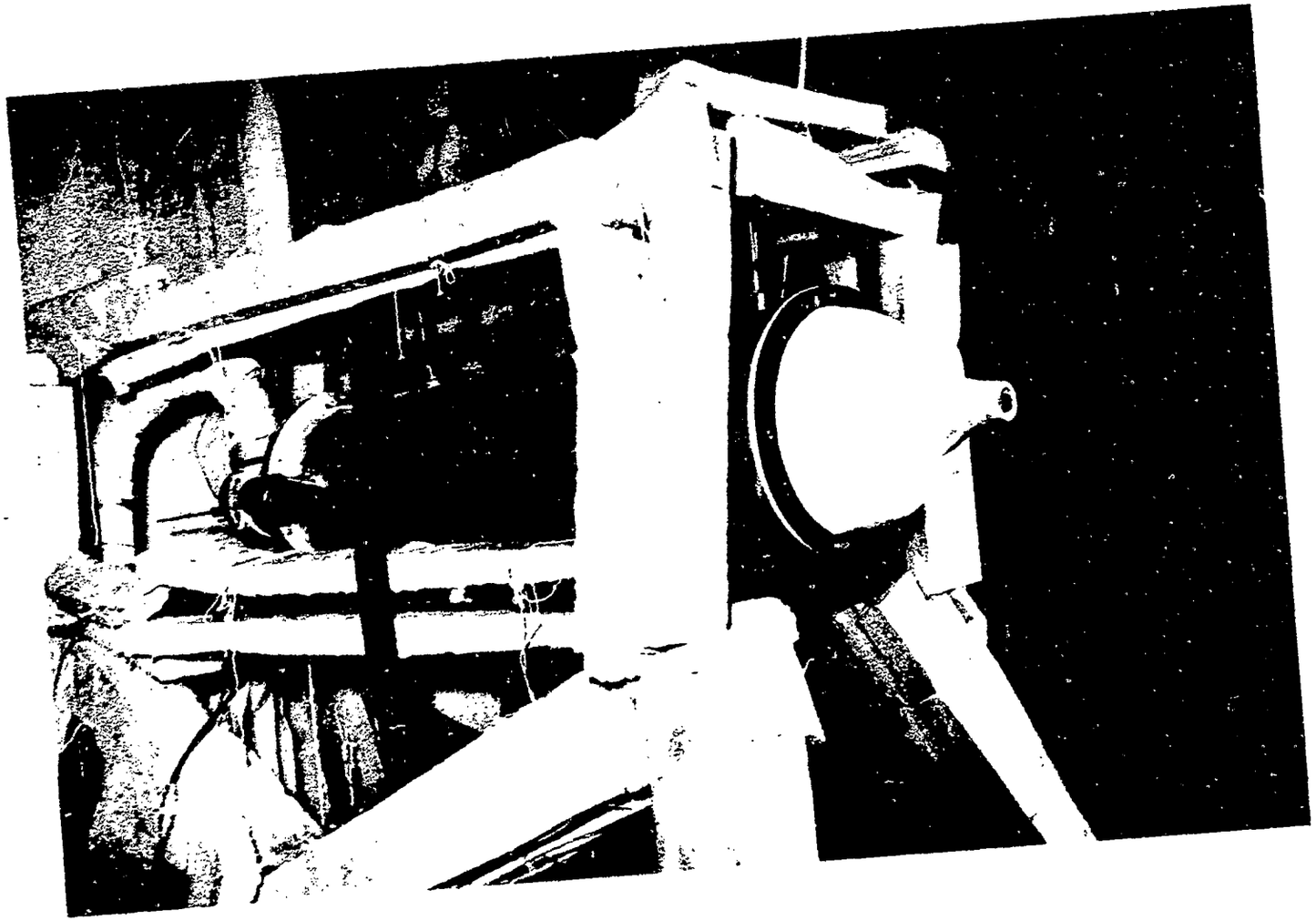

Figure 23. Photograph of Jet Flow Assembly

The complete coaxial system was supplied with air through flexible pipes and was suspended in a framework by wire ropes. The ends of the wire ropes were connected via universal joints to runners extending the length of the framework. The thrust of the operating jets was applied to a thrust gage mounted on the framework at the rear of the jet assembly. To ensure that no gap existed between the jet assembly and the thrust gage, and to bring the latter into the linear part of its operating range, a pre-load was applied to the gage. This was accomplished by securing a known weight to a cable running over a pulley attached to the rear of the jet rig support structure. The entire framework was covered with fiber glass to prevent acoustic reflections.

3.2.2 Jet Nozzles.

Three primary nozzles and four secondary nozzles, illustrated in Figures 24 and 25, were fabricated for these experiments. Figure 24 also shows the primary nozzle extension lengths. The primary nozzles were designed for pressure ratios of 1.6, 2.5 and 3.5. The internal exit diameters of each nozzle were as follows:

- Pressure ratio 1.6: Exit diameter 0.7495 inches
- Pressure ratio 2.5: Exit diameter 0.7457 inches
- Pressure ratio 3.5: Exit diameter 0.7533 inches

The external diameter of the primary nozzles was one inch, except for the last half-inch near the nozzle exit which tapered from one inch diameter to 0.8 inch at the exit plane. These nozzles were constructed of stainless steel to withstand the high primary flow temperatures.

The four secondary nozzles had internal exit diameters as follows:

- Nozzle No. 1: 1.288 inches
- Nozzle No. 2: 1.491 inches
- Nozzle No. 3: 1.955 inches
- Nozzle No. 4: 2.567 inches

These were manufactured from resin-bonded fiber glass. The actual ratio of the secondary nozzle flow area to primary nozzle exit area can be calculated from the above dimensions. In practice, the formation of boundary layers resulted in effective flow areas somewhat less than the theoretical. The effective flow areas were calculated from a knowledge of the experimentally determined mass flows through the nozzles and their pressure ratios for a velocity ratio of one.

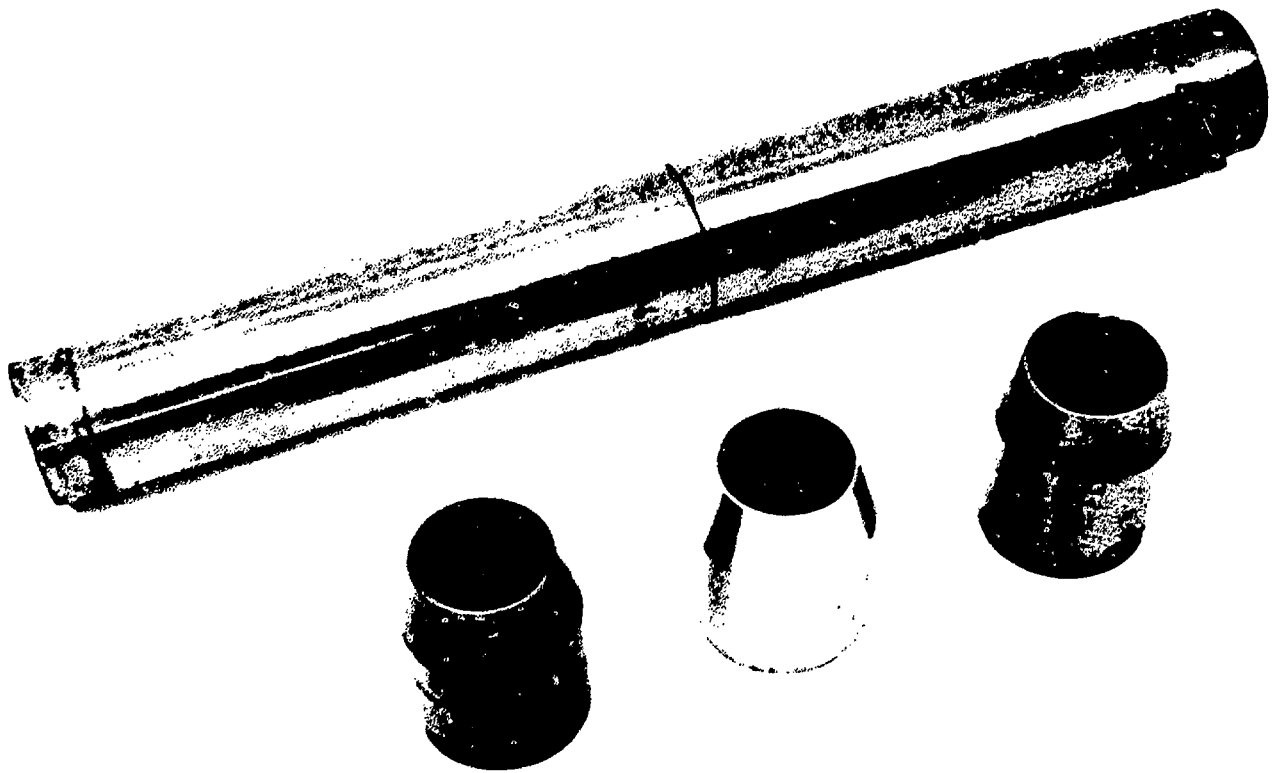

Figure 24. Primary Nozzles and Nozzle Extension Pieces.

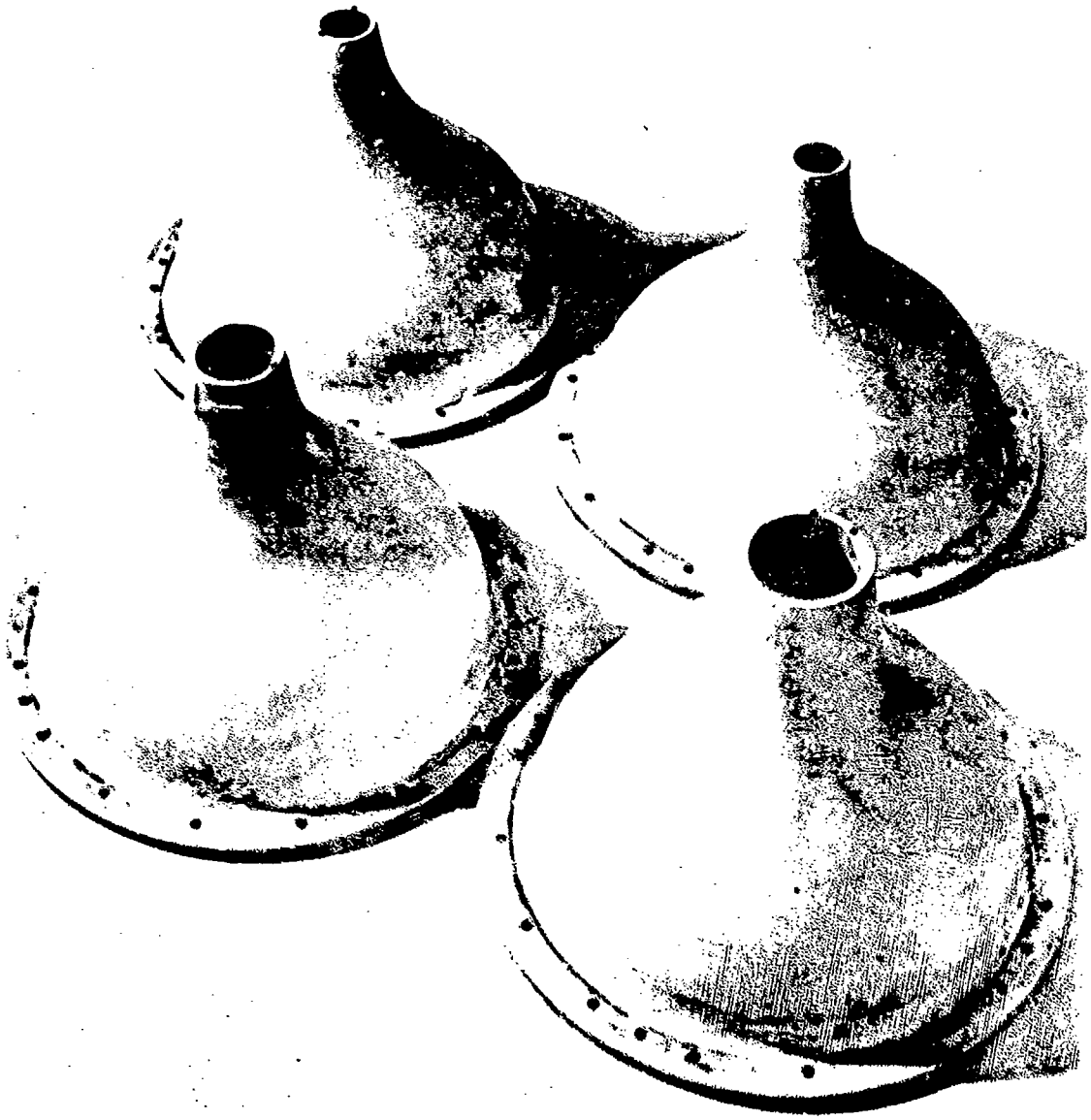

Figure 25. The Four Secondary Nozzles.

The nominal and effective area ratios for the four secondary nozzles are:

		(For Velocity Ratio of One)		
	Nominal	Effective Coplanar	1/2 Extended	Fully Extended
• Nozzle No. 1:	1	1.21	1.00	1.00
• Nozzle No. 2:	2	2.39	2.02	1.95
• Nozzle No. 3:	5	5.23	4.98	4.99
• Nozzle No. 4:	10	10.50	9.76	10.00

These values apply only for the condition when the secondary flow velocity approximated that of the primary. When the velocities were different, there were small variations in the effective area. For all conditions, however, the effective areas of the primary nozzles were within one percent of 0.00287 sq. ft., indicating a nozzle coefficient of approximately 94 percent.

3.2.3 Air Supply.

The air supplies for the primary and secondary nozzles were obtained from three 2-stage reciprocating air compressors with combined mass flow rates of 275 lbs per minute and with delivery pressures in the range 125 psig to 255 psig. A booster compressor was also available to increase the pressure from the compressors, with the lower delivery pressure up to a maximum of 300 psig.

The primary air supply was heated by a gas-fired heat exchanger capable of supplying 550,000 Btu per hour. With the air flows involved in this program and the length of line to the jet rig, the maximum static temperature attainable at the primary nozzles was approximately 900°F; this was attainable only for certain air flow rates. As a result, a primary flow temperature of 800°F was used for the majority of the hottest runs. Provision also was made in the air supply system for the mixing of cold air with the hot primary flow in order to achieve precise temperature control.

The mass flow of air to both primary and secondary nozzles was determined from the pressure drop across the orifice, which was measured by a mercury or red-oil manometer. The supply line air pressures upstream of the flow measuring orifices and in the settling chambers of the primary and secondary nozzles were measured by Ashcroft dial pressure gages, Models 1082A or 1279A, which have an accuracy of better than 0.5 percent. The flow temperatures upstream of the flow orifice and in the nozzle settling chambers were measured with thermocouple probes and recorded on a standard temperature recorder.

3.2.4 Jet Traversing Mechanism.

To investigate the jet velocity and temperature profiles (particularly for the purpose of checking the nozzle flows), three probes were traversed across the jet flow (Appendix B). To accomplish these traverses, the probes were mounted on a carriage which was driven across the jet axis by a leadscrew. The leadscrew, in turn, was driven by a variable-speed electric motor via a speed reducer. The shaft of a multi-turn potentiometer was coupled to the leadscrew, the potentiometer being supplied with direct current from a stabilized power supply. When the wiper of the potentiometer was connected to a chart recorder, the position of the probes across the jet was indicated as a chart pen deflection.

3.2.5 Anechoic Room.

The anechoic room used for the experiments was cylindrical in shape, approximately 30 feet in diameter and 21 feet high. To minimize acoustical background noise levels, the walls of the room were of high transmission loss construction. The lower section of the walls was constructed of cinder blocks, the courses filled with reinforced concrete and plastered on both sides, to a total wall thickness of 9 inches. The upper wall section was of staggered stud, wood frame construction, composed of the following layers (from interior to exterior wall surfaces):

- 1/2-inch gypsum wall board
- 1/2-inch wood fiber sound deadening board
- An air space of 5-1/2 inches
- 1-inch particle board mounted on the outer studs

Access to the room was via triple, solid-core doors separated by air spaces.

The basic anechoic treatment of the room was a curtain wall of 4-inch thick fiber glass spaced 6 to 10 inches from the interior wall surface. The floor of the room was treated in a similar fashion, and the suspended ceiling also consisted of a 4-inch layer of fiber glass. The basic acoustical treatment was supplemented by additional low frequency absorption in the form of wedges that were located in patches around the wall-floor perimeter.

The model jets used for the experiments were exhausted through a muffler to the external atmosphere. The muffler was designed to preserve the acoustical integrity of the anechoic room and consisted of a bent duct approximately 12 feet long and 4 feet square. The duct was lined with 4 inches of fiber glass spaced 4 inches from the interior walls. A fiber glass splitter vane divided the duct cross-section in half, over a longitudinal distance of 4 feet, to increase the high frequency absorption of the duct.

The suitability of the room for acoustic measurements such as were undertaken in this program is illustrated in Figure 26. These data show that the octave band acoustic levels in the room follow the inverse square law over the frequency band width and angular positions used for the measurement program.

3.3 Instrumentation

3.3.1 Acoustical Data Acquisition System.

The noise produced by the jets was measured by the system shown in Figure 27. This system consisted of a microphone mounted on a boom which slowly traversed a segment of a circle of radius 10.67 feet centered on the secondary nozzle. The segment ranged between 15 and 115 degrees from the jet axis. The microphone was a Bruel and Kjaer (B & K) half-inch plane wave condenser microphone, Type 4133, aligned to present the diaphragm at normal incidence to the noise from the jet. The microphone output was amplified by a B & K amplifier, Type 2603, and the amplified output fed to a B & K level recorder, Type 2305, and an Ampex two-track tape recorder. The system was calibrated using a B & K pistonphone, Type 4220. The system gain was increased as necessary to bring the signal level up toward the desired recording level (i.e., about 15 dB below the peak overload point). These gains were carefully noted for each run. The tape recordings were made at a tape speed of 15 inches per second to allow frequencies up to and including the 31.5 kHz octave band to be recorded.

The microphone traverse mechanism contained a microswitch trip mechanism which was actuated at 5-degree intervals (starting at 15 degrees from the jet axis). These 5-degree invervals were marked on the level recorder trace, using the event marker, and used to interrupt a 1 kHz tone which was then recorded on the second channel of the tape recorder. This provided a synchronized index signal of microphone position on the tape recording.

3.3.2 Acoustical Data Analysis System.

The on-line recordings of the jet noise were analyzed at a later date by the system shown in Figure 28. The first channel of the tape recorder contained the recorded jet noise. This was fed, via an attenuator and amplifier to a B & K level recorder and a Wyle analog-to-digital octave band analyzer. The 1000 Hz signal on the second channel of the tape recorder indicated the position of the microphone-traversing boom at 5-degree angular increments. This signal operated through a simple relay device to trigger the octave band digital analyzer and to indicate the angular positions on the event marker of the level recorder.

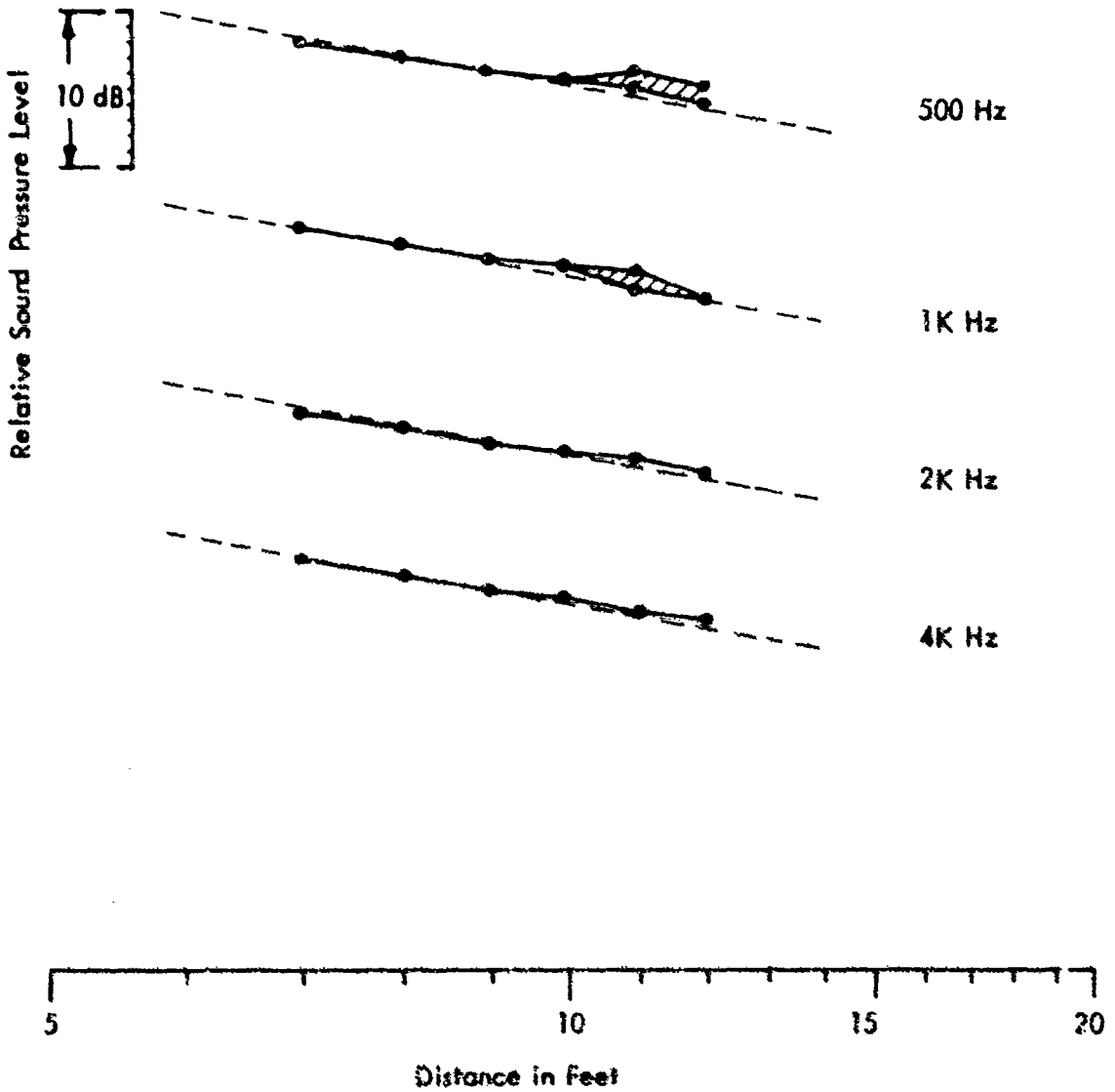

Figure 26. Inverse Square Law Measurements in the Anechoic Room Using Full Octave Bands of Random Noise. The broken lines indicate a slope of 6 dB per doubling of distance. The hatched area indicates the level variation found over a 120-degree sweep of the microphone boom.

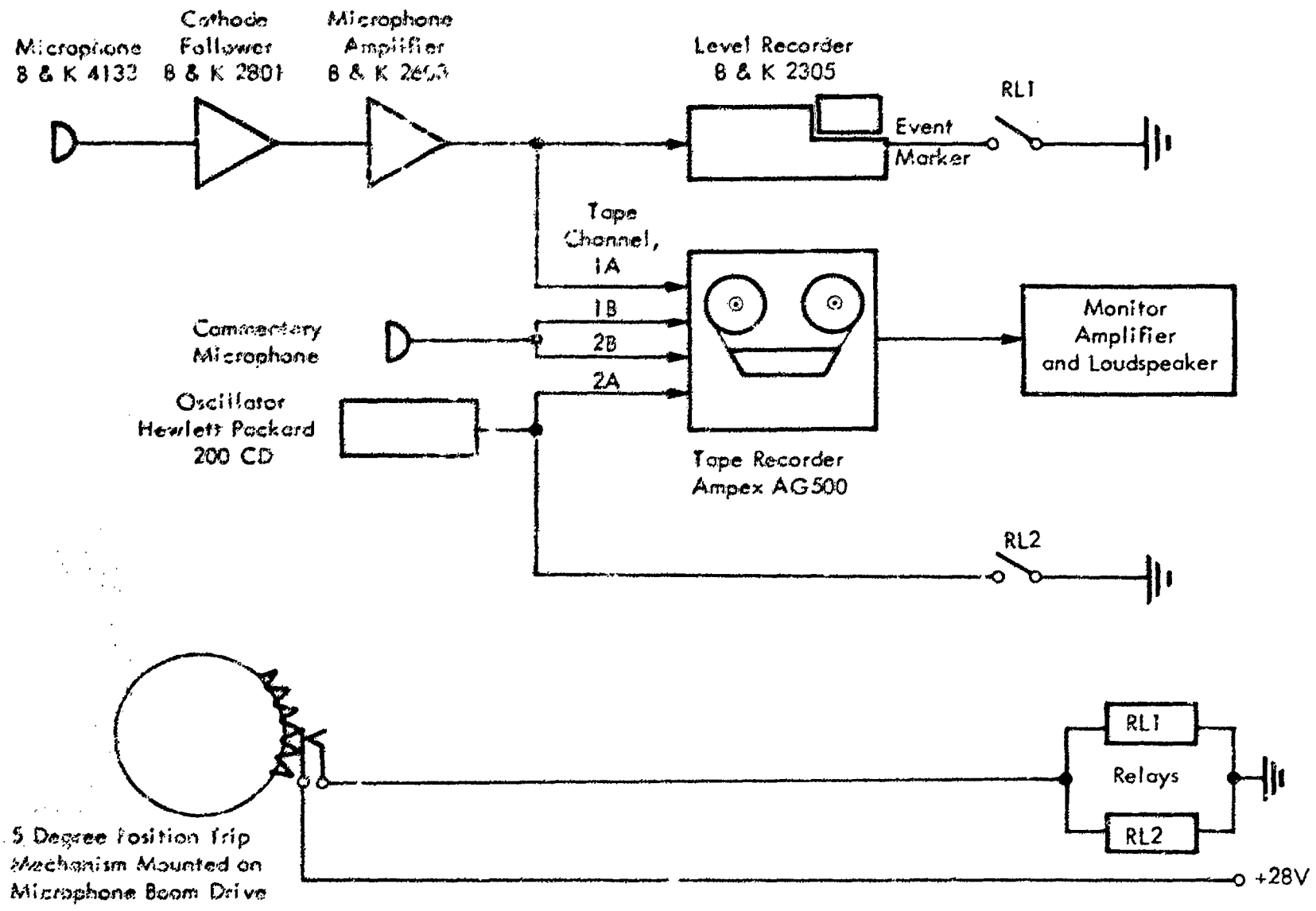

Figure 27. Block Diagram of Acoustic Data Acquisition System.

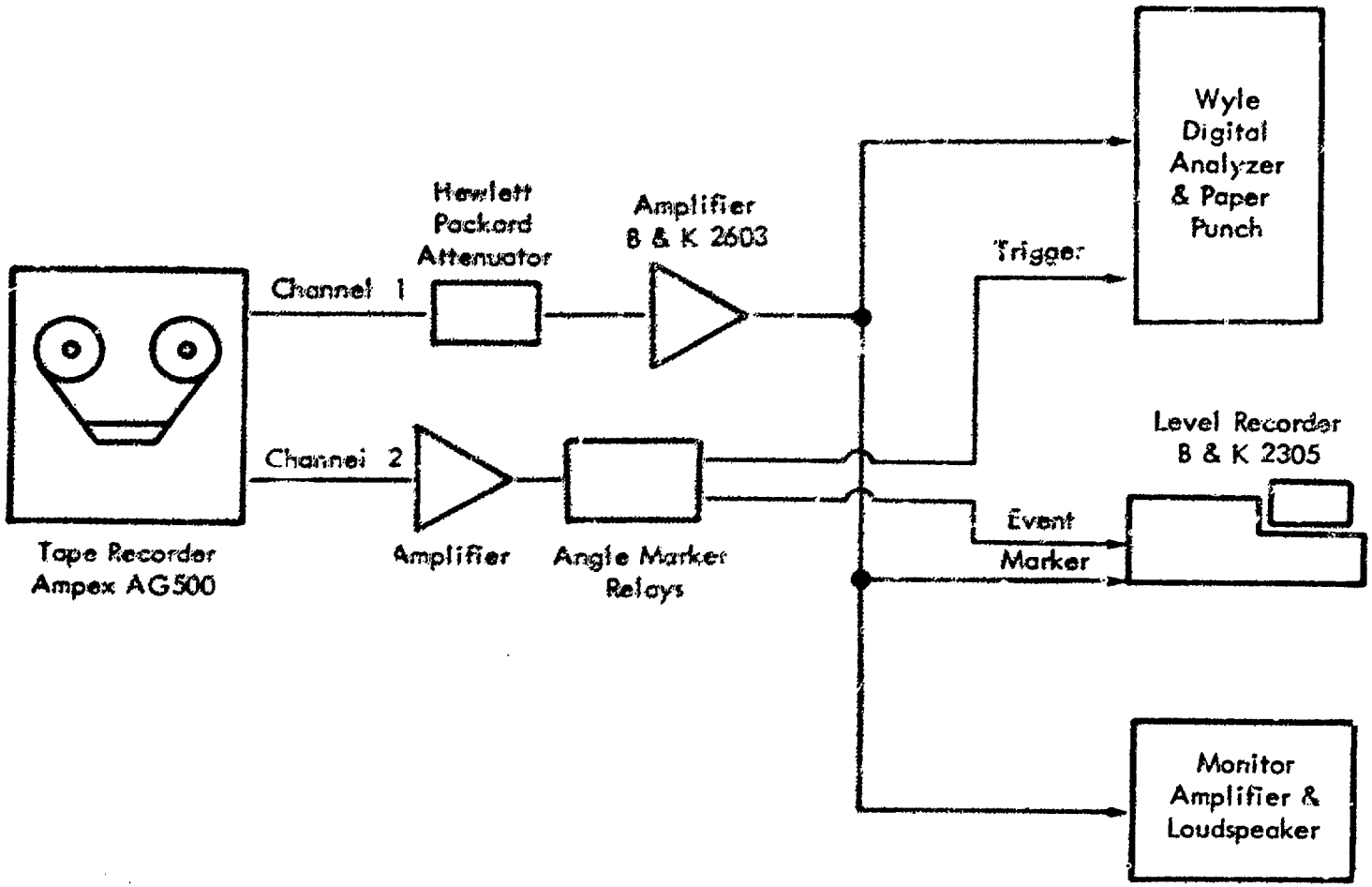

Figure 28. Block Diagram of Acoustic Data Analysis System.

The recorded signal was fed from the tape recorder through an attenuator and a booster amplifier to the digital analyzer which contains a set of parallel B & K octave band filters with center frequencies ranging from 63 Hz to 31.5 kHz. The filter outputs were then converted to dc levels, digitized and punched sequentially on a standard 8-hole ASCII paper tape punch as a 3-digit number. The value punched is proportional to the input voltage, i.e., it is linear, not logarithmic. Additional punching included the overall level, a reference level derived from a separate input, and a run number which was set by thumb switches on the analyzer. For this experiment, the reference signal and the lowest three octave bands were not used. Suitable line feed, carriage return and spacing characters were included on the paper tape so that the data could be printed in a legible tabular form by a teletype machine. The paper tape punch could be triggered either manually or by a separate triggering input.

Calibration of the system was undertaken using the 124 dB acoustic calibration signal recorded directly on the data magnetic tape prior to each run. The digital analyzer was adjusted so that 124 dB gave a maximum paper tape punch count of 999. A preliminary analysis of the overall sound pressure level was then made using only the level recorder with the same gain setting as was used when the recordings were made. The gain was then increased so that the maximum octave band level would register near 999 counts, obtaining the maximum dynamic range of the digital analyzer. For compatibility, the overall output channel was attenuated by 5 dB to insure that it would not overflow the counter. These gains and the original recorded 124 dB calibration signal were utilized to calculate a calibration factor in millivolts/dyne/cm for use in computer decoding of the digital tape.

Systems such as that described above for data acquisition and analysis do not have a completely flat response over the frequency range of interest for this project. Therefore careful calibrations were made to determine the octave band corrections that had to be applied to the final octave band analysis produced by the paper tape punch. These calibrations indicated that the following corrections had to be added:

Octave Band Center Frequency (kHz)	0.5	1	2	4	8	16	31.5	Overall
Correction (dB)	0	0.5	1.5	1.0	2.0	3.0	4.5	6.0

The overall correction factor accounts for the 5 dB added in the digital analysis as well as an approximate correction for the octave band correction factors. This latter correction obviously will be a function of spectrum shape and therefore is not an exact correction. Hence, whenever calculations were made on the octave band figures (as in the computer program to be described later), the overall value was calculated from the sum of the octave band levels.

3.3.3 Thrust Measurement.

The thrust of the model jets was measured by suspending the whole jet assembly (as shown in Figure 22) from a supporting frame so that it acted as a parallel pendulum. The assembly was then made to react against a force gage of the proving-ring type. This gage was manufactured by Wiancko Engineering Company (thrust gage, Type F1021). It utilized a differential transformer excited by a carrier signal to measure thrusts in the range zero to 100 lbs. The gage was pretensioned by a constant 5-lb load to eliminate initial non-linearity at the low end of the thrust range. Calibration was achieved by adding extra known weights to the preload system.

3.3.4 Jet Profile Measurements.

To investigate the velocity and temperature profiles of the jets, three probes were traversed sequentially across the jet flow. The three probes were modified types manufactured by United Sensor Control Corporation, Watertown, Massachusetts. The modifications consisted of stiffening the probes so that they would not vibrate in the jet. The three probes were:

- Total pressure probe, Type PT, 1/16-inch diameter
- Static pressure probe, Type PS, 1/16-inch diameter
- Total temperature probe, Type TC, 1/8-inch diameter

The probe pressures were converted to electrical signals by the use of carrier-type pressure transducers, the outputs of which were recorded on a multiple-channel strip chart recorder. The total pressure probe was used in conjunction with a 0-100 psig Statham pressure transducer, Type PG7317C-100-350, while the static pressure probe used a Statham ±5 psig pressure transducer, Type P60aTC ±5D-350. Both transducers used Sanborn carrier preamplifiers, Model 150-1100AS. The total temperature probe was connected, via a reference junction contained in an ice bath, to the input of a Sanborn stabilized dc preamplifier, Model 150-1800.

The pressure transducers and associated instrumentation were calibrated as systems by the introduction of known reference pressures at the transducers, the gains of the amplifiers then being adjusted to calibrate the chart records. The reference pressures at the transducers were measured by means of mercury manometers. The total temperature probe system was calibrated by the insertion of known voltages into the associated preamplifier, together with amplifier gain adjustment, to calibrate the chart records.

The insert voltages were derived from standard tables of the generated electromotive forces of Chromel-Alumel thermocouples at different temperatures. The probe calibration was checked periodically at two fixed temperature points by inserting the probe alternately into a melting ice bath and into boiling water.

3.3.5 Discrete Tones and the Resulting Hardware Modifications.

With very few exceptions, full-scale jet engine exhausts produce random noise without discrete tones. However, discrete tones are sometimes produced by model-scale jets. Because of this and the fact that occurrence of discrete tones would invalidate the data, all runs were monitored aurally, via a loudspeaker amplifier system connected to a microphone in the test room. The discrete tones thus encountered and the hardware modifications required to eliminate them will now be described.

The first discrete tone was encountered during one of the equipment-checkout runs, under the following conditions. The primary nozzle (design pressure ratio (R) = 3.5) and secondary nozzle No. 2 were installed in the coplanar position, but with no flow through the primary nozzle. As the secondary supply pressure was gradually brought forward (through the range to sonic secondary flow at 13.0 psig), the following sounds were observed. A pure tone was first heard at 4.7 psig; it gradually grew more intense until 6 psig was reached, remaining present at apparently constant intensity thereafter. Between 6 psig and 13.0 psig, several sudden jumps in pitch were observed as the pressure was increased. It was found that the tone could be completely "turned off" at will by placing a fingertip (or screwdriver) very slightly into the flow at the exit plane at any point on the periphery. Stopping the tone apparently depends upon destroying the perfect circularity of the nozzle exit by the very slightest amount. From this observation, plus the previously described jumps in pitch, it was concluded that the phenomenon observed was probably a ring tone which is known to depend on an acoustic feedback mechanism.

An experiment was made to determine whether a small button-shaped spoiler (washer) could be added at the periphery of the secondary nozzle without adding measurably to the random noise generation. Using the same conditions as Run No. 109, where there were no discretes present, a comparison was made of the overall noise (in a 120-degree sweep about the jet) with and without the spoiler, via on-line level recorder trace. There was no measurable difference. This test was followed by octave band sweeps (from the 125 Hz band through the 31.5 kHz band) using tape-recorded data. Again, with flow conditions set and held constant through the pair of tests, there was no measurable difference. Hence, it was concluded that the addition of the spoiler did not generate any measurable amount of additional random noise, and the spoiler was kept in place on secondary nozzle No. 2 during all subsequent production runs.

The second discrete tone was encountered during Run No. 125; by a process of elimination, it was found that the tone was being produced by the primary nozzle and occurred even when the secondary nozzle was removed. It was found that the tone or whistle disappeared if the operating pressure ratio was reduced from the design value of 2.5 to 2.45. This was confirmed by one-third octave band traces. Large, spatially-dependent spikes in several third-octave bands occurred during microphone sweeps when the audible whistle was present; these spikes disappeared when the whistle disappeared.

In later runs, it was found that this whistle (with this primary nozzle, and also with the high supersonic primary nozzle, R = 3.5) returned and could not be removed by slight alterations of the supply pressure. At this point, it was decided that these two primary nozzles would have to be modified slightly by adding a small brazing bead to the inner edge of the exit. This succeeded in eliminating the pure tone or whistle, again borne out by one-third octave band sweeps. The presence of the brazing beads did not add any measurable random noise, as determined from comparisons of level recorder traces in those third-octave bands in which tones were absent during occurrence of the whistle. All subsequent runs were made with these brazing beads affixed.

3.4 Analytical Basis for Data Reduction Computer Program

Upon completion of the model jet experiments, the acoustic data were in the form of octave band sound levels encoded as a series of 3-digit numbers. A computer program was therefore written to convert this data to model jet sound pressure levels in decibels relative to 2×10^{-4} dynes per square centimeter, and to scale these levels to the values for full-scale jet engines. Figure 29 indicates the calculations made by the computer program and the order in which they are carried out. The details of these calculations are given in this section. A description and listing of the computer program is given in Appendix C.

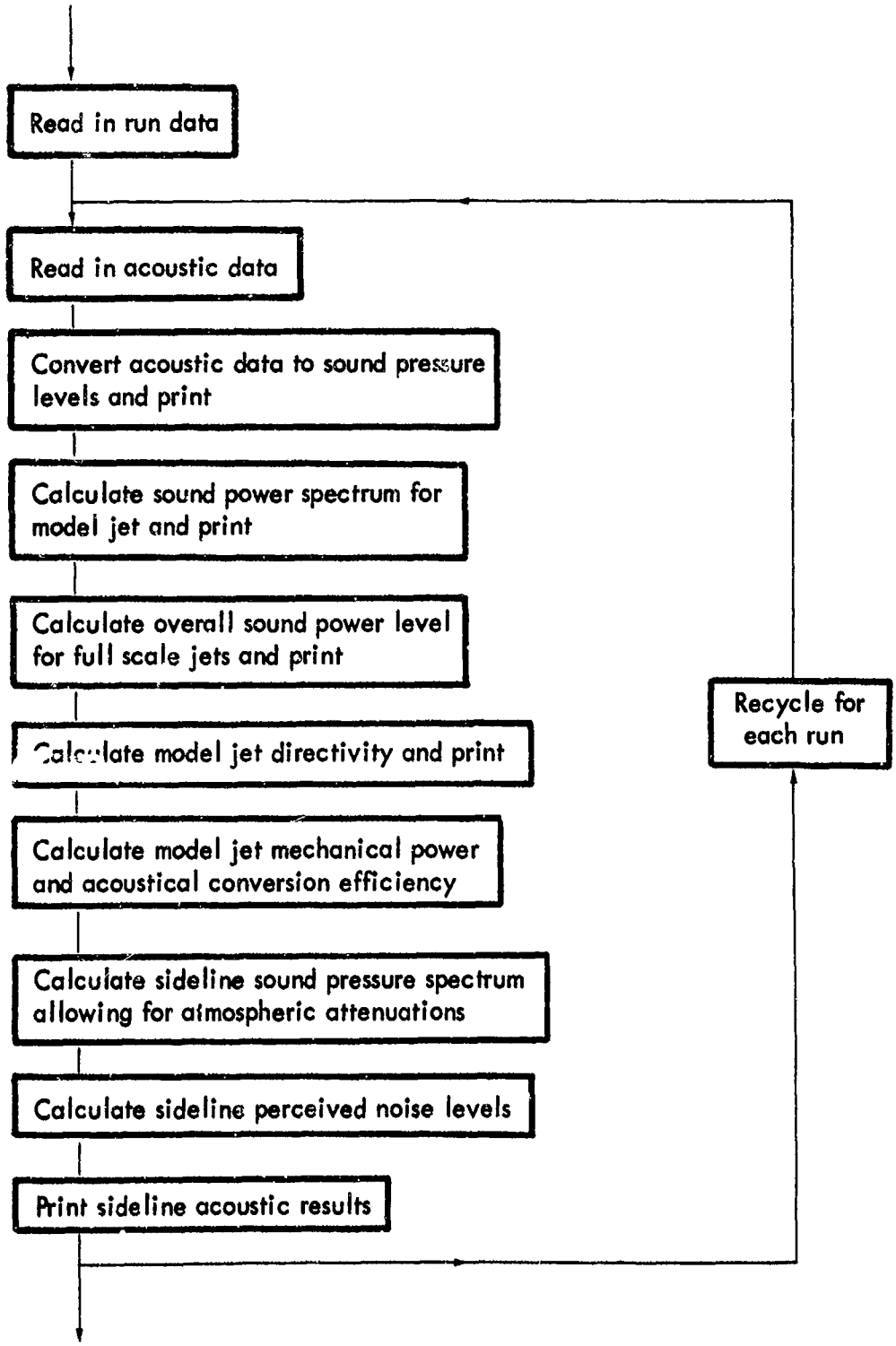

Figure 29. The Functional Flow Loop for the Computer Program.

3.4.1 Flow Velocities and Thrust.

During each model jet run, measurements were made of the primary and secondary mass flows and static (reservoir) temperature and pressure. These values were used to calculate the primary and secondary flow velocities. From Reference 31, the flow Mach number, M, as a function of the total pressure ratio, R, across the nozzle is given by:

$$M = \left[5\ (R^{.2857} - 1)\right]^{0.5} \tag{19}$$

and the nozzle flow temperature, T, is related to the total temperature, T_t, by:

$$T = T_t\ (1 + M^2/5)^{-1} \tag{20}$$

This temperature can then be used to determine the speed of sound, a, in the flow (assuming standard conditions of a_o = 1120 feet per second at 519°R). Thus:

$$a = a_o\ (T/T_o)^{1/2} \tag{21}$$

so that the nozzle velocity, U, is given by the product of the Mach number and the speed of sound:

$$U = Ma \tag{22}$$

Although the thrust of the model jets was measured during each run, it was found that there were some inconsistencies in the measurements of the early runs due to instrumentation-drift problems. These problems were overcome in the latter runs but in order to maintain consistency, the thrusts, F, were also calculated using the measured primary and secondary mass flows (m_p, m_s) and the calculated velocities (U_p, U_s). Thus:

$$F = \frac{m_p\ U_p + m_s\ U_s}{g} \tag{23}$$

A check was made between the calculated and measured values and the agreement found to be very good for all the latter run numbers. Therefore, calculated thrust values have been used for all subsequent analyses for these runs.

However, these equations must be modified for the runs in which the primary nozzle was retracted. The actual velocity, U_p', at the exit of the retracted primary is determined by the ratio of the primary nozzle pressure to the secondary nozzle pressure. The secondary flow is augmented by the mixing between the primary and secondary flows upstream of the secondary nozzle exit, and its velocity is a function of position across the nozzle. The flow velocity ratios tabulated for these retracted cases are U_s/U_p', where U_s is calculated for an ideal convergent nozzle, as previously. Also, the measured values of the thrusts were used for scaling and tabulation, since the calculated values are somewhat indeterminate because of the flow interaction. However, they were reasonably bounded by the minimum and maximum expected values given by:

$$\frac{m_p U_p' + m_s U_s}{g} \leq F \leq \frac{m_p U_p + m_s U_s}{g} \tag{24}$$

where prime indicates conditions at the exit plane of the retracted primary nozzle.

3.4.2 Sound Pressure Levels.

The measured acoustic pressure, p, was calculated from the product of the calibration factor (see Section 3.3.2) and the encoded 3-digit number. The sound pressure level (SPL) was then determined using:

$$SPL = 20 \log p + 74, \text{ dB re } 2 \times 10^{-4} \text{ dynes/cm}^2 \tag{25}$$

and the relevant octave band correction factors added (see Section 3.3.2). Since these correction factors are frequency-dependent, the correction factor for the overall level is dependent on spectrum shape. It is therefore not practical to calculate an overall level correction factor, so the measured overall level was replaced by the overall level computed from the sum of the octave band levels.

3.4.3 Sound Power Levels.

Since the acoustic data was taken in an anechoic room, the sound power radiated by the jets can be determined by integrating the acoustic intensity, I, over the surface of a sphere centered on the jet. The acoustic data was taken at 5-degree intervals. The sound pressure, p_i, measured at an angular position θ_i from the jet axis was therefore assumed to be representative of the sound pressure over an area A_i such that:

$$A_i = 2\pi r^2 (\cos(\theta_i - 2.5^\circ) - \cos(\theta_i + 2.5^\circ)) \tag{26}$$

This is the area of a strip of the spherical surface (radius r) centered on the jet axis at the plane of the secondary nozzle exit. The strip subtends an angle of 2.5 degrees either side of the measurement position θ_i and extends all the way around the jet axis. The sound was measured at 21 angular positions ranging from $\theta_1 = 15^\circ$ to $\theta_{21} = 115^\circ$; so the sound power, W, radiated is:

$$W = \sum_{i=1}^{21} (p_i^2 A_i/\rho a) \tag{27}$$

This summation was made for each octave band and the overall sound power calculated by summing the octave band powers. The octave band and overall sound power levels (PWL) were then determined as:

$$PWL = 10 \log W + 130, \text{ dB re } 10^{-13} \text{ watts} \tag{28}$$

The value of the characteristic acoustic impedance (ρa) used in the calculation was 41.5 cgs rayls at a pressure of 29.92 inches of mercury and absolute temperature of 519°R. The impedance was corrected for the ambient temperature, T_a, and pressure, P_a, measured for each run, so that the value of acoustic impedance used in Equation (27) was:

$$\rho a = 41.5\ (P_a/29.92)\ (519/T_a)^{0.5} \text{ cgs rayls} \tag{29}$$

The radius, r, at which the sound measurements were made was measured in feet, so area A_i from Equation (26) is in square feet. If the acoustic pressure, P_i, is in dynes per square centimeter, the dimensional constant required in Equation (27) is 9.29×10^{-5} so that it should read:

$$W = 9.29 \times 10^{-5} \sum_{i=1}^{21} p_i^2 A_i/\rho a, \text{ watts} \tag{30}$$

The above calculations have been limited to the acoustic power produced by the model jet. Each model jet has a different thrust, so for comparison it is convenient to scale the overall sound power produced by the model jet, PWL_m, with thrust F_m to give the sound power produced by an engine with a standard thrust, F_S. This requires the scaling of the model jet by scaling the nozzle exit area, which is directly proportional to thrust, since the flow characteristics of the model and scaled jets are the same.

The scaled power level, PWL_S, is therefore given by:

$$PWL_S = PWL_m + 10 \log (F_S/F_m) \tag{31}$$

Throughout the computer program, four standard thrusts with values of 10,000 pounds, 20,000 pounds, 40,000 pounds and 80,000 pounds were used.

3.4.4 Directivity Patterns.

Having calculated the model power spectra, the directivity index, DI, can be found using the expression:

$$DI = SPL - PWL + 20 \log r + 10.5 - 10 \log \rho a/41.5 \tag{32}$$

In this expression, SPL is the measured octave band sound pressure level at distance r (in feet) from the jet and PWL is the measured octave band power level. The constant in Equation (32) assumes a reference sound power of 10^{-13} watts and a reference sound pressure of 2×10^{-4} dynes per square centimeter.

At this point in the computer program, an indication is given of the level of the noise floor relative to the zero level on the directivity. This is a function of the calibration factor for the sound pressure measurements, and was provided as a system check.

3.4.5 Acoustic Conversion Efficiency.

The ratio of the acoustic power, W, produced by the jet to the mechanical power in the jet, E, is one additional measure of the acoustic performance of the jet. The mechanical power in watts is given by:

$$E = 0.0211 \, (m_p U_p^2 + m_s U_s^2) \tag{33}$$

when the primary and secondary mass flows (m_p, m_s) are in units of pounds per second and the velocities (U_p, U_s) in feet per second. Using the acoustic power, W, determined earlier, the acoustic efficiency, η, is given as:

$$\eta = W/E \tag{34}$$

3.4.6 Sideline Sound Pressure Levels for Full-Scale Engines.

The scaling of the model acoustic data to give the sound pressure levels on a sideline parallel to the jet axis due to a full-scale engine requires the following operations on the model data:

- Determine scale factor to scale-model thrust to standard thrust.
- Shift model frequency to frequency of standard thrust nozzle by the inverse of the square root of the scale factor.
- Apply inverse square law appropriate for the desired distance.
- Apply atmospheric attenuation as appropriate.

In scaling the measured data to the equivalent values on a sideline, the physical situation is as shown in Figure 30. The data taken on the circular arc (radius r) must be scaled to lie on the sideline. The position of this sideline is characterized by the sideline distance L_d (see Figure 30). For the purposes of this project, two sideline distances of 500 feet and 1500 feet were chosen. The sound pressure measured on the model jet at coordinate (r, θ) is therefore scaled to the point (L, θ) on one of these sidelines. The sound pressure decreases by $20 \log (L/r)$ due to this change.

In order to scale the results to allow for a change of thrust, the engine thrust must be increased without altering any of the jet flow parameters. Thus, the scaling is done purely by changing the nozzle area. The thrust change is then directly proportional to the change in area. For the same flow velocity and density, the acoustic output is also proportional to area. Hence, if the thrust is scaled from a model thrust of F_m to a full-scale thrust of F_S, the sound pressure level at a fixed radius will change by $10 \log (F_S/F_m)$.

For this project, the full-scale thrusts (F_S) lie in the range 10,000 pounds to 80,000 pounds while the model jets had thrusts ranging from 6 pounds to 120 pounds. Similarly, for the 1500-foot sideline, the propagation distances range from 1500 feet to 6000 feet, compared to a model-jet measurement distance of 10.67 feet. For these values, the combined distance and thrust scaling correction varies over a range from -2 dB to -36 dB.

The atmospheric absorption data were taken from Reference 32. The data for a standard day with a temperature of 519°R and relative humidity of 70 percent were used and are plotted in Figure 31.

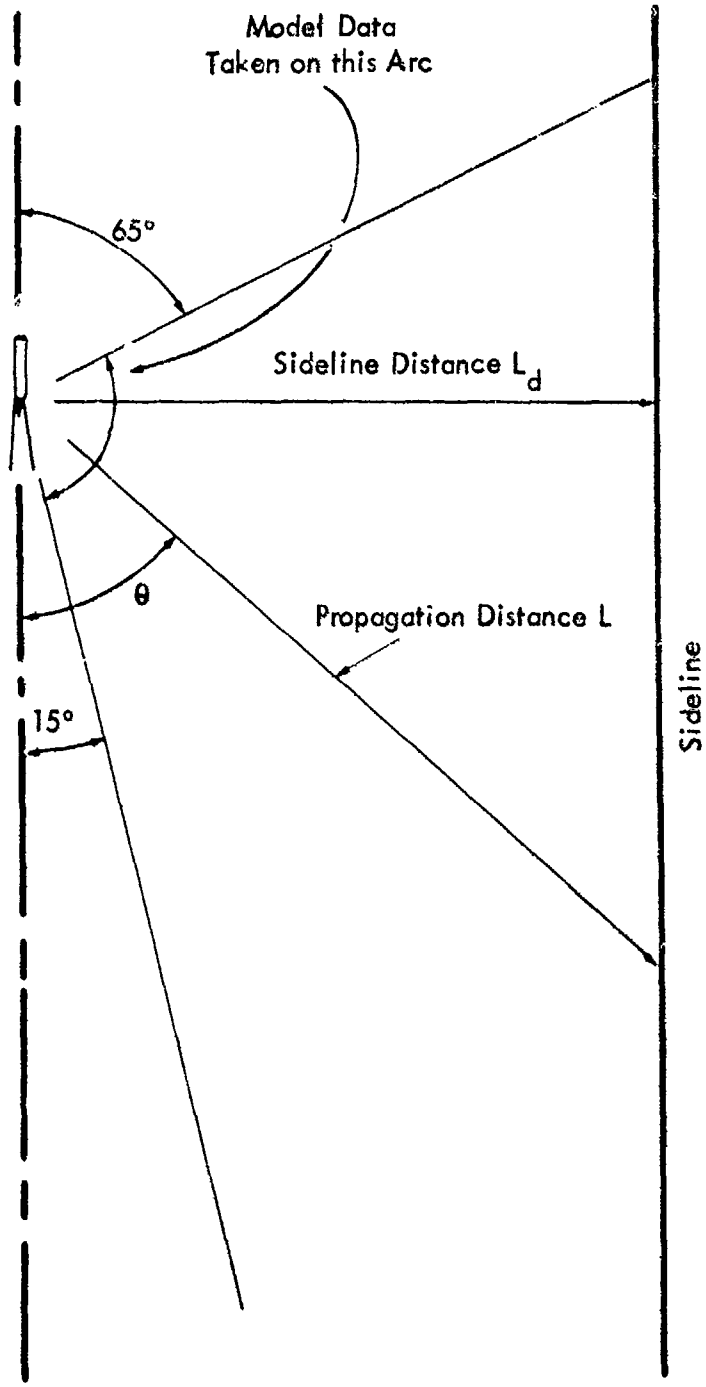

Figure 30. Geometry for Obtaining Sideline Sound Pressure Levels from Measured Data.

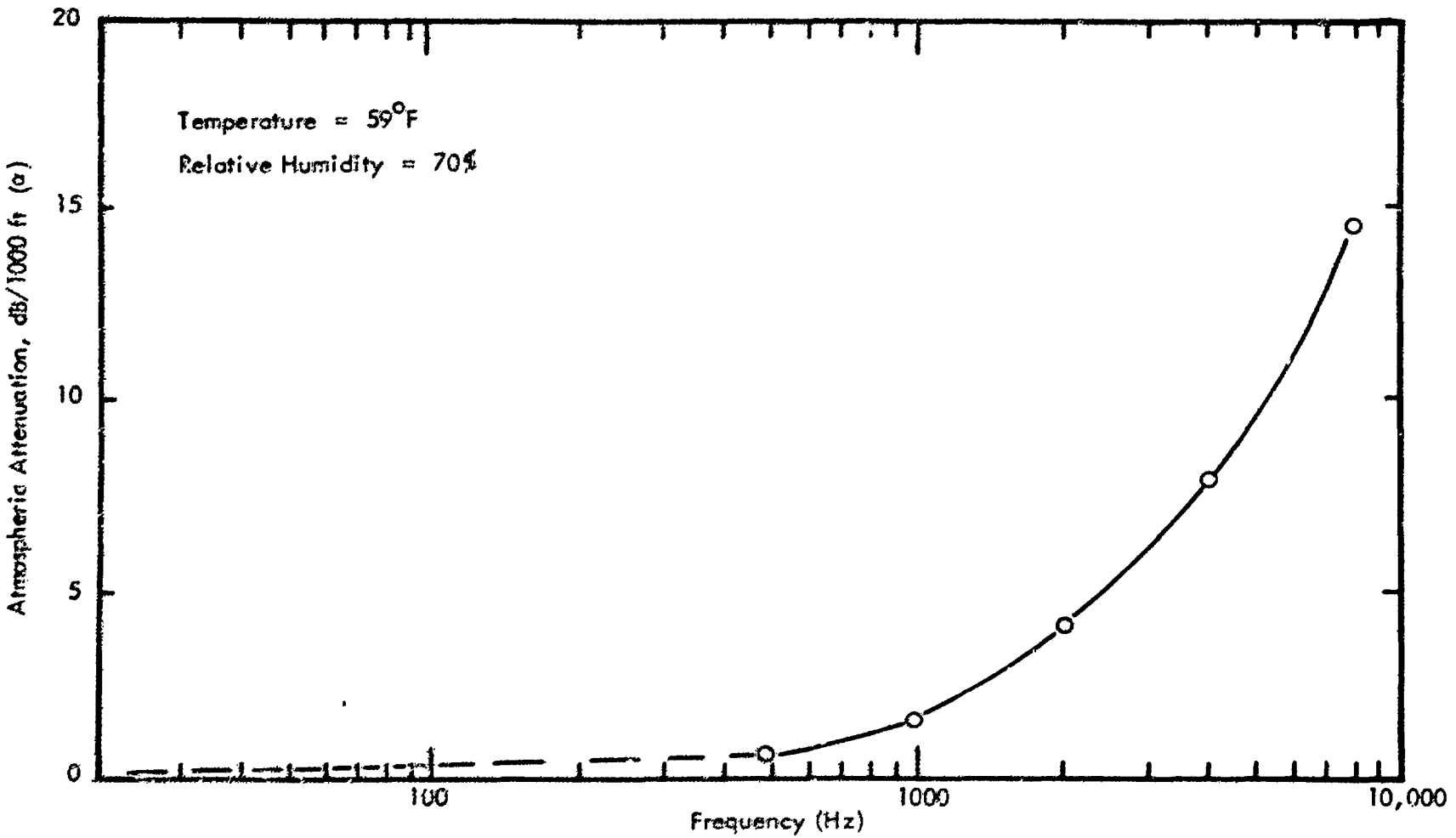

Figure 31. Atmospheric Attenuation Utilized to Compute Sideline Sound Pressure Level. (From Reference 32.)

For the computer program, it was desirable to fit a curve through the data points. This resulted in the following empirical equation for the absorption $\alpha(f_S)$ in dB per 1000 feet:

$$\alpha(f_S) = 10^{b(f_S)} \tag{35}$$

where

$b(f_S) = \alpha_o + \log(f_S/1000)(\alpha_1 + \alpha_2 \log(f_S/1000))$

f_S is the octave band center frequency for the full-scale engine

$\alpha_o = 0.127$

$\alpha_1 = 1.338$

$\alpha_2 = -0.207$

This expression was chosen solely for convenience in the computer analysis. It provided values for air absorption over the full-scale frequency range which were in substantial agreement with values computed by a more exact theoretical model for the measured data (Reference 33). Absorption corrections were not required for the model data because the distance from the model jet to the measured point was small.

Combining these factors, the total change from the model sound pressure level, SPL_m, to full-scale sound pressure level, SPL_S, is given by:

$$SPL_S = SPL_m + 10 \log(F_S/F_m) + 20 \log(r/L) - L\,\alpha(f_S)/1000 \tag{36}$$

The change in frequency accompanying this change in level is based on the use of a constant Strouhal number, S, before and after the scaling process. Thus:

$$S = fd/U = \text{constant} \tag{37}$$

where f is a frequency, d is a typical dimension of the jet, and U is a typical jet velocity. We have specified constant flow conditions in the scaling process. Hence, U is unaltered by the scaling. However, the area of the jet is altered in proportion to the thrust, so a typical linear dimension changes according to the square root of the thrust. Thus, if f_m is a typical frequency of the model jet, applying Equation (37) yields:

$$f_S = f_m (F_m/F_S)^{0.5} \tag{38}$$

This equation governs the frequency scaling and also is used to define the full-scale frequency used in Equation (35).

3.4.7 Perceived Noise Level.

Once the sideline octave band levels have been determined, the perceived noise levels can be calculated. The method used is specified in Reference 34, utilizing the equations given in Table II of that reference to calculate the Noy values. Under certain circumstances, the lowest and highest octave bands of sideline sound pressure fall outside the range of 50 Hz to 10 kHz covered by this reference. For octave band frequencies below 50 Hz, the Noy value was calculated as if the octave band frequency were 50 Hz. Frequencies above 10 kHz were assumed to make no contribution to the perceived noise level and were therefore ignored.

The original model-jet sound pressure measurements were taken in seven octave bands up to and including the 31.5 kHz band. When these data are scaled to the higher thrust values, the upper frequency band does not always extend above the frequency containing the peak in the Noy curves. This condition often occurred with the largest scaled thrust of 80,000 pounds, sometimes resulting in erroneously low perceived noise level values. To overcome this deficiency, the model data were extrapolated by adding four extra octave bands above the 31.5 kHz band, assuming a 3 dB per octave decrease in level from the 31.5 kHz band. In many cases, the atmospheric attenuation reduces these extra bands to negligible small levels when they are scaled to the sideline. In certain cases for the higher scaled thrusts, the first of these added bands has a significant effect on the perceived noise level. In order to indicate the magnitude of this effect, the perceived noise level calculations were made twice and printed out by the computer. The first value of PNL was obtained using all octave bands, including the four extra bands. The second value of PNL (printed in parenthesis) utilizes only the original seven octave bands of data. In this way, the effect of the added bands is clearly seen for each case.

4.0 DESCRIPTION OF THE EXPERIMENTAL DATA

During the course of this program, the sound from over 310 model jet configurations was measured and processed by the computer program. An effective presentation of all of these detailed data could not be made within one cover. Thus, the principal results are given in this report, supplemented by a detailed tabulation of the results in Volume II. Appendix A, in Volume I, gives a detailed listing of the run numbers and associated run conditions. This section describes the format of the detailed data and discusses a few pertinent points concerning the results.

4.1 Computer Output Data

For each experimental run condition, the output of the computer program consists of the following major items of information:

(1) The basic run conditions, including such items as mass flow, velocity, thrust and pressure ratio.

(2) The octave band sound pressure levels for the model jet. The data are presented in seven octave bands with frequencies ranging from 500 Hz to 31.5 kHz, and an overall level computed as the sum of the octave band levels. Levels are given at 5-degree angular increments, starting at an angle of 15 degrees from the jet axis in the flow direction and extending to 115 degrees around an arc of 10.67 feet radius.

(3) The model jet sound power octave band spectrum and overall level. This information is the result of an integration of the sound power over a spherical surface within the angular limits specified in (1) above.

(4) The overall sound power level for full-scale jets with thrusts of 10,000 pounds, 20,000 pounds, 40,000 pounds and 80,000 pounds.

(5) The model jet directivity index.

(6) The model jet mechanical power and acoustical conversion efficiency.

(7) The octave band sound pressure levels, overall sound pressure levels and perceived noise levels on a 500-foot sideline. These levels are given for each of the 5-degree angular positions used in the model sound pressure level measurement (see (1) above). The coordinate defining position on this output (L) is the distance from the jet to the sideline at various angles. Two values of the perceived noise level are printed, as explained earlier in Section 3.4.7. The first value is computed from

the measured plus extrapolated octave band levels. The value in parentheses utilizes only the seven measured octave bands in the perceived noise level calculation.

(8) The same information as in item (7) above, but for a 1500-foot sideline.

This information occupies many pages of computer output and was condensed for presentation in Volume II in the format shown in Figure 32. The data presented include items (1), (2), (3), (4) and (8) for the 20,000 pound thrust case only. From these data, two sets of summary plots were made. The first set gives the overall sound power level for a 20,000 pound thrust engine as a function of mass flow ratio (ratio of secondary mass flow to primary mass flow), and the second presents the maximum 1500-foot sideline perceived noise level as a function of mass flow ratio. For each of these sets of plots, each graph represents one combination of primary nozzle temperature, primary pressure ratio and primary axial position. Thus, 28 plots are required for each set to cover all run conditions measured in the experiment. The complete set of plots for overall power level and for perceived noise level are given in Appendices D and E, respectively.

For illustration, an example from each set is presented in Figures 33 (overall sound power level) and 34 (perceived noise level). Each of these graphs contains a point on the vertical axis, giving the result for the primary nozzle alone, and four solid lines for the four different values of the nominal ratio of secondary nozzle area to primary nozzle area. (See Section 3.2.1 for the exact values.) The experimental points on each of the four lines correspond to various velocity ratios.

The experiments documented in this report include the determination of the directivity of the jets measured in an anechoic room where there was no reflecting ground plane and the possibility of the jet exhaust being deflected by low velocity air currents was eliminated. Many of the measurements of directivity patterns previously reported were made in the open where the presence of a ground plane can significantly affect the measured results (References 5 and 35), and a slight breeze can markedly bend the jet exhaust plume and hence distort the directivity. It is therefore felt that a useful side benefit from the present tests is a set of single-nozzle directivity patterns from which all ground plane and cross-wind effects have been removed. Consequently, a set of directivity plots and sound power spectra for each of the primary nozzles acting alone is presented in Appendix F.

RUN NUMBER	=	103.000
AXIAL POSITION OF PRIMARY NOZ. SECONDARY (INS.)	=	8.000
PRIMARY TEMPERATURE (R)	=	525.000
SECONDARY TEMPERATURE (R)	=	525.000
PRIMARY PRESSURE RATIO	=	1.000
AREA RATIO	=	1.000
VELOCITY RATIO	=	.700
PRIMARY VELOCITY (FT/SEC)	=	881.562
MASS FLOW RATIO	=	.937
PRIMARY MASS FLOW (LB/SEC)	=	.217
THRUST (LBS)	=	9.932
ENVIRONMENTAL TEMPERATURE (R)	=	523.500
ENVIRONMENTAL PRESSURE (IN.HG)	=	29.810
ENVIRONMENTAL HUMIDITY (PER CENT)	=	67.000
CALIBRATION FACTOR (W/ TO DY/SQ CM)	=	.007
INSTRUMENTATION NOISE FLOOR (DB)	=	46.500

ACOUSTIC POWER AND SOUND POWER LEVEL FOR MODEL JET

FREQUENCY	POWER(WATTS)	POWER LEVEL(DB)
OVERALL	1.15353E-01	120.6
500	1.30182E-03	101.1
1000	7.36225E-03	108.6
2000	2.53555E-02	114.0
4000	3.12544E-02	114.9
8000	2.74616E-02	114.4
16000	1.60264E-02	112.0
31500	6.65123E-03	108.2

OVERALL SOUND POWER LEVEL,SCALED FOR THRUST

THRUST	POWER LEVEL(DB)
10000	150.6
20000	153.7
40000	156.7
80000	159.7

EXPERIMENTAL DATA
TABLE SHOWING OCTAVE BAND AND OVERALL SOUND PRESSURE LEVEL VARIATION WITH ANGLE

ANGLE (DEG)	OCTAVE BAND SOUND PRESSURE LEVELS 500	1000	2000	4000	8000	16000	31500	OVER ALL
15.0	80.5	88.4	92.5	89.6	82.5	76.3	71.6	95.7
20.0	79.6	87.8	92.5	90.4	84.2	78.0	73.6	95.9
25.0	77.8	86.1	91.4	90.6	86.0	79.9	75.1	95.5
30.0	76.8	84.5	89.9	90.2	87.4	82.0	77.4	95.0
35.0	74.6	82.3	88.1	89.1	87.8	83.4	78.1	94.1
40.0	72.9	80.6	86.7	88.9	87.9	84.3	79.5	93.6
45.0	71.3	78.8	84.9	87.2	87.3	84.7	80.4	92.7
50.0	70.2	77.6	84.1	86.3	86.6	84.6	80.5	92.0
55.0	69.7	76.7	82.9	85.2	85.8	84.0	80.6	91.2
60.0	69.8	76.0	82.0	84.5	85.2	83.4	79.9	90.6
65.0	69.8	76.1	81.6	84.4	85.1	83.2	80.2	90.5
70.0	69.4	75.6	80.9	83.8	84.4	83.0	79.6	89.9
75.0	68.7	75.3	81.0	83.7	84.1	82.6	79.3	89.6
80.0	68.6	74.5	80.5	83.9	83.6	82.0	78.5	89.0
85.0	68.3	74.5	80.1	83.0	83.8	81.8	78.1	88.9
90.0	68.0	74.2	79.7	82.2	83.4	81.5	78.0	88.6
95.0	67.3	74.2	80.1	81.9	83.3	81.7	78.1	88.6
100.0	66.6	73.6	79.5	81.5	82.7	81.2	77.6	88.0
105.0	65.5	73.0	79.5	81.4	82.3	81.1	77.5	87.8
110.0	65.5	72.6	78.9	81.0	81.9	81.0	76.7	87.4
115.0	65.5	72.2	78.7	80.6	81.5	80.9	76.5	87.1

MODEL THRUST = 9.932 FULL SCALE THRUST = 20000.000

LB	PNDB	OASPL	OCTAVE BAND SOUND PRESSURE LEVELS 11.1	22.3	44.6	89.1	178.3	356.6	712.6	1424.0	2785.6	5571.3	11142.5
5796.6	67.4(66.5)	73.9	58.85	66.48	70.78	67.73	60.23	52.84	45.18	34.86	16.13	-18.35	-77.98
4384.7	71.8(70.6)	76.6	60.35	68.51	73.20	71.05	64.46	57.39	50.70	42.16	27.20	.44	-45.41
3548.3	75.2(73.6)	77.9	60.41	69.71	73.94	73.13	69.26	61.40	54.82	47.33	34.70	12.42	-25.26
3000.0	78.2(76.3)	78.9	60.96	68.80	73.93	74.18	71.19	65.17	58.95	52.16	41.02	21.72	-10.59
2615.2	79.8(77.7)	79.1	59.83	67.58	73.31	74.32	72.74	67.85	61.20	54.90	44.80	27.59	-.96
2333.6	81.4(78.9)	79.6	58.18	66.83	72.87	74.66	73.94	69.87	63.84	57.90	48.56	32.80	7.09
2121.3	82.4(79.5)	79.6	58.32	65.84	71.93	74.23	74.12	71.13	65.73	60.05	51.29	36.77	13.04
1958.1	83.0(79.9)	79.6	57.94	65.17	71.84	73.96	74.15	71.72	66.61	61.14	52.82	39.18	17.05
1831.2	83.2(79.9)	79.4	58.04	65.09	71.23	73.49	73.97	71.75	67.39	62.08	54.11	41.16	20.27
1732.1	83.1(79.7)	79.2	58.62	64.78	70.77	73.28	73.89	71.67	67.25	62.00	54.36	41.95	22.03
1655.1	83.6(80.1)	79.5	59.01	65.28	70.81	73.56	74.21	71.97	68.02	62.93	55.44	43.45	24.28
1596.9	83.5(80.0)	79.3	58.92	65.17	70.66	73.09	73.91	72.02	67.88	62.84	55.51	43.84	25.26
1549.9	83.5(79.9)	79.3	58.51	65.03	70.73	73.42	73.70	71.90	67.75	62.79	55.57	44.14	25.96
1521.1	83.1(79.5)	78.8	58.58	64.43	70.43	72.78	73.40	71.47	67.24	62.31	55.18	43.90	26.02
1509.7	83.0(79.5)	78.9	58.31	64.53	70.17	73.00	73.32	71.40	66.91	62.01	54.92	43.74	26.03
1500.0	82.7(79.1)	78.5	58.10	64.31	69.73	72.27	73.32	71.15	66.82	61.92	54.85	43.70	26.05
1489.7	82.8(79.1)	78.5	57.30	64.21	70.17	71.88	73.24	71.26	66.91	62.01	54.92	43.74	26.03
1521.1	82.1(78.5)	77.8	56.51	63.59	69.60	71.35	72.51	70.64	66.27	61.34	54.21	42.93	25.05
1552.9	81.7(78.1)	77.5	55.36	62.79	69.27	71.13	71.98	70.18	66.00	61.04	53.83	42.39	24.22
1598.3	81.0(77.6)	76.8	55.02	62.10	68.47	70.49	71.28	70.00	64.94	59.92	52.59	40.92	22.32
1636.1	80.4(77.0)	76.2	54.71	61.39	67.90	69.77	70.55	69.61	64.34	59.25	51.76	39.77	20.68

Reproduced from best available copy.

Figure 32. Example of Computer Output for One Computer Run.

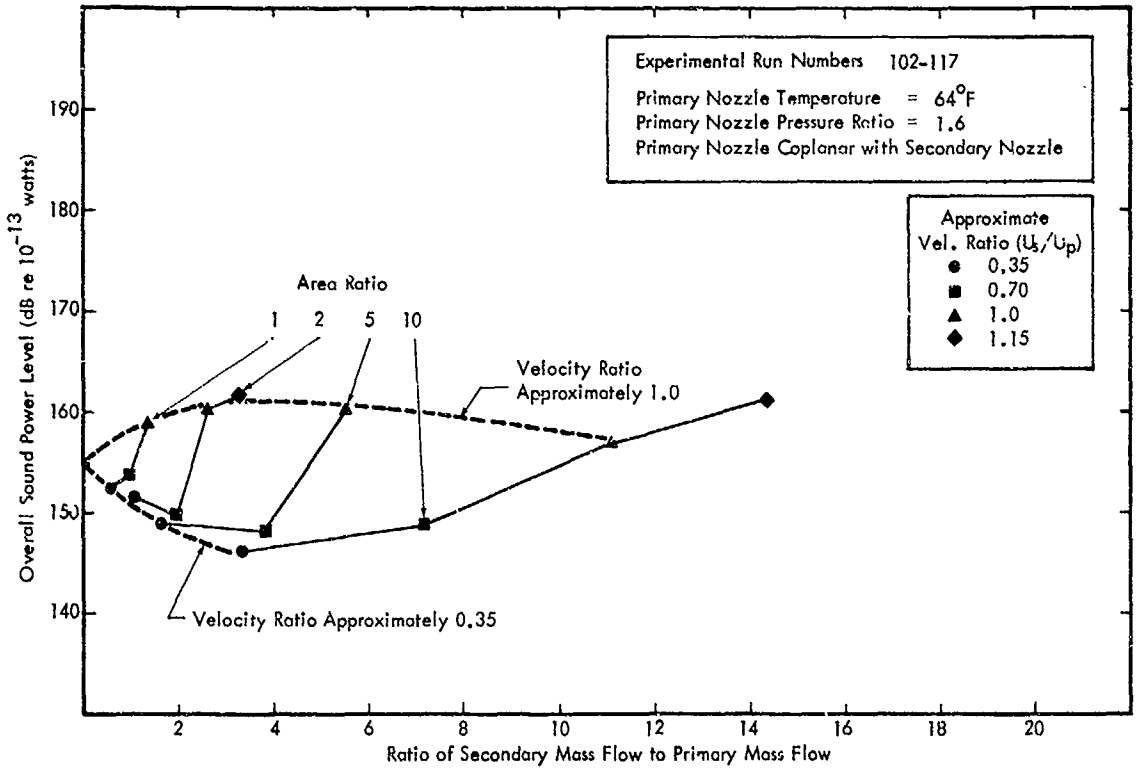

Figure 33. Variation in Overall Sound Power with Bypass Ratio for Thrusts Scaled to 20,000 Lbs.

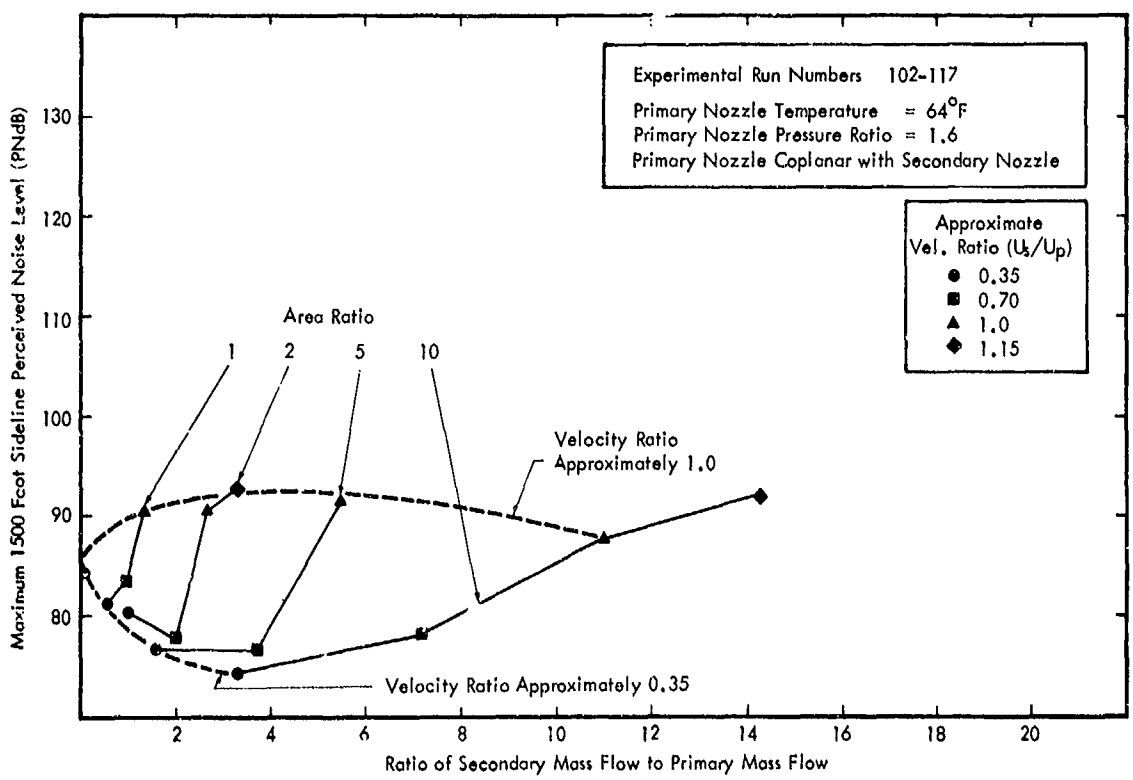

Figure 34. Variation in Maximum Perceived Noise Level on a 1500-Foot Sideline with Bypass Ratio for Thrusts Scaled to 20,000 Lbs.

4.2 Some Experimental Anomalies

Some of the results of this program depart from the expected trends. These anomalies are discussed in the following paragraphs.

The first anomaly occurred when the secondary flow velocity equaled the primary velocity. Evidence of this is to be found in Figures 33 and 34, for Run Numbers 102 to 117. Here, for unity velocity ratio, the scaled power level and perceived noise level values for the coaxial nozzles are in excess of the level produced by the primary nozzle alone. One would expect the scaled noise produced by nozzles with a velocity ratio of unity to be the same as that produced by the primary alone, if any interaction effect between the primary and secondary flow is neglected. In this case, the primary nozzle acting alone has been checked extensively and there is no doubt as to the reliability of the data. In addition, its noise output agrees well with the level predicted by Reference 5. This indicates that the increase in level is due to the presence of the coaxial nozzles. The exact cause of this discrepancy is not known, but an examination of the acoustic power spectra shows that additional noise sources are present which increase the middle and high frequency content of the spectra. The worst case is illustrated in Figure 35.

Examination of all of the power spectra show that this increase in the high frequency region of the normalized power spectra is most significant for the coplanar cold 1.6 pressure ratio nozzle. There is little or no effect for the lower area ratio secondary nozzles with the half and fully extended primaries, whereas with the coplanar nozzles these area ratios exhibited the largest effect. Also, examination of all the coplanar nozzle power spectra for lower velocity ratios indicated that this effect was generally not present.

These results are consistent with the possibility that the additional source is associated with the contraction of the external diameter of the primary nozzle pipe from 1.0 to 0.8 inches over a distance of 1/2-inch forward of the nozzle. This contraction in the primary pipe diameter creates a slightly divergent secondary nozzle for the coplanar case, with the throat approximately 1/2-inch upstream of the nozzle plane. The amount of divergence decreases with increasing area ratio, as can be seen by comparing the area ratios given in Section 3.2 for the coplanar and extended primary nozzle cases. Consequently, the effect would be expected to be greatest for the smaller area ratio secondary nozzles. Also, the acoustic effect would be expected to be greatest for flow velocities in the sonic region where the divergence acts as a supersonic diffuser, accelerating the flow rather than slowing it.

Additionally, as shown in Appendix B, the boundary layer shed from the outside of the primary nozzle prevents the coplanar nozzles from having completely uniform

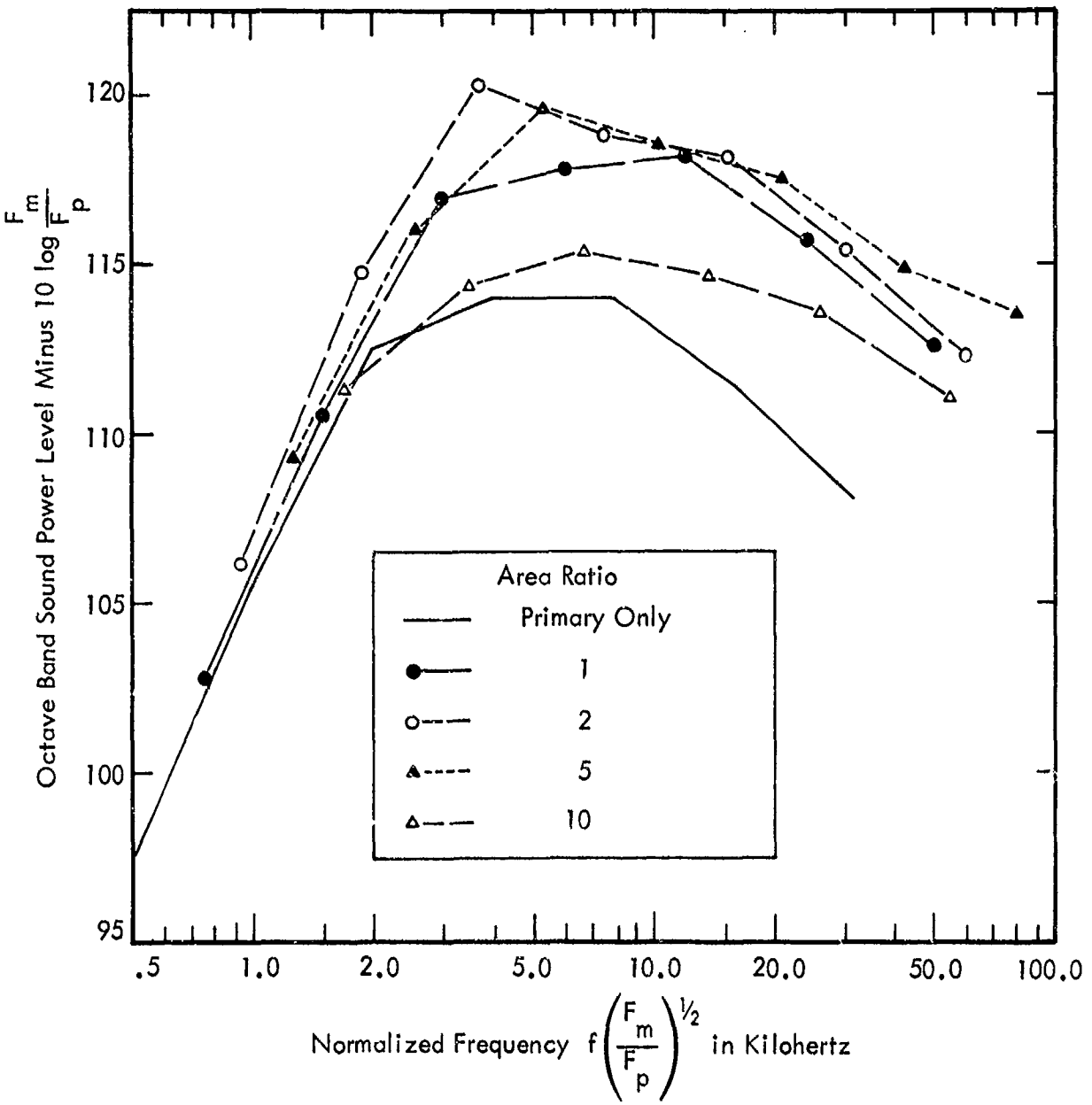

Figure 35. Power Spectra for Unity Velocity Ratio and Various Area Ratios for Coplanar Jet with Primary Nozzle Pressure Ratio of 1.6 and Temperature of 60°F. (Data are normalized to primary nozzle thrust.)

velocity profiles. The turbulence induced by this velocity defect probably causes additional sound generation at a frequency associated with the scale of the contraction ($\approx$ 0.1 inch) and with a magnitude which increases proportional to a power of the secondary flow velocity. A similar condition would undoubtedly be present on a real full-sized jet engine, although its magnitude may well vary considerably with variations in internal nozzle geometry, and hence would not necessarily scale correctly from these model jet results.

The second anomaly is associated with the secondary nozzle which has an area ratio of 2. This effect is illustrated in Figure 36 for Run Numbers 176 to 187, where the noise for the area ratio 2 nozzle is greater than would be expected. Examination of the nozzle showed that it had been over-heated when the primary was run with high temperature air, since the inside had become roughened and charred. This roughness would cause an unusually turbulent boundary layer to be produced inside the mouth of the nozzle. From an examination of the data, the over-heating appears to have happened just before Run 148; for all run numbers below 148, the nozzle produces results consistent with those produced by the other nozzles, but thereafter it appears to produce too much noise. The results for this area ratio for run numbers greater than 147 should therefore be treated with caution.

The third anomaly concerns a noise source associated with the two supersonic primary nozzles. In the majority of the runs with these nozzles, the model directivity pattern in the higher octave bands (principally the 31.5 kHz and 16 kHz bands) showed an unexpected increase at angles near 90 degrees to the jet axis. The maximum value of this increase was usually found near 110 degrees.

This phenomenon is shown in Figure 37 for Run 128, which had a primary nozzle with pressure ratio 2.5 and temperature of 64°F, together with a coplanar secondary nozzle of area ratio 10 and velocity ratio of 0.38. This figure illustrates one of the worst examples of this phenomenon. It shows the directivity patterns for the 5 highest octave bands. The 31.5 kHz and 16 kHz bands are seen to be 10 to 12 dB high at 110 degrees while the remaining bands form a consistent group, decreasing in level with increasing angle. It is obvious that such a discrepancy cannot be truly representative of a full-size jet and that the model data should be corrected. Fortunately, the peaks in the forward direction of directivity pattern for both the anomalous octave bands have not been affected (this was always the case in all runs with this fault) so that the correction to the directivity and computer corrections could be made.

As part of an evaluation of this phenomena, a one-tenth octave analysis was made of the sound at 110 degrees from the jet axis and at frequencies up to 25 kHz. This analysis is shown in Figure 38. It does not show any evidence of a discrete frequency, but rather a broad peak with a bandwidth of approximately one octave.

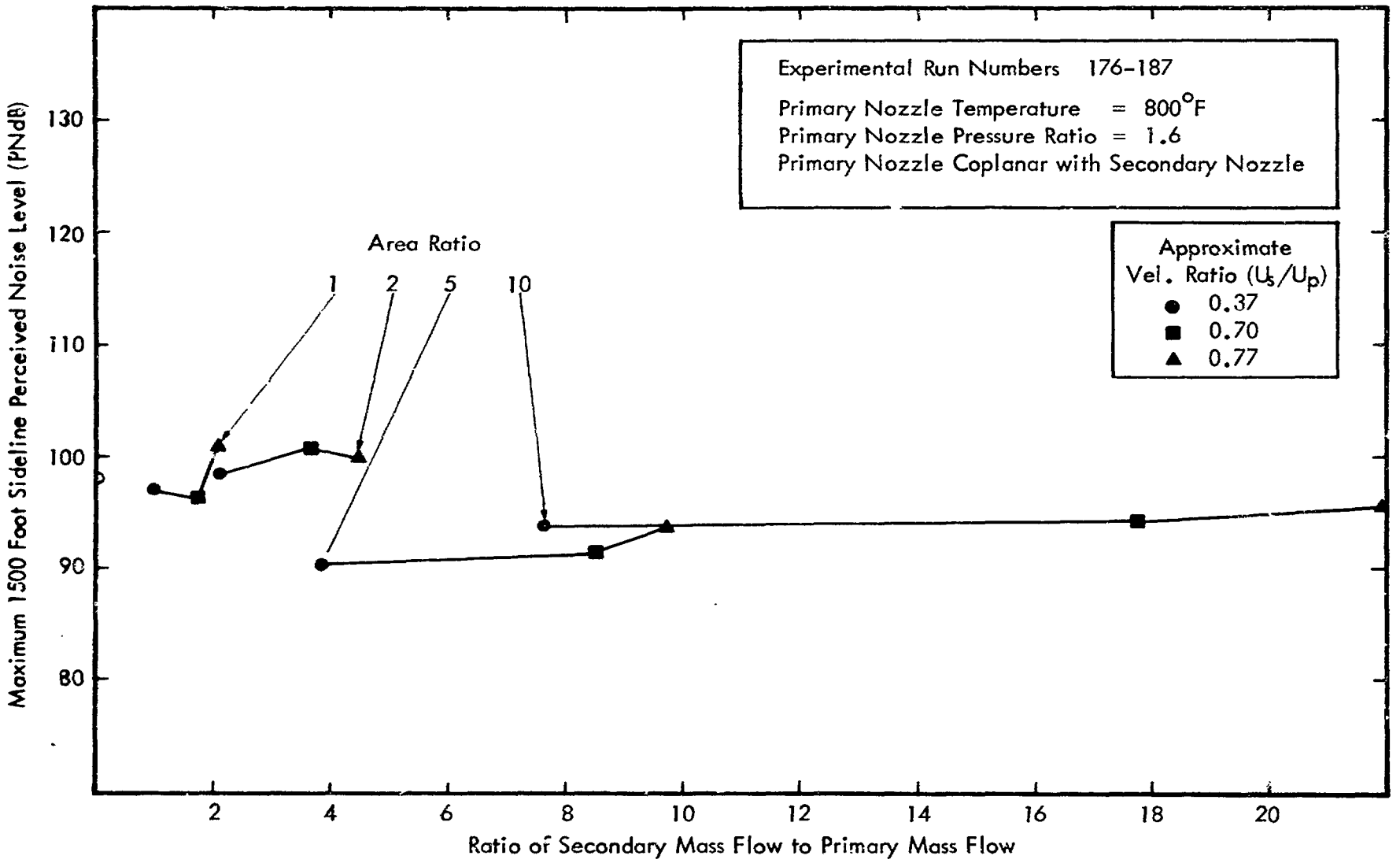

Figure 36. Variation in Maximum Perceived Noise Level on a 1500-Foot Sideline with Bypass Ratio for Thrusts Scaled to 20,000 Lbs.

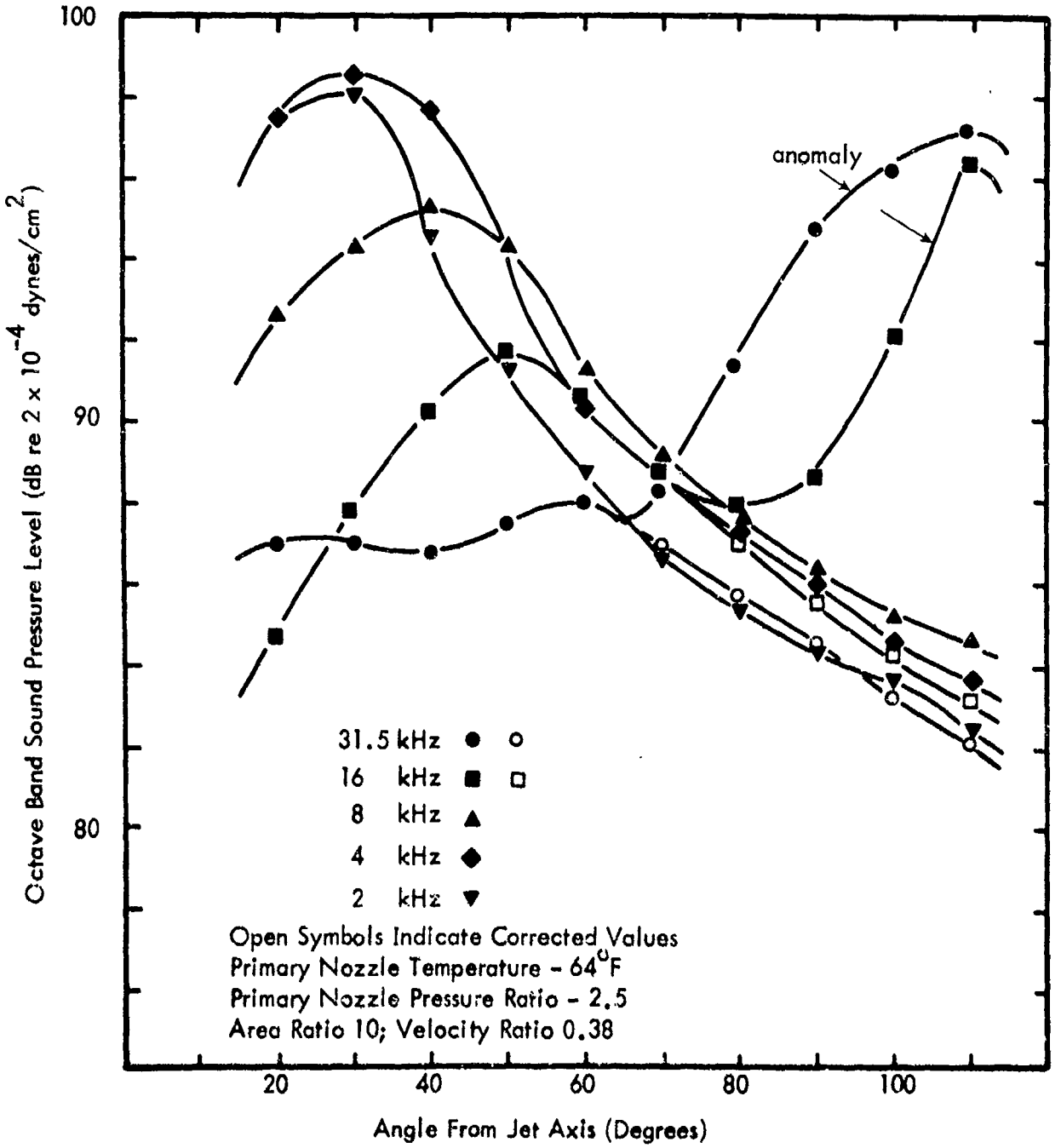

Figure 37. Directivity Pattern for Run 128 (Coplanar) Showing the Anomaly in the High Octave Bands.

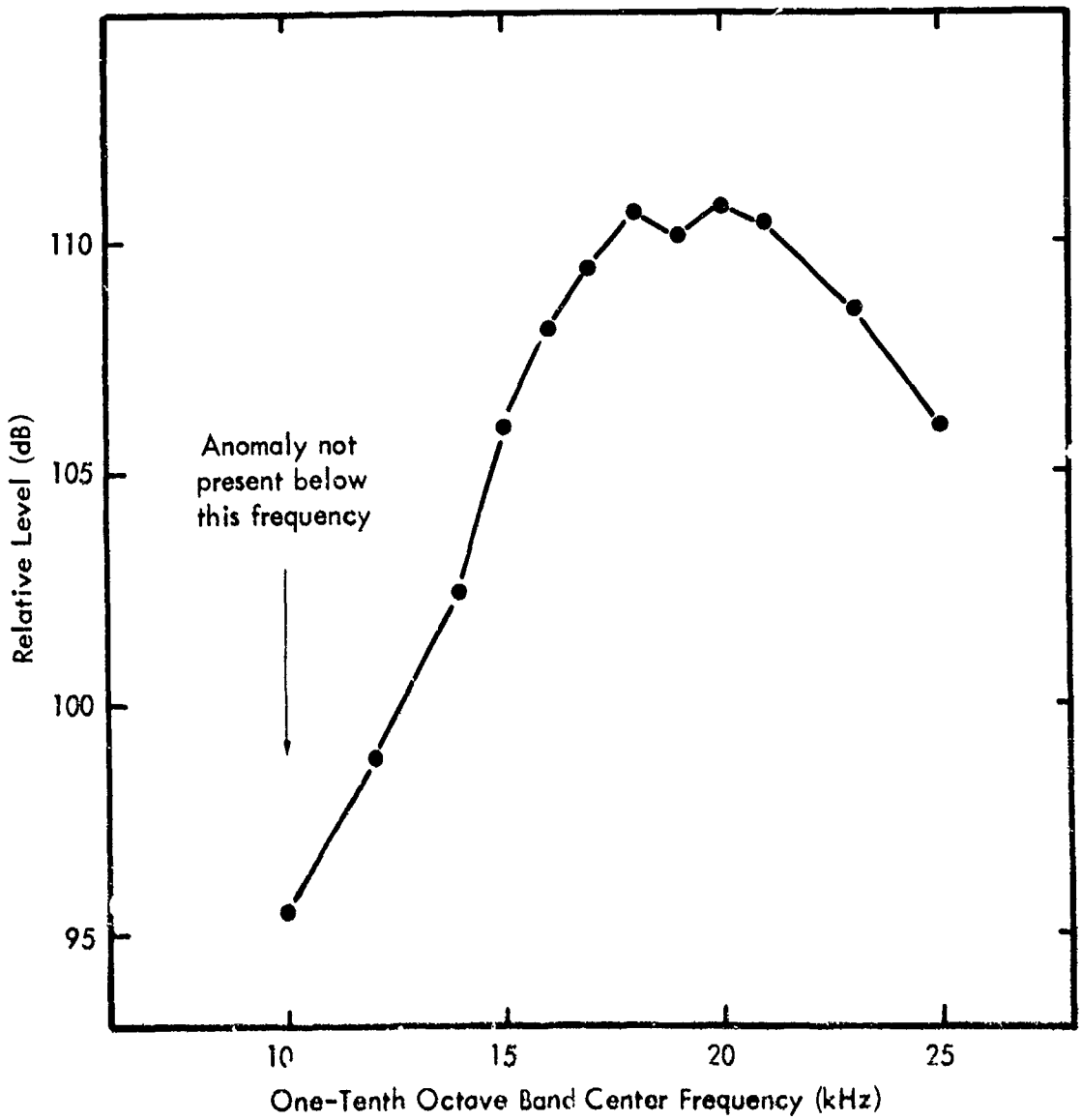

Figure 38. One-Tenth Octave Band Analysis of Directivity Anomaly for Run 128 at 110 Degrees.

Finally, a check was made to determine the effect of this anomaly on the computed sound power levels and sideline perceived noise level. The corrections indicated in Figure 37 lowered the sound power level in both the 16 kHz and 31.5 kHz bands. The resulting overall sound power levels decreased 1.5 dB. The sideline perceived noise levels were then checked. It was found that the true maximum sideline perceived noise level was not altered by this change in the higher two bands for any of the full-scale jet thrusts. Similar checks were made on other runs where this problem was severe, with the same basic conclusions. These results indicate that the scaled overall sound power level plots, of which Figure 33 is an example, are altered slightly when the anomaly under discussion is at its worst, but that the maximum sideline perceived noise level is not altered. On this basis, all runs which showed this anomaly were corrected, as in Figure 37, and are noted by an asterisk (*) in the run number schedule in Appendix A.

The cause for this anomaly is not known. It appeared in almost all of the coplanar and extended nozzle configurations, in a few of the half retracted configurations, and none of the fully retracted runs. It was only slightly in evidence ($\approx$ 2 dB at 31.5 kHz) when the 2.5 pressure ratio nozzle was run alone. However, it was present in most of the runs of the 3.5 pressure ratio nozzle which was operated at several pressure ratios. These latter results, shown in Appendix G, indicate that the effect is present for all pressure ratios greater than 2.0, generally increasing in magnitude with increasing pressure ratio.

Intentionally Left Blank

5.0 DISCUSSION OF RESULTS AND THEIR APPLICATION TO FULL-SCALE ENGINES

This section reviews the principal experimental results which are relevant to predicting the noise of full-scale engines and to understanding the noise reduction characteristics of coaxial jet flows in terms of the analysis in Section 2.3. These results are utilized to develop a prediction method for full-scale engines and to evaluate the differences between the noise characteristics of practical full-scale coaxial jet engines and those of idealized single-nozzle engines with a similar exit velocity.

5.1 Discussion of Principal Experimental Results

The experimental results will be examined with a view to determining the noise reduction characteristics of coaxial jets. The noise reduction of a coaxial jet is defined to be the difference between the noise of the coaxial jet and that of a single-nozzle jet which has the same thrust as does the coaxial jet and the same flow conditions as those of the primary nozzle of the coaxial jet. This comparison eliminates the gross variations due to changes in primary velocity and temperature. The following paragraphs examine the noise produced by the primary nozzles alone and the changes in sound power, directivity and maximum sideline perceived noise level resulting from the coaxial jet flow.

5.1.1 Noise of the Primary Nozzles.

Figures 39, 40 and 41 show the sound produced by the three primary nozzles with the three pressure ratios and three total temperatures as shown, as a function of the flow velocity. Figure 39 shows the measured overall sound power level for the model primary nozzles. The dashed curve for the overall sound power level shows reasonable agreement with the data except for the 60-degree, pressure ratio 3.5 nozzle. The line can be represented by:

$$PWL = 123.6 + 80 \log \frac{U_p}{1000} \text{ in dB re } 10^{-13} \text{ watts} \qquad (39)$$

where U_p is the primary velocity. This curve is 2 dB greater than that given in Figure 1, which is based principally on data obtained over a ground plane and assumed to have hemispheric radiation. Since the data in this report were taken in free spherical space, the difference might indicate that the typical ground plane in Figure 1 provided some absorption and reflection losses, partially invalidating the assumption of ideal hemispheric radiation.

Preceding page blank

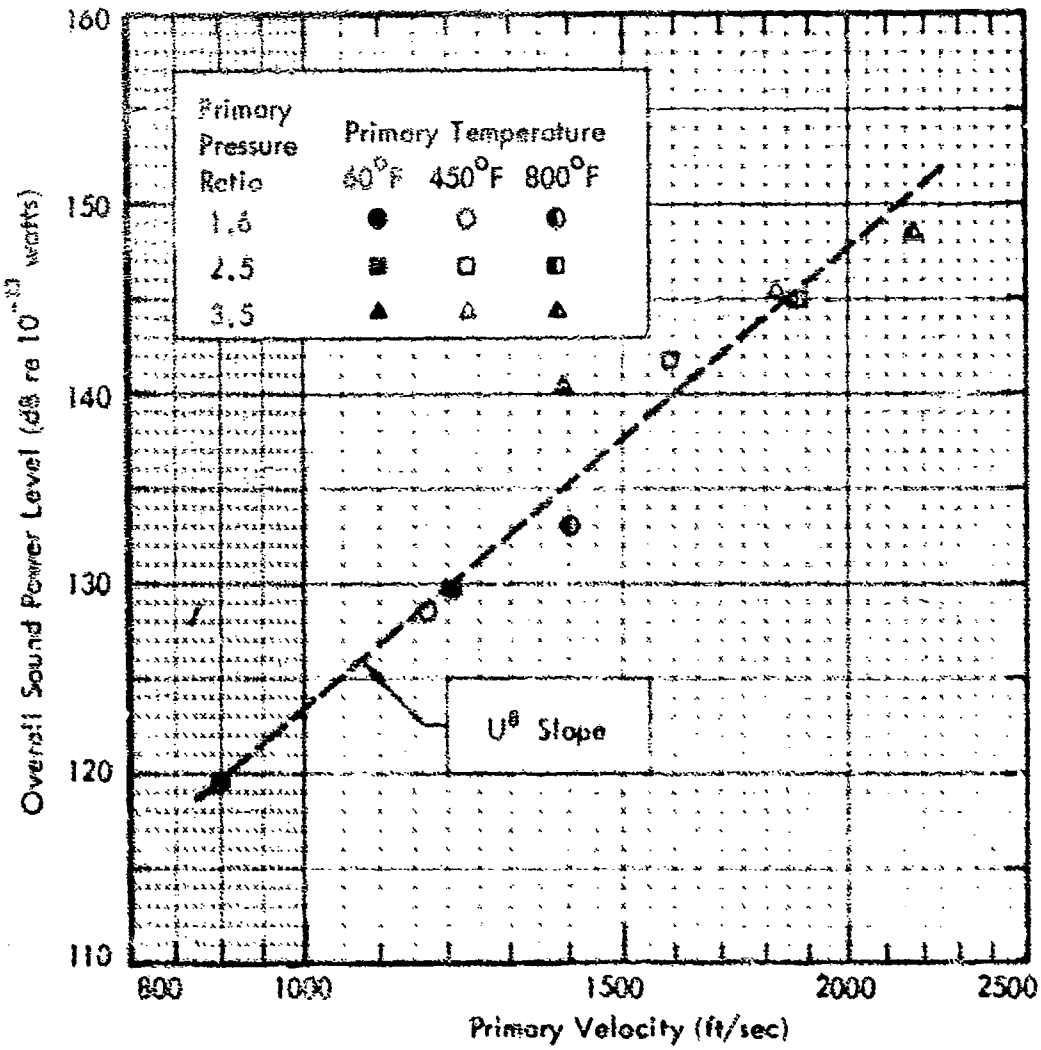

Figure 39. Variation in Measured Overall Sound Power Level with Velocity for the Model Scale Primary Nozzles Alone.

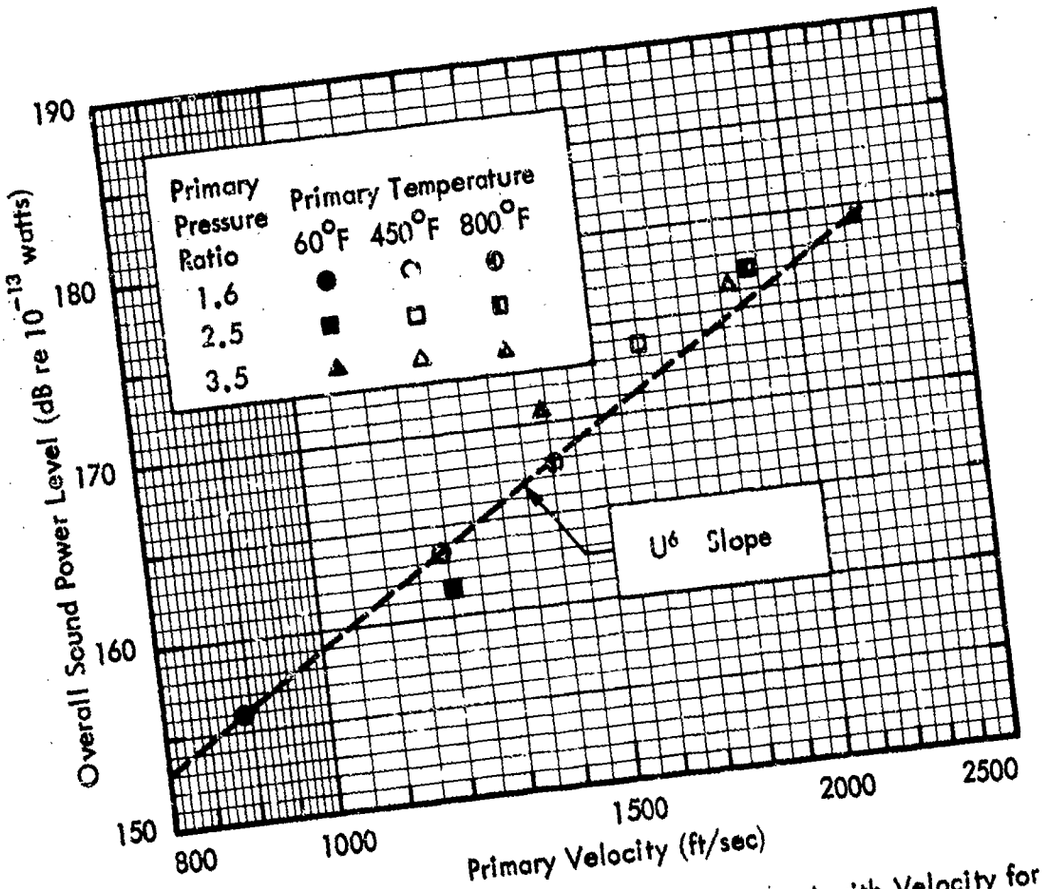

Figure 40. Variation in Overall Sound Power Level with Velocity for the Primary Nozzles Alone, Scaled to 20,000 Lbs Thrust.

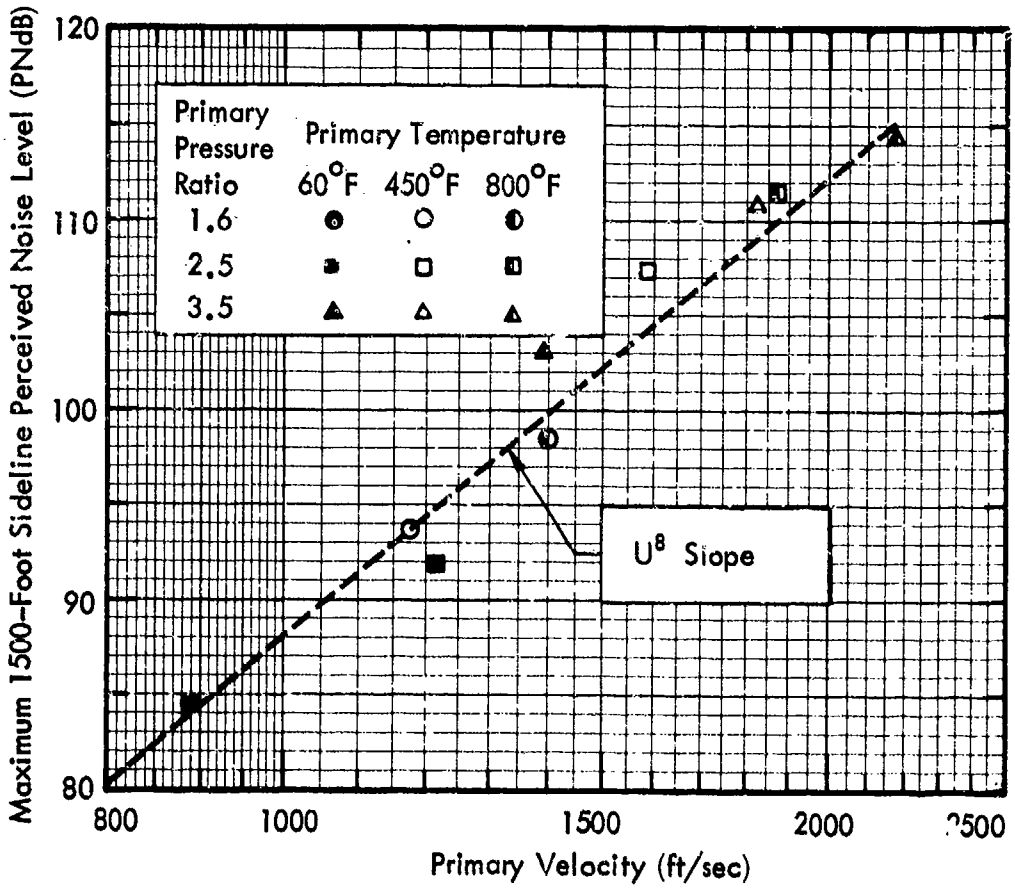

Figure 41. Variation in Maximum 1500-Foot Sideline Perceived Noise Level for the Primary Nozzles Alone, Scaled to 20,000 Lbs Thrust.

Figure 40 shows the same data scaled to a thrust of 20,000 pounds. The dashed line represents the curve of Figure 39 scaled in accordance with the following expression:

$$PWL_{(20,000\ lbs)} = 159 + 60 \log \frac{U_p}{1000} \text{ in dB re } 10^{-13} \text{watts} \qquad (40)$$

The change in the velocity exponent from 8 to 6 results from the thrust scaling.

Figure 41 gives the maximum perceived noise level on a 1500-foot sideline for these jets scaled to a thrust of 20,000 pounds. These results appear to be proportional to U^8. To calculate the overall power for a thrust other than 20,000 pounds, the results on Figure 40 can be scaled by ten times the ratio of the new thrust to 20,000 pounds. However, this simple rule does not apply to the maximum sideline perceived noise level because it is also a function of the noise spectrum. To determine the magnitude of this effect, the change in maximum 1500-foot sideline perceived noise level was calculated for thrusts of 10,000, 20,000, 40,000 and 80,000 pounds. The results are shown in Figure 42, along with the extent of the scatter. The mean line through the data has a slope proportional to $F^{.83}$, indicating that doubling the thrust produces a maximum perceived noise level increase of approximately 2.5 PNdB.

5.1.2 Reduction in Overall Sound Power Level Associated with Coaxial Jet Flows.

To determine the sound power level reductions associated with the various coaxial jet configurations, the overall sound power level of each coaxial jet was compared to the overall sound power level of its primary jet operating alone, with all data scaled to a constant thrust of 20,000 pounds. Figure 43 shows the change in overall sound power level for the coplanar nozzles as a function of velocity ratio, with the simple theoretical estimates of Section 2.3 included for comparison. The data exhibited three anomalies: (1) an increase of noise for coaxial nozzles of unity velocity ratio, (2) relatively poor noise reduction performance for the nozzle with an area ratio of two, and (3) the distinctly lesser noise reductions associated with the primary nozzle with pressure ratio 2.5 when operating at 60°F.

The first two of these anomalies have been discussed in Section 4.2. The third anomaly is present throughout the data. It occurs for cold flows only, not being apparent in the cases when the jet was heated. A uniform reduction of approximately 4 dB would bring the cold 2.5 pressure ratio data into line, suggesting that the sound power of the primary nozzle might be low. However, inspection of Figure 39 shows the noise of this primary nozzle to be consistent with that of the other eight primaries, and other data. Thus, the cause remains a mystery and the data for the cold pressure ratio 2.5 nozzle will be ignored in the remaining discussions.

The data for the coplanar nozzles with area ratios of 5 and 10, and to a lesser extent area ratio 1, show rather good agreement with the simple theory. Further, there seem

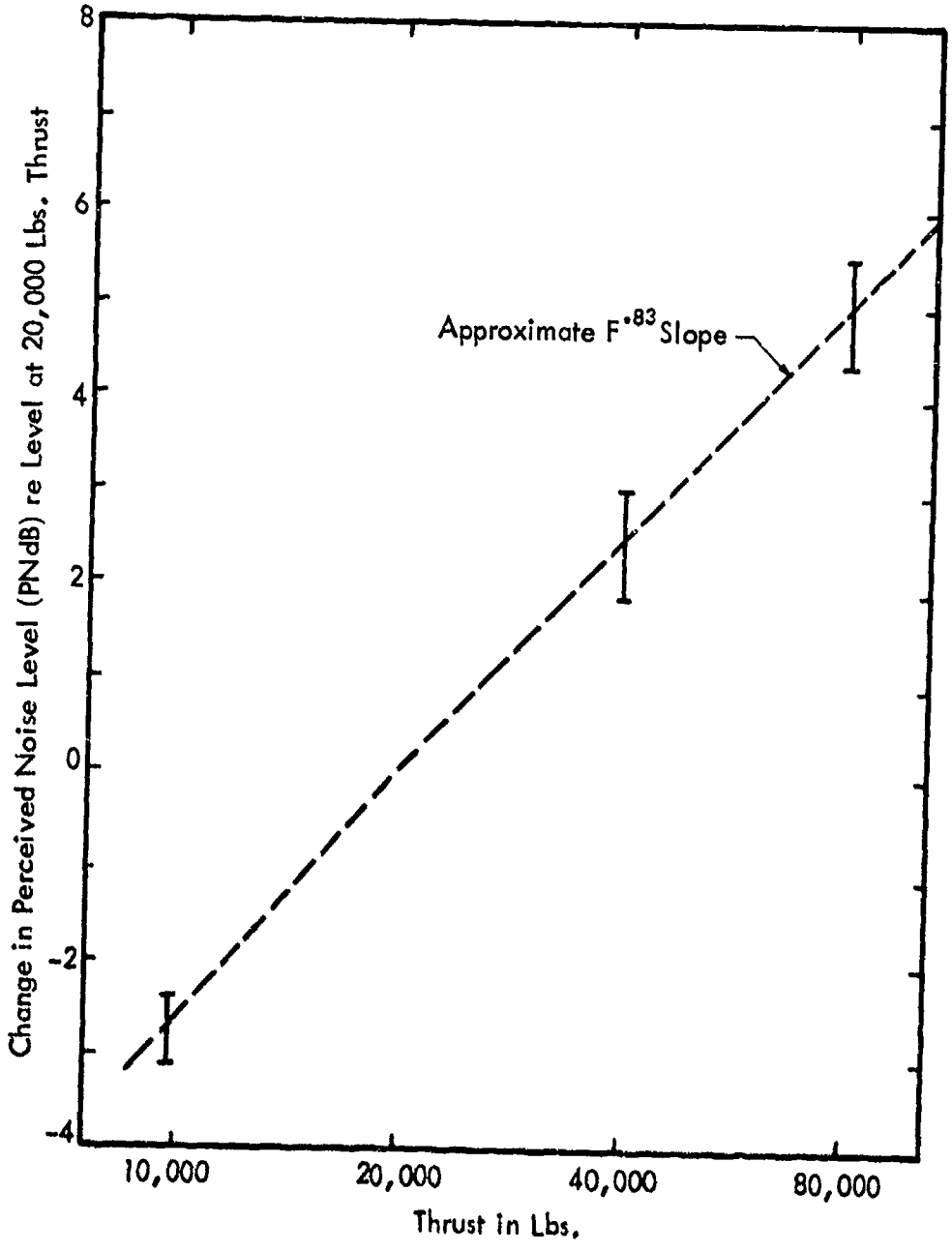

Figure 42. Effect of Jet Thrust on Calculated Maximum Perceived Noise Level on 1500-Foot Sideline for the Primary Nozzles of Figure 41.

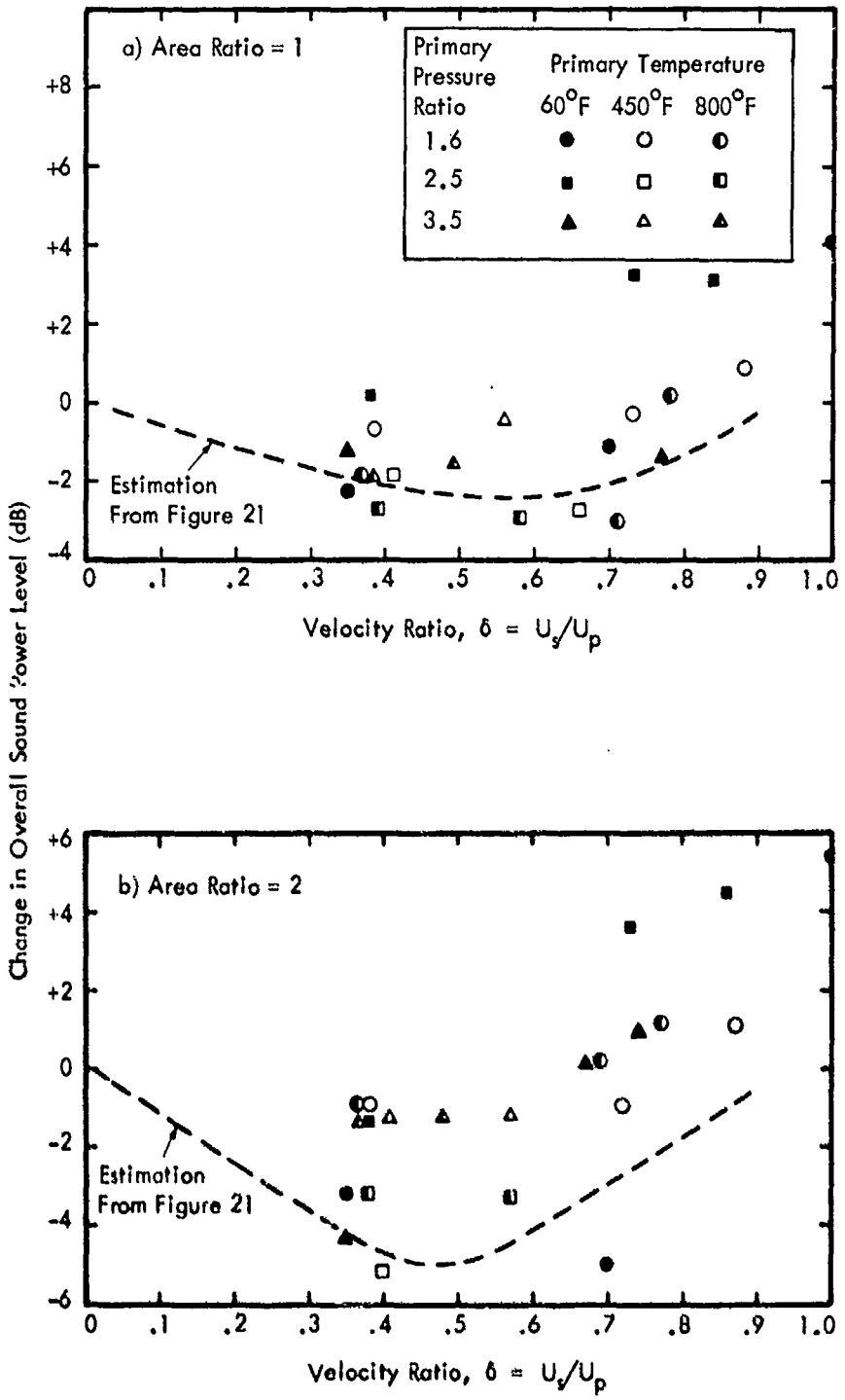

Figure 43. Change in Overall Sound Power Level with Velocity Ratio for Coplanar Coaxial Jets of 20,000 Lbs Thrust and Four Area Ratios. Change is Measured Relative to a Single-Nozzle Jet which has Equal Thrust and a Velocity Equal to U_p.

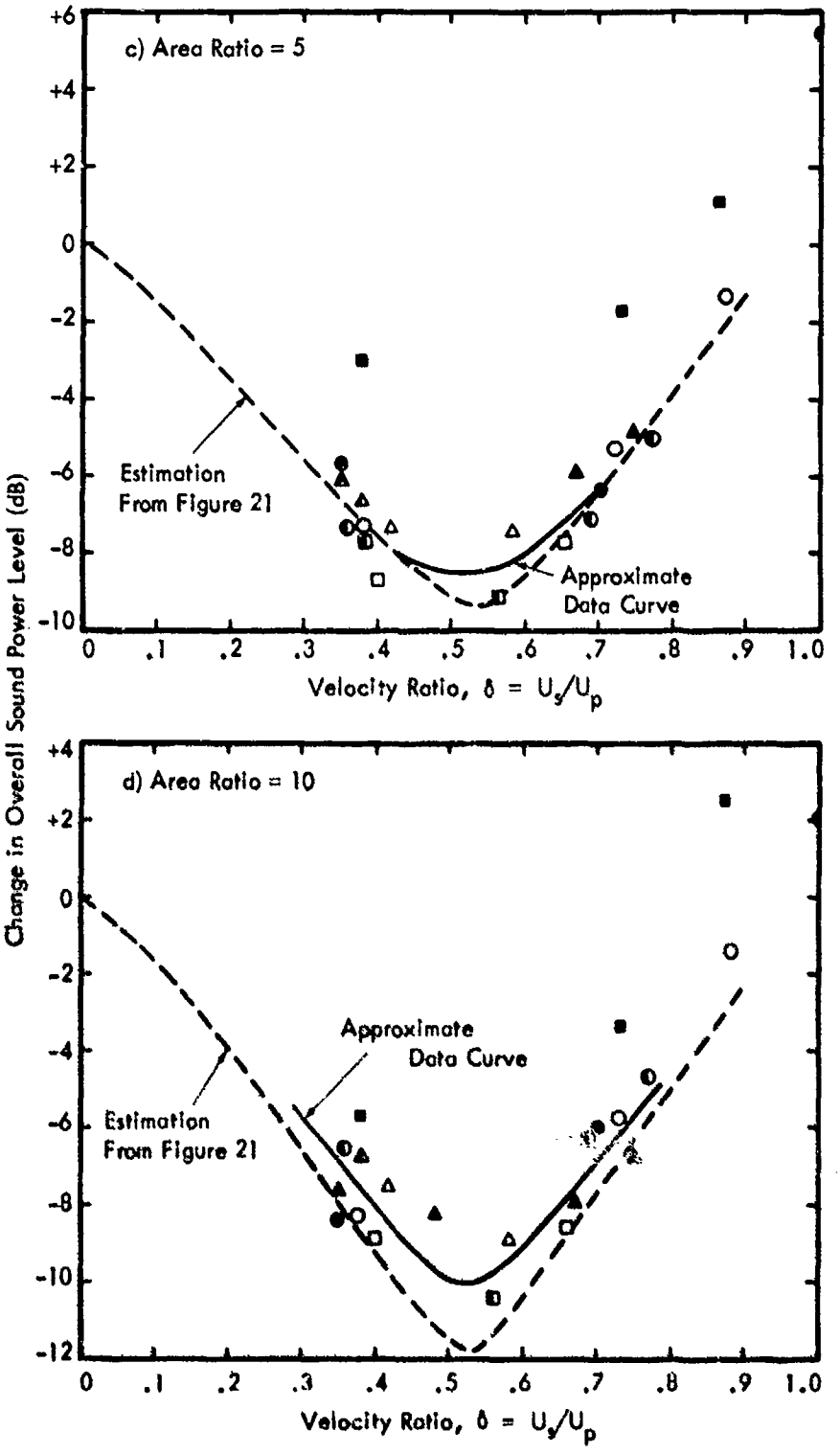

Figure 43. continued ... Change in Overall Sound Power with Velocity Ratio for Coplanar Coaxial Jets of 20,000 Lbs Thrust and Four Area Ratios. Change is Measured Relative to a Single-Nozzle Jet which has Equal Thrust and a Velocity Equal to U_p.

to be no consistent effects of either temperature or primary pressure ratio on the reductions of overall sound power level. Hence, it would appear that predictions of the sound power of the jet flow from modern high bypass ratio fan engines with coplanar coaxial nozzles can be made considering only the area and velocity ratios of the two flows.

The effect of extending the primary nozzle 5.5 primary nozzle diameters beyond the plane of the secondary nozzle (one-half extension) and 11 diameters (full extension) is illustrated in Figures 44 through 47. Again, the theoretical estimate of the change in overall sound power is included for reference, although its derivation assumed coplanar nozzles.

The results for the nozzle of area ratio 1, given in Figure 44, show an improvement over the coplanar performance. This may result from an improvement in its ability to shroud the core since the theory of Section 2.3 indicated that this nozzle was not large enough to shroud the primary core. However, with the extended primary nozzle, the secondary flow should be significantly larger than its initial diameter when it passes through the plane of the primary nozzle. At this plane, it will be slower than indicated by its exit velocity ratio, thus extending the shrouding regime to higher velocity ratios than predicted for coplanar nozzles in Section 2.3. Unfortunately, there are no velocity profiles available to test this conjecture.

The data for the nozzle with an area ratio of 2 are contained in Figure 45. They show improvement over the coplanar case, but the scatter is large and the roughness of this nozzle makes any evaluation questionable. The data for the nozzle with area ratio 5, Figure 46, show little change from the coplanar case, except for a small increase in scatter. However, the data for the fully extended nozzle of area ratio 10, Figure 47, show a decrease in noise reduction relative to the coplanar case. The reason for this change in performance is not known; however, the data appear consistent and the results must be considered valid.

The acoustic performance of retracted primary nozzle configurations can be expected to differ from that of the coplanar and extended primary nozzle configurations since the flows and acoustic boundary conditions are different. During all tests, the nozzles were operated at a fixed set of total pressures such that the velocity ratios for the non-retracted cases were consistent among runs which had the same primary nozzle and temperature. However, when the primary nozzle is retracted within the secondary plenum, its effective pressure ratio is decreased and its velocity is similarly decreased. Its initial mixing with the secondary flow occurs within the plenum, where the secondary flow velocity is quite low; however, the noise generated by this mixing is somewhat shielded by the walls of the secondary nozzle.

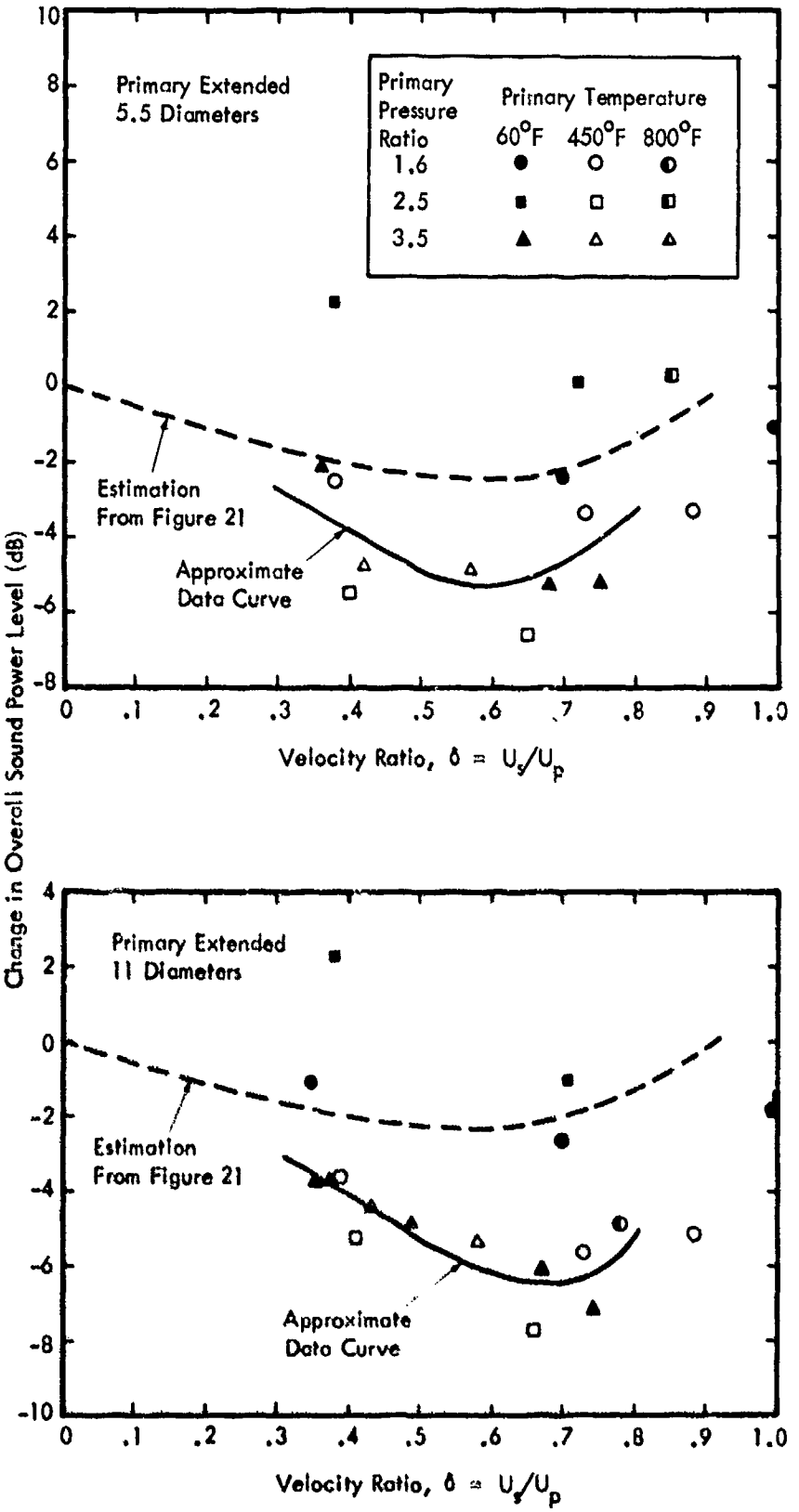

Figure 44. Change in Overall Sound Power Level with Velocity Ratio for Coaxial Jets with a Nozzle Area Ratio of 1 and Thrust of 20,000 Lbs. Change is Measured Relative to a Single-Nozzle Jet which has Equal Thrust and a Velocity Equal to U_p.

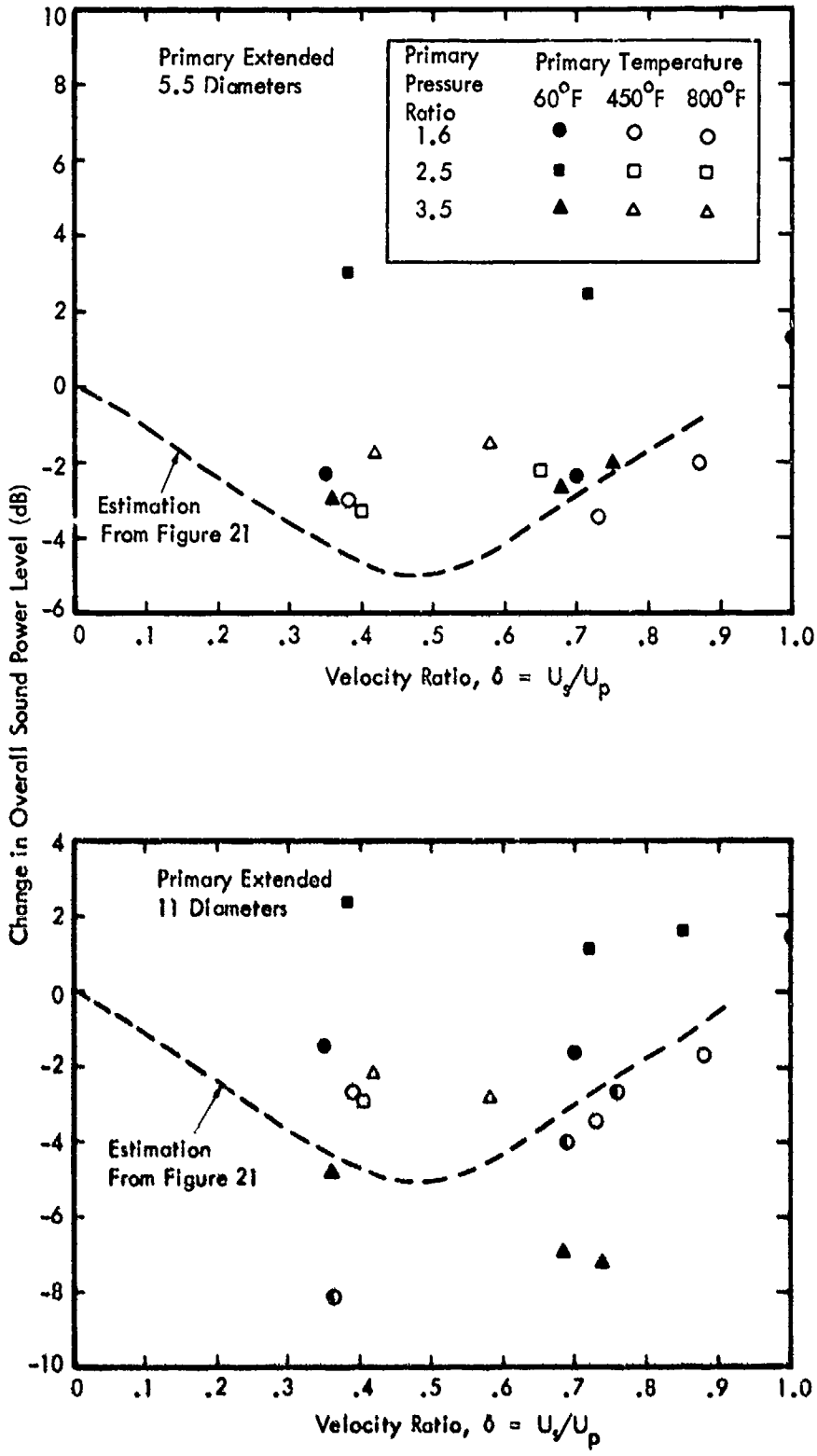

Figure 45. Change in Overall Sound Power Level with Velocity Ratio for Coaxial Jets with a Nozzle Area Ratio of 2 and Thrust of 20,000 Lbs. Change is Measured Relative to a Single-Nozzle Jet which has Equal Thrust and a Velocity Equal to U_p.

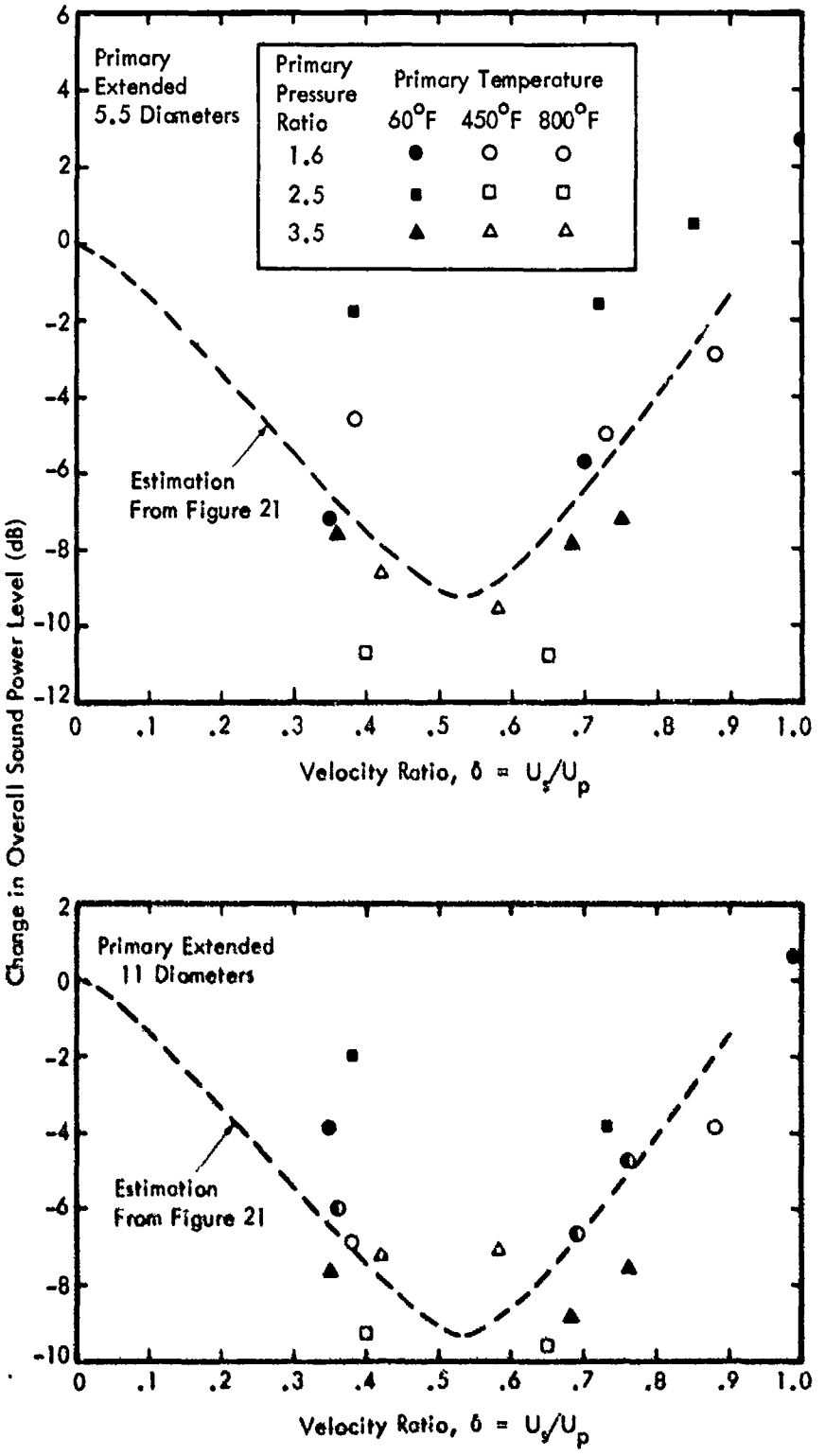

Figure 46. Change in Overall Sound Power Level with Velocity Ratio for Coaxial Jets with a Nozzle Area Ratio of 5 and Thrust of 20,000 Lbs. Change is Measured Relative to a Single-Nozzle Jet which has Equal Thrust and a Velocity Equal to U_p.

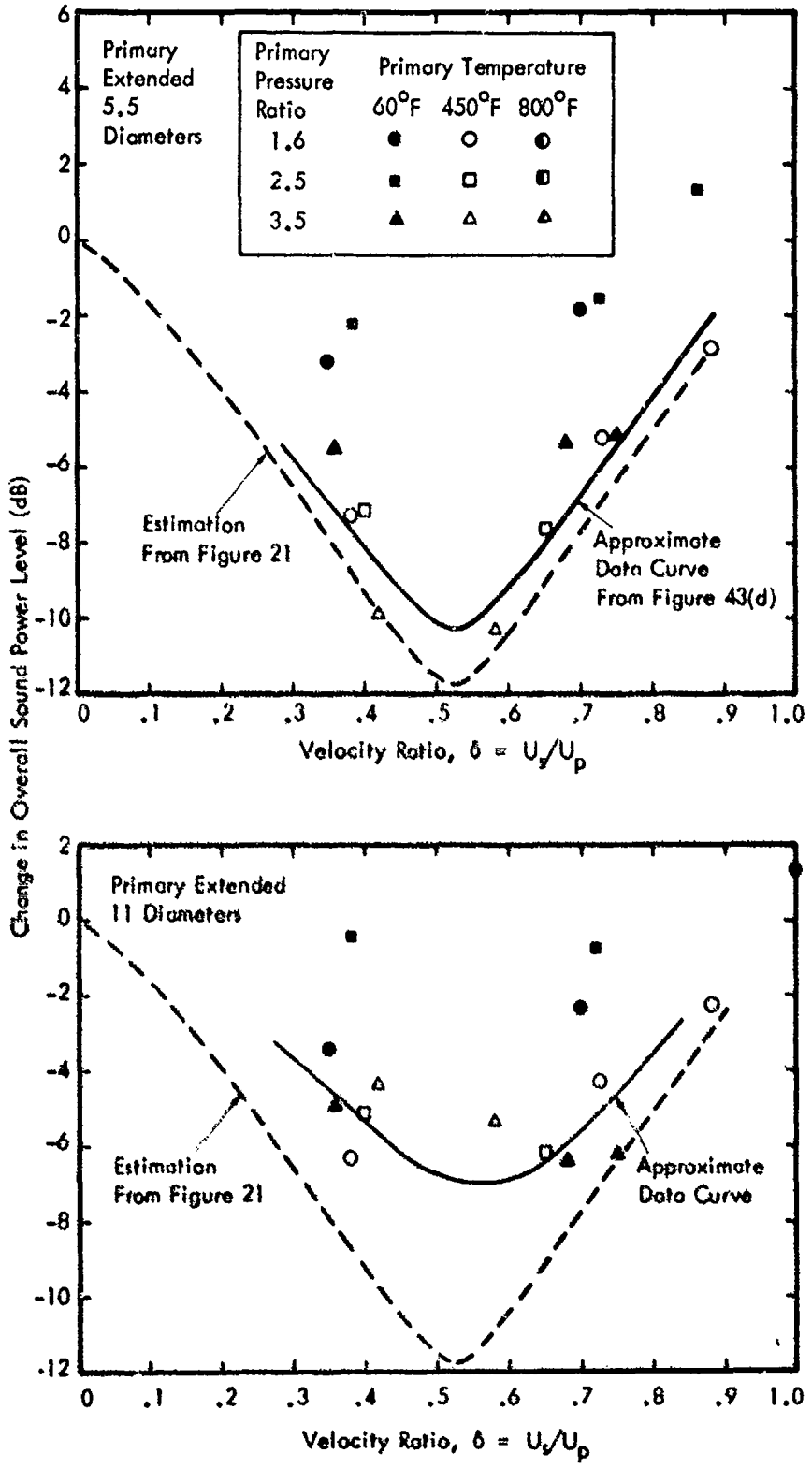

Figure 47. Change in Overall Sound Power Level with Velocity Ratio for Coaxial Jets with a Nozzle Area Ratio of 10 and Thrust of 20,000 Lbs. Change is Measured Relative to a Single-Nozzle Jet which has Equal Thrust and a Velocity Equal to U_p.

Assuming that the primary is retracted sufficiently that it completely mixes with the secondary flow prior to exiting from the secondary nozzle and its noise does not radiate through the nozzle, the average or effective velocity through the nozzle would be expected to be given by:

$$U_e \cong \frac{4(m_s + m_p)}{g} \tag{41}$$

The acoustic power should be proportional to:

$$W_m \sim d_s^2 U_e^8 \tag{42}$$

This situation represents a lower bound on the expected results which was not approached with the configurations evaluated in this study. The obvious upper bound is given by the assumption that all the noise of the primary mixing into the slow moving secondary is radiated through the nozzle and adds to the noise generated by the jet issuing from the secondary nozzle as it mixes with the ambient. Also, at low pressure ratios, additional noise might be expected from the turbulence generated in the plenum as it is convected downstream, outside of the secondary nozzle. The true situation for these data obviously lies between these two bounds.

The basic results for the variation of axial position, including the retracted primary nozzle cases, are given for the pressure ratio 3.5 primary nozzle in Figure 48. The 3.5 pressure ratio nozzle was chosen for discussion because its behavior is reasonably typical of the average data in the coplanar and extended primary nozzle cases, and because its flow parameters underwent the least change in the retracted cases. The changes in noise level for all cases in Figure 48 were based, as before, on the noise of the primary nozzle operating at a fixed total pressure and exhausting into the ambient.

The results illustrate the small increase in noise relative to the coplanar configuration for the area ratio 10 nozzle at both extended positions, as previously discussed. No change is exhibited for the retracted nozzles. For the area ratio 1 and 5 nozzles, however, a small reduction relative to the coplanar case is found in the retracted cases, as well as in the extended cases. The more limited data for the pressure ratio 1.6 nozzle indicate slight increases relative to the coplanar cases for the retracted cases. However, it is not presented in detail since its flow was drastically affected by the secondary plenum pressure, and is not representative of full-scale engine design conditions.

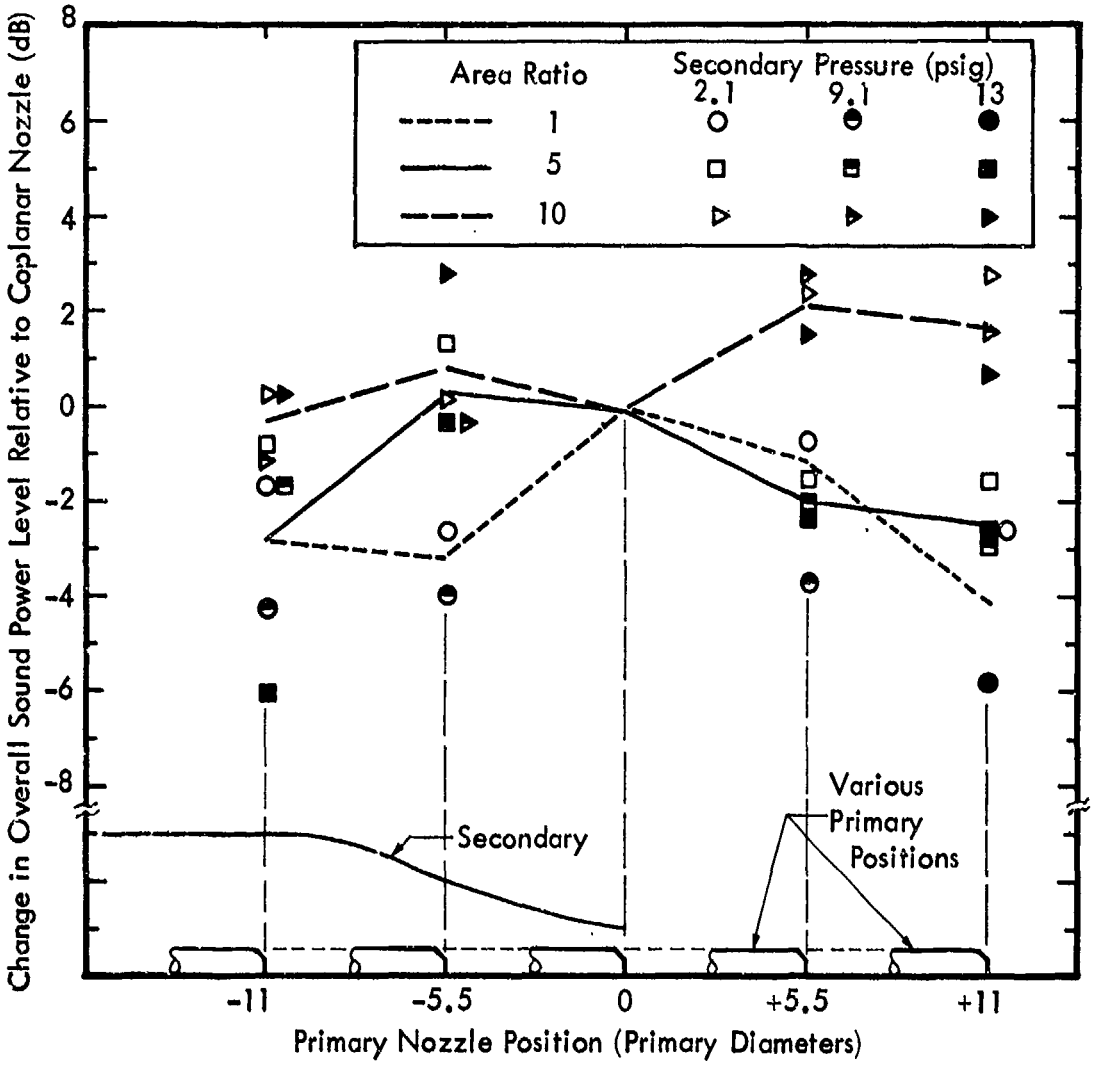

Figure 48. Effect of Axial Position of the Primary Nozzle as Measured by the Change in Overall Sound Power Level Relative to the Level for Each Nozzle and Pressure Combination in the Coplanar Position. In all Cases, the Primary Total Pressure is 36.5 psig (Nominal 3.5 Pressure Ratio) and Total Temperature is Ambient. Lines Connect Averages for Each Area Ratio.

5.1.3 Changes in Sound Power Spectra and Directivity.

The principal changes in overall sound power associated with coaxial jet flows are also illustrated in examining a few typical sound power spectra. Figure 49 shows the sound power spectrum for a model jet configuration which has a primary nozzle with a pressure ratio of 1.6 and total temperature of 450°F, and a coplanar secondary nozzle with an area ratio of 10. The spectra are given for four velocity ratios ranging from zero (primary nozzle alone) to 0.88. The spectrum for the velocity ratio of 0.38 is 6 to 7 dB lower than the spectrum for the primary alone in the frequency range above the peak in the spectrum, while at low frequencies its sound power level is slightly above the level of the primary alone. The overall sound power level (at model thrust) is approximately 3 dB lower. This reduction of levels at the higher frequencies demonstrates that the low velocity secondary flow is shrouding the primary flow, thus reducing its acoustical output. The secondary flow would be expected to reduce the high frequencies in preference to the low frequencies because the high frequency acoustic sources are located in the initial mixing region of the primary jet where the effect of the secondary flow is greatest, whereas the lower frequencies are produced downstream where the secondary flow has less effect. Conversely, the increase in low frequency noise generation is to be expected as a result of the larger diameter equivalent jet resulting from the combined flows.

When the secondary velocity is increased to give a velocity ratio of 0.73, the equivalent jet becomes the dominating factor. The spectrum for this jet has a shape that should be expected of a single-nozzle jet with an exit area approximately ten times that of the primary nozzle alone. A final increase in secondary velocity to give a velocity ratio of 0.88 does not significantly change the spectrum shape, but does increase the spectrum levels in proportion to the eighth power of the change in secondary velocity. All of these results are consistent with the simple theoretical model postulated in Section 2.3.

Figure 50 shows the effect of extending the primary nozzle beyond the secondary. Comparing Figures 49 and 50, the effect of shrouding the primary can be seen to have nearly disappeared for the velocity ratio of 0.38 when the primary nozzle is extended eleven (11) primary diameters beyond the secondary nozzle. The spectra for velocity ratios of 0.725 and 0.878 appear to have a few dB less power when the primary is extended than in the coplanar case.

Comparison at a velocity ratio of 0.88 shows little change in the high frequency portion of the spectrum which should be controlled by the initial mixing region of the secondary jet. However, the low frequency portion of the spectrum of the extended primary is lower in level than that of the coplanar case. This result is consistent with the hypothesis that the equivalent jet for the extended nozzle cases should be defined by the flow conditions existing in the plane of the extended primary.

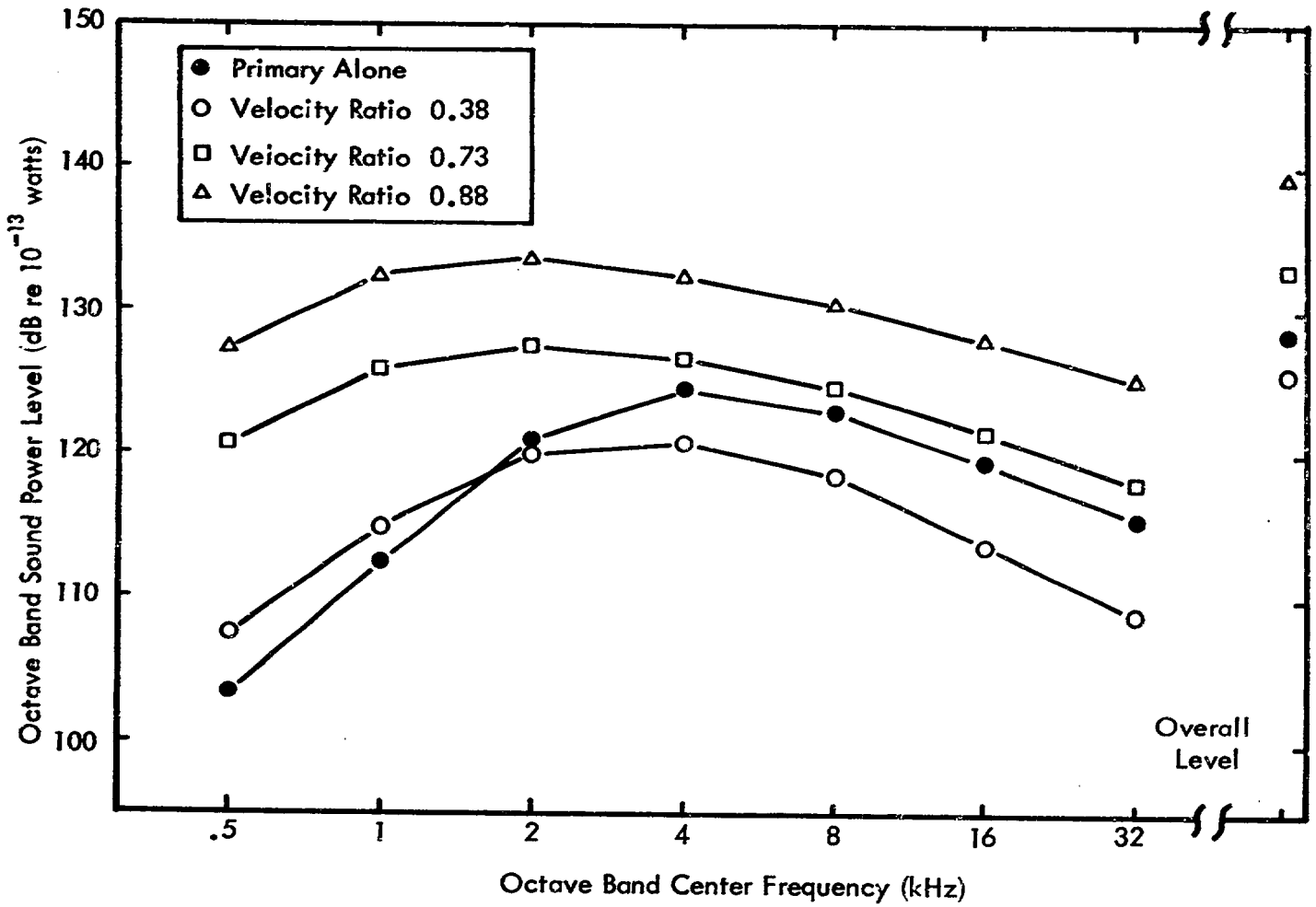

Figure 49. Model Jet Sound Power Spectrum for Coplanar Nozzles (Primary Nozzle Pressure Ratio 1.6, Primary Nozzle Temperature 450°F, Area Ratio 10, Thrust Variable).

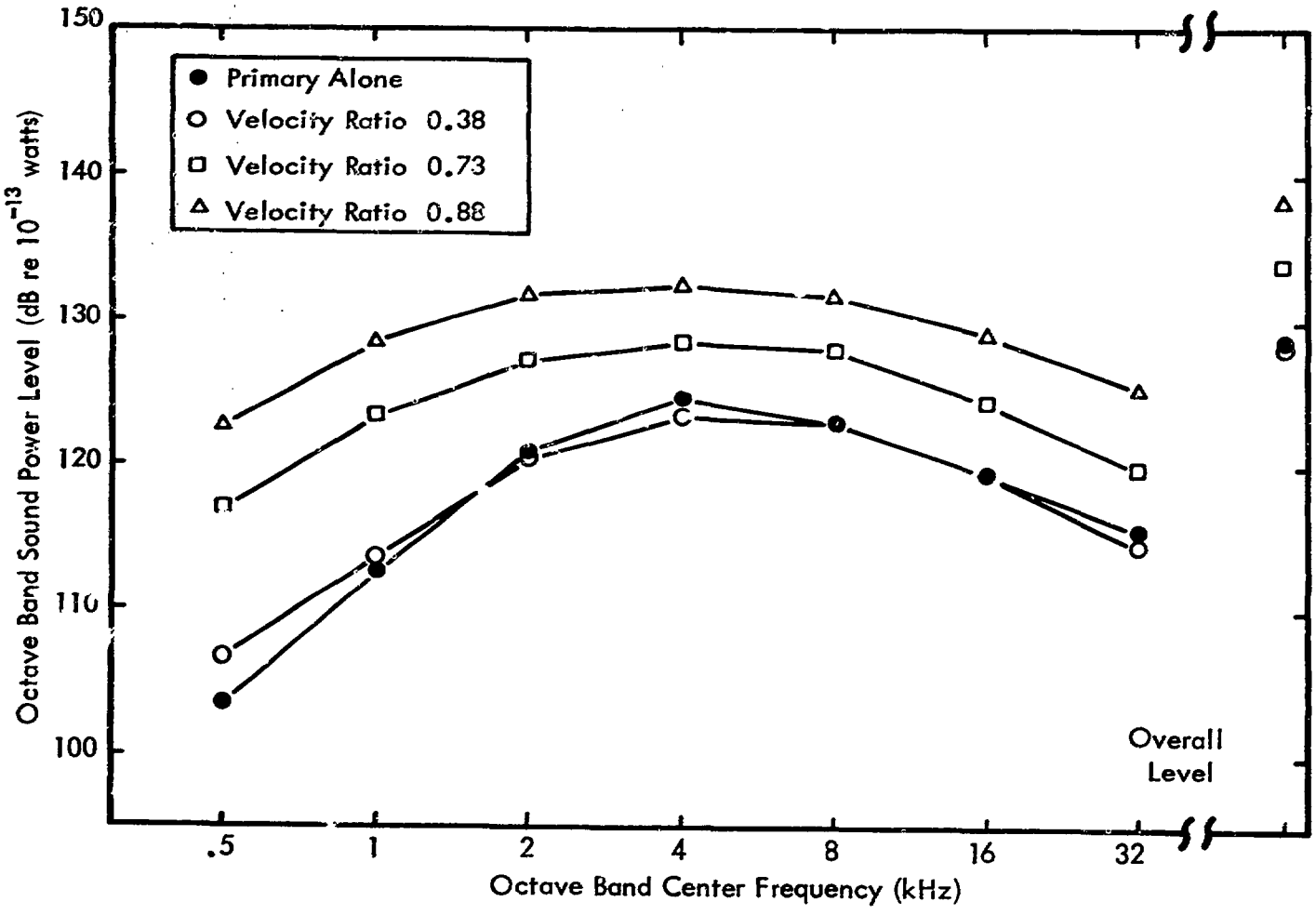

Figure 50. Model Jet Sound Power Spectrum for Fully Extended Primary Nozzle (Primary Nozzle Pressure Ratio 1.6, Primary Nozzle Temperature 450°F, Area Ratio 10, Thrust Variable).

In Figure 51, the effect of area ratio on the shrouding of the primary nozzle is shown for coplanar nozzles at a velocity ratio of 0.38. These results demonstrate that flows from coaxial nozzles with small area ratios have little apparent shrouding effect, whereas flows from the larger secondary nozzles have considerable effect. This result is in accordance with the simple theory, since a secondary nozzle which has an area ratio of only 1 or 2 results in a fairly thin layer of secondary flow around the primary jet. Within a very few nozzle diameters downstream from the nozzle, the primary flow will have developed into a diameter larger than the original secondary nozzle diameter. The primary nozzle flow will therefore tend to behave over most of its length as if there were no secondary flow. It should be emphasized that these spectra are from the model jet, and hence no allowance has been made for varying thrusts. If they were corrected to an equal thrust, a small shrouding effect would be seen for the lower area ratios and an even larger effect would be observed for the higher area ratios.

Accompanying the changes in spectrum are changes in the acoustic radiation directivity pattern. Figures 52 through 55 show the directivity patterns for the flow cases whose spectra are shown in Figure 49. These results show that as the velocity ratio increases, proportionally more sound is radiated at larger angles from the jet flow direction. The 500 Hz and 1000 Hz octave bands do not change directivity very much, but the remainder are affected. The angular position of the peaks in the octave band directivity indices move by a maximum of 10 degrees; but at angles away from the peak, the directivity indices vary by as much as 12 dB in extreme cases near the jet axis and by up to 4 dB at 110 degrees from the axis. As a result, the angle at which the directivity index is zero increases by up to 30 degrees in both cases.

5.1.4 Change in Maximum Sideline Perceived Noise Level.

The effect of the various configurations on the maximum perceived noise level on the 1500-foot sideline is summarized for the coplanar nozzle configurations in Figure 56. This figure gives the data for perceived noise level in the same format used for the overall sound power level in Figure 43, and includes the theoretical prediction curve for power level reduction for reference. There is much similarity between the two sets of figures, although the maximum reduction in perceived noise level for area ratios 5 and 10 is nearly 1 dB greater than the maximum reduction in power level. All the general comments made previously concerning the change in overall sound power level are applicable to perceived noise level.

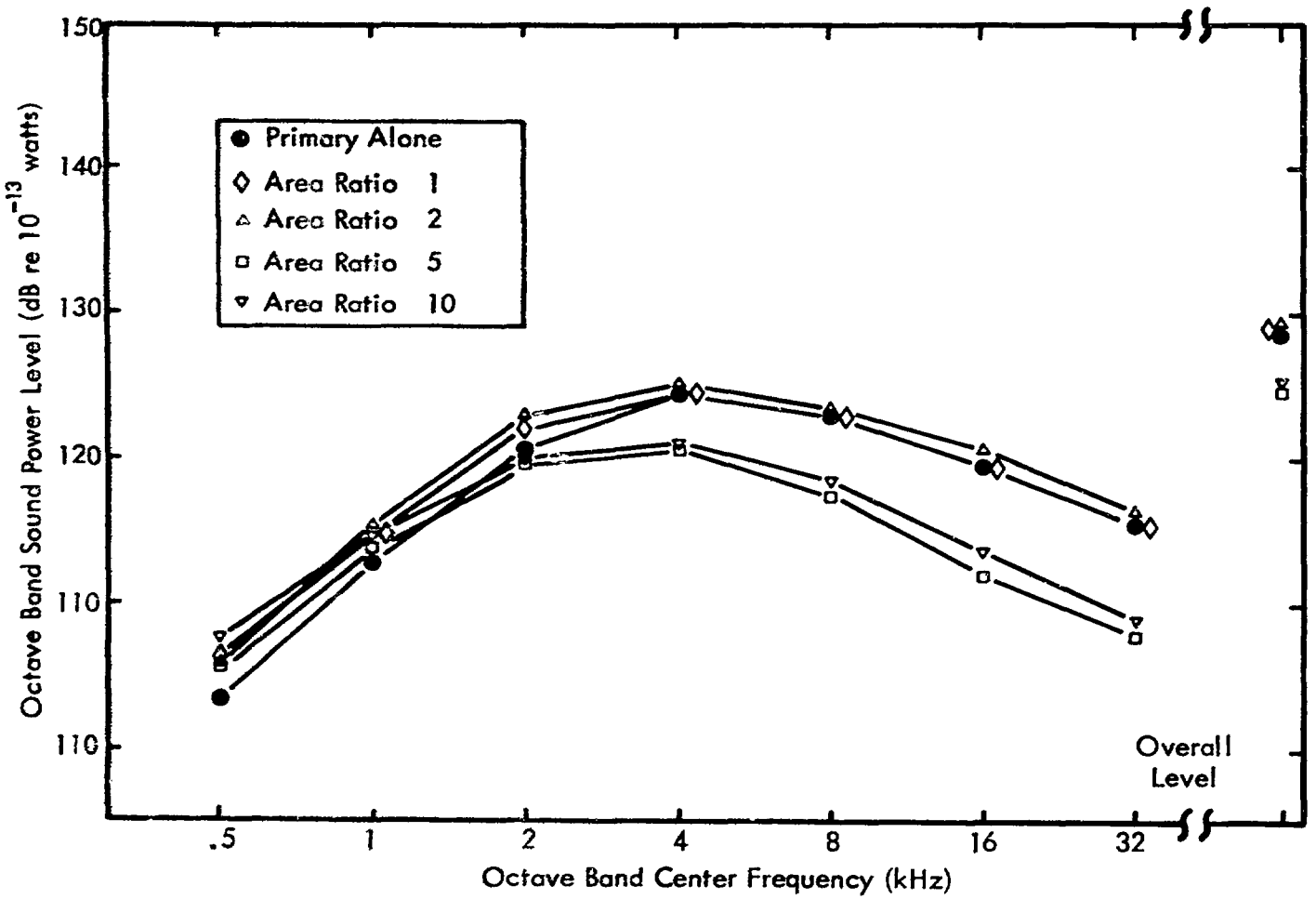

Figure 51. Effect of Area Ratio of Shrouding of Model Primary Jet (Primary Nozzle Pressure Ratio 1.6, Primary Nozzle Temperature 450°F, Velocity Ratio 0.38, Thrust Variable).

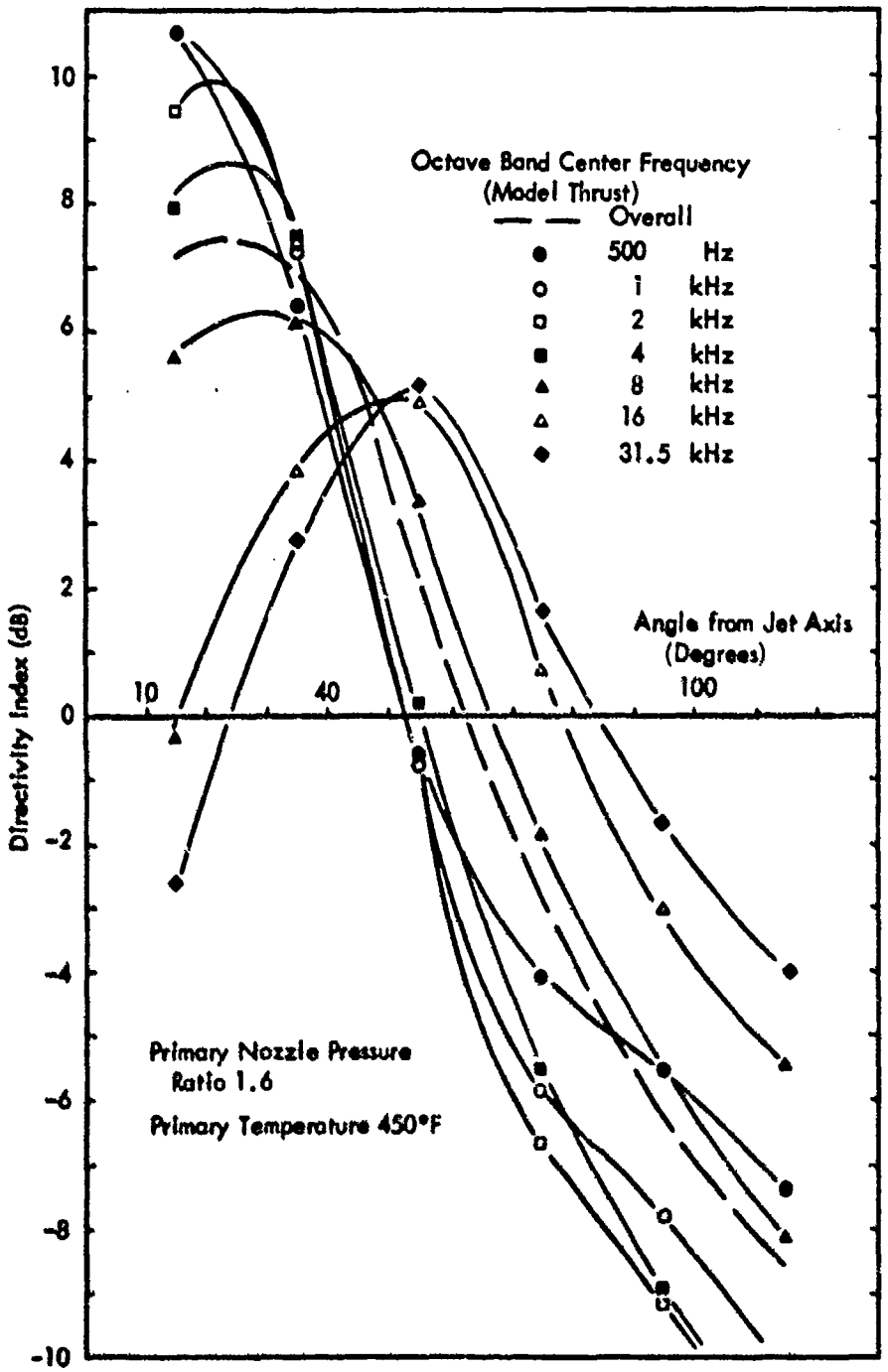

Figure 52. Directivity Pattern for a Primary Nozzle Alone.

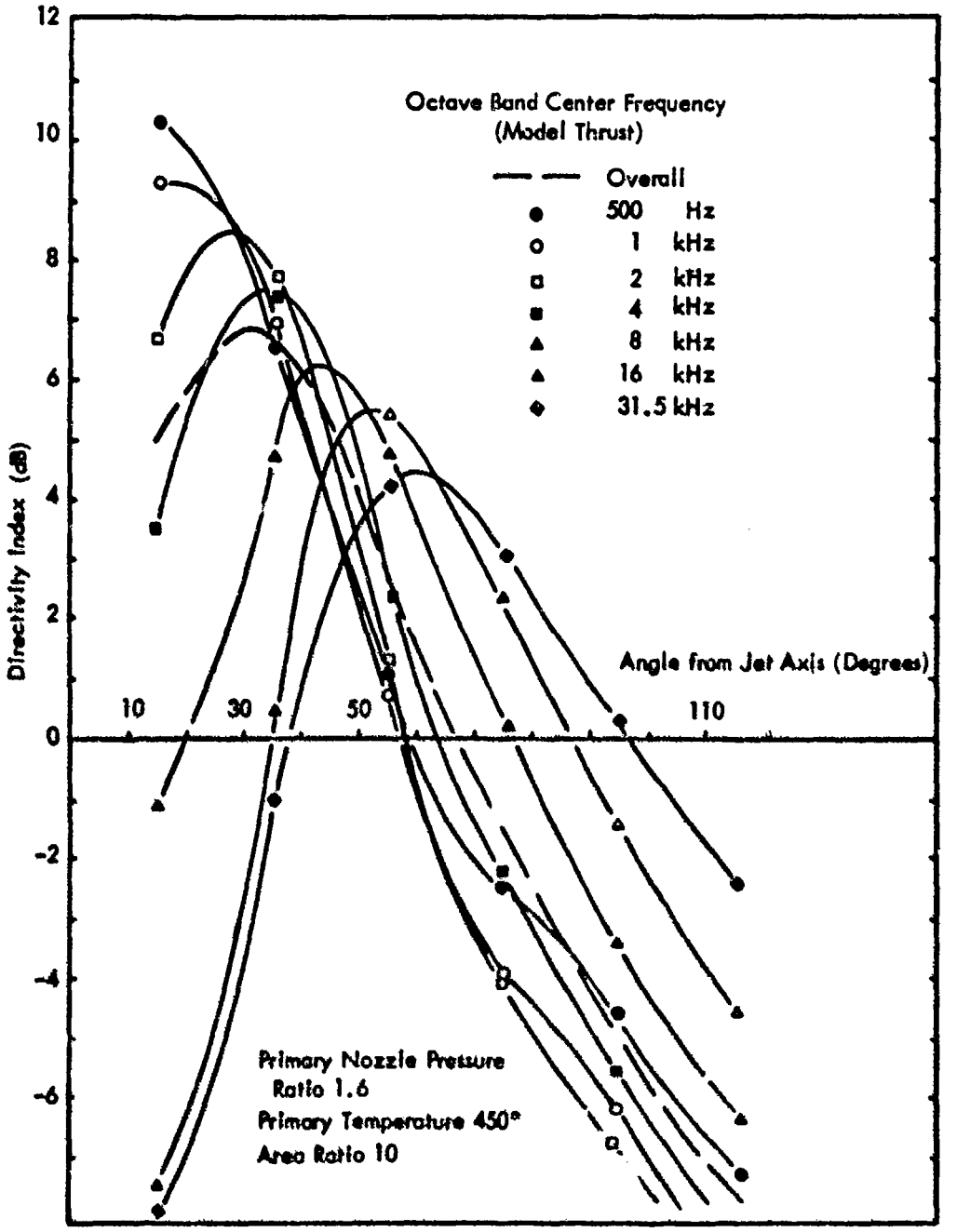

Figure 53. Directivity Pattern of Coplanar Nozzle with Velocity Ratio of 0.375.

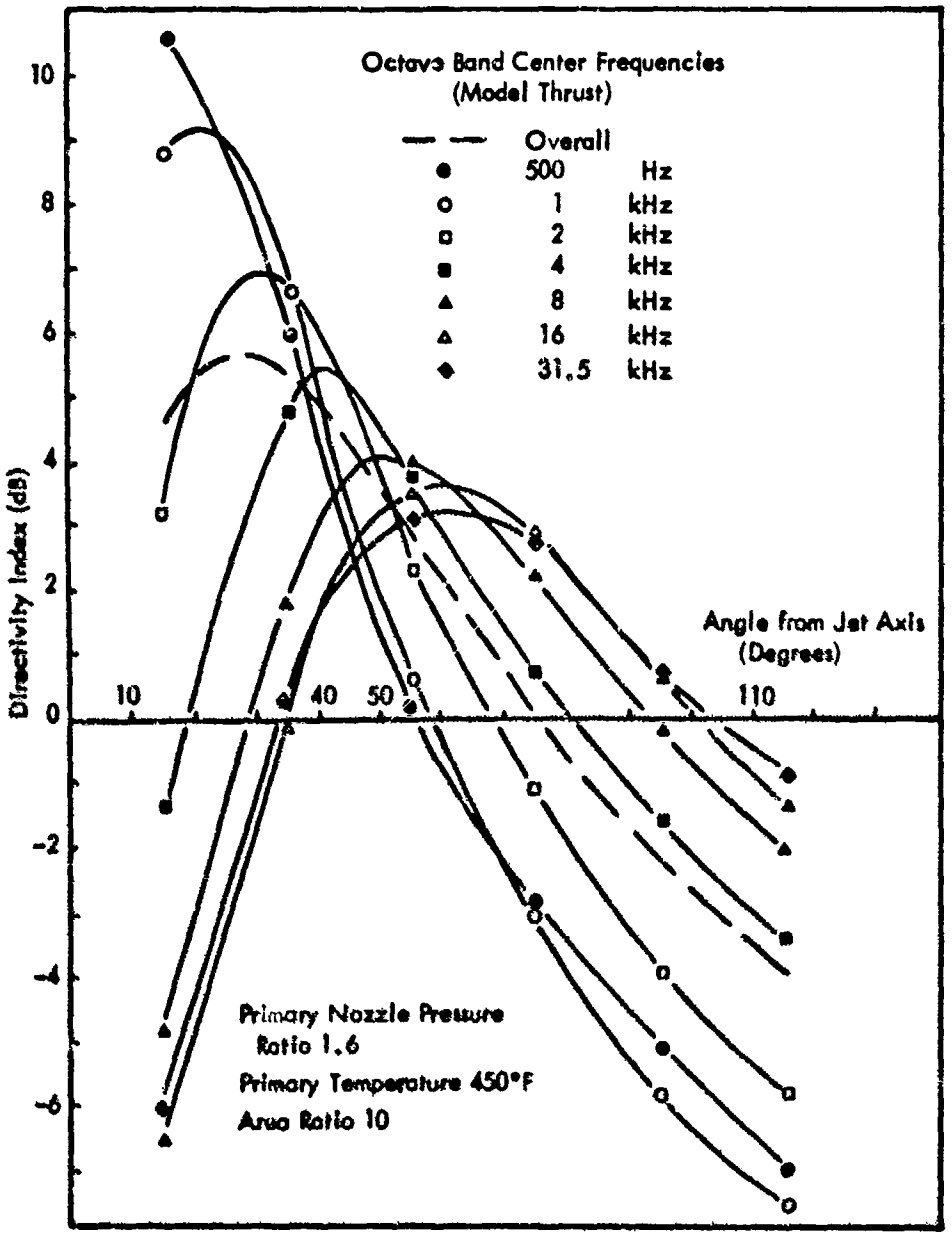

Figure 54. Directivity Pattern for Coplanar Nozzle with Velocity Ratio of 0.731.

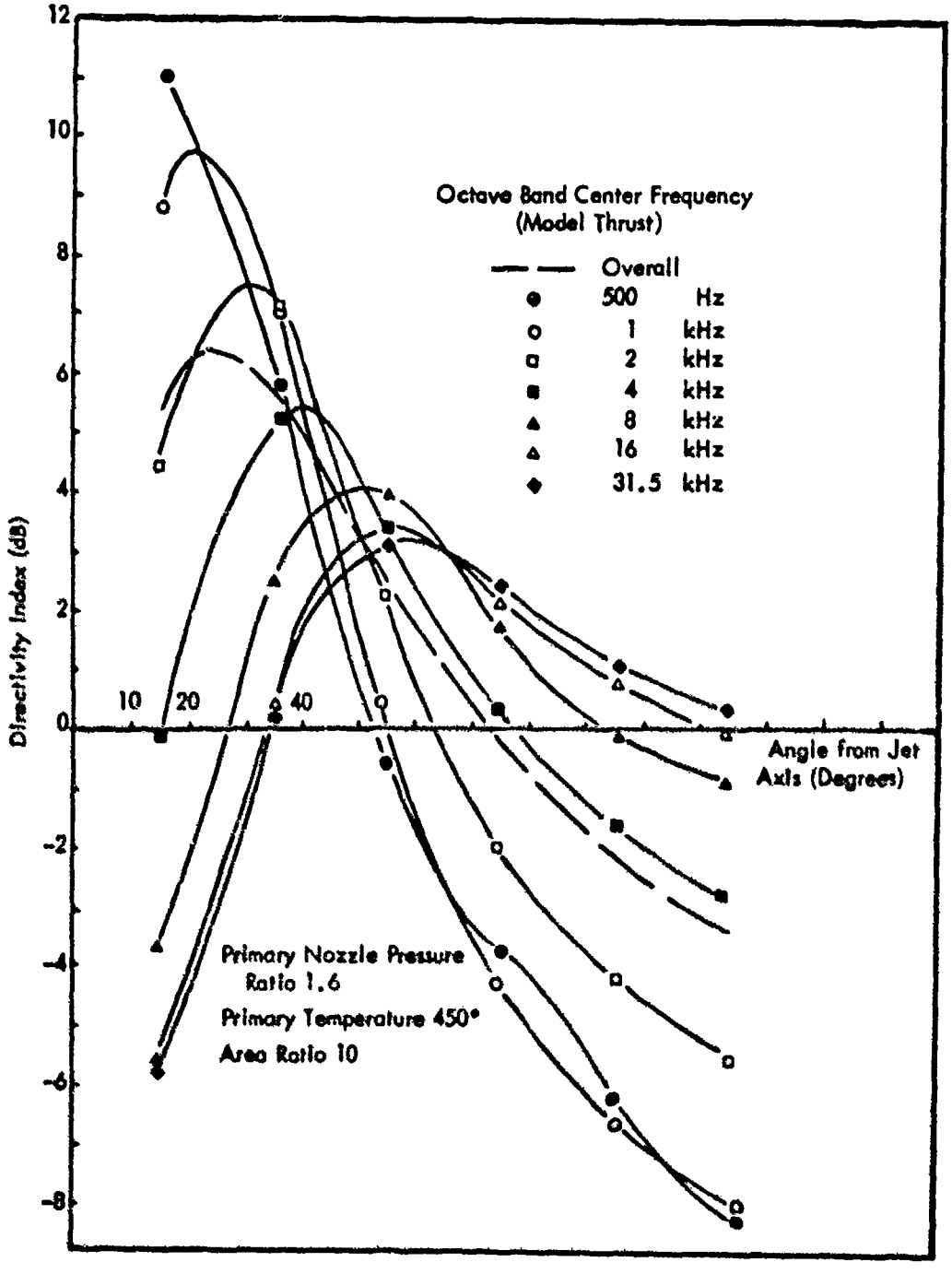

Figure 55. Directivity Pattern for Coplanar Nozzle with Velocity Ratio of 0.88.

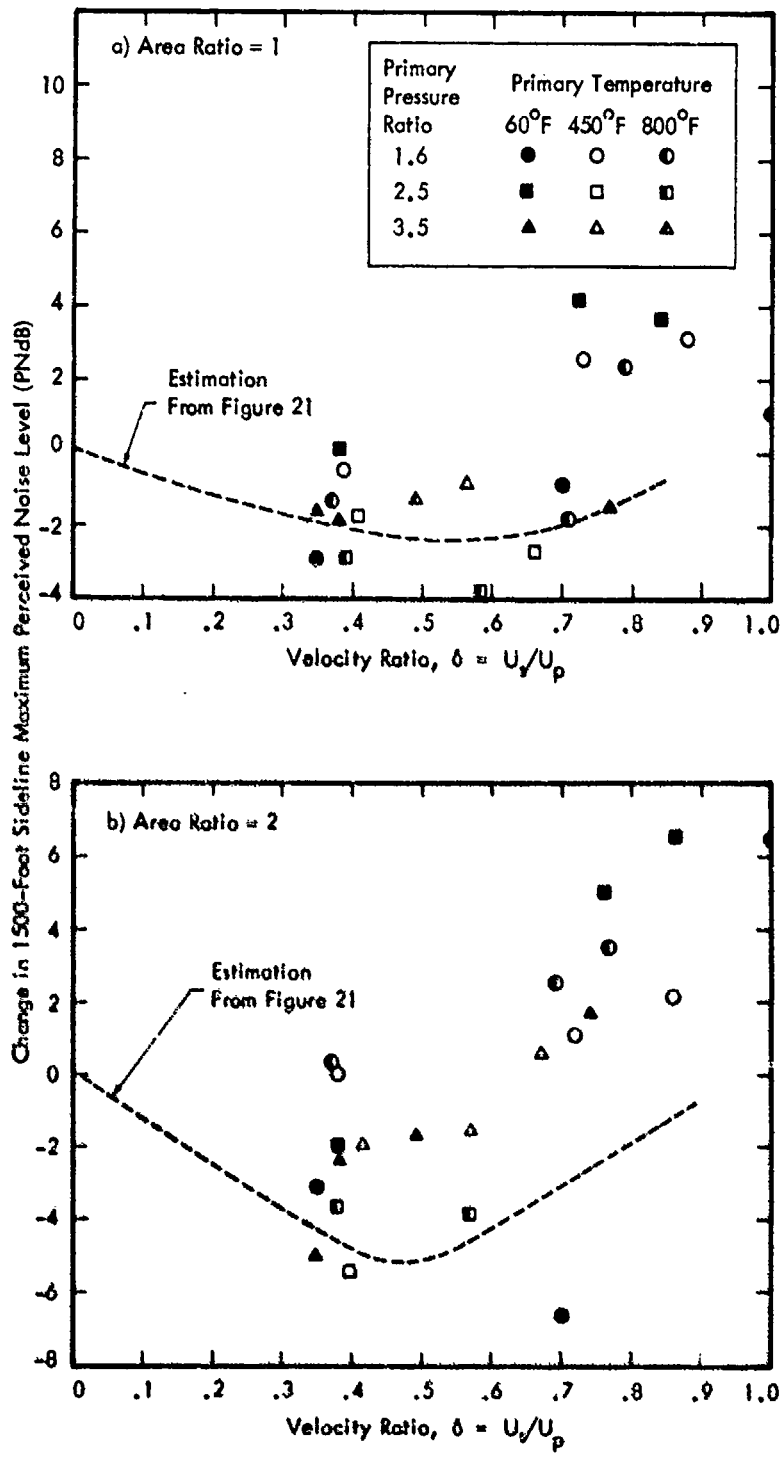

Figure 56. Change in 1500-Foot Sideline Maximum Perceived Noise Level with Velocity Ratio for Coplanar Coaxial Jets of 20,000 Lbs Thrust and Four Area Ratios. Change is Measured Relative to a Single-Nozzle Jet which has Equal Thrust and a Velocity Equal to U_p.

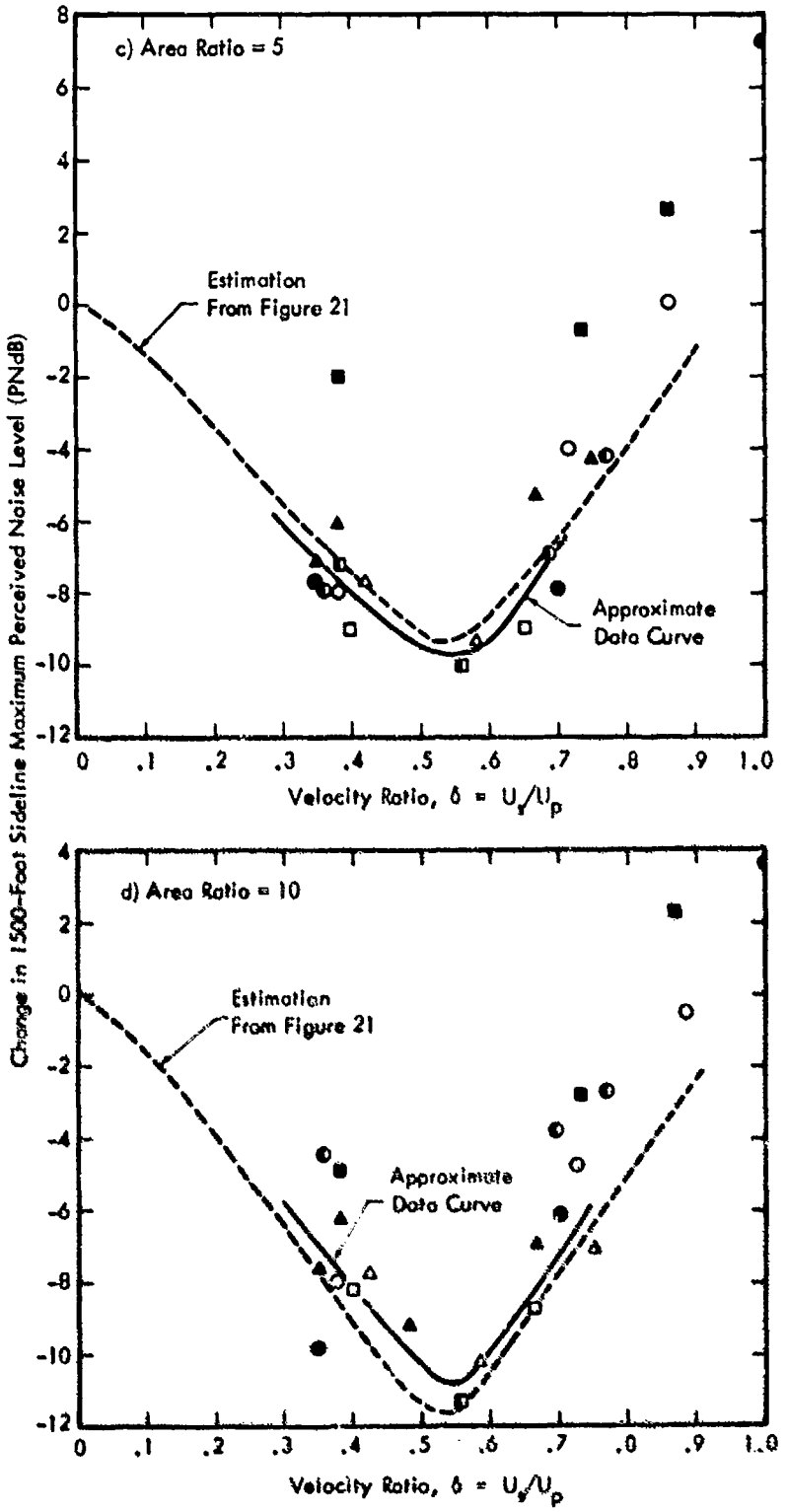

Figure 56. continued ... Change in 1500-Foot Sideline Maximum Perceived Noise Level with Velocity Ratio for Coplanar Coaxial Jets of 20,000 Lbs Thrust and Four Area Ratios. Change is Measured Relative to a Single-Nozzle Jet which has Equal Thrust and a Velocity Equal to U_p.

Figure 57 shows the data for one-half and full extension of the primary nozzle for area ratio 5. The data appear slightly more scattered than the associated overall sound power level data shown in Figure 46. However, they appear reasonably well represented by the coplanar data curve.

Figure 58 gives a presentation of the effect of axial position on the 1500-foot sideline perceived noise level, analogous to the sound power data of Figure 48. The results are similar, but with slightly more scatter.

In general, the changes in maximum perceived noise level are very similar to those of overall sound power level, except that there is a tendency for slightly more scatter in the data. This tendency may result partially from the fact that the maximum perceived noise level is dependent upon a single angular measurement, whereas the sound power is a function of measurements at many angular positions. Also, the perceived noise level is more sensitive to the level in a few octave bands, whereas the overall sound power is a function of most of the octave bands. For both these reasons, the perceived noise level measurement may be inherently more susceptible to minor variations in the experimental process.

In addition, the perceived noise level is affected by any changes in directivity which are associated with the various configurations. The effect of the directivity changes on the variation in perceived noise level along the 1500-foot sideline, shown in Figures 52 through 55, is given in Figure 59. Zero feet on the sideline corresponds to the point directly opposite the jet (i.e., at 90 degrees to the jet axis). The data show that the maximum sideline level shifts along the sideline towards zero feet as the velocity ratio increases. In addition, there is a slight change in the rate at which the perceived noise level falls with increasing distance along the sideline.

5.2 Prediction of the Noise Characteristics of Full-Scale Coaxial Jets

The data and theory presented in this report can be used as the basis for the prediction of the noise characteristics of full-scale coaxial jets. This section develops prediction methods for both the overall sound power level and the 1500-foot sideline maximum perceived noise level, the latter being the principal goal of this study. The principal emphasis is on coplanar coaxial nozzles which are of considerable practical interest. For prediction of non-coplanar coaxial jets, the reader is referred to the discussions in Section 5.1 which consider the effects of axial displacement of the primary nozzle relative to the secondary nozzle. Caution should be exercised in applying this latter data to full-scale geometries which differ significantly from the models studied here.

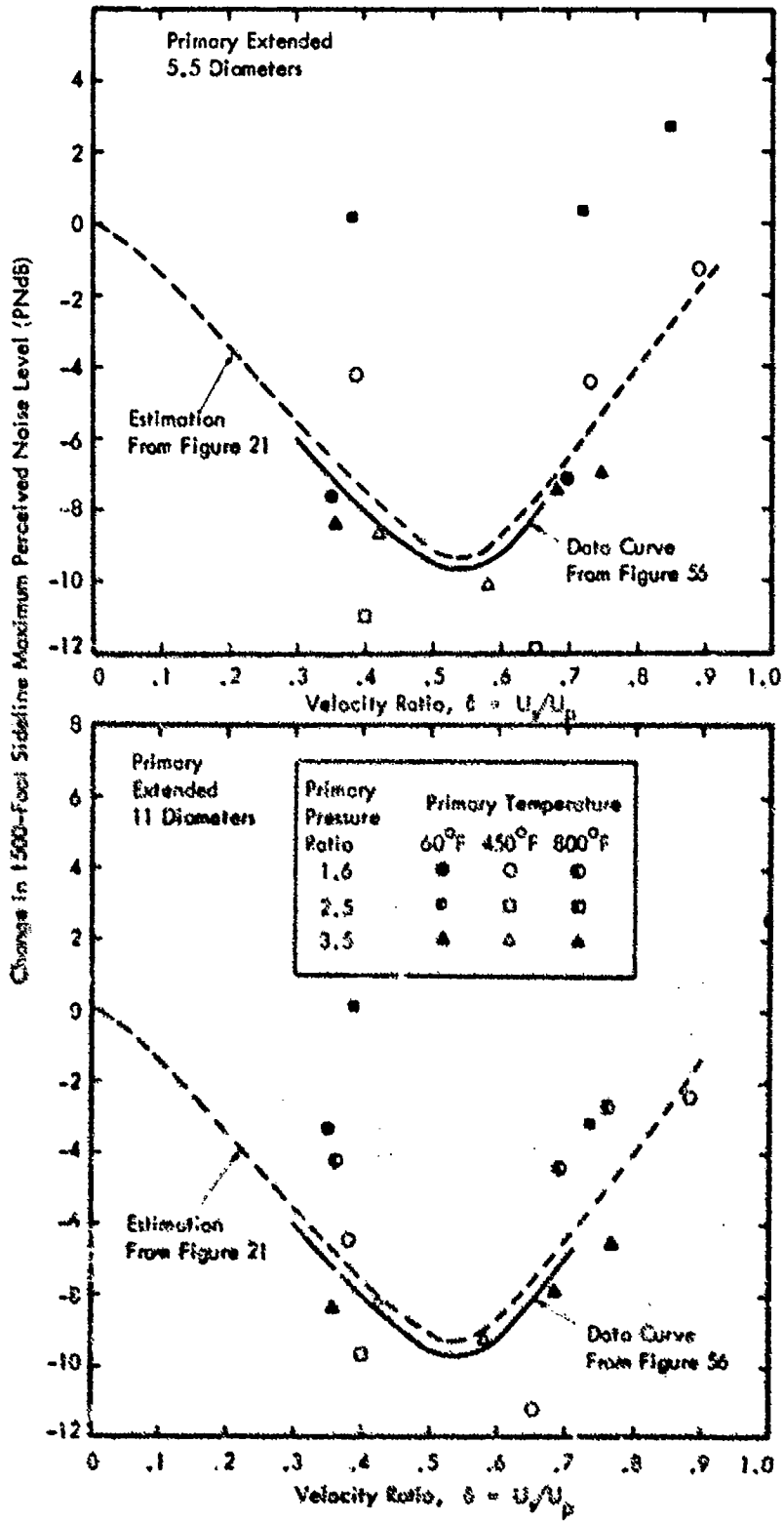

Figure 57. Change in 1500-Foot Sideline Maximum Perceived Noise Level with Velocity Ratio for Coaxial Jets with a Nozzle Area Ratio of 5 and Thrust of 20,000 Lbs. Change is Measured Relative to a Single-Nozzle Jet which has Equal Thrust and a Velocity Equal to U_p.

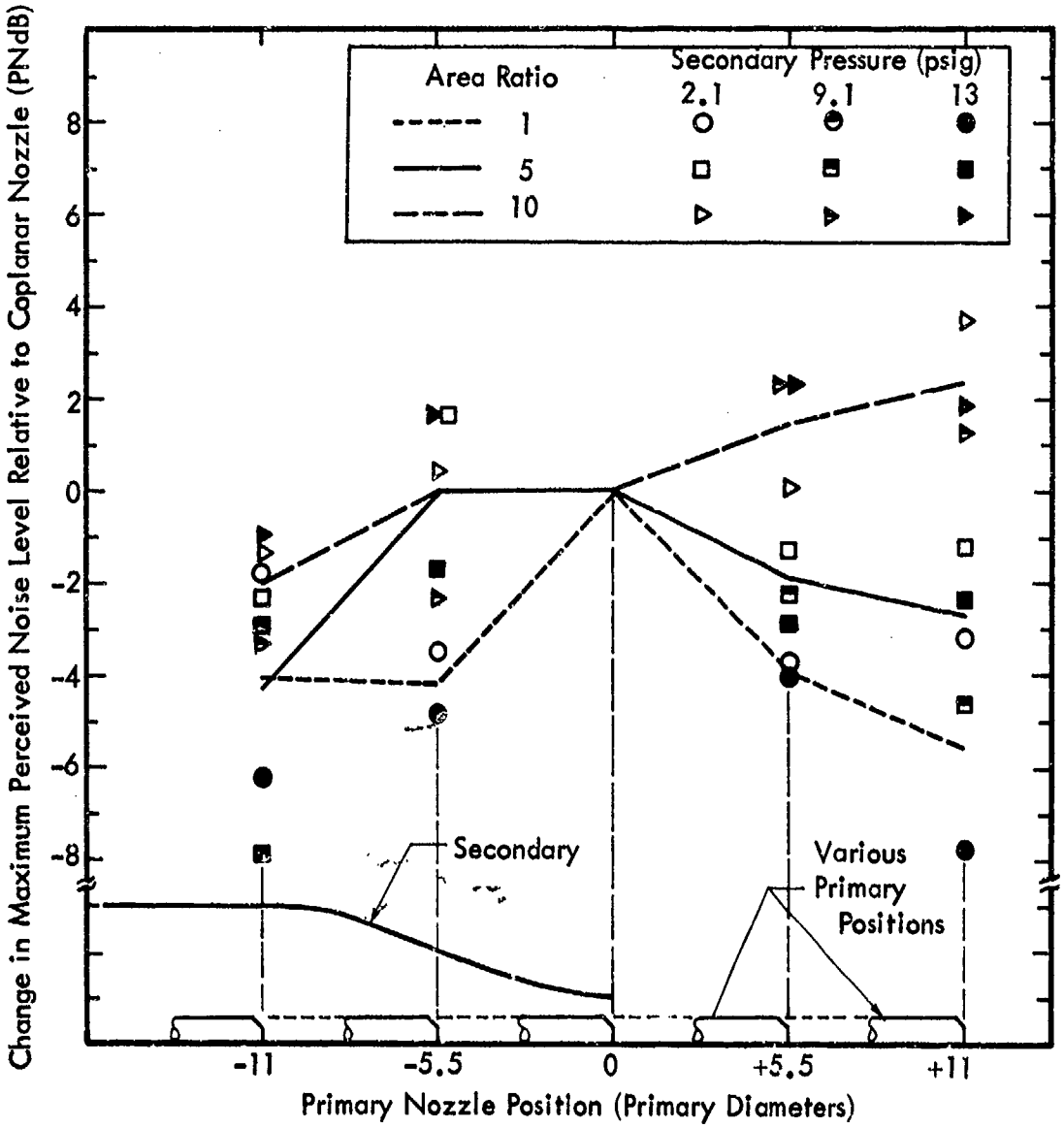

Figure 58. Effect of Axial Position of the Primary Nozzle as Measured by the Change in Maximum Perceived Noise Level in the 1500-Foot Sideline Relative to the Level for Each Nozzle and Pressure Combination in the Coplanar Position. In all Cases, the Primary Total Pressure is 36.5 psig (Nominal 3.5 Pressure Ratio) and Total Temperature is Ambient. Lines Connect Averages for Each Area Ratio.

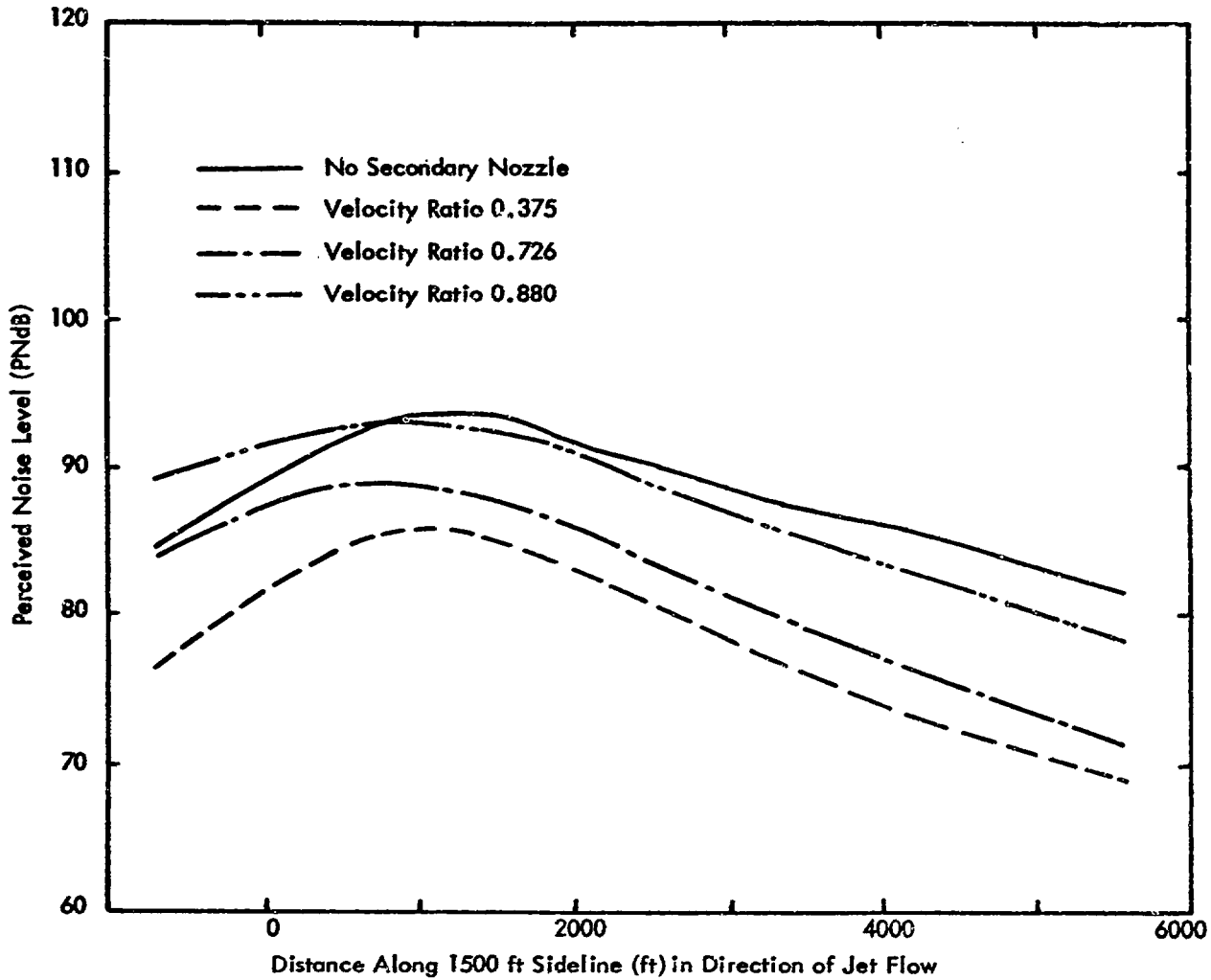

Figure 59. Effect of Velocity Ratio of 1500-Foot Sideline Perceived Noise Level for Coplanar Nozzle (Primary Nozzle Pressure Ratio 1.6, Primary Nozzle Temperature 450°F, Area Ratio 10, Data Scaled to 20,000 Lb Thrust).

The basic predictions for sound power level are developed directly from Figures 40 and 43. The results are given in Figure 60. When $\Delta_{DW} = 0$, the equation at the top of the figure represents the relationship found for zero secondary flow (primary only) from Figure 40 and the basic jet noise scaling laws. The curves which give the decrease of overall sound power level as a function of coaxial jet velocity ratio were obtained from Figure 43. They are based on the approximate data curves, where given in Figure 43, and are supplemented by the theoretical curves from Figure 21 as required for completeness.

Figure 61 presents a similar prediction method for the 1500-foot sideline maximum perceived noise level. When $\Delta_{DP} = 0$, the equation represents the results for the primary flows given in Figures 41 and 42. The curves giving the decrease of perceived noise level as a function of velocity ratio were obtained from Figure 56 in a manner similar to the development of the sound power level prediction curves.

There are two basic potential sources of error in using these two figures for prediction of the noise of a specific full-scale engine which has coplanar nozzles. First is the potential error in estimating the noise for the reference primary jet which may be expected to vary approximately ± 2 dB about the mean data line. Second, the model data for the coaxial flows, ignoring anomalous data, show a scatter of ± 1-2 dB about the mean curves, describing the decrease of noise as a function of velocity and area ratio. These two errors might be expected to add in a mean square sense to give a total error of just under ± 3 dB for a specific prediction.

However, for tradeoff studies leading to engine optimization for noise, these prediction methods should be quite accurate, particularly since the simple theory appears to be in basically good agreement with the mean of the experimental results.

Figures 60 and 61 again demonstrate that the minimum noise for a coplanar coaxial jet with a fixed primary velocity and thrust occurs at a velocity ratio of approximately 0.5. The noise characteristics for a family of engines meeting this criterion and having 20,000 lbs. thrust and various area ratios are given in Figures 62 (power) and 63 (perceived noise).

From one viewpoint, however, the results presented in Figures 62 and 63 are more an indication of the potential remedial effects of a secondary flow. From a purely design viewpoint, the approach to optimization proceeds in a different manner. In engine design, the design thrust is one of the principal specified objectives. For a single nozzle with a given pressure ratio, the thrust produced is independent of the flow temperature. However, the noise produced by the jet is not independent of temperature since higher temperatures imply higher nozzle velocities, and hence more noise.

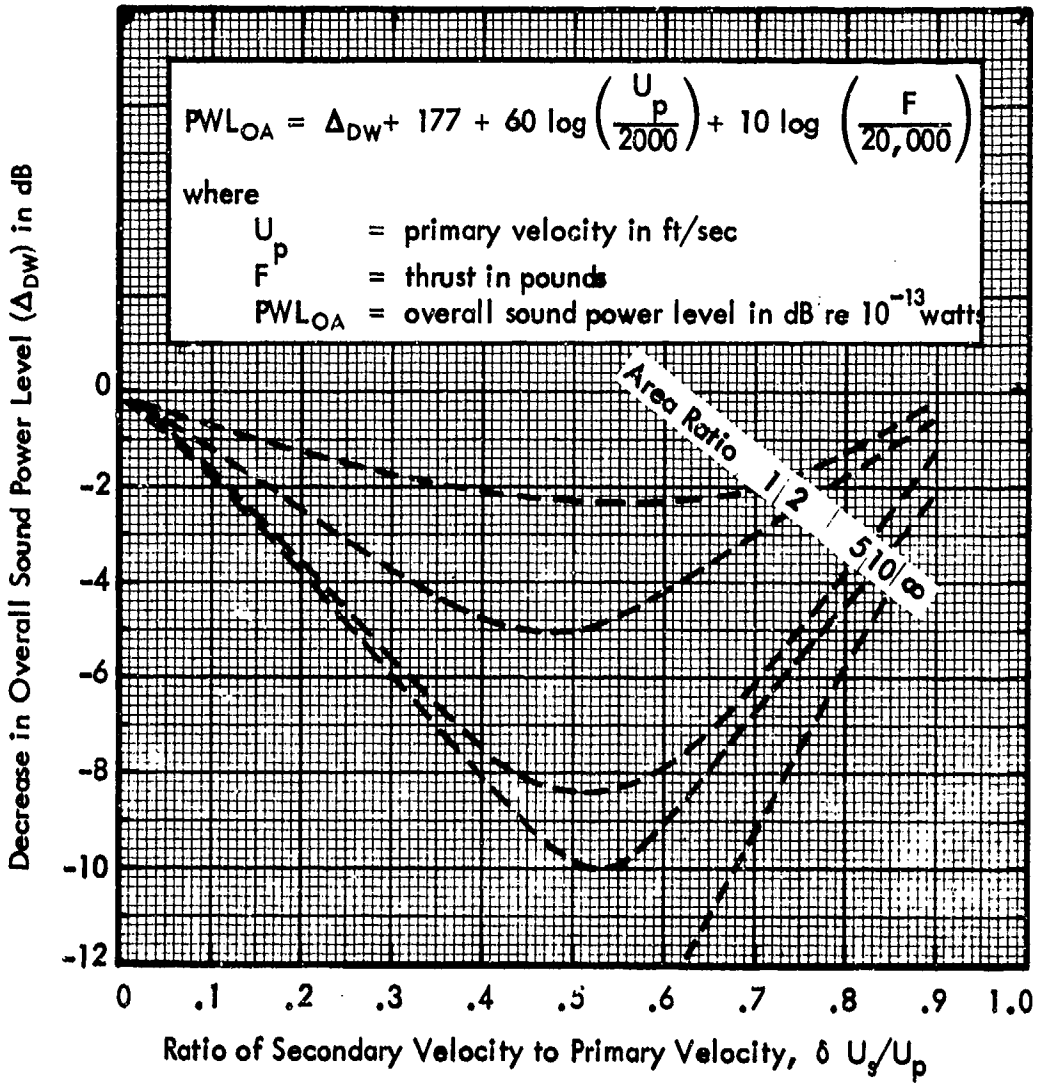

Figure 60. Prediction of Overall Sound Power Level Based on Primary Nozzle Data in Figure 40 and Mean Curves of Experimental Variation in the Decrease in Overall Sound Power with Velocity Ratio for Jets with Coplanar Coaxial Nozzles and Fixed Thrust. Decrease of Coaxial Jet Sound Power Level is Measured Relative to a Baseline Single-Nozzle Jet which has Equal Thrust and a Velocity Equal to the Primary Velocity.

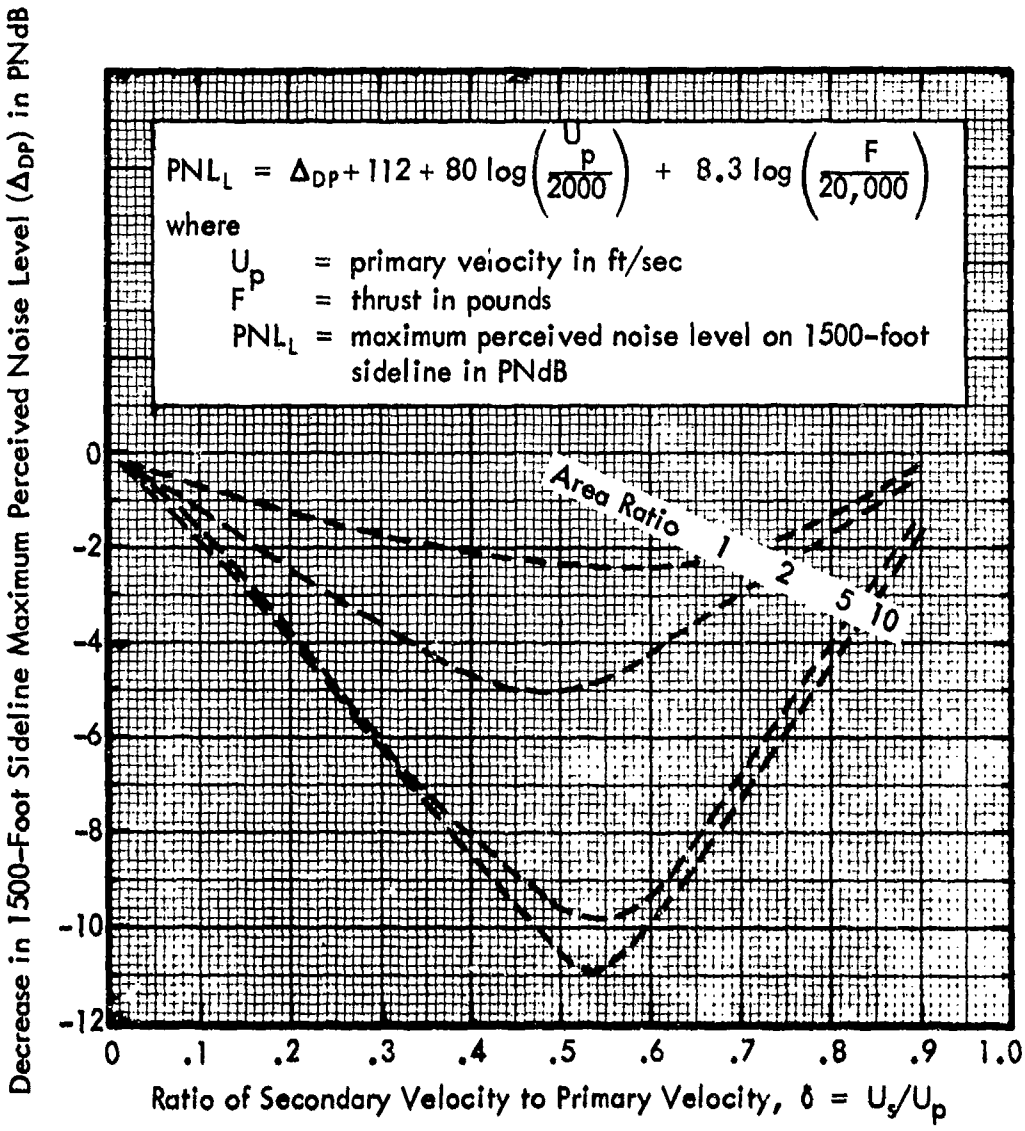

Figure 61. Prediction of 1500-Foot Sideline Perceived Noise Level Based on Primary Nozzle Data in Figures 41 and 42 and Mean Curves of Experimental Variation in the Decrease in 1500-Foot Sideline Maximum Perceived Noise Level for Jets with Coplanar Coaxial Nozzles and Fixed Thrust. Decrease of Sideline Perceived Noise Level is Measured Relative to a Baseline Single-Nozzle Jet which has Equal Thrust and a Velocity Equal to the Primary Velocity.

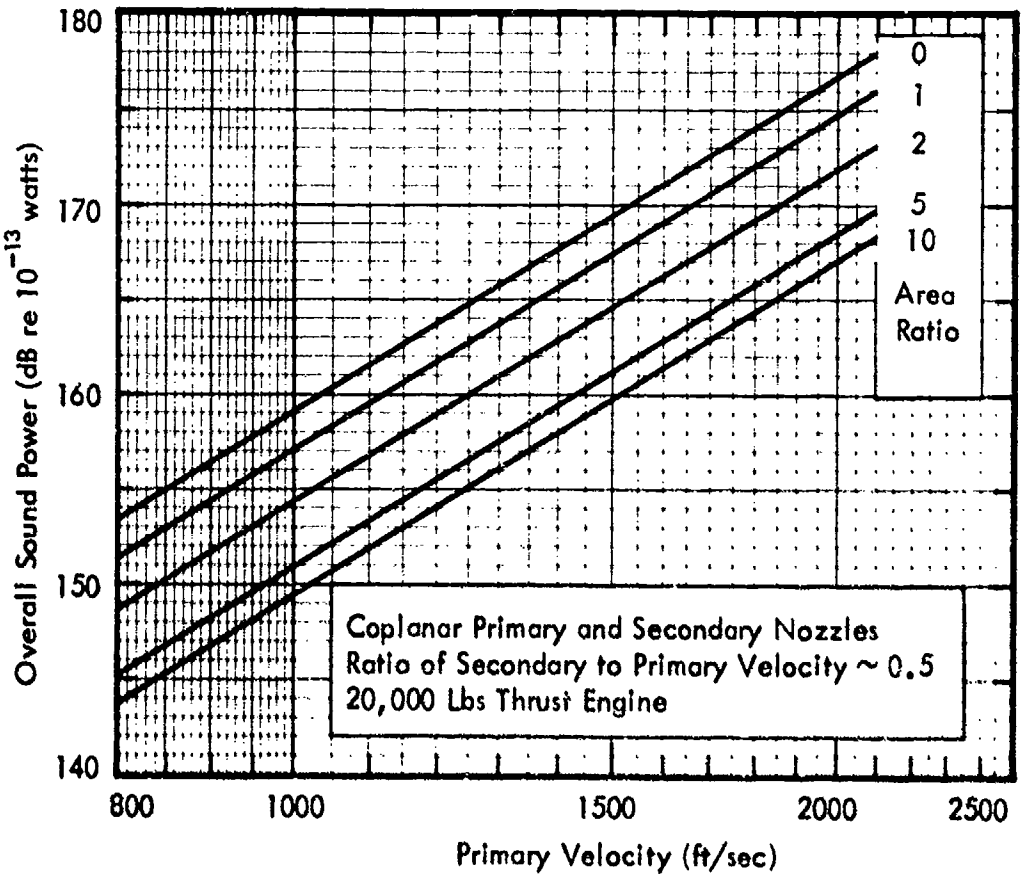

Figure 62. Variation of Minimum Sound Power as a Function of Area Ratio and Primary Velocity.

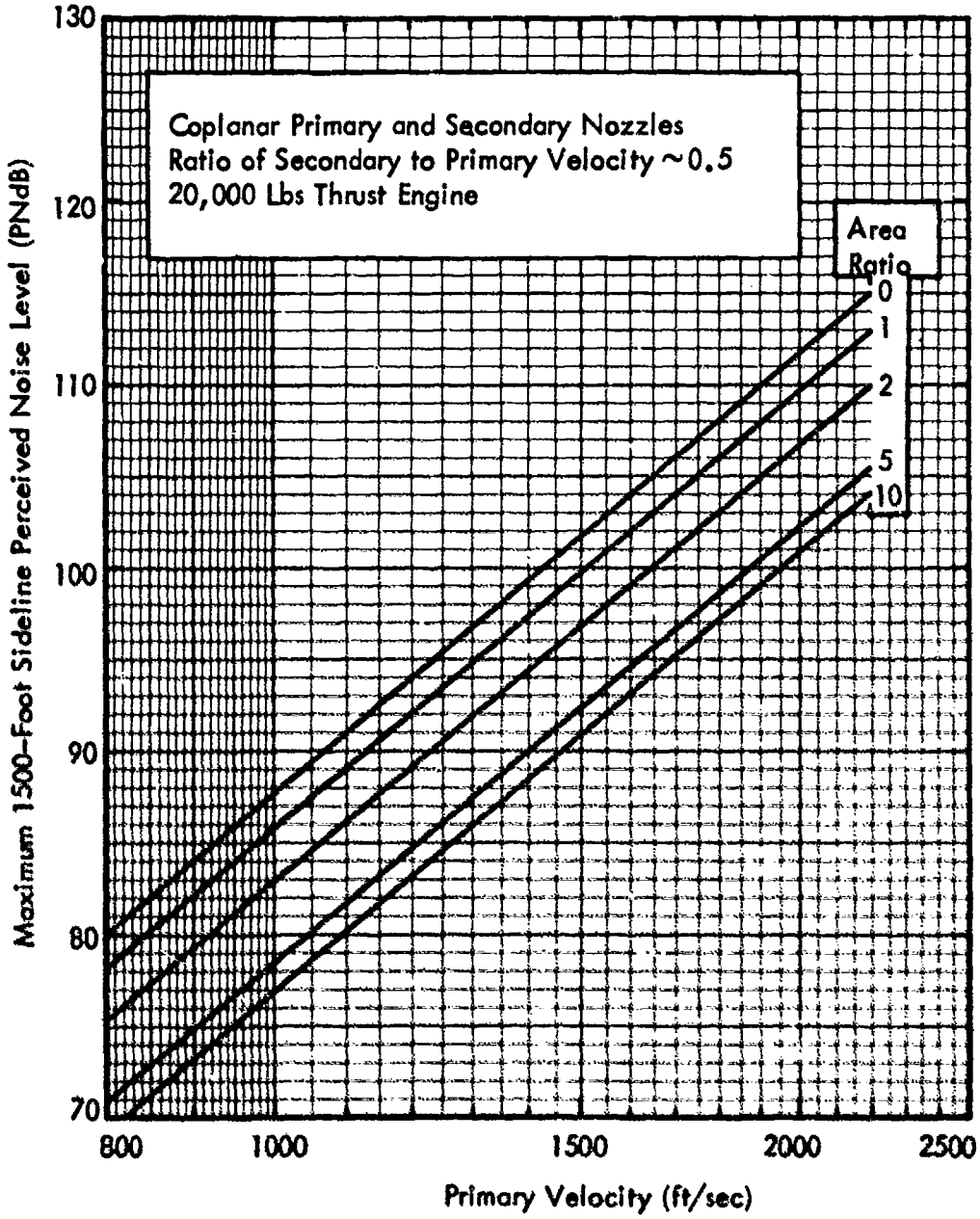

Figure 63. Variation of Minimum Value of the Maximum Perceived Noise Level on a 1500-Foot Sideline as a Function of Area Ratio and Primary Velocity.

From an acoustic viewpoint, it is therefore important to keep the jet temperature as low as possible, which means that a jet total temperature equal to ambient temperature is the possible minimum. The jet exhaust velocity, and hence the noise, can be reduced still further by reducing the nozzle pressure ratio as much as possible. There is obviously some practical minimum to the pressure ratio so that the resultant jet engine will produce the necessary thrust without becoming unnecessarily large with attendant weight and drag penalties. For takeoff conditions and engines with fixed convergent nozzles, that practical pressure ratio is most likely to be somewhere in the region of the critical pressure ratio, or slightly below, so that the engine is still efficient at cruise conditions. From an acoustic viewpoint, therefore, a practical optimum single jet engine should produce a jet exhaust at sonic pressure ratio with an exhaust temperature as near ambient as possible.

These conclusions were reached from an examination of a single jet nozzle. But for present-day jet engines, the requirements for optimum conditions actually apply to the bypass flow of practical bypass jet engines. For modern engines, the secondary flow temperature is only slightly greater than ambient temperature, and optimum overall performance generally dictates that the pressure ratio at takeoff thrust be slightly less than critical. For such designs, it is very instructive to interpret the noise reduction results using the secondary flow velocity as a fixed parameter and determine the amount of the detrimental effect on the engine's noise characteristics resulting from a higher temperature, higher velocity primary flow.

Figure 64 shows the predicted increase in overall sound power level (Δ_{lw}) for various values of aaea ratio as a function of the ratio of primary jet velocity to secondary jet velocity. The equation for the predicted sound power level and the design curves in the figure is a restatement of the information in Figure 60.

Figure 65 gives a similar presentation of the increase in the maximum perceived noise level on a 1500-foot sideline, developed from Figure 61.

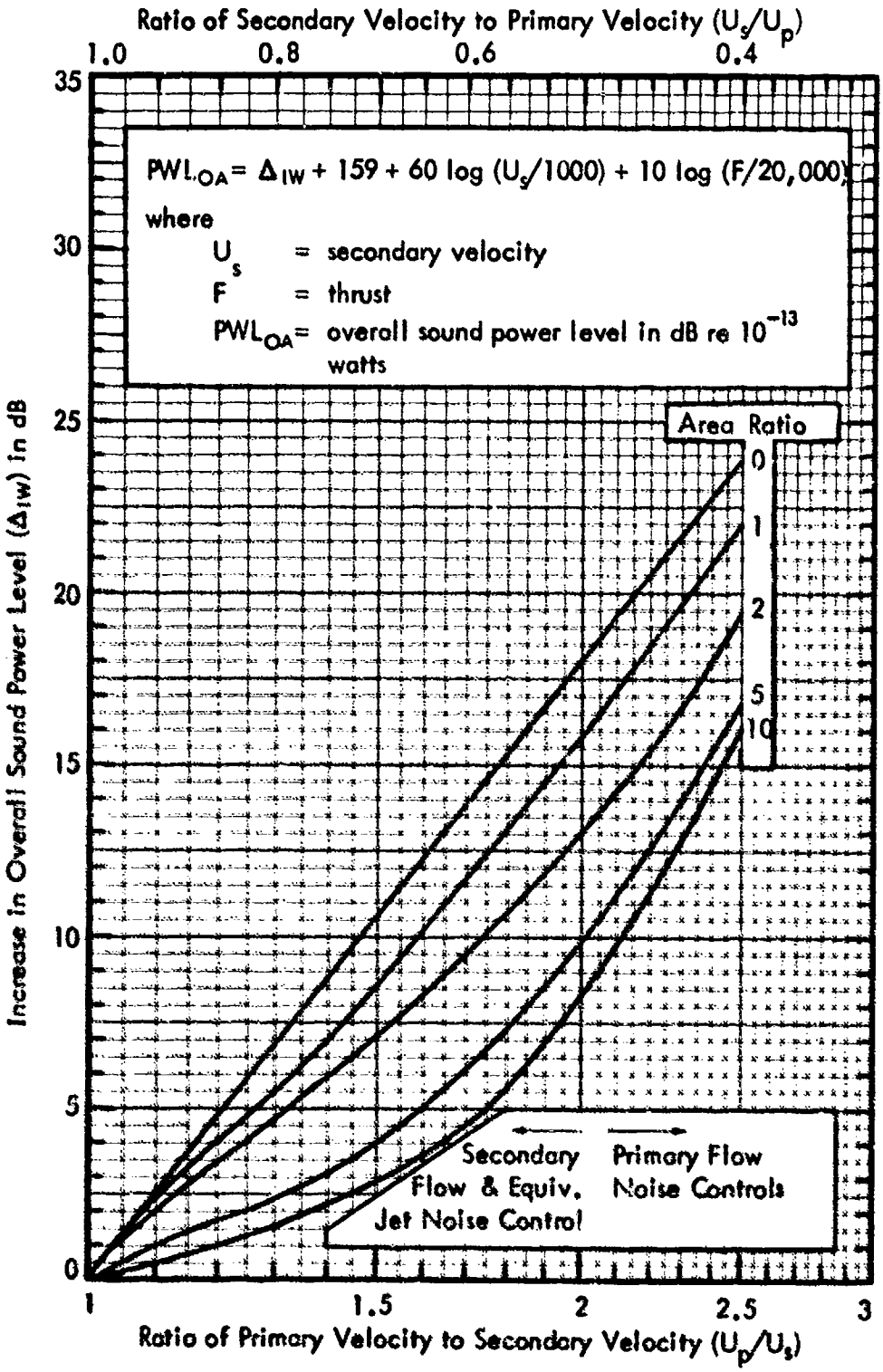

Figure 64. Prediction of Sound Power Level for a Coaxial Jet Using Secondary Velocity for Reference.

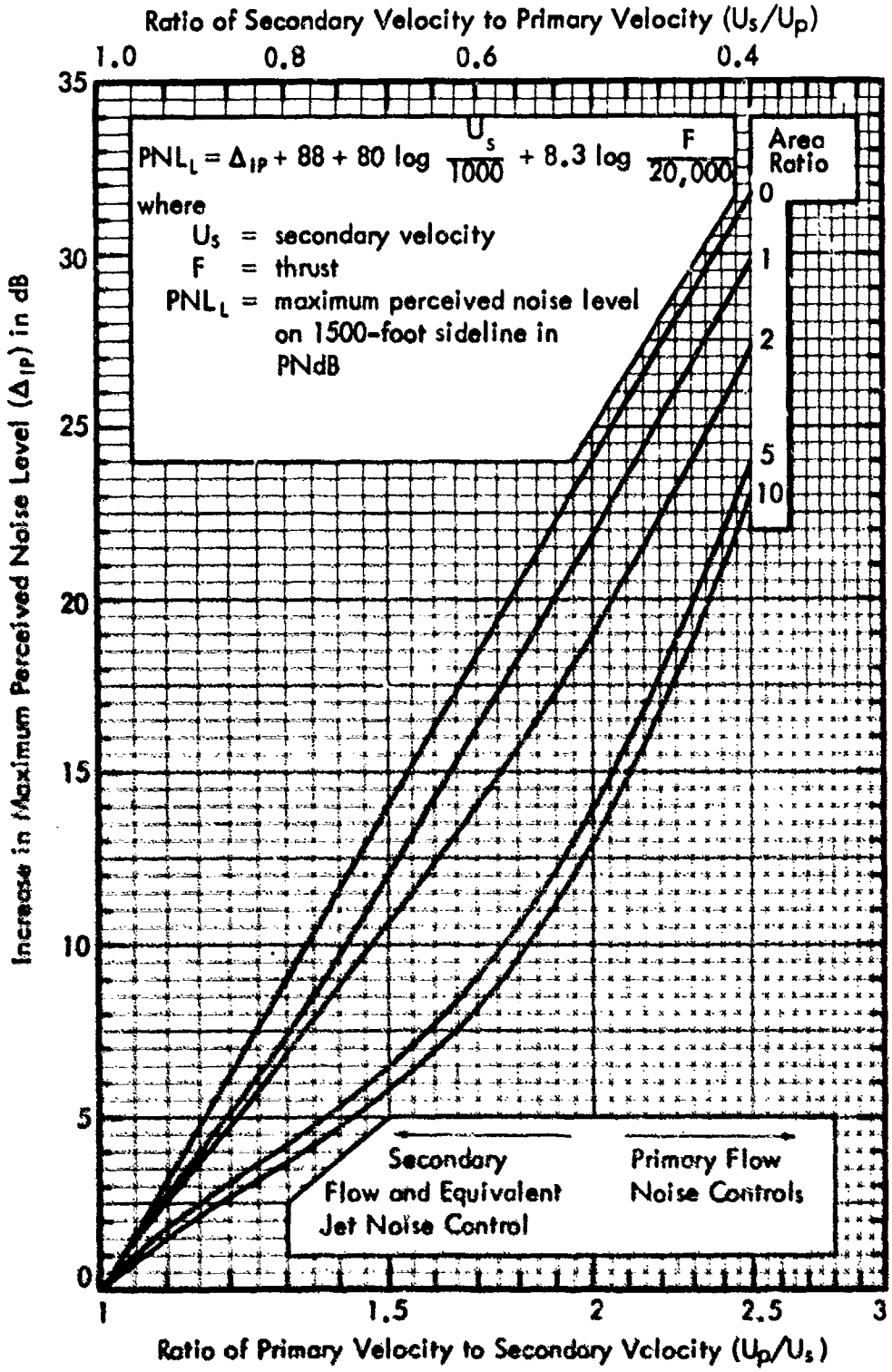

Figure 65. Prediction of Maximum Perceived Noise Level on a 1500-Foot Sideline for a Coaxial Jet Using Secondary Velocity for Reference.

Tables 3 and 4 give the velocity ratios (primary velocity to secondary velocity) which cause either a 3 dB or 6 dB increase in overall sound power or maximum perceived noise level on a 1500-foot sideline relative to the noise at a velocity ratio of 1. It will be noticed that there is a considerable difference between power level and perceived noise level in sensitivity to the ratio of primary-to-secondary flow velocity. For example, for a coplanar nozzle with area ratio of 10 and primary velocity ratio of approximately 1.5, there is only a 3 dB increase in overall sound power output, but a 6 dB increase in 1500-foot sideline perceived noise level. These differences are the penalties resulting from having a primary velocity 50 percent greater than that of the secondary. This greater sensitivity of perceived noise level to changes in velocity ratio is due to the fact that the overall power level for fixed thrust increases in proportion to velocity to the sixth power, whereas the perceived noise level increases in proportion to velocity to the eighth power.

Table 3

Primary Velocity Ratios (U_p/U_s) for a 3 dB and 6 dB Increase in Overall Power Level from Figure 64

Power Level Increase	Area Ratio			
	1	2	5	10
3 dB	1.14	1.17	1.40	1.52
6 dB	1.34	1.42	1.70	1.85

Table 4

Primary Velocity Ratios (U_p/U_s) for a 3 dB and 6 dB Increase in Sideline Perceived Noise Level from Figure 65

Perceived Noise Level Increase	Area Ratio			
	1	2	5	10
3 PNdB	1.11	1.12	1.18	1.23
6 PNdB	1.29	1.22	1.37	1.53

It should be noted that a primary-secondary velocity ratio of 1.5 is typical of current high bypass ratio engine design, primarily for non-acoustic reasons. This velocity ratio is in the region where the noise produced by the secondary mixing with the ambient and the equivalent jet control the overall sound power characteristics, except at low area ratios where the primary is inadequately shrouded. These concepts were developed in Section 2.3, particularly with reference to Figures 18 and 20.

5.3 Comparison of Noise Characteristics of Practical Coaxial Jet Engines with Optimum Single-Nozzle Engines

If the heat could be extracted from the primary jet, reducing its temperature to near ambient, its velocity would be approximately equal to that of the secondary. In this case, no noise penalty would be associated with the higher speed primary jet and the resulting engine would have near optimum performance and noise characteristics. The following paragraphs compare the acoustic characteristics of such an engine with those of currently feasible coaxial jet engines.

The model jet that comes nearest to this idealized jet is the primary nozzle with a pressure ratio of 1.6 and a flow temperature of 60°F. Its acoustic characteristics can be compared with those of the coplanar jets, which had area ratios of 5 and 10 and primary nozzles with pressure ratio 1.6 but flow temperature of 450°F. These two coplanar jets have primary velocity to secondary velocity ratios of approximately 1.35 and secondary flow velocities of 890 feet per second. The secondary flow therefore has nearly the same flow conditions as the 60°F primary nozzle acting alone, so that these two coplanar runs correspond approximately to the conditions for the area ratio 5 nozzle indicated in Tables 3 and 4, which give a 6 dB increase in sideline perceived noise level and a 3 dB increase in overall sound power.

Figure 66 gives the acoustic power spectra for a 20,000 lb. thrust jet for these three configurations. It shows that the coplanar nozzles with the higher temperature and higher velocity primary jet produce considerably more high frequency noise than does the single-nozzle cold jet. This increased acoustic power at higher frequencies gives an indication as to why the coplanar jet shows a larger increase in perceived noise level than is indicated by the increase in overall sound power level. This conclusion is reinforced by a comparison of the octave band sound pressure spectra shown in Figure 67 for the position on the 1500-foot sideline which has the maximum perceived noise level. This position is at an angle of 55 degrees from the jet axis for the primary jet alone, but is at 65 degrees for the coplanar jets, which indicates the effect of changes in the directivity pattern.

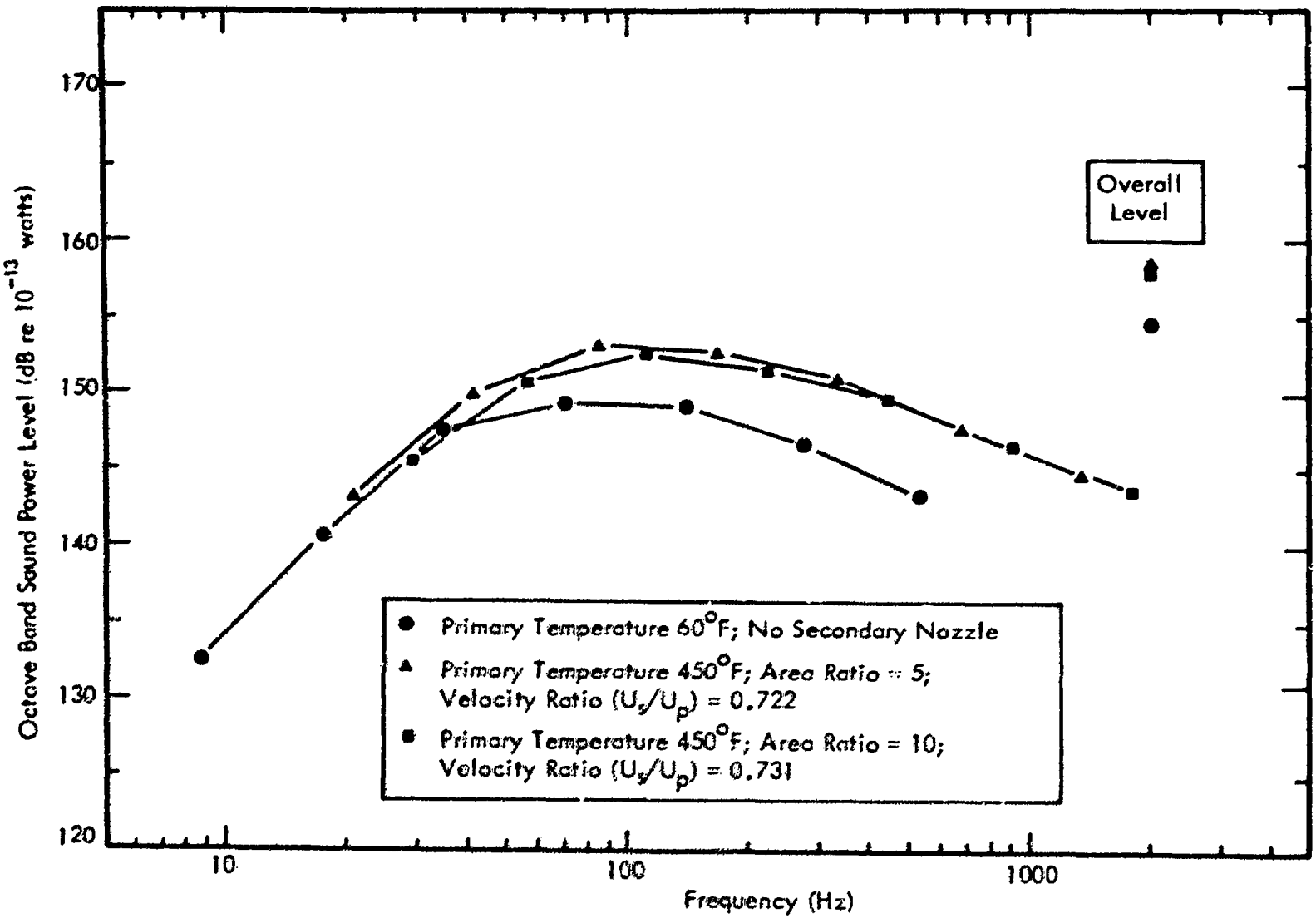

Figure 66. Sound Power Spectrum for Coplanar Nozzles, Primary Nozzle Pressure Ratio 1.6, Data Scaled to 20,000 Lbs Thrust.

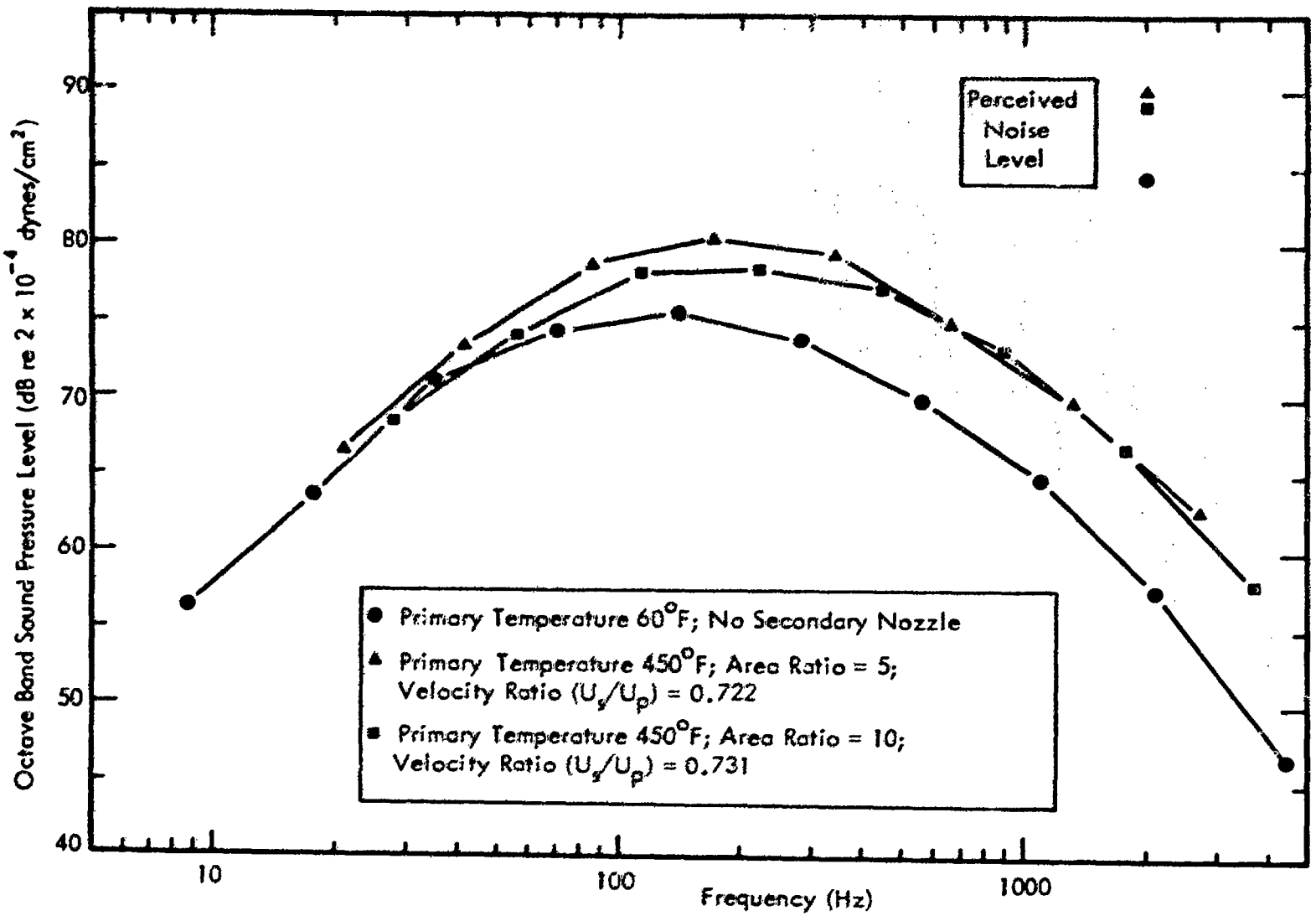

Figure 67. Octave Band Sound Pressure Spectrum at Position of Maximum Perceived Noise Level on 1500-Foot Sideline. Primary Nozzle Pressure Ratio 1.6, Thrust 20,000 Lbs.

Figures 68, 69 and 70 present the octave band directivity patterns for these three jets. The directivity maxima increase in angle by about 10 degrees when secondary flow is present. There is also a change in the shape of directivity pattern, so that the largest angle at which the directivity index is zero increases by as much as 25 degrees. These angular changes are reflected in Figure 71 which shows the 1500-foot sideline perceived noise level for the three jets. The changes in directivity cause the perceived noise level to drop more rapidly from the maximum value for the coaxial jets than is the case for the primary nozzle alone. Thus, at the peak level the coaxial jets produce about 6 PNdB more noise, whereas at large distances along the sideline in the direction of the jet exhaust, the difference is only 2 PNdB.

The above results have been presented for a 20,000 lb. thrust engine. It has already been shown (Figure 42) that on the average, the maximum perceived noise level increases by 2.5 PNdB for every doubling of jet thrust in the range of thrust from 10,000 lbs. to 80,000 lbs. This scaling factor generally holds over the complete sideline curve, as demonstrated in Figure 72 which gives the calculated values of the sideline perceived noise levels for four different thrusts for the jet with pressure ratio of 1.6 and total temperature of 60°F.

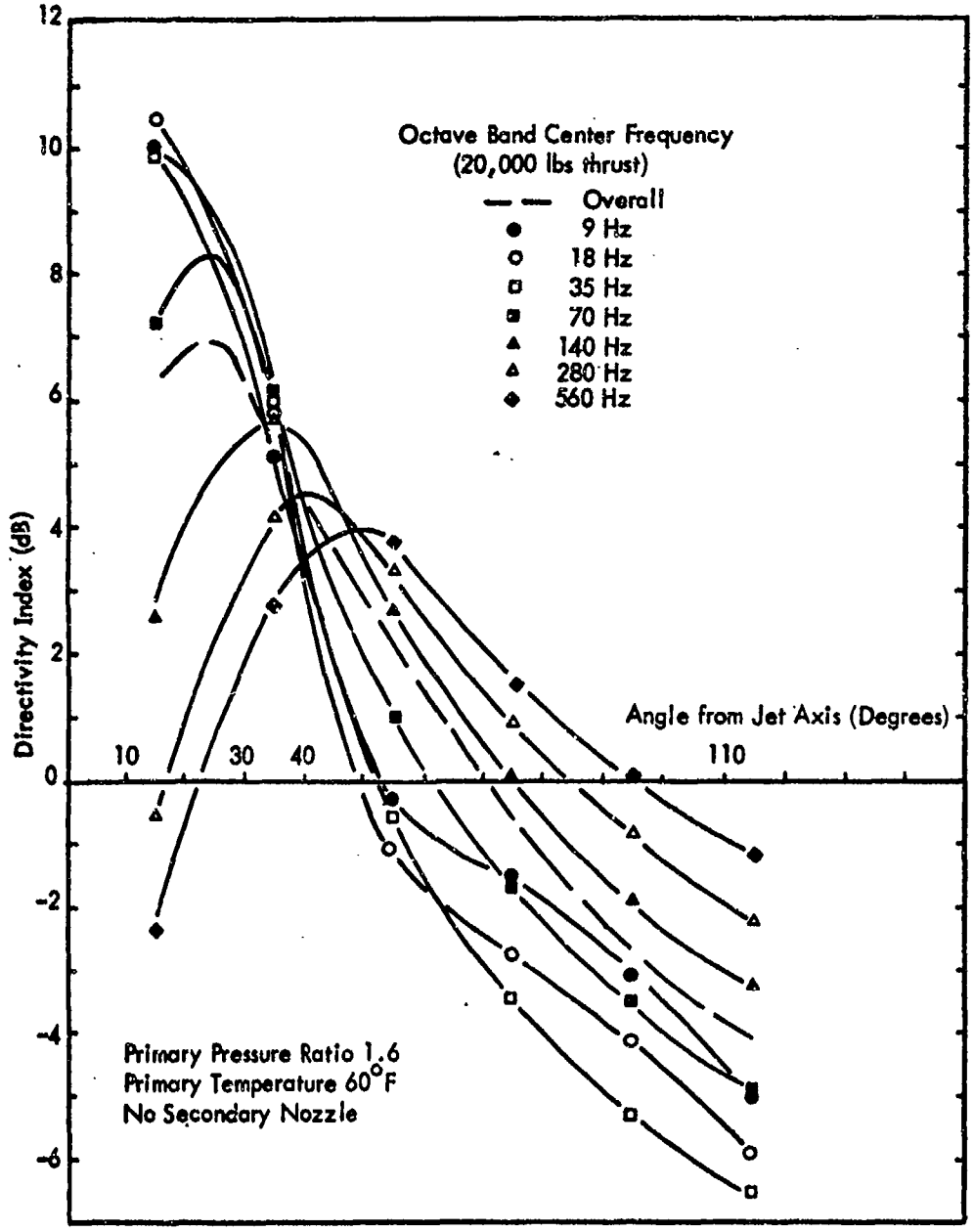

Figure 68. Directivity Pattern for Primary Nozzle Alone.

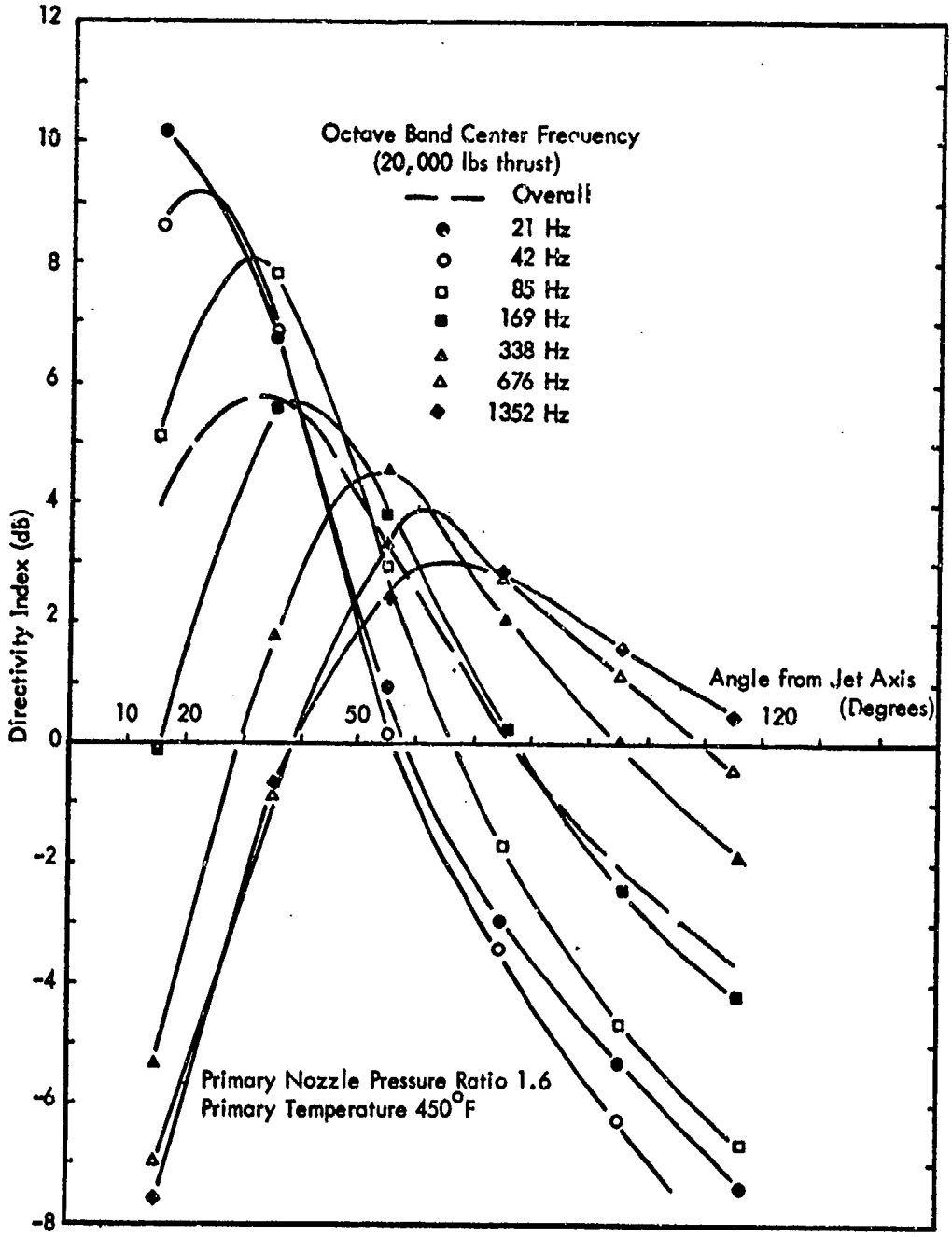

Figure 69. Directivity Pattern for Coplanar Nozzles with Area Ratio 5, Velocity Ratio 0.722.

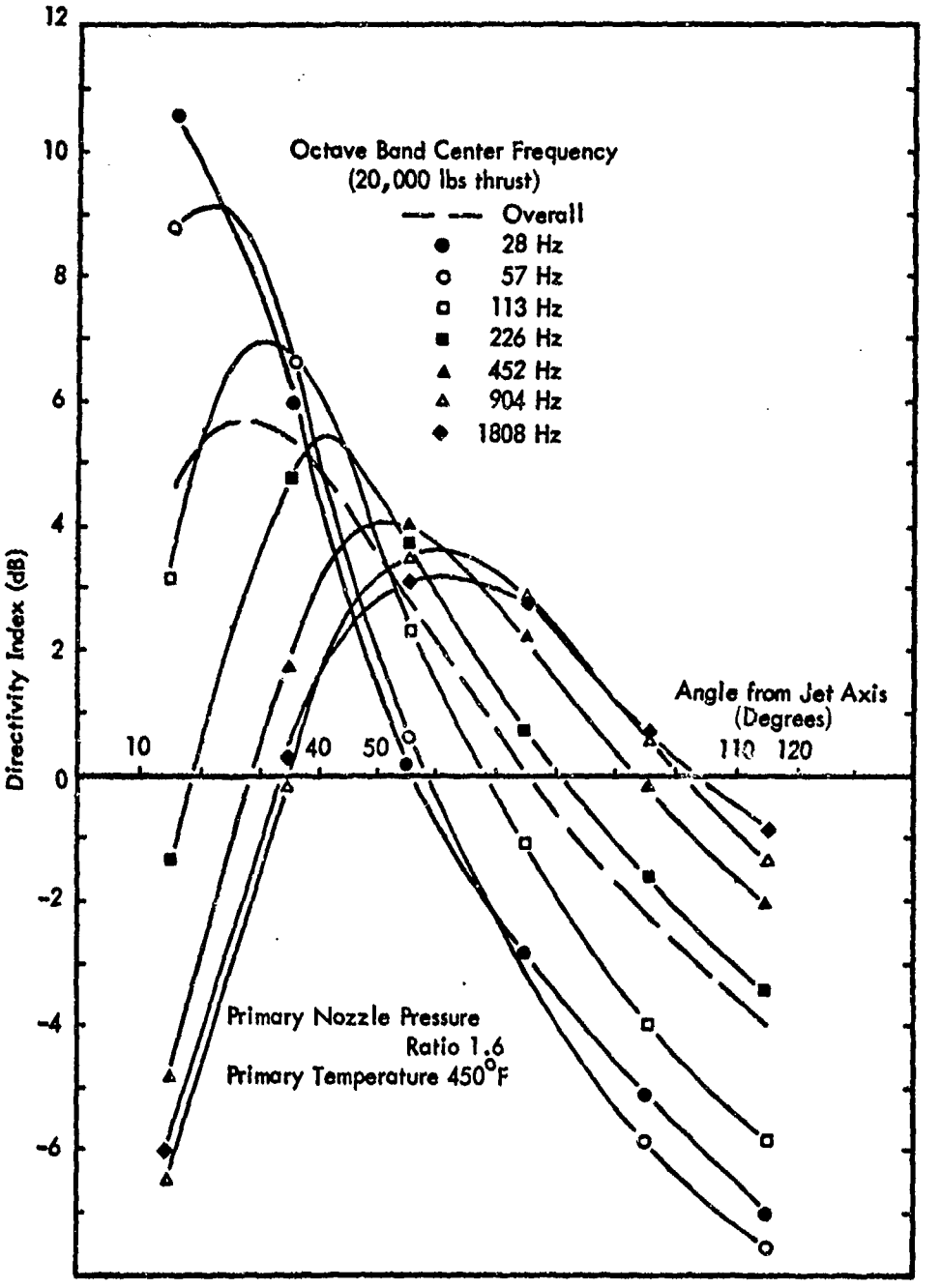

Figure 70. Directivity Pattern for Coplanar Nozzles with Area Ratio 10, Velocity Ratio 0.731.

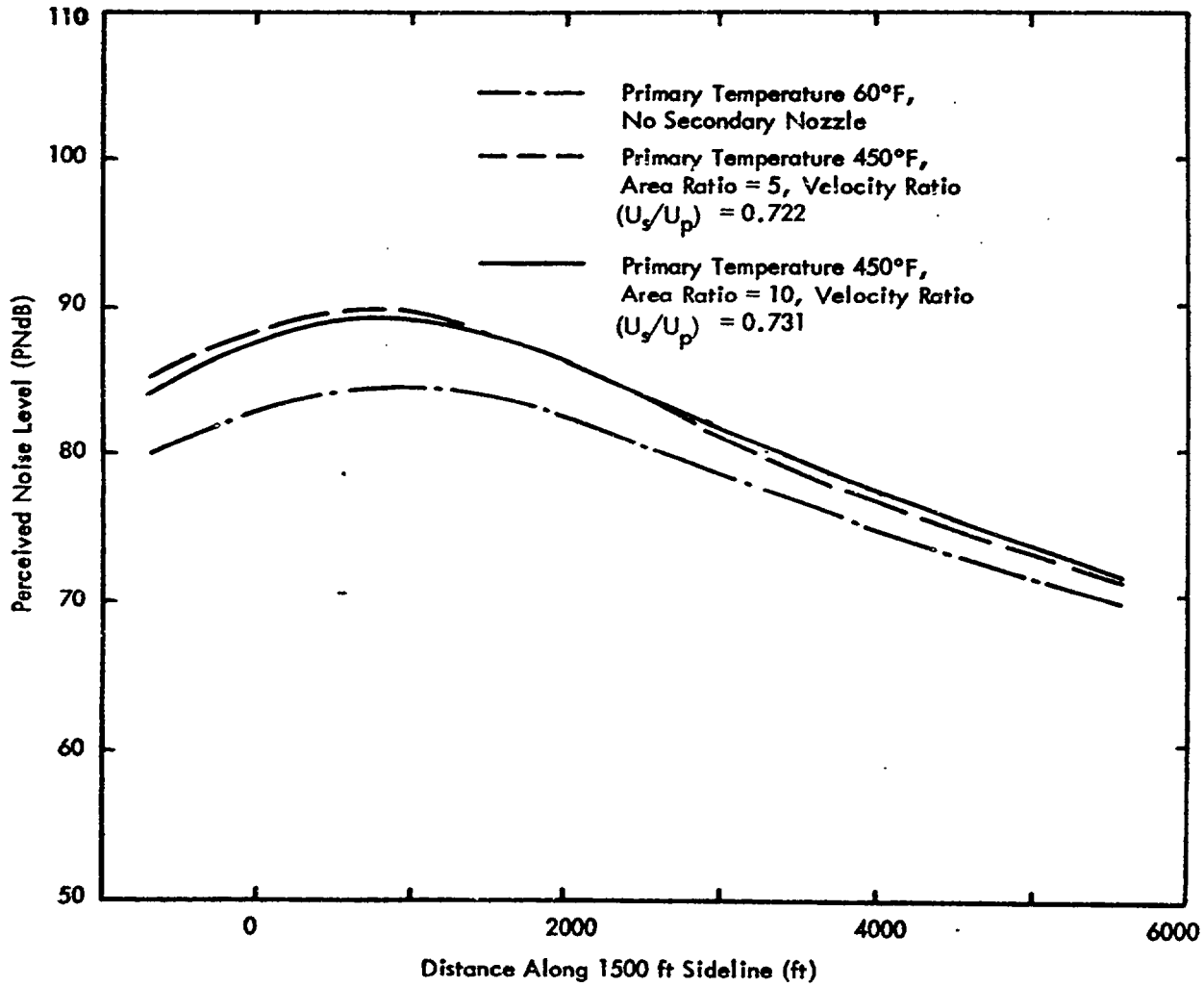

Figure 71. 1500-Foot Sideline Perceived Noise Level for Three Configurations Scaled to 20,000 Lbs Thrust, Primary Nozzle Pressure Ratio 1.6.

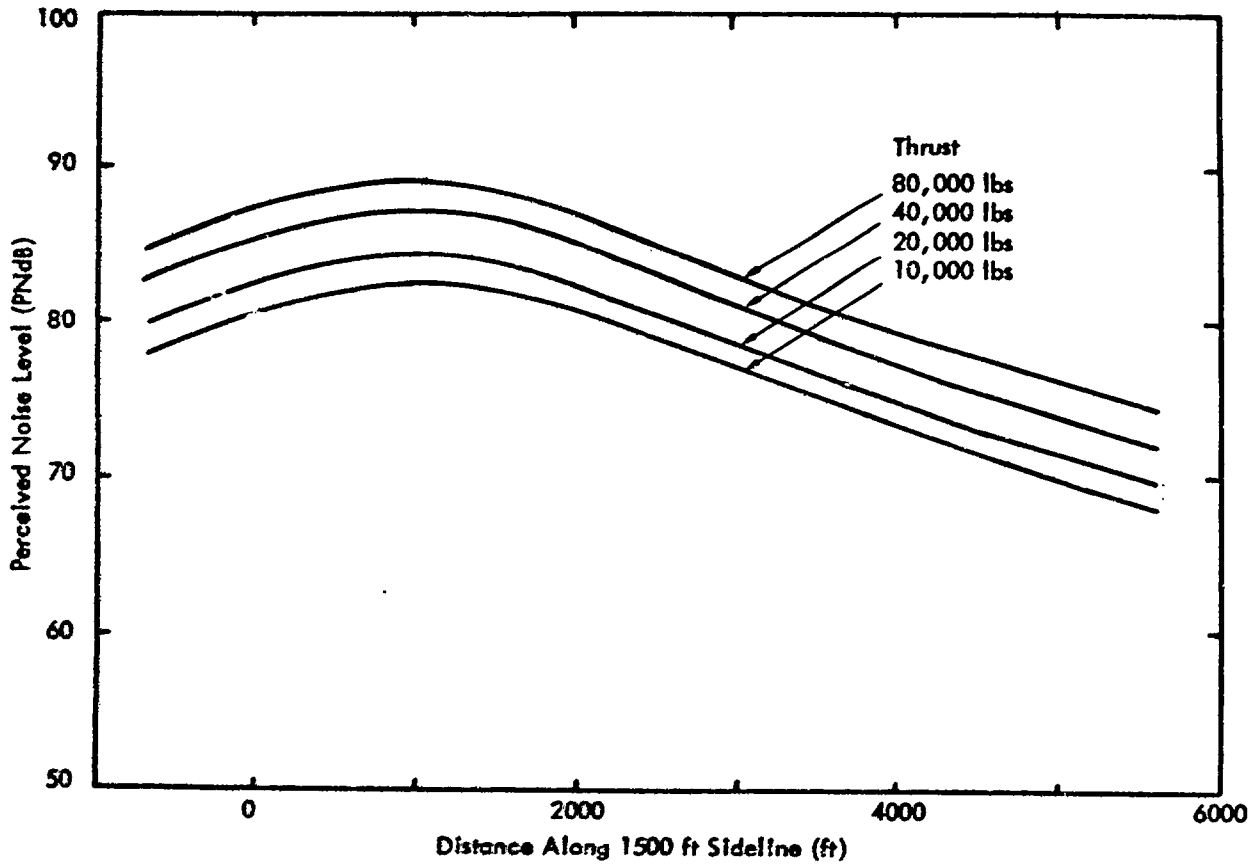

Figure 72. Effect of Jet Thrust on 1500-Foot Sideline Perceived Noise Level for Near-Optimum Jet with 20,000 Lbs Thrust (Nozzle Pressure Ratio 1.6, Temperature 60°F, No Secondary Nozzle).

6.0 SUMMARY AND CONCLUSIONS

The acoustic output of more than three hundred (300) different model coaxial jet configurations has been analyzed and used to determine the effect of the slower secondary (or bypass) air flow on the sound output of coaxial jets. The model data were scaled to give the sound power output of a full-scale jet engine, and the sound pressure levels and perceived noise levels determined along a sideline parallel to the jet axis. Noise reductions for coaxial jets were computed relative to a baseline single-nozzle jet which had the same thrust as that of the coaxial jet and a velocity equal to the coaxial jet primary. The principal conclusions from this work are as follows:

(1) The jet noise for coaxial jets with fixed thrust and area ratio was found to be minimum when the ratio of secondary velocity to primary velocity was approximately 0.5.

(2) The reduction in jet noise for fixed velocity ratio and thrust increases with increasing area ratio for coplanar or nearly coplanar nozzles. The maximum reduction in overall sound power was found to be 10 dB, and the maximum reduction in sideline perceived noise level was 11 PNdB for the nozzle which had a secondary to primary area ratio of 10. However, the reductions for an area ratio of 5 were approximately only 1 dB less than those for area ratio 10. These experimental results largely substantiate the simple theory of the noise of coplanar coaxial jets which was developed in this study.

(3) These noise reductions were found to be largely independent of the pressure ratio of the primary nozzle and the total temperature of the primary flow over the range of pressure ratios (1.6 - 3.5) and temperatures (60°F - 800°F) covered in the experimental program.

(4) While for a fixed velocity and temperature condition the overall sound power output is directly proportional to engine thrust, the maximum perceived noise level on a 1500-foot sideline was found to increase by only 2.5 PNdB each time the thrust was doubled, over a thrust range from 10,000 lbs. to 80,000 lbs. The maximum perceived noise level is therefore proportional to thrust raised to the power 0.833, when velocity and temperature conditions are held constant.

(5) At fixed thrust and area ratio, the maximum perceived noise level on a 1500-foot sideline was found to increase as the eighth power of velocity, whereas the overall sound power level increases as the sixth power.

(6) An engine designed to have maximum thrust per unit area will generally have minimum weight and drag per unit thrust. Assuming the secondary flow is limited by aerodynamic constraints to sonic or nearly sonic flow speeds, the acoustically optimum engine will have primary and secondary velocities of approximately 1000 feet per second. This implies that the acoustically optimum primary flow temperature should be very near ambient and the pressure ratio no greater than that of the secondary. Although the pressure ratio condition is essentially achieved in current high bypass ratio jets, the temperature condition is difficult to achieve, although it represents increased cycle efficiency.

(7) If all conditions of conclusion (6) could be achieved with a 20,000 lb. thrust engine, it would have an estimated overall sound power output of 159 dB relative to 10^{-13} watts and a maximum perceived noise level on a 1500-foot sideline of 88 PNdB.

(8) Small increases in the primary velocity relative to the secondary velocity produce small increases in acoustic output, their magnitudes being a function of area ratio. Tables 5 and 6 give the ratios of primary velocity to secondary velocity which results in either 3 dB or 6 dB increase in noise relative to the noise of an engine which has a velocity ratio of unity and the same secondary velocity and total thrust. The tables therefore give the velocity ratio which results in the specified noise increase compared to the optimum engine discussed in conclusions (6) and (7). The marked differences between the two tables results from the difference between the sensitivities of the overall sound power and perceived noise level to changes in primary velocity.

Table 5

Secondary-Primary Velocity Ratio for
Specified Increase in Overall Sound Power

Power Level Increase	Area Ratio			
	1	2	5	10
3 dB	1.14	1.17	1.40	1.52
6 dB	1.34	1.42	1.70	1.85

Table 6

Secondary-Primary Velocity Ratio for
Specified Increase in Perceived Noise Level

Perceived Noise Level Increase	Area Ratio			
	1	2	5	10
3 PNdB	1.11	1.12	1.18	1.23
6 PNdB	1.29	1.22	1.37	1.53

(9) It is probable that the noise reduction associated with coplanar coaxial jets can be increased by designing the nozzles to promote more rapid mixing. Such nozzles would probably enable the design of engines with jet noise characteristics approaching the optimums discussed in conclusions (6) and (7).

(10) The extension of the primary nozzle up to eleven (11) primary nozzle diameters beyond the secondary nozzle produced an increase in the noise reduction for nozzles of area ratio 1, little change in the noise reduction for nozzles of area ratio 2 and 5, and a decrease in the noise reduction for nozzles with area ratio 10.

(11) Significant retractions of the primary nozzle inside the secondary nozzle tended to decrease the noise relative to that produced by coplanar nozzles for all of the secondary nozzles when the primary nozzle had a high pressure ratio (3.5), but to increase the noise when the convergent primary nozzle with a subsonic pressure ratio (1.6) was used. However, the flow conditions for this latter primary nozzle were not characteristic of practical engines, and it is concluded that retracted primaries can be beneficial when properly designed.

Intentionally Left Blank

REFERENCES

1. Lighthill, M.J., "On Sound Generated Aerodynamically: I, General Theory," Proceedings of the Royal Society, A, Vol. 211, p 564, 1952.

2. Lighthill, M.J., "On Sound Generated Aerodynamically: II, Turbulence as a Source of Sound," Proceedings of the Royal Society, A, Vol. 222, p 1, 1954.

3. Plumblee, H.E., Wynne, G.A. and Zinn, B.T., "Effect of Jet Temperature on Jet and Pure Tone Noise Radiation," NASA CR-1472, 1969.

4. Plumblee, H.E., "Effect of Duct Heating on Jet and Fan Noise," Proceedings of Basic Aerodynamics Noise Research Conference, NASA Headquarters, Washington, D.C., NASA SP-207, July 1969.

5. Eldred, K.M., White, R.W., Mann, M.A. and Cottis, M.G., "Suppression of Noise with Emphasis on the Near Field," Report ASD-TDR-62-578, Wright-Patterson Air Force Base, Ohio, 1963.

6. Eldred, K.M., "Review of the Noise Generation of Rockets and Jets," JASA, Vol. 32, No. 11, p 1502.

7. Rollins, V.G., "Effect of Jet Temperature on Jet-Noise Generation," NACA TN-4217, March 1958.

8. Eldred, K.M., "Acoustic Loads Generated by the Propulsion System," NASA SP-8072, June 1971.

9. Grande, E., "Refraction of Sound by Jet Flow and Jet Temperature, II" University of Toronto, Institute of Aerospace Studies, UTIAS Report 110, 1966.

10. Atvars, J., Schubert, L.K., Grande, E. and Ribner, H.S., "Refraction of Sound by Jet Flow or Jet Temperature," NASA CR-494, May 1966.

11. Lighthill, M.J., "The Bakerian Lecture, 1961, Sound Generated Aerodynamically," Proceedings of the Royal Society, A, Vol. 267, p 147, 1962.

12. Howes, W.L., Callaghan, E.E., et al, "Near Noise Field of a Jet Engine Exhaust," NACA Report 1338, 1957.

13. Laurence, J.C., "Intensity, Scale and Spectra of Turbulence in Mixing Region of Free Subsonic Jet," NACA Report 1292, 1956.

Preceding page blank

14. Johannesen, N.H., "The Mixing of Free Axially Symmetrical Jets of Mach Number 1.40," ASTIA AD-203564, January 1957.

15. Pitkin, E.T., Glassman, "Experimental Mixing Profiles of a Mach 2.6 Free Jet," ASTIA AD-202294, August 1958.

16. Anderson, Arthur, Johns, Frank, "Non-Dimensional Characteristics of Free and Deflected Supersonic Jets Exhausting into Quiescent Air," WADC-ED-5401, March 1954.

17. Dyer, I., "Distribution of Sound Sources in a Jet Stream," Journal of Acoustical Society of America, Vol. 31, p 1016, 1959.

18. Ribner, H.S., "On the Strength Distribution of Noise Sources Along a Jet," University of Toronto, Institute of Aerospace Studies, UTIAS Report No. 51, 1958.

19. Westley, R. and Lilley, G.M., "An Investigation of the Noise Field from a Small Jet and Methods for its Reduction," Report No. 53, College of Aeronautics, Cranfield, England, 1952.

20. Greatrex, F.B., "Aeronautical Acoustics - in Particular Jet Noise," Journal of Royal Aeronautical Society, London, April 1954.

21. Greatrex, F.B., "Engine Noise," Joint Symposium on Aeronautical Acoustics, London, May 1953.

22. Mercer, D.M.A., et al, "The Effect of 'Teeth' on the Noise from a Jet Engine," WADC TR 54-224, September 1954.

23. Colloghan, E.E., et al, "Tooth Type Noise Suppression Devices on a Full-Scale Axial Flow Turbojet Engine," NACA RM E54-B01, March 1954.

24. North, W.J., "Summary Evaluation of Toothed Nozzle Attachments as a Jet Noise Suppression Device," NACA TN 3516, July 1955.

25. Laurence, J.C. and Benninghoff, J.M., "Turbulence Measurements in Multiple Interfering Air Jets," NACA TN 4029, December 1957.

26. Ciepluch, et al, "Acoustic, Thrust, and Drag Characteristics of Several Full-Scale Noise Suppressors for Turbojet Engines," NACA TN 4261, April 1958.

27. Greatrex, F.B., "Bypass Engine Noise," Society of Automotive Engineers, Reprint 162C, 1960.

28. Pao, S.P. and Lowson, M.V., "Spectral Techniques in Jet Noise Theory," Wyle Laboratories Research Staff Report WR 68-21, April 1969.

29. Lowson, M.V., "Some Applications of Jet Noise Theory," Wyle Laboratories Research Staff Report WR 69-21, October 1969.

30. Aviation Week and Space Technology, "Forecast and Inventory Issue," March 10, 1969.

31. Ames Research Staff, "Equations, Tables and Charts for Compressible Flow," National Advisory Committee for Aeronautics, Report 1135, Ames Aeronautical Laboratory, Moffett Field, California, 1953.

32. Society of Automotive Engineers, "Standard Values of Atmospheric Absorption as a Function of Temperature and Humidity for use in Evaluating Aircraft Flyover Noise," Aerospace Recommended Practice (ARP) 866, August 1964.

33. Evans, L.B. and Sutherland, L.C., "Investigation of Anomalous Behavior of Sound Absorption by Molecular Relaxation," Wyle Laboratories Research Staff Technical Memorandum, TM 70-4, May 1970.

34. Society of Automotive Engineers, "Definitions and Procedures for Computing the Perceived Noise Level for Aircraft Noise," Draft Revision ARP 865. Original date - October 15, 1964.

35. Hermes, P.H. and Smith, D.L., "Measurement and Analysis of the J57-P21 Noise Field," AFFDL-TR-66-147, Wright-Patterson Air Force Base, Ohio, 1966.

Intentionally Left Blank

APPENDIX A

DIRECTORY OF EXPERIMENTAL RUNS

This appendix contains a listing of the experimental runs that were made in the course of this project.

Table A-1 shows the groups of experimental runs associated with the various flow conditions of the primary nozzles and the relative position of the primary and secondary nozzles. Half extended or retracted means the primary nozzle is displaced 5.5 primary nozzle diameters axially from the exit plane of the secondary nozzle. Fully retracted or extended refers to 11 diameters. Within each group of runs indicated in the table, there is an equal number of runs for each of the four secondary nozzles. For each secondary nozzle, the secondary flow velocity is varied between that required to give a velocity ratio (secondary to primary) of one-third, up to a sonic velocity. Intermediate velocity ratios of two-thirds and unity are interposed between these extremes if this does not require the secondary velocity to be supersonic.

Table A-2 gives a detailed listing of the actual completed runs, giving the following data:

- Run Number (numbers in parentheses are reruns; asterisks indicate corrections were made to correct the high frequency data in the vicinity of 110 degrees for the third anomaly discussed in Section 4.2)
- Nozzle Position
- Nominal Area Ratio
- Primary Temperature
- Primary Pressure Ratio
- Primary Velocity
- Velocity Ratio (secondary/primary)
- Mass Flow Ratio (secondary/primary)

For additional detail, see Volume II.

Preceding page blank

Table A-1. Directory of Experimental Run Conditions

	Primary Nozzle Flow Temperature								
	60°F			450°F			800°F		
	Primary Pressure Ratio			Primary Pressure Ratio			Primary Pressure Ratio		
	1.6	2.5	3.5	1.6	2.5	3.5	1.6	2.5	3.5
Primary Nozzle Alone	101	118	131 600-606	144	157	166	175	188	197
Coplanar Nozzles	102-117	119-130	132-143	145-156	158-165	167-174	176-187	189-196	198-205
Fully Extended Primary	215-230	231-242	243-254	255-266	267-274	275-282	283-294 (1)	-	303-310 (1)
Fully Retracted Primary	311-326 (2)	327-338 (2)	339-350 (2)	-	-	-	-	-	-
Half Extended Primary	407-422	423-434	435-446	447-458	459-466	467-474	-	-	-
Half Retracted Primary	503-516	519-530	531-592	-	-	-	-	-	-

(1) Some runs not made in these groups (see Table A-2 for details).

(2) Runs not made when secondary supply pressure greater than primary supply pressure. Primary plenum pressures for these runs were identical with those of all other runs; however, actual pressure ratios across primary exhausting into secondary were lower and are given in Table A-2.

Table A-2

Experimental Run Conditions

Run Number	Nozzle Position	Nom. Area Ratio	Primary Temp. ~ °F Average	Primary Pressure Ratio	Primary Velocity Ft/Sec	Velocity Ratio	Mass Flow Ratio
101	Primary Nozzle Alone	–	64	1.5	899	–	–
102	Coplanar	1	64	1.6	900	0.35	0.58
103	Coplanar	1	64	1.6	894	0.70	0.93
104	Coplanar	1	64	1.6	894	1.0	1.33
105	Omitted	–	–	–	–	–	–
106	Coplanar	2	64	1.6	891	0.35	1.10
107 (705)	Coplanar	2	64	1.6	893	0.70	1.99
108 (722)	Coplanar	2	64	1.6	892	1.0	2.61
109	Coplanar	2	64	1.6	893	1.15	3.25
110 (706)	Coplanar	5	64	1.6	892	0.35	1.63
111 (723)	Coplanar	5	64	1.6	892	0.70	3.79
112 (803)	Coplanar	5	64	1.6	894	1.0	5.50
113	Omitted	–	–	–	–	–	–
114 (708)	Coplanar	10	64	1.6	895	0.35	3.30
115 (804)	Coplanar	10	64	1.6	899	0.70	7.15
116	Coplanar	10	64	1.6	878	1.0	11.03
117 (726)	Coplanar	10	64	1.6	881	1.16	14.28
118	Primary Nozzle Alone	–	64	2.5	1204	–	–
119 (709)	Coplanar	1	64	2.5	1199	0.38	0.46
120 (710)	Coplanar	1	64	2.5	1199	0.73	0.79
*121 (713)	Coplanar	1	64	2.5	1207	0.84	1.04
*122 (714)	Coplanar	2	64	2.5	1195	0.38	0.92
*123	Coplanar	2	64	2.5	1193	0.73	1.61
*124 (715)	Coplanar	2	64	2.5	1193	0.86	2.03
*125 (717)	Coplanar	5	64	2.5	1182	0.38	1.67
*126	Coplanar	5	64	2.5	1177	0.73	3.34
127 (719)	Coplanar	5	64	2.5	1177	0.86	4.14
*128	Coplanar	10	64	2.5	1184	0.38	3.18
*129	Coplanar	10	64	2.5	1194	0.73	6.69
*130	Coplanar	10	64	2.5	1195	0.87	8.38
*131	Primary Nozzle Alone	–	64	3.5	1380	–	–
*132	Coplanar	1	64	3.5	1374	0.35	0.38
*133	Omitted	–	–	–	–	–	–
*134	Coplanar	1	64	3.5	1382	0.74	0.76
*135 (720)	Coplanar	2	64	3.5	1370	0.35	0.68
*136 (809)	Coplanar	2	64	3.5	1368	0.67	1.31
*137	Coplanar	2	64	3.5	1374	0.74	1.48
*138	Coplanar	5	64	3.5	1376	0.35	1.40
*139	Coplanar	5	64	3.5	1376	0.67	2.96
*140	Coplanar	5	64	3.5	1367	0.75	3.36
*141 (721)	Coplanar	10	64	3.5	1387	0.35	2.64
*142	Coplanar	10	64	3.5	1383	0.67	5.88
*143	Coplanar	10	64	3.5	1387	0.75	6.67
144	Primary Nozzle Alone	–	450	1.6	1176	–	–
145	Coplanar	1	450	1.6	1176	0.38	0.78
146	Coplanar	1	450	1.6	1176	0.73	1.43
147	Coplanar	1	450	1.6	1176	0.88	1.89
148	Coplanar	2	450	1.6	1176	0.38	1.38
149	Coplanar	2	450	1.6	1176	0.72	3.05
150 (811)	Coplanar	2	450	1.6	1176	0.87	4.09
151	Coplanar	5	450	1.6	1176	0.38	3.29
152	Coplanar	5	450	1.6	1176	0.72	6.65
153	Coplanar	5	450	1.6	1176	0.87	9.04
154 (727)	Coplanar	10	450	1.6	1176	0.38	6.02
155	Coplanar	10	450	1.6	1176	0.73	13.38
156 (729)	Coplanar	10	450	1.6	1176	0.88	18.38
*157	Primary Nozzle Alone	–	450	2.5	1590	–	–
*158	Coplanar	1	450	2.5	1590	0.41	0.68
*159	Coplanar	1	450	2.5	1590	0.66	1.18
*160	Coplanar	2	450	2.5	1590	0.40	1.48
161	Omitted	–	–	–	–	–	–
*162	Coplanar	5	450	2.5	1590	0.41	3.07
163	Coplanar	5	450	2.5	1590	0.65	5.10
*164 (812)	Coplanar	10	450	2.5	1590	0.40	5.42
165	Coplanar	10	450	2.5	1590	0.66	10.22
*166	Primary Nozzle Alone	–	450	3.5	1817	–	–
*167 (732)	Coplanar	1	450	3.5	1817	0.57	1.02
168	Omitted	–	–	–	–	–	–
*169	Coplanar	2	450	3.5	1817	0.42	1.38
*170 (734)	Coplanar	2	450	3.5	1817	0.57	1.96
*171	Coplanar	5	450	3.5	1817	0.42	3.00
*172 (736)	Coplanar	5	450	3.5	1817	0.58	4.15
*173	Coplanar	10	450	3.5	1817	0.42	5.42
*174	Coplanar	10	450	3.5	1817	0.58	8.45
175	Primary Nozzle Alone	–	800	1.6	1401	–	–
176	Coplanar	1	800	1.6	1401	0.37	1.01
177	Coplanar	1	800	1.6	1362	0.71	1.90
178	Coplanar	1	800	1.6	1362	0.78	2.03
179	Coplanar	2	800	1.6	1364	0.37	2.07
180 (737)	Coplanar	2	800	1.6	1359	0.69	3.62
181	Coplanar	2	800	1.6	1361	0.77	4.53
182	Coplanar		800	1.6	1369	0.36	3.83
183 (738)	Coplanar	5	800	1.6	1362	0.69	8.48
184 (739)	Coplanar	5	800	1.6	1366	0.77	9.84
185 (815)	Coplanar	10	800	1.6	1366	0.36	7.67
186	Coplanar	10	800	1.6	1359	0.69	17.68
187	Coplanar	10	800	1.6	1359	0.77	21.85
*188	Primary Nozzle Alone	–	800	2.5	1864	–	–
*189	Coplanar	1	800	2.5	1853	0.39	0.78
*190	Coplanar	1	800	2.5	1856	0.58	1.38
191	Coplanar	2	800	2.5	1855	0.38	1.84
192	Coplanar	2	800	2.5	1856	0.57	2.65
*193	Coplanar	5	800	2.5	1854	0.38	3.79
194 (741)	Coplanar	5	800	2.5	1853	0.56	5.98
195	Omitted	–	–	–	–	–	–
196	Coplanar	10	800	2.5	1852	0.56	12.00

Table A-2 – continued

Run Number	Nozzle Position	Nom. Area Ratio	Primary Temp. ~°F Average	Primary Pressure Ratio	Primary Velocity Ft/Sec	Velocity Ratio	Mass Flow Ratio
*197	Primary Nozzle Alone	–	800	3.5	2169	–	–
*198	Coplanar	1	800	3.5	2183	0.38	0.84
*199	Coplanar	1	800	3.5	2178	0.49	1.08
*200	Coplanar	2	800	3.5	2179	0.38	1.74
201	Coplanar	2	800	3.5	2183	0.48	2.27
*202 (744)	Coplanar	5	800	3.5	2183	0.38	3.84
203	Omitted	–	–	–	–	–	–
*204	Coplanar	10	800	3.5	2180	0.38	7.29
205	Coplanar	10	800	3.5	2184	0.48	10.08
206 -214	Omitted	–	–	–	–	–	–
215	Fully Extended Primary	1	66	1.6	898	0.35	0.32
216	Fully Extended Primary	1	66	1.6	896	0.70	0.82
217	Fully Extended Primary	1	66	1.6	900	0.99	1.21
218	Fully Extended Primary	1	66	1.6	898	1.14	1.49
219	Fully Extended Primary	2	66	1.6	892	0.35	0.60
220	Fully Extended Primary	2	66	1.6	892	0.70	1.34
221	Fully Extended Primary	2	66	1.6	895	1.0	2.79
222	Fully Extended Primary	2	66	1.6	895	1.14	3.36
223	Fully Extended Primary	5	66	1.6	894	0.34	1.60
224	Omitted	–	–	–	–	–	–
225	Fully Extended Primary	5	66	1.6	895	0.99	6.09
226	Fully Extended Primary	5	66	1.6	900	1.15	7.01
227	Fully Extended Primary	10	66	1.6	887	0.35	3.20
228	Fully Extended Primary	10	66	1.6	895	0.70	6.65
229	Fully Extended Primary	10	66	1.6	898	1.0	10.58
230	Fully Extended Primary	10	66	1.6	898	1.16	12.44
*231	Fully Extended Primary	1	66	2.5	1210	0.38	0.32
*232	Fully Extended Primary	1	66	2.5	1221	0.71	0.68
*233	Fully Extended Primary	1	66	2.5	1220	0.84	0.88
*234	Fully Extended Primary	2	66	2.5	1209	0.38	0.58
*235	Fully Extended Primary	2	66	2.5	1217	0.72	1.26
*236	Fully Extended Primary	2	66	2.5	1204	0.95	1.54
*237	Fully Extended Primary	5	66	2.5	1200	0.38	1.60
*238	Fully Extended Primary	5	66	2.5	1187	0.73	3.24
*239	Omitted	–	–	–	–	–	–
*240	Fully Extended Primary	10	66	2.5	1208	0.38	2.44
*241	Fully Extended Primary	10	66	2.5	1208	0.72	5.31
242	Omitted	–	–	–	–	–	–
*243	Fully Extended Primary	1	66	3.5	1378	0.36	0.27
*244	Fully Extended Primary	1	66	3.5	1333	0.67	0.59
*245	Fully Extended Primary	1	66	3.5	1384	0.74	0.70
*246	Fully Extended Primary	2	66	3.5	1367	0.36	0.51
*247	Fully Extended Primary	2	66	3.5	1374	0.68	1.05
*248	Fully Extended Primary	2	66	3.5	1380	0.74	1.29
*249	Fully Extended Primary	5	66	3.5	1374	0.35	1.30
*250 (747)	Fully Extended Primary	5	66	3.5	1370	0.68	2.81
*251	Fully Extended Primary	5	66	3.5	1378	0.76	3.23
*252	Fully Extended Primary	10	66	3.5	1388	0.36	2.47
*253	Fully Extended Primary	10	66	3.5	1388	0.68	5.46
*254	Fully Extended Primary	10	66	3.5	1387	0.75	6.31
255	Fully Extended Primary	1	450	1.6	1177	0.39	0.50
256	Fully Extended Primary	1	450	1.6	1184	0.73	1.77
257	Fully Extended Primary	1	450	1.6	1183	0.88	1.56
258	Fully Extended Primary	2	450	1.6	1187	0.39	1.04
259	Fully Extended Primary	2	450	1.6	1187	0.73	2.34
260	Fully Extended Primary	2	450	1.6	1184	0.88	3.02
261	Fully Extended Primary	5	450	1.6	1185	0.38	2.85
262	Omitted	–	–	–	–	–	–
263	Fully Extended Primary	5	450	1.6	1183	0.88	7.96
264	Fully Extended Primary	10	450	1.6	1186	0.38	5.44
265 (750)	Fully Extended Primary	10	450	1.6	1185	0.72	11.66
266	Fully Extended Primary	10	450	1.6	1186	0.88	16.15
*267	Fully Extended Primary	1	450	2.5	1605	0.41	0.54
*268	Fully Extended Primary	1	450	2.5	1594	0.66	1.15
*269	Fully Extended Primary	2	450	2.5	1604	0.40	0.95
*270	Omitted	–	–	–	–	–	–
*271	Fully Extended Primary	5	450	2.5	1601	0.40	2.62
*272	Fully Extended Primary	5	450	2.5	1605	0.65	4.88
*273	Fully Extended Primary	10	450	2.5	1603	0.40	5.07

Table A-2 – continued

Run Number	Nozzle Position	Nom. Area Ratio	Primary Temp. ~°F Average	Primary Pressure Ratio	Primary Velocity Ft/Sec	Velocity Ratio	Mass Flow Ratio
*274	Fully Extended Primary	10	450	2.5	1604	0.65	9.62
*275 (751)	Fully Extended Primary	1	450	3.5	1802	0.42	0.64
*276	Fully Extended Primary	1	450	3.5	1800	0.58	0.98
*277	Fully Extended Primary	2	450	3.5	1800	0.42	0.72
*278 (752)	Fully Extended Primary	2	450	3.5	1800	0.58	1.07
*279	Fully Extended Primary	5	450	3.5	1798	0.42	1.52
*280	Fully Extended Primary	5	450	3.5	1800	0.58	2.19
*281	Fully Extended Primary	10	450	3.5	1803	0.42	5.17
*282	Fully Extended Primary	10	450	3.5	1802	0.58	7.96
283-284	Omitted	–	–	–	–	–	–
285	Fully Extended Primary	1	800	1.6	1372	0.78	1.74
286	Fully Extended Primary	2	800	1.6	1374	0.37	1.33
287 (754)	Fully Extended Primary	2	800	1.6	1376	0.69	2.92
288	Fully Extended Primary	2	800	1.6	1379	0.76	3.58
289	Fully Extended Primary	5	800	1.6	1377	0.36	3.57
290	Fully Extended Primary	5	800	1.6	1374	0.69	7.63
291	Fully Extended Primary	5	800	1.6	1374	0.76	8.82
292-302	Omitted	–	–	–	–	–	–
*303 (753)	Fully Extended Primary	1	800	3.5	2182	0.39	0.62
*304	Fully Extended Primary	1	800	3.5	2185	0.49	0.96
305-310	Omitted	–	–	–	–	–	–
311	Fully Retracted Primary	1	74	1.52	846	0.37	0.71
312	Fully Retracted Primary	1	74	1.29	664	0.94	1.80
313-314	Omitted	–	–	–	–	–	–
315	Fully Retracted Primary	2	74	1.52	845	0.37	0.99
316	Fully Retracted Primary	2	74	1.29	663	0.94	2.15
317-319	Omitted	–	–	–	–	–	–
320	Fully Retracted Primary	5	74	1.29	664	0.94	4.34
321-322	Omitted	–	–	–	–	–	–
323	Fully Retracted Primary	10	74	1.52	853	0.37	3.63
324	Fully Retracted Primary	10	74	1.29	669	0.94	7.70
325-327	Omitted	–	–	–	–	–	–
328 (832)	Fully Retracted Primary	1	74	1.61	896	0.96	1.16
329 (762)	Fully Retracted Primary	1	74	1.32	700	1.47	1.68
330	Fully Retracted Primary	2	74	2.23	1146	0.40	0.76
331	Fully Retracted Primary	2	74	1.61	906	0.96	1.66
332	Fully Retracted Primary	2	74	1.32	702	1.47	2.49
333	Fully Retracted Primary	5	74	2.23	1141	0.40	1.79
334	Fully Retracted Primary	5	74	1.56	872	1.03	3.68
335	Fully Retracted Primary	5	74	1.32	705	1.47	4.98
336	Fully Retracted Primary	10	74	2.23	1148	0.40	3.20
337	Fully Retracted Primary	10	74	1.61	904	0.96	6.34
338	Fully Retracted Primary	10	74	1.32	705	1.47	8.85
339	Fully Retracted Primary	1	74	3.06	1330	0.37	0.46
340	Fully Retracted Primary	1	74	2.09	1114	0.84	0.89
341 (763)	Fully Retracted Primary	1	74	1.85	1025	1.01	1.12
342	Fully Retracted Primary	2	74	3.06	1331	0.37	0.74
343	Fully Retracted Primary	2	74	2.09	1114	0.84	1.43
344	Fully Retracted Primary	2	74	1.85	1024	1.01	1.68
345	Fully Retracted Primary	5	74	3.06	1331	0.37	1.62
346	Fully Retracted Primary	5	74	2.09	1109	0.85	3.09
347 (764)	Fully Retracted Primary	5	74	1.85	1024	1.01	3.57
348	Fully Retracted Primary	10	74	3.06	1335	0.37	2.88
349	Fully Retracted Primary	10	74	2.09	1115	0.85	6.05
350	Fully Retracted Primary	10	74	1.85	1023	1.02	6.69
351-407	Omitted	–	–	–	–	–	–
408 (823)	Half Extended Primary	1	60	1.6	896	0.70	0.63
409	Half Extended Primary	1	60	1.6	894	1.0	1.04
410	Half Extended Primary	1	60	1.6	895	1.15	1.28
411	Half Extended Primary	2	60	1.6	894	0.35	0.55
412	Half Extended Primary	2	60	1.6	896	0.70	1.27
413	Half Extended Primary	2	60	1.6	897	1.0	2.12
414 (756)	Half Extended Primary	2	60	1.6	895	1.15	2.59
415	Half Extended Primary	5	60	1.6	886	0.35	1.54
416	Half Extended Primary	5	60	1.6	883	0.70	3.28
417 (824)	Half Extended Primary	5	60	1.6	887	1.01	5.14

Table A-2 – continued

Run Number	Nozzle Position	Nom. Area Ratio	Primary Temp. ~°F Average	Primary Pressure Ratio	Primary Velocity Ft/Sec	Velocity Ratio	Mass Flow Ratio
418	Half Extended Primary	5	60	1.6	887	1.16	5.98
419	Half Extended Primary	10	60	1.6	887	0.35	2.94
420	Half Extended Primary	10	60	1.6	887	0.70	6.12
421	Half Extended Primary	10	60	1.6	894	1.01	9.75
422	Half Extended Primary	10	60	1.6	892	1.16	11.90
*423	Half Extended Primary	1	60	2.5	1198	0.38	0.26
*424	Half Extended Primary	1	60	2.5	1198	0.72	0.60
*425	Half Extended Primary	1	60	2.5	1202	0.85	0.75
*426	Half Extended Primary	2	60	2.5	1202	0.38	0.56
*427	Half Extended Primary	2	60	2.5	1202	0.72	1.21
*428	Omitted	–	–	–	–	–	–
*429	Half Extended Primary	5	60	2.5	1202	0.38	1.43
*430	Half Extended Primary	5	60	2.5	1205	0.72	3.02
*431	Half Extended Primary	5	60	2.5	1211	0.85	3.85
*432	Half Extended Primary	10	60	2.5	1210	0.38	2.79
*433	Half Extended Primary	10	60	2.5	1205	0.72	5.94
434	Half Extended Primary	10	60	2.5	1208	0.86	7.48
*435	Half Extended Primary	1	60	3.5	1356	0.36	0.24
*436	Half Extended Primary	1	60	3.5	1360	0.68	0.54
*437	Half Extended Primary	1	60	3.5	1363	0.75	0.62
*438	Half Extended Primary	2	60	3.5	1366	0.36	0.48
*439	Half Extended Primary	2	60	3.5	1366	0.68	1.12
*440	Half Extended Primary	2	60	3.5	1367	0.75	1.29
*441	Half Extended Primary	5	60	3.5	1370	0.36	1.22
*442	Half Extended Primary	5	60	3.5	1374	0.68	2.73
*443	Half Extended Primary	5	60	3.5	1380	0.75	3.14
*444	Half Extended Primary	10	60	3.5	1376	0.36	2.44
*445	Half Extended Primary	10	60	3.5	1378	0.68	5.27
*446	Half Extended Primary	10	60	3.5	1380	0.75	6.08
447	Half Extended Primary	1	460	1.6	1189	0.38	0.52
448	Half Extended Primary	1	460	1.6	1189	0.73	1.14
449	Half Extended Primary		460	1.6	1185	0.88	1.63
450	Half Extended Primary	2	460	1.6	1187	0.38	0.99
451	Half Extended Primary	2	460	1.6	1185	0.72	2.42
452	Half Extended Primary	2	460	1.6	1188	0.87	3.14
453	Half Extended Primary	5	460	1.6	1187	0.38	2.64
454 (759)	Half Extended Primary	5	460	1.6	1186	0.73	5.81
455	Half Extended Primary	5	460	1.6	1186	0.88	7.63
456	Half Extended Primary	10	460	1.6	1183	0.38	5.38
457	Half Extended Primary	10	460	1.6	1186	0.73	11.52
458	Half Extended Primary	10	460	1.6	1186	0.88	15.09
*459	Half Extended Primary	1	460	2.5	1601	0.40	0.52
*460	Half Extended Primary	1	460	2.5	1597	0.65	0.97
*461	Half Extended Primary	2	460	2.5	1601	0.40	1.00
*462 (826)	Half Extended Primary	2	460	2.5	1596	0.65	1.09
*463	Half Extended Primary	5	460	2.5	1600	0.40	2.68
*464	Half Extended Primary	5	460	2.5	1599	0.65	4.96
*465	Half Extended Primary	10	460	2.5	1601	0.40	5.18
*466	Half Extended Primary	10	460	2.5	1601	0.65	9.67
*467	Half Extended Primary	1	460	3.5	1829	0.42	0.52
*468	Half Extended Primary	1	460	3.5	1824	0.57	0.76
*469	Half Extended Primary	2	460	3.5	1827	0.42	0.94
*470	Half Extended Primary	2	460	3.5	1828	0.58	1.52
*471	Half Extended Primary	5	460	3.5	1828	0.42	2.66
*472	Half Extended Primary	5	460	3.5	1825	0.58	3.86
*473	Half Extended Primary	10	460	3.5	1828	0.42	4.83
*474	Half Extended Primary	10		3.5	1828	0.58	7.76
475-503	Omitted	–	–	–	–	–	–
504	Half Retracted Primary	1	70	1.29	664	0.94	1.59
505 (765)	Half Retracted Primary	2	70	1.52	847	0.37	1.06
506 (766)	Half Retracted Primary	2	70	1.29	663	0.94	2.24
507-510	Omitted	–	–	–	–	–	–
511	Half Retracted Primary	5	70	1.52	843	0.37	7.03
512	Half Retracted Primary	5	70	1.29	661	0.94	4.42
513-514	Omitted	–	–	–	–	–	–

Table A-2 – concluded

Run Number	Nozzle Position	Nom. Area Ratio	Primary Temp. ~°F Average	Primary Pressure Ratio	Primary Velocity Ft/Sec	Velocity Ratio	Mass Flow Ratio
515	Half Retracted Primary	10	70	1.52	843	0.37	3.52
516	Half Retracted Primary	10	70	1.29	667	0.94	7.68
517-518	Omitted	–	–	–	–	–	–
519	Half Retracted Primary	1	70	2.23	1149	0.40	0.69
*520	Half Retracted Primary	1	70	1.61	903	0.97	1.33
*521	Half Retracted Primary	1	70	1.32	702	1.47	1.92
522	Half Retracted Primary	2	70	2.23	1144	0.40	1.01
523	Half Retracted Primary	2	70	1.61	894	0.97	1.92
*524	Half Retracted Primary	2	70	1.32	698	1.47	2.78
*525	Half Retracted Primary	5	70	2.23	1138	0.40	1.95
526	Half Retracted Primary	5	70	1.61	895	0.97	3.90
*527	Half Retracted Primary	5	70	1.32	699	1.48	5.29
528	Half Retracted Primary	10	70	2.23	1144	0.40	3.19
529	Half Retracted Primary	10	70	1.61	898	0.97	6.03
530	Half Retracted Primary	10	70	1.32	702	1.45	9.16
*531	Half Retracted Primary	1	70	3.06	1314	0.37	0.67
*532	Half Retracted Primary	1	70	2.09	1095	0.85	1.10
*533 (767)	Half Retracted Primary	1	70	1.85	1017	1.02	1.27
*534	Half Retracted Primary	2	70	3.06	1320	0.37	0.88
*535	Half Retracted Primary	2	70	2.09	1100	0.85	1.58
*536	Half Retracted Primary	2	70	1.85	1030	1.02	1.88
*537	Half Retracted Primary	5	70	3.06	1331	0.37	1.63
538	Omitted	–	–	–	–	–	–
*539	Half Retracted Primary	5	70	1.85	1073	1.02	3.47
*540	Half Retracted Primary	10	70	3.06	1333	0.37	2.87
541	Half Retracted Primary	10	70	2.09	1108	0.85	5.84
542	Half Retracted Primary	10	70	1.85	1020	1.02	6.72
543-599	Omitted	–	–	–	–	–	–
600	Primary Nozzle Alone	–	74	2.0	1036	–	–
601	Primary Nozzle Alone	–	74	2.5	1271	–	–
*602	Primary Nozzle Alone	–	74	3.0	1318	–	–
*603	Primary Nozzle Alone	–	74	3.5	1397	–	–
*604 (836)	Primary Nozzle Alone	–	74	4.0	1450	–	–
*605	Primary Nozzle Alone	–	74	5.4	1570	–	–
*606	Primary Nozzle Alone	–	74	7.8	1688	–	–

Intentionally Left Blank

APPENDIX B

JET FLOW PROFILE MEASUREMENTS

Measurements were made of the total pressure, static pressure and total temperature profile at the exit plane of the model jets prior to initiating the acoustic tests. These tests were conducted primarily to check the velocity profile at the exit of the primary and secondary jets. In addition, the data provided an independent check on the thrust measurements. A few profile measurements were also made well downstream of the exit plane to investigate the spreading characteristics of a coaxial jet. Typical results from these measurements are presented in this appendix. The instrumentation and apparatus used has been described in Sections 3.2.4 and 3.3.4.

B-1 Test Conditions

Test conditions for which significant flow profile data were obtained are summarized in Table B-1. The first series of runs were made without any secondary nozzle. The remaining runs were made with both nozzles in place, although in some cases there was no air flow through one of the nozzles. It is apparent that only a small number of the possible configurations were used for obtaining flow profile data.

B-2 Test Results

Figure B-1 presents a sample of the raw data taken directly from the chart recorder, showing a total pressure profile measurement for a primary nozzle with a pressure ratio of 1.6. Data of this type is the basis for the calculation of flow velocity. Figure B-2 shows the velocity profile at the exit plane of the nozzle with pressure ratio 1.6 as a function of total temperature of the flow. As would be expected from aerodynamic considerations, the boundary layer tends to become thinner with increasing temperature. Note that the abscissa is broken to expand the scale within the region of interest. Figure B-3 shows a similar set of profiles, except that in this case the flow total temperature is held at approximately 850°F while the nozzle pressure ratio is changed. It should be noted that these three profiles were made by three different nozzles, not by one nozzle with a varying pressure ratio.

Table B-1
Test Conditions for Flow Profile Data

Nominal Area Ratio	Primary				Secondary(1)		Profiles(4)		
	Nozzle Position	Pressure Ratio		T_t	Pressure Ratio		P_t	P	T_t
		Nominal	Actual	°F	Nominal	Actual			
0	Alone	1.6	1.58	58	None		x		
			1.58	460			x		
			1.59	800			x		
		2.5	2.53	900			x		x
			1.5-2.6	900			x		
		3.5	2.7-3.7	820			x		
1	Coplanar	2.5	off		1.89	1.83	x		
2						1.87	x		
5						1.84	x		
10						1.89	x		
			2.1	790		1.5	x	x	x (2)
			2.43	790	1.27	1.27	x	x	x
			2.43	790	off		x	x	
		3.5	3.2-4.1	820	1.89	1.89	x		
			3.5	820	off		x	x	x(2)
5	Retracted(3)	2.5	off		1.89	1.84	x		x
10	Retracted(3)		2.49	790		1.92	x		x
1	Extended(3)		2.45	880		1.89	x	x	x
1	Extended(3)		2.45	880	off		x	x	x

(1) Total Temperature of Secondary varied from 70°F to 90°F.
(2) Profile Measurements also taken at Positions Downstream of Nozzle Exit Plane.
(3) Fully Retracted or Fully Extended Position.
(4) P_t = Total Pressure, P = Static Pressure, T_t = Total Temperature.

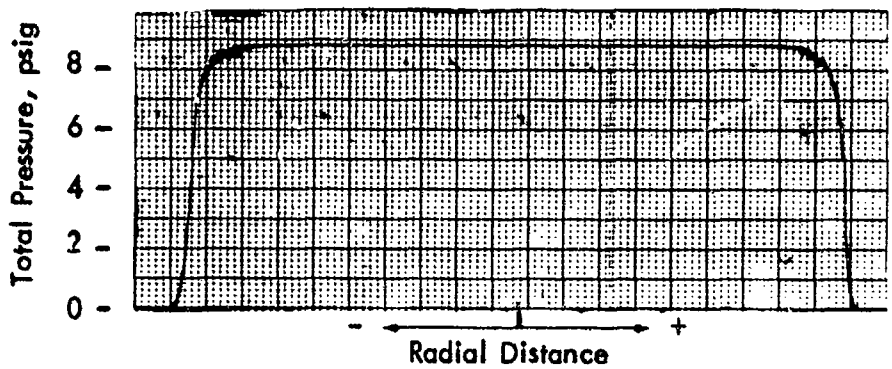

Figure B-1. Typical Graphic Record of Total Pressure Profile for a Primary Nozzle with Pressure Ratio 1.6.

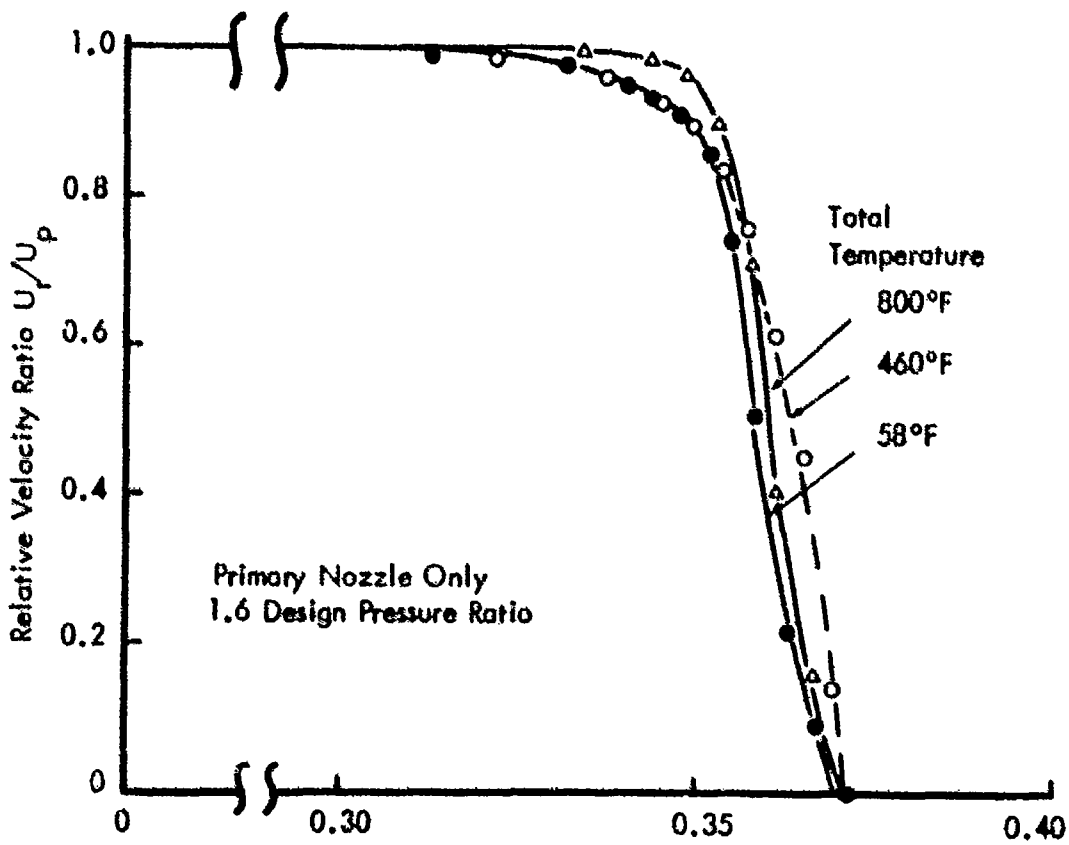

Figure B-2. Effect of Temperature on Boundary Layer at the Exit of Primary Nozzle.

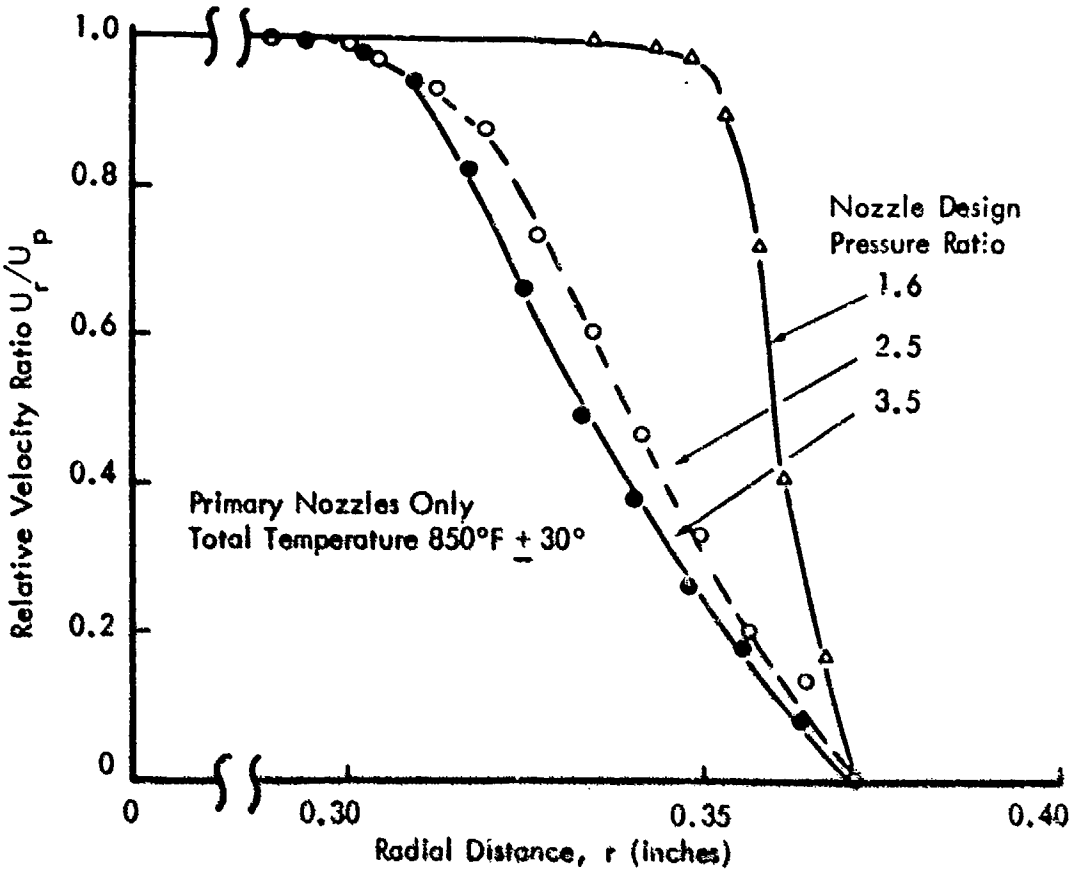

Figure B-3. Typical Flow Velocity Profiles Through Exit Plane Boundary Layer for the Three Primary Nozzles.

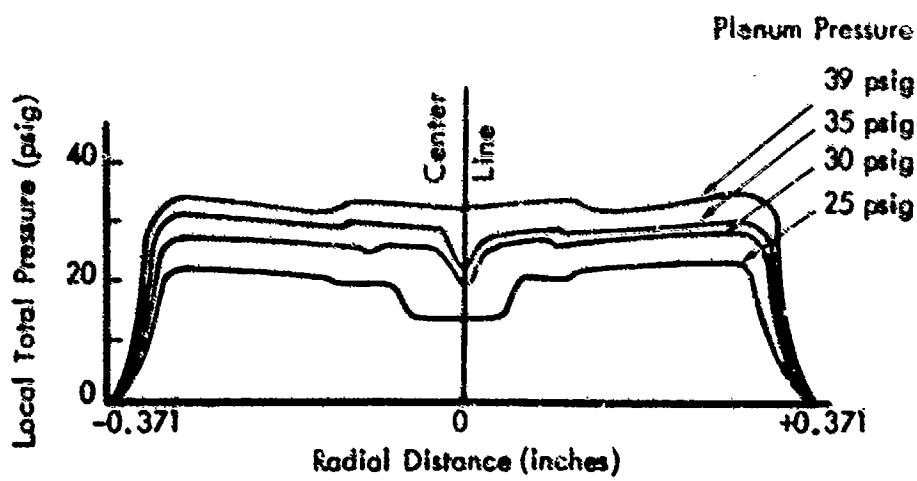

Figure B-4. Typical Profile of Total Pressure at Exit Plane of Supersonic Nozzle (Pressure Ratio 3.5) Operating at Off-Design Conditions.

The complete velocity profile for the supersonic nozzles was found to be very sensitive to changes in pressure ratio. Figure B-4 illustrates the changes that occur for the nozzle designed for a pressure ratio of 3.5. The correct plenum pressure for this nozzle is 37 psig, which unfortunately was not included in the series of runs. However, the figure still indicates that the discontinuities in the velocity profile decrease as the correct pressure ratio is approached.

Figure B-5 shows the total pressure profiles for the flow from the secondary nozzles with a primary nozzle in position but without any airflow through it. The profiles were made on a single traverse across a diameter of the jet. For presentation, the profiles for both sides of the jet are placed on the same graph. A slight lack of symmetry which decreases with area ratio is displayed on these figures. This was due partly to off-center fitting of the primary nozzle which was rectified by improving the location and fixing of the primary nozzles. Note that on the figure for area ratio 10, a dashed line is included to show the profile that was measured when the primary nozzle, without any airflow through it, was retracted inside the secondary nozzle. In this case, the flow at the exit plane is essentially uniform across the whole diameter of the nozzle.

The remaining figures show measurements made with airflow in both the primary and secondary nozzles. Figure B-6 shows the total pressure and total temperature profiles at several axial positions for a nozzle with area ratio 10. The primary nozzle was designed to run at a pressure ratio of 2.5 but for this series of traverses was actually run at 2.1. The secondary nozzle was operated at a pressure ratio of 1.5. There is evidence of the operation of the primary nozzle below its design pressure ratio shown by the discontinuous form of the total pressure profile at the exit plane within the region of the primary flow. It will also be noted that there is a sharp dip in the total pressure profile at the edge of the primary nozzle caused by the finite thickness of the edge of the primary nozzle and the boundary layer shed from the inside and outside of the primary nozzle. As the profile station is moved downstream, the evidence of the shock structure in the primary flow grows weaker and the mixing process between primary and secondary flow becomes apparent. Figure B-7 shows a similar series of profiles for the primary nozzle with pressure ratio 3.5. Again, the nozzle is operating slightly off design pressure ratio. It is also apparent that the rate of decay of total pressure in a radial direction is much more rapid than the decay in temperature. This is a characteristic of the mixing process in jet flow.

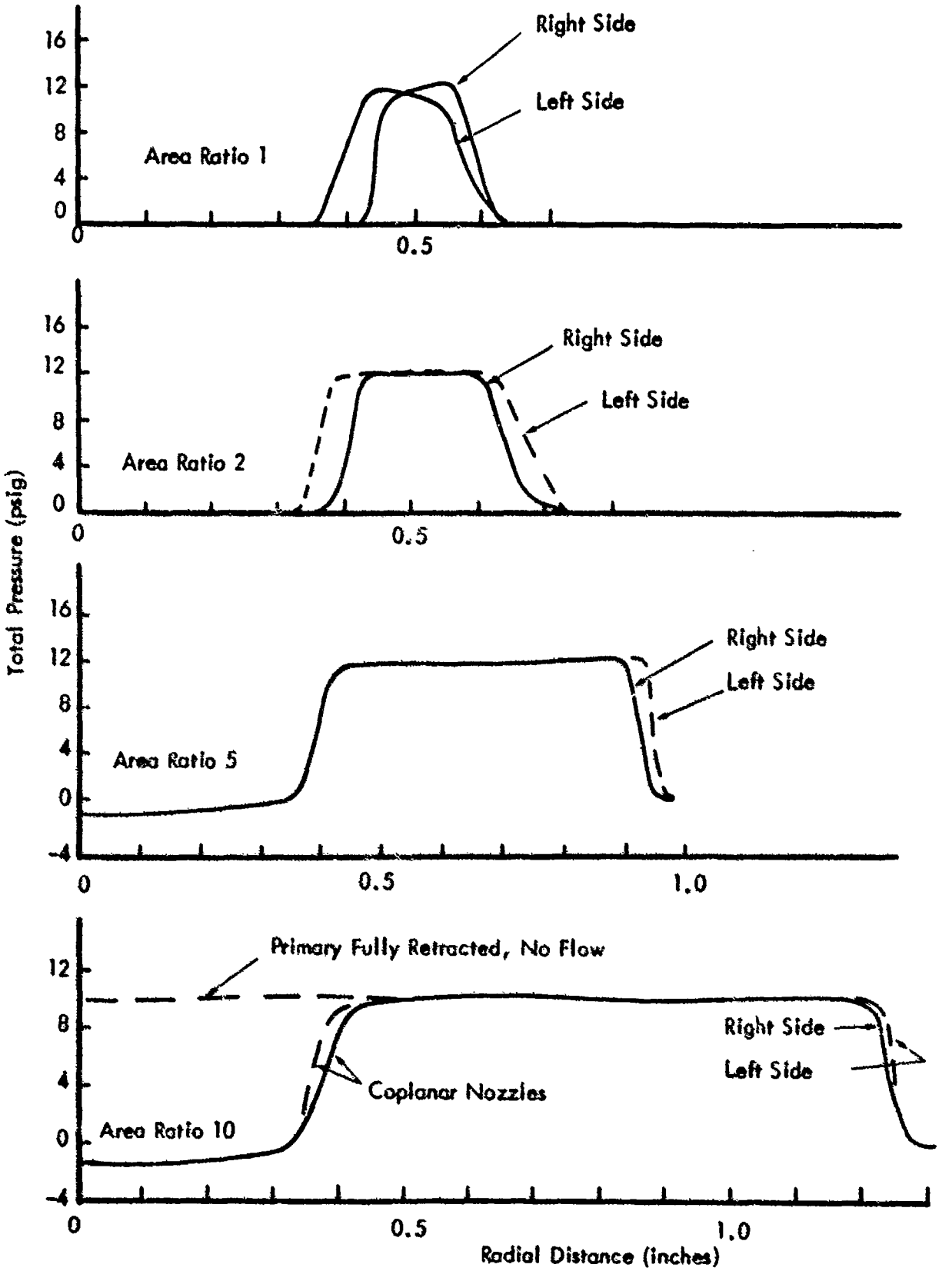

Figure B-5. Total Pressure Profiles at Exit Plane of Secondary Nozzle (Coaxial Nozzles with No Flow in Primary Nozzle).

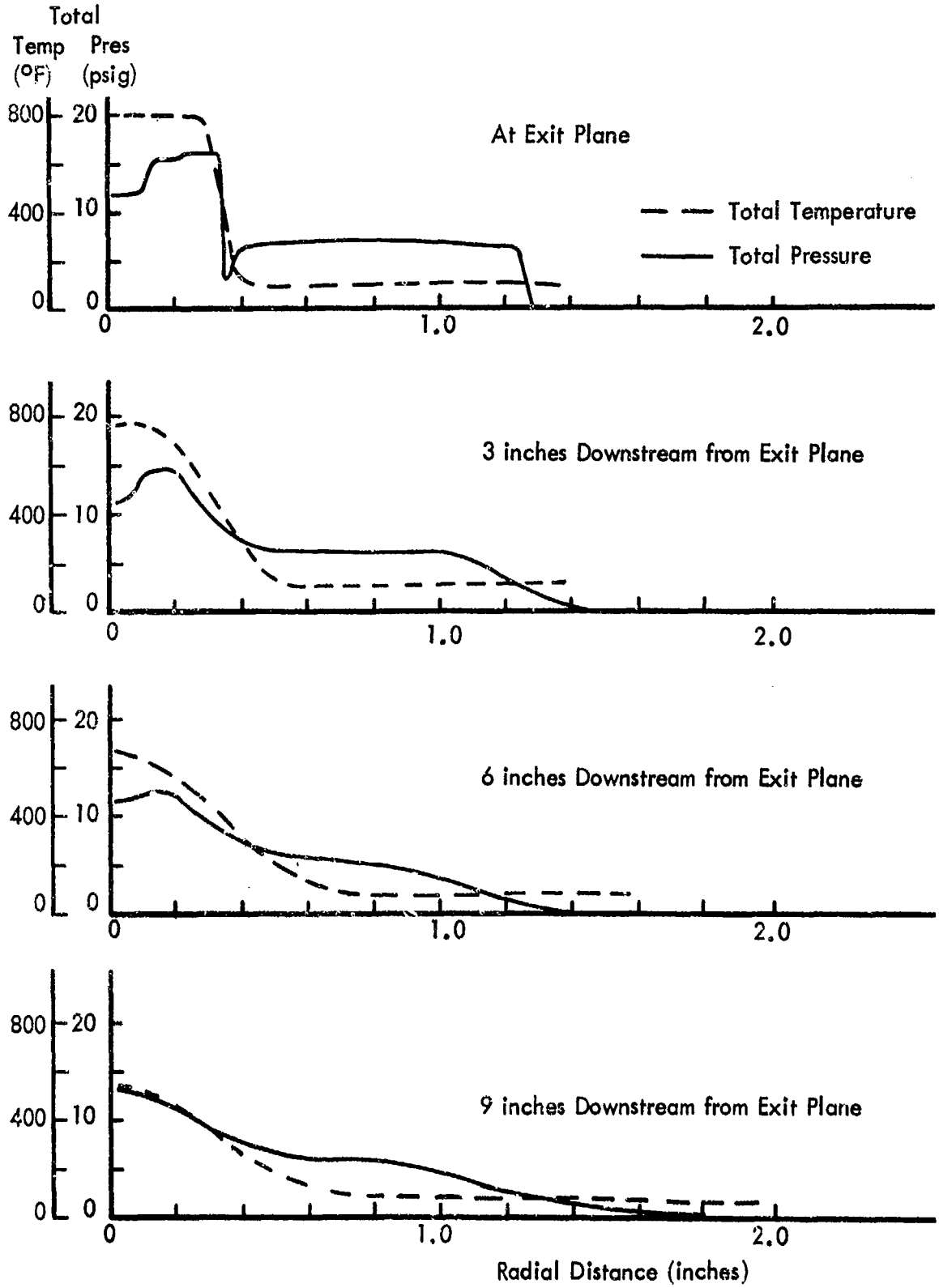

Figure B-6. Total Pressure and Temperature Profiles at Several Axial Positions for Coplanar Nozzles with Area Ratio 10. Primary Pressure Ratio 2.1, Secondary Pressure Ratio 1.5. (Primary Operating Below Design Pressure Ratio.)

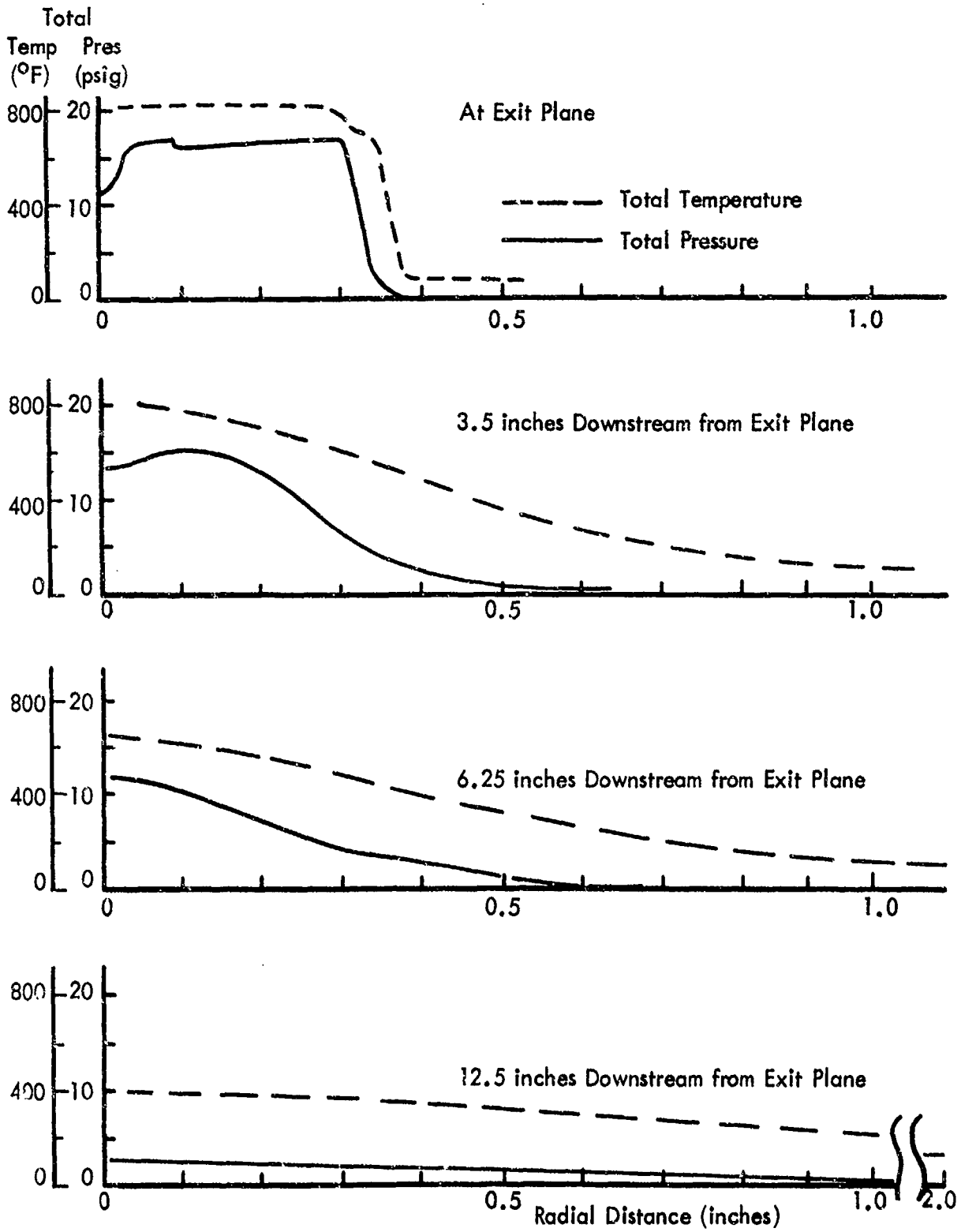

Figure B-7. Total Pressure and Temperature Profiles at Several Axial Positions for Pressure Ratio 3.5 Primary Nozzle Alone. (Operating Slightly Below Design Pressure.)

The profiles measured with the primary nozzle fully extended or fully retracted did not show particularly striking features. The only case illustrated (Figure B-8) shows the total pressure and temperature profile across the exit plane of the secondary nozzle (area ratio 10) with the primary nozzle fully retracted. The primary nozzle was run at a temperature of 790°F. There is a very slight bulge in the pressure and temperature profiles at the exit plane, which indicates that considerable mixing of the secondary and primary flows has taken place. Profile measurements made with the primary fully extended were distinguished by the absence of any significant difference between these profiles and the profiles obtained for the primary alone. This is not too surprising in view of the relatively long distance (8.5 inches) between the secondary and primary nozzles.

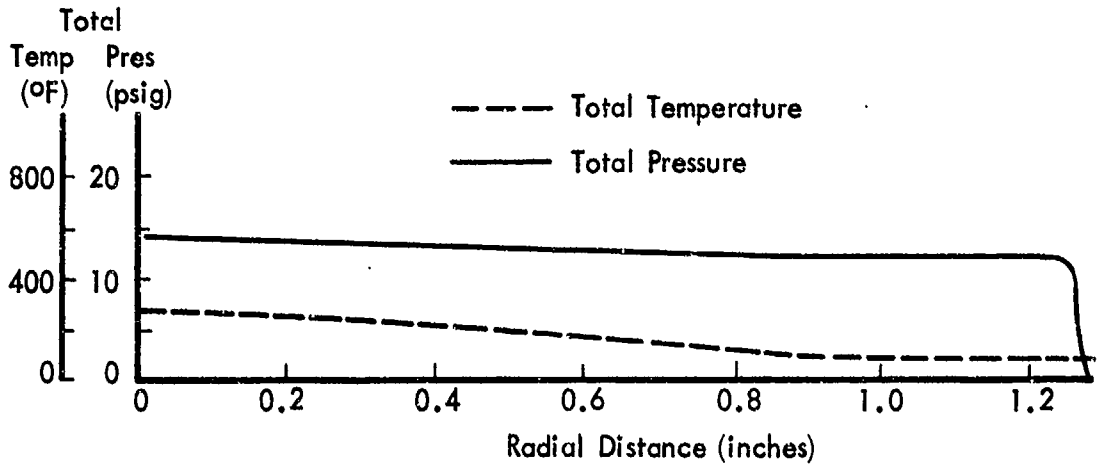

Figure B-8. Total Pressure and Temperature Profiles at Exit Plane of Secondary Nozzle (Pressure Ratio 1.89, Area Ratio 10) with Primary Nozzle (Pressure Ratio 2.5, Total Temperature 790°F) Fully Retracted.

Intentionally Left Blank

APPENDIX C

COMPUTER PROGRAM FOR DATA ANALYSIS

Section 3.3 of this report has given details of the analytic methods used to process the experimentally-obtained data and to scale them to obtain results applicable to full-scale jets. The details of the programs used for accomplishing these analyses are given in this appendix.

The data obtained from the experiment was in two forms. The basic data giving flow conditions, pressures and temperatures for each run was noted on run sheets and then transcribed and punched on FORTRAN data cards. The remaining octave band and overall sound pressure data obtained from the traverse of the jet sound field was stored on magnetic tape and later processed by an automatic octave band analyzer which punched the data on eight-hole paper tape. A preliminary program was therefore required to reproduce this data on FORTRAN data cards. This reproduction program was written at the Control Data Corporation (CDC) Data Center at Los Angeles to run on a small CDC 160A computer. This was a machine language program and is not reproduced here.

The main portion of the data processing was done using a FORTRAN program written for the CDC 6600 computer at Los Angeles. Details of this program are given in the following pages. The program was written as a series of subprograms. The connections between these subprograms are shown in Figure C-1. A brief description of each of these subprograms is then given, followed by a complete listing.

C-1 Controlling Program A1901

Purpose

This is the controlling program for the reduction and analysis of the model jet acoustical data. It accepts the model data and scales it to equivalent full size bypass jet engine exhaust noise data.

Argument List

The elements in the argument list for this routine are control information required by the particular CDC 6600 Computer System on which this program was run.

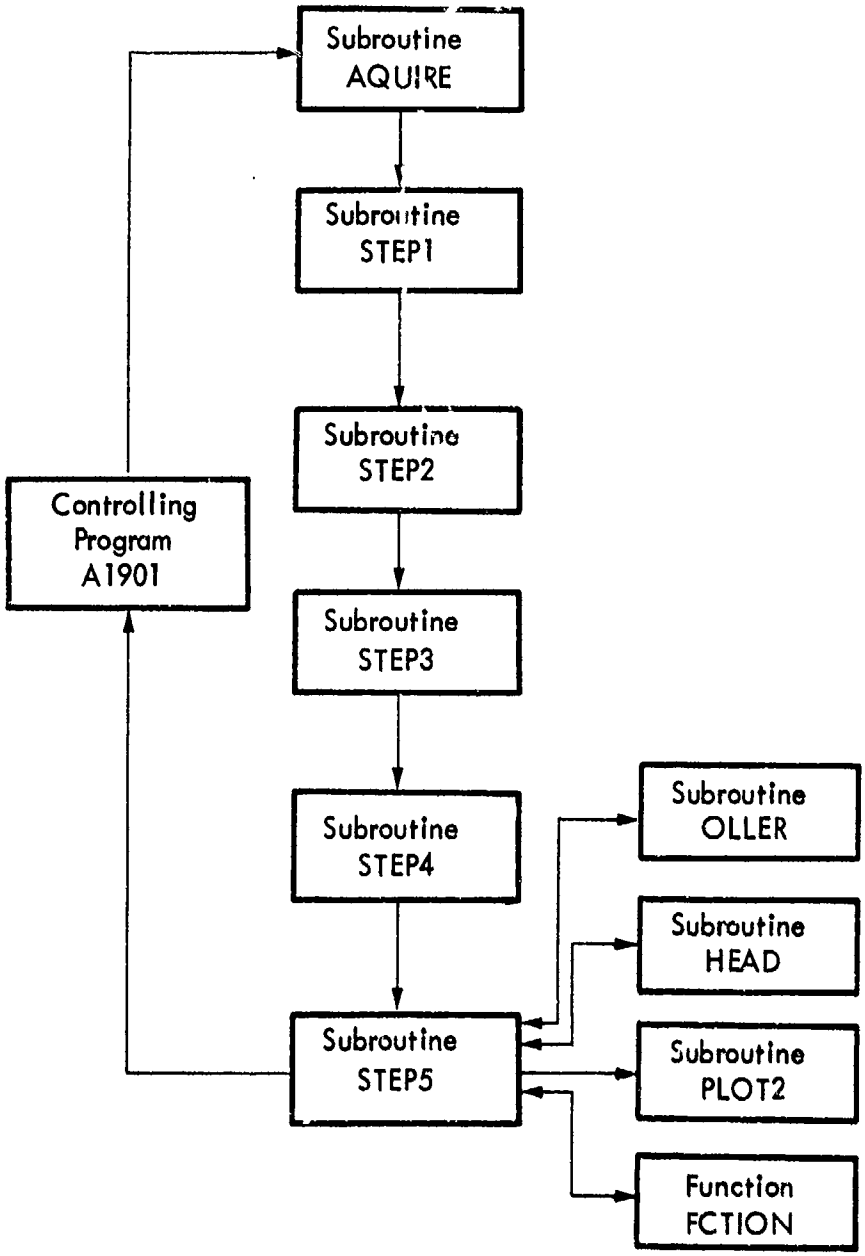

Figure C-1. Basic Flow Diagram for Complete Data Reduction Computer Program

Common Storage

/DATA1/

FF contains one-third octave band center frequencies (these are set in a DATA statement).

M1, L1, LC, M2, L2 are constants (set in a DATA statement) utilized in subroutine OLLER for perceived noise level calculations.

/DATA2/

ICH is a counter used in subroutine AQUIRE (set as a DATA statement).

PI is the constant π.

AB0, AB1, AB2 are constants used in function FCTION (set as DATA).

/DATA3/

The items in this common data store are as defined below as input to this routine (except that at input, the first character is repeated; e.g., RRM at input is equivalent to RM in DATA3).

/DATA4/

RC is the value of specific acoustic impedance (ρc, cgs rayls).

R is the radius of the boom (ft) of the traverse microphone.

VM is the velocity of the microphone on the boom (ft/sec).

DT is the time to take one sound level reading with the traversing microphone (sec).

TH contains a list of the angles relative to the jet axis at which sound measurements were made.

XR1, XR2 are the two sideline distances.

THR1, THR2, THR3 and THR4 are the four full-scale jet thrusts.

F contains the octave band center frequencies.

All the above data were set as a DATA statement.

/DATA5/

N, N1, NC are integers controlling the amount of the experimental data that is used in the analysis (set as DATA).

V is storage space for the experimental data.

DBMS is the instrumentation noise floor.

IND is used in subroutine STEP3.

Unnamed Common Storage

Used as required throughout the computer program.

Method

See Section 3.3.

Other Routines Used

This controlling program uses subroutines STEP1, STEP2, STEP3, STEP4, STEP5, PLOT2, OLLER and HEAD, and function FCTION. In addition, certain plotting routines are called which were incorporated within the software of the computer system used.

Data Required

Some of the invariant data used are set within this program. The remaining data required is information concerning the flow conditions of the runs being analyzed. The data is required in the following order:

NJOB: The total number of runs to be processed.

NCASES: Not used in this particular version of the program.

J: Any integer. This is used purely to ensure that a read error will be produced should the data cards get out of sequence.

RRN: The number assigned to the particular run.

AAP: Axial position of primary jet with respect to the secondary jet (in inches).

TTT1: Primary jet temperature (^{o}R).

TTT2: Secondary jet temperature (^{o}R).

PPR: Pressure ratio across the primary nozzle.

AAR: The ratio of the area of the secondary nozzle to the area of the primary.

VVR: The static pressure (reservoir pressure, psig) for the secondary nozzle. Immediately after this number is read in, it is used in conjunction with the data in VV1 to calculate the ratio of the secondary nozzle velocity to the primary nozzle velocity. This velocity ratio is then stored in this location.

VV1: The static pressure (reservoir pressure, psig) for the primary nozzle. Immediately after this information is read in, it is used to calculate the exit velocity for the primary nozzle. This velocity is then stored in this location.

RRMM: The mass flow through the secondary nozzle (lbs/min).

EEM1: The mass flow through the primary nozzle (lbs/min).

TTHR: The thrust of the model jet (lbs).

TT: The ambient temperature (^{o}R).

PP: The ambient pressure (inches of mercury).

HH: The ambient relative humidity (percent).

CCF: The calibration factor relating millivolt output of the octave band analyses to sound pressure (dynes per cm^2/millivolt).

TTB: The angle (in degrees) from the jet exhaust axis at which the total sound power integration was begun. In the present series of tests, this was constant at 12.5 degrees.

Further data is then required for subroutine AQUIRE.

Printing

This routine prints the number of experimental runs to be processed, followed by the invariant data set within the program. As each run is processed, it prints out the data previously read in (as in the preceding section). Additional output is produced by subroutines STEP1, STEP2, STEP3, STEP4 and HEAD.

Miscellaneous

There is a limit of 200 on the total number of experimental runs that can be processed in any one run on the computer.

C-2 Subroutine AQUIRE

Purpose

Reads in, checks and converts to floating point form the sound level data from each experiment.

Argument List

NR: The number of the run for which acoustic data is sought.

VX: Storage for the acoustic data as processed by this subroutine.

ISTOP: This is set equal to +1 if an error is found in the data (in which case the controlling program A1901 does not attempt to process the data). Otherwise, ISTOP equals zero.

Common Storage

For details, see Controlling Program A1901.

Method

The routine searches for the character "L." Having found one, it checks to see if the next three (3) characters from the run number NR. This process is continued until the correct run number is found. The following thirty-six (36) characters are then processed in groups of three (3) to form millivolt values corresponding to measured sound pressure levels. It searches for 21 groups of such data and processes them.

Data Required

This routine requires 21 groups of forty (40) characters. Each group should begin with the character "L." The next 3 characters in each group constitute the run number. The remaining twelve (12) sets of 3 characters correspond to 12 sound pressure level readings. These 12 are a reference level, ten (10) octave band levels (up to 31.5 kHz band) and the overall sound pressure level. The 21 groups of 40 characters are the sound levels at 5-degree intervals, starting at 15 degrees from the axis of the jet.

Miscellaneous

There are three (3) error stops in this routine. They occur if (1) there is too much data, (2) there is too little data, or (3) a character other than a numeral or "L" is found. In the first two cases, ISTOP is set equal to unity. In the second, the whole computer run is aborted.

C-3 Subroutine STEP1

Purpose

Converts the millivolt sound level readings to decibel readings relative to 0.0002 dynes/cm^2.

Common Storage

See Controlling Program A1901.

Method

The data obtained by subroutine AQUIRE is converted first to sound pressure in dynes per square centimeter (arrays X and V) and then to sound pressure levels re 2×10^{-4} dynes per square centimeter (array Y). In this conversion, the following correction factors determined from the instrumentation checkout (see Section 3.2.2) were included.

Octave Band Center Frequency (kHz)	0.5	1	2	4	8	16	31.5	Overall
Correction	0	0.5	1.5	1.0	2.0	3.0	4.5	6.0

The reference level and 63 Hz, 125 Hz and 250 Hz octave bands are ignored since they are not relevant to this experiment. In addition, the overall level is calculated from the sum of the octave band levels. This value replaces the experimentally-determined value which will not be correct because of the coupling between the spectrum shape and the correction factors given in the above table.

Printing

The octave band and overall sound pressure levels in decibels for the model jet are printed for twenty-one (21) angular positions at 5-degree intervals, starting 15 degrees from the axis of the jet exhaust.

C-4 Subroutine STEP2

Purpose

To determine the total power radiated from the model jet.

Common Storage

See Controlling Program A1901.

Method

The radiated sound from the jet is assumed to be cylindrically symmetric about the jet axis. The total sound power (in watts) is therefore found by integrating the sound intensity over a sphere centered on the jet nozzle. This integration is carried out both for overall sound power radiated and for the power in the octave bands. The power level is then determined by converting to decibels relative to 10^{-13} watts.

Finally, the overall sound power level is scaled to give the values for full-scale engines with 10,000 lbs, 20,000 lbs, 40,000 lbs and 80,000 lbs thrust.

Printing

The overall and octave band sound power (in watts) and sound power level (in dB relative to 10^{-13} watts) are printed for the model jet. The overall sound power levels for the four (4) full-scale jet engines are listed.

C-5 Subroutine STEP3

Purpose

To calculate the directivity pattern for the jet noise.

Common Storage

See Controlling Program A1901.

Method

The overall and octave band directivity are calculated based on the definition of directivity as the difference between the actual sound pressure level and the sound pressure level that would pertain if the total sound power output of the jet were radiated equally in all directions.

Printing

The overall and octave band directivity indices are printed, along with an indication of the noise floor for that particular octave band.

C-6 Subroutine STEP4

Purpose

To calculate the jet mechanical power and acoustic conversion efficiency.

Common Storage

See Controlling Program A1901.

Method

The mechanical power is defined in Section 3.3 and is calculated in watts. The acoustic conversion efficiency is the ratio of the total acoustic power to the jet mechanical power.

C-7 Subroutine STEP5

Purpose

To calculate the sideline overall and octave band sound pressure levels and the sideline perceived noise levels.

Common Storage

See Controlling Program A1901.

Method

The theoretical basis for this subroutine is given in Section 3.3. The four (4) extra octave bands are added in this routine, assuming a constant decrease in level of 3 dB per octave above the 31.5 kHz band. The routine allows for attenuation due to distance (inverse square law) and atmospheric attenuation. Two sideline distances (500 feet and 1500 feet) and four full-scale jet thrusts (10,000 lbs, 20,000 lbs, 40,000 lbs and 80,000 lbs) are considered. The positions on the sidelines correspond to five-degree angle increments starting at 15 degrees from the jet axis. The attenuation effects are calculated in the main part of this routine. Subroutine OLLER is used to calculate the perceived noise levels.

Other Routines Used

This routine calls subroutines OLLER, HEAD and PLOT2, and function subroutine FCTION.

Printing

Subroutine HEAD prints the sideline sound level information. (For further details see the specification for subroutine HEAD.)

C-8 Subroutine OLLER

Purpose

Calculates the sideline perceived noise levels (PNL in units of PNdB), given the sideline octave band sound pressure levels.

Argument List

F is a one-dimensional array giving the center frequencies of the octave bands.

THR is the thrust of the model jet.

THRI is the thrust of the full-scale engine.

SL is the two-dimensional array containing the sideline octave band information.

PN is the array which contains (on exit from the routine) the sideline perceived noise level (PNdB).

Common Storage

See Controlling Program A1901.

Method

Outlined in Society of Automotive Engineers "Definitions and Procedures for Computing the Perceived Noise Level of Aircraft Noise," Aerospace Recommended Practice (ARP) 865, dated October 15, 1964.

Miscellaneous

(1) The noy curves (tables) exist only for frequencies in the range 50 Hz $\leq f \leq$ 10,000 Hz. The routine allows for lower frequencies by extending the noy curves as a constant (independent of frequency) below 50 Hz. At frequencies above 10,000 Hz, the contribution to the perceived noise is assumed to be negligible.

(2) If any octave band sound pressure level should exceed 136.0 dB, the routine places 777.0 PNdB in the appropriate place in the PNdB table.

C-9 Subroutine HEAD

Purpose

Prints the sideline octave band and overall sound pressure levels and the perceived noise level.

Argument List

THR is the thrust of the model jet.

THRI is the thrust of the full-scale jet.

SL is a two-dimensional array containing the octave band and overall sideline sound pressure levels.

PN is a one-dimensional array containing the sideline perceived noise levels.

AL is a one-dimensional array listing the positions along the sideline at which the sound levels, et cetera, are determined.

Common Storage

See Controlling Program A1901.

Printing

This routine prints sideline sound pressure level and perceived noise levels at twenty-one (21) positions along the sideline. These positions are at 5-degree intervals from the jet axis, starting at 15 degrees from the axis. For each sideline position, the printing consists of:

(1) The distance in feet to the point on the sideline at which the sound levels are calculated.

(2) The perceived noise level at that point. The first value is obtained by including eleven (11) octave bands in the perceived noise level calculation. The value in parenthesis is the value obtained without using the top four (4) octave bands. These are the bands that were extrapolated in Subroutine STEP5.

(3) The overall sound pressure level.

(4) Eleven (11) octave band sound pressure levels. It should be noted that the center frequencies of these octave bands will vary because they are scaled from the model frequencies by the square root of the ratio of the model thrust to full-scale thrust.

C-10 Subroutine PLOT2

Purpose

Plots the perceived noise level on the 1500-foot sideline for full-scale jet engines with thrusts of 10,000 lbs, 20,000 lbs, 40,000 lbs and 80,000 lbs.

Argument List

X is the distance from the jet to the point on the 1500-foot sideline.

Y1, Y2, Y3 and Y4 are the column arrays containing the perceived noise levels for the four (4) full-scale jet engines.

RN is the run number being analyzed.

Method

The four (4) sideline perceived noise levels are plotted and labeled appropriately. The scales are not marked on the axes, but the vertical axis has a range of perceived noise levels from 50 PNdB to 130 PNdB while the horizontal axis gives distance along the sideline in the range -1000 feet to +6000 feet. The zero point on this axis corresponds to the point on the sideline nearest to the jet, i.e., the point at which a line from the jet, at right angles to the jet axis, intersects the sideline.

Other Routines Used

Subroutines PLOT, SYMBOL and NUMBER were used. These were part of the FORTRAN operating system on which this complete computer program was run and therefore were not provided as separate routines with the program card deck. Subroutine PLOT is the routine for drawing lines and moving the pen and subroutines SYMBOL and NUMBER are the routines for writing Hollerith characters and numbers, respectively, on the graph.

Miscellaneous

The output from this routine was plotted off-line on a CALCOMP plotter.

C-11 Function FCTION

Purpose

Used in computation of atmospheric attenuation.

Method

Calculates an attenuation factor from a measured attenuation curve as outlined in Section 5.

Argument List

J is an integer indicating the frequency being considered.

THRI is the full-scale jet thrust.

Common Storage

See Controlling Program A1901.

Intentionally Left Blank

```
      PROGRAM A1901(INPUT,OUTPUT,TAPE60=INPUT,TAPE61=OUTPUT,TAPE7)
      REAL M1,M2,L1,L2,LC
C *****
      COMMON/DAT1/ FF(24),M1(24),L1(24),LC(24),M2(24),L2(24)
      COMMON/DAT2/ ICH,PI,AB0,AB1,AB2
      COMMON/DAT3/ RN,AP,TT1,TT2,PR,AR,VR,V1,RMM,EM1,THR,T,P,H,CF,TB
      COMMON/DAT4/ RC,R,VM,DT,TH(21),XR1,XR2,THR1,THR2,THR3,THR4,F(14)
      COMMON/DAT5/ N,N1,NC,M,V(13,21) ,DBNS,IND(11)
C *****
      DIMENSION BUFF(1024)
      DIMENSION DD(1)
      EQUIVALENCE (DD(1),RN)
C *****
      COMMON EM,EM2,V2,X(12,21),Y(12,21),A(21),W(11),PW(11),DI(11,21)
      COMMON CE(1),SLL1(15,21),SLL2(15,21),AL1(21),AL2(21)
      COMMON PN11(21),PN12(21),PN13(21),PN14(21),PN1(21),PN2(21)
      COMMON PN21(21),PN22(21),PN23(21),PN24(21)
      COMMON SL11(15,21),SL12(15,21),SL13(15,21),SL14(15,21)
      COMMON SL21(15,21),SL22(15,21),SL23(15,21),SL24(15,21)
C *****
      DIMENSION RRN(200),AAP(200),TTT1(200),TTT2(200),PPR(200),AAR(200),
     1VVR(200),VV1(200),RRMM(200),EEM1(200),TTHR(200),TT(200),PP(200),HH
     2(200),CCF(200),TTB(200),JJ(200),KK(273),DDBNS(200)
      EQUIVALENCE (JJ(1),HH(1)),(KK(1),V(1))
C *****
      DATA (AB0=0.127032),(AB1=1.338286),(AB2=-0.207140)
      DATA ((TH(I),I=1,21)=15.0,20.0,25.0,30.0,35.0,40.0,45.0,50.0,55.0,
     160.0,65.0,70.0,75.0,80.0,85.0,90.0,95.0,100.0,105.0,110.0,115.0)
      DATA (R=10.667),(VM=1.2),(DT=0.273),(RC=41.5)
      DATA (N=21),(N1=21),(NC=21),(M=664)
      DATA (ICH=81),(PI=3.14159265)
      DATA (XR1=500.0),(XR2=1500.0)
      DATA (THR1=10000.0),(THR2=20000.0),(THR3=40000.0),(THR4=80000.0)
      DATA ((F(I),I=1,14)=63.0,125.0,250.0,500.0,1000.0,2000.0,4000.0,80
     100.0,16000.0,31500.0,63000.0,125000.0,250000.0,500000.0)
      DATA ((KK(I),I=1,40)=4HTHIS,4H TAP,4HE CO,4HNTAI,4HNS T,4HHE R,4HE
     1SUL,4HTS O,4HF JE,4HT NO,4HISE ,4HEXPE,4HRIME,4HNT, ,4HWORK,4H PER
     2,4HFORM,4HED U,4HNDER,4H CON,4HTRAC,4HT FO,4HR TH,4HE FA,4HA, P,4H
     3ROGR,4HAM W,4HRITT,4HEN F,4HOR T,4HHE C,4HDC. ,4H6600,4H. FI,4HRST
     4 ,4HTEST,4H ON ,4H12/1,4H3/68,4H.    )
      DATA ((FF(I),I=1,24)=50.0,63.0,80.0,100.0,125.0,160.0,200.0,250.0,
     1315.0,400.0,500.0,630.0,800.0,1000.0,1250.0,1600.0,2000.0,2500.0,3
     1150.0,4000.0,5000.0,6300.0,8000.0,10000.0)
      DATA ((M1(I),I=1,24)=0.043478,0.04057,2(0.036931),0.035336,2(0.033
     1333),0.032051,0.030675,6(0.030103),7(0.02996),2(0.042285))
      DATA ((L1(I),I=1,24)=64.0,60.0,56.0,53.0,51.0,48.0,46.0,44.0,42.0,
     15(40.0),38.0,34.0,32.0,30.0,2(29.0),30.0,31.0,37.0,41.0)
      DATA ((LC(I),I=1,24)=91.01,85.88,87.32,79.85,79,76,75.96,73.96,74.
     191,94.63,13(0.0),44.29,50.72)
      DATA ((M2(I),I=1,24)=15(0.030103),9(0.029960))
      DATA ((L2(I),I=1,24)=52.0,51.0,49.0,47.0,46.0,45.0,43.0,42.0,41.0,
     15(40.0),38.0,34.0,32.0,30.0,2(29.0),30.0,31.0,34.0,37.0)
C *****
      DIMENSION OUTLAB(483),OUTBLA(2999)
      EQUIVALENCE(OUTLAB(1),FF(1))
      EQUIVALENCE(AP,IAP),(TTT2,TT2),(IAR,AR),(IVR,VR),(IRMM,RMM)
      CALL PLOTS(BUFF,1024,7)
```

```
      CALL PLOT(0.0,0.5,-3)
      READ (60,1) NJOB,NCASES
1     FORMAT (2I5)
      WRITE (61,600)
 600  FORMAT (1H1)
      WRITE (61,2) NJOB
    2 FORMAT (10X,34HANALYSIS OF JET NOISE EXPERIMENTS./10X,33(1H-)///10
     1X,I5,2X,28HEXPERIMENTS TO BE PROCESSED.////)
      IF (NJOB.GT.200) 3,4
    3 STOP
    4 WRITE (61,5) (DD(I),I=17,20)
    5 FORMAT(10X,38HLISTING OF STANDING DATA FOR ALL RUNS./10X,38(1H-)/
     1/10X,49HSPECIFIC ACOUSTIC IMPEDANCE OF AIR AT STD. CONDS.,11X,2H=
     2,F10.4/10X,28HMICROPHONE BOOM SWEEP RADIUS,32X,2H= ,F10.4/10X,25HM
     3ICROPHONE SWEEP VELOCITY,35X,2H= ,F10.4/10X,33HTIME BETWEEN SEQUEN
     4TIAL PRINTOUTS,27X,2H= ,F10.4)
      WRITE (61,6) (DD(I),I=42,47)
    6 FORMAT (10X,24HFIRST SIDE-LINE DISTANCE,36X,2H= ,F10.4/10X,25HSECO
     1ND SIDE-LINE DISTANCE,35X,2H= ,F10.4/10X,34HFIRST THRUST REFERENCE
     2 FOR SCALING,26X,2H= ,F10.4/10X,35HSECOND THRUST REFERENCE FOR SCA
     3LING,25X,2H= ,F10.4/10X,34HTHIRD THRUST REFERENCE FOR SCALING,26X,
     42H= ,F10.4/10X,35HFOURTH THRUST REFERENCE FOR SCALING 25X,2H= ,F10
     5.4////)
      WRITE (61,7) (TH(I),I=1,21)
    7 FORMAT (10X,54HANGULAR POSITIONS OF MICROPHONE TO JET STREAM (THET
     1A),,// 7X,21F6.1////)
      WRITE (61,8) (F(I),I=4,10)
    8 FORMAT (10X,44HORIGINAL FREQUENCIES OF OCTAVE BAND CENTERS,//10X,
     17F9.1/1H1)
      DO 10 I=1,NJOB
      READ (60,111) J,RRN(I)
111   FORMAT (I5,F10.0)
      READ (60,9) AAP(I),TTT1(I),TTT2(I),PPR(I),AAR(I),VVR(I),VV1(I),RRM
     1M(I)
    9 FORMAT (8F10.0)
      READ (60,29)EEM1(I),TTHR(I),TT(I),PP(I),HH(I),CCF(I),TTB(I)
   29 FORMAT (7F10.0)
   10 CONTINUE
      DO 16 I=1,NJOB
      RN=RRN(I)
      TT1=TTT1(I)
      IF(AAP(I).GE.-0.5)  400,401
 401  V1=(VV1(I) + 14.6)/(VVR(I) + 14.6)
      PR=V1
      PPR(I)=V1
      GO TO 402
 400  CONTINUE
      PR=PPR(I)
      V1=(VV1(I) + 14.6)/14.6
 402  CONTINUE
      VR=(VVR(I) + 14.6)/14.6
      V1=(5.0*(V1**0.28571 - 1.0))**0.5
      VR=(5.0*(VR**0.28571 - 1.0))**0.5
      VV1(I)= TTT1(I)/(1.0 + (V1**2)/5.0)
      VVR(I)= TTT2(I)/(1.0 + (VR**2)/5.0)
      VV1(I)=1120.0*(VV1(I)/520.0)**0.5
      VVR(I)=1120.0*(VVR(I)/520.0)**0.5
      V1=V1*VV1(I)
```

```
      VV1(I)=V1
      VVR(I)=VR*VVR(I)
      IF(AAP(I).GE.-0.5) 405,406
  406 THR=TTHR(I)
      GO TO 407
  405 CONTINUE
      THR=(VV1(I)*EEM1(I) + VVR(I)*RRMM(I))/(60.0*32.2)
  407 CONTINUE
C   NOTE.......THE NOZZLE VELOCITIES ARE CALCULATED FROM THE MEASURED PRESSURE
C              RATIOS AND STATIC TEMPERATURES.  WITH RETRACTED PRIMARY,THE
C              CALCULATED SECONDARY VELOCITY WILL BE WRONG IF THE PRIMARY
C              TEMPERATURE DIFFERS FROM THE SECONDARY TEMPERATURE.   FOR
C              COPLANER NOZZLES AND EXTENDED PRIMARY,THRUST IS CALCULATED
C              FROM FLOW DATA.    FOR RETRACTED PRIMARY,THRUST IS THE MEASURED
C              THRUST.
      VVR(I)=VVR(I)/V1
      RRMM(I)=RRMM(I)/EEM1(I)
      EEM1(I)=EEM1(I)/60.0
      EM1=EEM1(I)
      T=TT(I)
      P=PP(I)
      H=HH(I)
      CF=CCF(I)
      TB=TTB(I)
      DBNS=(CCF(I)/0.063246)**2.0
      DBNS=65.6 + 10.0*ALOG10(DBNS)
      DDBNS(I)=DBNS
      IF(TTT2(I))20,25,20
   25 IAP=ITT2=IAR=IVR=IRMM=10H     NONE
      GO TO 30
   20 ENCODE(8,980,AP)AAP(I)
      ENCODE(8,980,TT2)TTT2(I)
      ENCODE(8,980,AR)AAR(I)
      ENCODE(8,980,VR)VVR(I)
      ENCODE (8,980,RMM) RRMM(I)
  980 FORMAT (F8.3)
   30 CONTINUE
      WRITE (61,600)
      WRITE (61,11) (DD(I),I=1,8)
   11 FORMAT (10X 10HRUN NUMBER,50X,2H= , F8.3/10X,47HAXIAL POSITION OF
     1PRIMARY WRT. SECONDARY (INS.),13X,2H= ,A8    /10X,23HPRIMARY TEMPER
     2ATURE (R),37X,2H= , F8.3/10X,25HSECONDARY TEMPERATURE (R),35X,2H=
     3,A8    /10X,22HPRIMARY PRESSURE RATIO,39X,2H= , F8.3/10X,10HAREA RA
     4TIO,50X,2H= ,A8    /10X,14HVELOCITY RATIO,46X,2H= ,A8    /10X,25HPRI
     5MARY VELOCITY (FT/SEC),35X,2H= , F8.3)
      WRITE (61,12) (DD(I),I=9,15)
   12 FORMAT (10X,15HMASS FLOW RATIO,45X,2H= ,A8    /10X,29HPRIMARY MASS
     1FLOW (LB/SEC)    ,31X,2H= , F8.3/10X,12HTHRUST (LBS),48X,2H= , F8.3
     2/10X,29HENVIRONMENTAL TEMPERATURE (R),31X,2H= , F8.3/10X,30HENVIRO
     3NMENTAL PRESSURE (IN.HG),30X,2H= , F8.3/10X,33HENVIRONMENTAL HUMID
     4ITY (PER CENT),27X,2H= , F8.3/10X,35HCALIBRATION FACTOR (MV TO DY/
     5SQ CM),25X,2H= , F8.3)
      WRITE (61,970) DBNS
  970 FORMAT (10X 32HINSTRUMENTATION NOISE FLOOR (DB) , 28X 2H= ,
     1 F8.3, ////45X 45(1H-), ////)
      IF(TTT2(I)) 35,40,35
   35 VR=VVR(I)
      RMM=RRMM(I)
```

```
 40 CONTINUE
    NRN=INT(RN)
 15 CALL AQUIRE (NRN,V,ISTOP)
    IF(ISTOP.EQ.1) 16,777
777 CONTINUE
    CALL STEP1
    CALL STEP2
    CALL STEP3
    CALL STEP4
    CALL STEP5
 16 CONTINUE
    CALL PLOT (0.0, 0.0, 999)
    WRITE (61,17)
 17 FORMAT (1X,10HEND OF RUN)
    STOP
    END


    SUBROUTINE AQUIRE (NR,VX,ISTOP)
    DIMENSION V(13,22),II(80),VX(13,21)
    COMMON/DAT2/ ICH
    ISTOP=0
    KJ=1
    MK=1
  1 IF (ICH.GT.80) 2,4
  2 READ (60,3) (II(I),I=1,80)
  3 FORMAT (80R1)
    ICH=1
  4 I=II(ICH)
    ICH=ICH+1
    IF (I.EQ.1RL)5,1
  5 NX=0  S  KI=0
    DO 8 J=1,3
    IF (ICH.GT.80) 6,7
  6 READ (60,3) (II(I),I=1,80)
    ICH=1
  7 NX = NX*10+II(ICH)-27
  8 ICH=ICH+1
    IF (NX.EQ.NR) 16,9
  9 IF (MK.EQ.1) 1,10
 10 IF (KJ-22)30,31,34
 30 WRITE(61,998) NR
998 FORMAT (1H0, 10X 10HRUN NUMBER, I5, X 18HINSUFFICIENT DATA,     )
 32 ISTOP=1
    GO TO 36
 31 JS=1
    JE=21
 38 K=0
    DO 33 J=JS,JE
    K=K+1
    DO 33 I=1,13
    VX(I,K)=V(I,J)
```

```
   33 CONTINUE
   36 RETURN
   34 IF(KJ.GT.23) 35,37
   35 WRITE (61,997) NR
  997 FORMAT (1H0,10X,10HRUN NUMBER,I5,2X,14HTOO MUCH DATA.)
      GO TO 32
   37 JS=2
      JE=22
      WRITE (61,996)
  996 FORMAT (2X,48HBEWARE. THERE ARE 22 PIECES OF DATA IN THIS RUN. )
      GO TO 32
C************
C     THE ABOVE THREE CARDS SHOULD BE REPLACED BY THE STATEMENT--GO TO 38 --
C          IF THE OPTION OF PROCESSING 22 PIECES OF DATA PER RUN IS REQUIRED.
C************
   16 KI=KI+1
      IF (NX)27,25,27
   26 V(KI,KJ) = 0.5
      GO TO 28
   27 V(KI,KJ)=FLOAT(NX)
   28 NX=0    $  MK=2
      DO 25 J=1,3
   17 IF (ICH.GT.80) 18,19
   18 READ (60,3) (II(I),I=1,80)
      ICH=1
   19 I=II(ICH)
      ICH=ICH+1
      IF(I.EQ. IRL)55,23
   55 KJ=KJ+1
      GO TO 5
   23 IF(I.GT.36) 21,24
   24 NX=NX*10+I-27
   25 CONTINUE
      GO TO 16
   21 WRITE (61,22)
   22 FORMAT (10X,27HINPUT ERROR IN SUBR. AQUIRE)
      STOP
      END
```

```
      SUBROUTINE STEP1
      REAL M1,M2,L1,L2,LC
      COMMON/DAT1/ FF(24),M1(24),L1(24),LC(24),M2(24),L2(24)
      COMMON/DAT2/ ICH,PI,AB0,AB1,AB2
      COMMON/DAT3/ RN,AP,TT1,TT2,PR,AR,VR,V1,RMM,EM1,THR,T,P,H,CF,TB
      COMMON/DAT4/ RC,R,VM,DT,TH(21),XR1,XR2,THR1,THR2,THR3,THR4,F(14)
      COMMON/DAT5/ N,N1,NC,M,V(13,21)
      COMMON EM,EM2,V2,X(12,21),Y(12,21),A(21),W(11),PW(11),DI(11,21)
      COMMON CE(1),SL11(15,21),SL12(15,21),AL1(21),AL2(21)
      COMMON PN11(21),PN12(21),PN13(21),PN14(21),PN1(21),PN2(21)
      COMMON PN21(21),PN22(21),PN23(21),PN24(21)
      COMMON SL11(15,21),SL12(15,21),SL13(15,21),SL14(15,21)
      COMMON SL21(15,21),SL22(15,21),SL23(15,21),SL24(15,21)
      DO 200 J=1,21
      V(3,J)=0.5
      V(4,J)=0.5
  200 V(5,J)=0.5
      DO 100 I=2,13
      DO 100 J=1,N
      V(I,J)=V(I,J)*CF
  100 CONTINUE
      DO 1 I=1,N1
      K=I
      X(1,K)=V(2,I)
      Y(1,K)=ALOG10(X(1,K)*X(1,K))*10.0+74.0
      DO 1 J=3,13
      L=J-1
      X(L,K)=V(J,I)
      Y(L,K)=ALOG10(X(L,K)*X(L,K))*10.0+74.0
    1 CONTINUE
      DO 25 I3=1,NC
C*******
C     THIS LOOP INSERTS THE FOLLOWING OCTAVE BAND CORRECTION FACTORS
C          250HZ        0DB.
C         1000HZ      +0.5DB.
C         2000HZ      +1.5DB.
C         4000HZ      +1.0DB.
C         8000HZ      +2.0DB.
C        16000HZ      +3.0DB.
C        31500HZ      +4.5DB.
C         OVERALL       +6.0DB.
C*******
      Y( 6,I3)=Y( 6,I3) + 0.5
      Y( 7,I3)=Y( 7,I3) + 1.5
      Y( 8,I3)=Y( 8,I3) + 1.0
      Y( 9,I3)=Y( 9,I3) + 2.0
      Y(10,I3)=Y(10,I3) + 3.0
      Y(11,I3)=Y(11,I3) + 4.5
      Y(12,I3)=Y(12,I3) + 6.0
      V( 7,I3) = X( 6,I3) = X( 6,I3)*(10.0**(0.5/20.0))
      V( 8,I3) = X( 7,I3) = X( 7,I3)*(10.0**(1.5/20.0))
      V( 9,I3) = X( 8,I3) = X( 8,I3)*(10.0**(1.0/20.0))
      V(10,I3) = X( 9,I3) = X( 9,I3)*(10.0**(2.0/20.0))
      V(11,I3) = X(10,I3) = X(10,I3)*(10.0**(3.0/20.0))
      V(12,I3) = X(11,I3) = X(11,I3)*(10.0**(4.5/20.0))
      V(13,I3) = X(12,I3) = X(12,I3)*(10.0**(6.0/20.0))
   25 CONTINUE
```

```
      DO 9 I=1,NC
      SUM=0.0
      DO 8 K=5,11
    8 SUM=SUM+10.0**(Y(K,I)/10.0)
      Y(12,I)=10.0*ALOG10(SUM)
    9 CONTINUE
      WRITE (61,2)
    2 FORMAT (10X,17HEXPERIMENTAL DATA /10X,79HTABLE SHOWING OCTAVE BAND
     * AND OVERALL SOUND PRESSURE LEVEL VARIATION WITH ANGLE  ///)
      WRITE (61,12) (F(I),I=4,10)
   12 FORMAT (6X,5HANGLE,17X,65HOCTAVE     BAND     SOUND     PRESSURE     L
     1EVELS ,17X,4HOVER /6X,5H(DEG), 5X,7(F6.0,4X),5X,3HALL /)
      DO 3 I=1,NC
      J=I
      WRITE(61,4) TH(J),(Y(K,I),K=5,12)
    4 FORMAT (5X,F6.1, 5X,7(F6.1,4X),2X,F6.1)
    3 CONTINUE
      WRITE (61,5)
    5 FORMAT (///////)
      DO 6 J=1,N
      XX=V(2,J)
      V(2,J)=V(13,J)
      V(13,J)=XX
    6 CONTINUE
      DO 7 J=1,21
      XX=X(1,J)
      X(1,J)=X(12,J)
      X(12,J)=XX
      XX=Y(1,J)
      Y(1,J)=Y(12,J)
      Y(12,J)=XX
    7 CONTINUE
      RETURN
      END
```

```
      SUBROUTINE STEP2
      REAL M1,M2,L1,L2,LC
      COMMON/DAT1/ FF(24),M1(24),L1(24),LC(24),M2(24),L2(24)
      COMMON/DAT2/ ICH,PI,A30,A31,A32
      COMMON/DAT3/ RV,AP,TT1,TT2,PR,AR,VR,V1,RMM,EM1,THR,T,P,A,CF,TB
      COMMON/DAT4/ RC,R,VM,DT,TH(21),XR1,XR2,THR1,THR2,THR3,THR4,F(14)
      COMMON/DAT5/ N,N1,NC,M,V(13,21)
      COMMON EM,EM2,V2,X(12,21),Y(12,21),A(21),W(11),PW(11),DI(11,21)
      COMMON CE(1),SLL1(15,21),SLL2(15,21),AL1(21),AL2(21)
      COMMON PN11(21),PN12(21),PN13(21),PN14(21),PN1(21),PN2(21)
      COMMON PN21(21),PN22(21),PN23(21),PN24(21)
      COMMON SL11(15,21),SL12(15,21),SL13(15,21),SL14(15,21)
      COMMON SL21(15,21),SL22(15,21),SL23(15,21),SL24(15,21)
      RCS=RC*29.92/P*SQRT(T/519.0)
      T2=12.5*PI/180.0
      DO 1 I=1,NC
      T1=T2
      T2 = (TH(I.   +2.5)*PI/180.
      A(I)=PI*2.0*R*R*(COS (T1)-COS (T2))
    1 CONTINUE
      W(1)=0.0
      DO 3 J=5,11
      W(J)=0.0
      DO 2 I=1,NC
      W(J)=W(J)+X(J,I)*X(J,I)*A(I)
    2 CONTINUE
      W(J)=W(J)*929.03E-7/RCS
      W(1)=W(1)+W(J)
      PW(J)=ALOG10(W(J))*10.0+130.0
    3 CONTINUE
      PW(1)=10.0*ALOG10(10.0**(PW(5)/10.0)+10.0**(PW(6)/10.0)+10.0**(PW(
     17)/10.0)+10.0**(PW(8)/10.0)+10.0**(PW(9)/10.0)+10.0**(PW(10)/10.0)
     2+10.0**(PW(11)/10.0))
      WRITE (61,45)
   45 FORMAT (1H1///51H ACOUSTIC POWER AND SOUND POWER LEVEL FOR MODEL J
     *ET )
      WRITE (61,4)
    4 FORMAT(//5X,9HFREQUENCY,9X,12HPOWER(WATTS),6X,15HPOWER LEVEL(DB)/)
      WRITE (61,6) W(1),PW(1)
    6 FORMAT (6X,7HOVERALL,8X,E12.5,7X,F7.1/)
      DO 10 I=5,11
      J=I-1
      WRITE (61,8) F(J),W(I),PW(I)
   10 CONTINUE
    8 FORMAT (7X,F6.0,8X,E12.5,7X,F7.1)
      WRITE (61,100)
  100 FORMAT (///64H OVERALL SOUND POWER LEVEL,SCALED FOR THRUST//7X,6HT
     *HRUST,6X,15HPOWER LEVEL(DB) )
      W(2)=PW(1) + 10*ALOG10(THR1/THR)
      WRITE (61,101) THR1,W(2)
      W(2)=PW(1) + 10*ALOG10(THR2/THR)
      WRITE (61,101) THR2,W(2)
      W(2)=PW(1) + 10*ALOG10(THR3/THR)
      WRITE (61,101) THR3,W(2)
      W(2)=PW(1) + 10*ALOG10(THR4/THR)
      WRITE (61,101) THR4,W(2)
  101 FORMAT (7X,F6.0,8X,F7.1)
      WRITE (61,7)
    7 FORMAT (4/////)
      RETURN
      END
```

```
      SUBROUTINE STEP3
      REAL M1,M2,L1,L2,LC
      COMMON/DAT1/ FF(24),M1(24),L1(24),LC(24),M2(24),L2(24)
      COMMON/DAT2/ ICH,PI,AB0,AB1,AB2
      COMMON/DAT3/ RN,AP,TT1,TT2,PR,AR,VR,V1,RHM,EM1,THR,T,P,M,CF,TB
      COMMON/DAT4/ RC,R,VM,DT,TH(21),XR1,XR2,THR1,THR2,THR3,THR4,F(14)
      COMMON/DAT5/ N,N1,NC,M,V(13,21),OBNS,IND(11)
      COMMON EM,EM2,V2,X(12,21),Y(12,21),A(21),W(11),PW(11),DI(11,21)
      COMMON CF(11),SLL1(15,21),SLL2(15,21),AL1(21),AL2(21)
      COMMON PN11(21),PN12(21),PN13(21),PN14(21),PN1(21),PN2(21)
      COMMON PN21(21),PN22(21),PN23(21),PN24(21)
      COMMON SL11(15,21),SL12(15,21),SL13(15,21),SL14(15,21)
      COMMON SL21(15,21),SL22(15,21),SL23(15,21),SL24(15,21)
      DIMENSION ISLL1(209)
      EQUIVALENCE (ISLL1(1),SLL1(1))
      CON=ALOG10(R)*20.0+10.6
      DO 1 I=1,11
      CC=PW(I)
      DO 1 J=1,NC
      DI(I,J)=Y(I,J)-CC+CON
    1 CONTINUE
      WRITE (6,2)
    2 FORMAT (1H1/10X,29HTABLE OF DIRECTIVITY INDICES,/10X,23(1H-)///10X
     1,6HTHETA,, 3X 7HOVERALL,4X,6H500 HZ, 5X,5H1 KHZ, 5X,5H2 KHZ, 5X,5H
     2A KHZ, 5X,5HB KHZ, 4X,6H16 KHZ, 3X,8H31.5 KHZ, /)
      DO 3 J=1,NC
      ENCODE (110,4,ISLL1) (DI(I,J),I=1,11)
    4 FORMAT (11(F6.2, 4X))
      K=J
      WRITE (6,5) TH(K),ISLL1(1),(ISLL1(I),I=5,11)
    5 FORMAT (10X,F6.1,2X,8(2X,A8))
    3 CONTINUE
      DO 20 I=1,11
      PW(I)=OBNS-PW(I)+CON
   20 CONTINUE
      WRITE (6,21) PW(1),(PW(I),I=5,11)
   21 FORMAT (///29X,65H TABULATED VALUES ARE DOUBTFUL IF THEY ARE LESS
     *THAN THESE VALUES ,//10X,8(F10.2))
      RETURN
      END
```

```
      SUBROUTINE STEP4
      REAL M1,M2,L1,L2,LC
      COMMON/DAT1/ FF(24),M1(24),L1(24),LC(24),M2(24),L2(24)
      COMMON/DAT2/ [illegible],ABO,ABI,ABZ
      COMMON/DAT3/ RV,AP,TT1,TT2,VB,AR,VR,Z1,RHM,EN1,THR,T,P,H,CF,TB
      COMMON/DAT4/ RC,N,VM,DT,TH(2),X1,X2,THR1,THR2,THR3,THR4,F(14)
      COMMON/DAT5/ N,N1,NC,M,K(13,21)
      COMMON EM,EM2,V2,X(12,21),Y(12,21),A(21),W(11),PW(11),DI(11,21)
      COMMON CE(11),SL1(15,21),SL2(15,21),SL1(21),SL2(21)
      COMMON PN1(21),PN2(21),PN3(21),PN4(21),PN1(21),PN2(21)
      COMMON PN21(21),PN22(21),PN23(21),PN24(21)
      COMMON SL11(15,21),SL12(15,21),SL13(15,21),SL14(15,21)
      COMMON SL21(15,21),SL22(15,21),SL23(15,21),SL24(15,21)
      EQUIVALENCE (EMM,AMM)
      DATA1.0/10.7376*2.0*32.17
      IF (EMM .EQ. 10^4    NONE    ) 20,10
20    EM = V2 = 0.
      GO TO 30
10    CONTINUE
      EM2=EM1*EMM
      V2=V1*VR
30    EM=CON*(EM1*V1*V1+EM2*V2*V2)
      CE(1)=W(1)/EM
      WRITE (6,2) EM,CE(1)
2     FORMAT (4(/) 10X 20HJET MECHANICAL POWER, 3X 2H= , E14.5, /
     210X 21HCONVERSION EFFICIENCY 24 2H= , E14.5)
      RETURN
      END
```

```
      SUBROUTINE STEPS
      REAL M1,M2,L1,L2,LC
      COMMON/DAT1/ FF(24),M1(24),L1(24),LC(24),M2(24),L2(24)
      COMMON/DAT2/ ICH,PI,AB0,AB1,AB2
      COMMON/DAT3/ RN,AP,TT1,TT2,PR,AR,VR,V1,RMM,EM1,THR,T,P,H,CF,TB
      COMMON/DAT4/ RC,R,V4,DY,TH(21),XR1,XR2,THR1,THR2,THR3,THR4,F(14)
      COMMON/DAT5/ N,N1,NC,M,V(13,21)
      COMMON EM,EM2,V2,X(12,21),Y(12,21),A(21),W(11),PW(11),DI(11,21)
      COMMON CE(1),SLL1(15,21),SLL2(15,21),AL1(21),AL2(21)
      COMMON PN11(21),PN12(21),PN13(21),PN14(21),PN1(21),PN2(21)
      COMMON PN21(21),PN22(21),PN23(21),PN24(21)
      COMMON SL11(15,21),SL12(15,21),SL13(15,21),SL14(15,21)
      COMMON SL21(15,21),SL22(15,21),SL23(15,21),SL24(15,21)
      DO 3 I=1,NC
      AL1(I)=XR1/SIN (TH(I  )*PI/180.0)
      AL2(I)=XR2/SIN (TH(I  )*PI/180.0)
      WZ1=ALOG10(AL1(I)/R)*20.0
      WZ2=ALOG10(AL2(I)/R)*20.0
      DO 1 J=1,11
      SLL1(J,I)=Y(J,I)-WZ1
      SLL2(J,I)=Y(J,I)-WZ2
    1 CONTINUE
      DO 4 J=1,4
      J1=J+11
      J2=J+10
      SLL1(J1,I)=SLL1(J2,I)-3.0
      SLL2(J1,I)=SLL2(J2,I)-3.0
    4 CONTINUE
      SS11=SS12=SS13=SS14=SS21=SS22=SS23=SS24=0.0
      WZ1=AL1(I)/1000.0
      WZ2=AL2(I)/1000.0
      DO 2 J=2,15
      ALF = 10.**FCTION(J,THR1)
      SF = 10.*ALOG10(THR1/THR)
      SL11(J,I)=SLL1(J,I)-ALF*WZ1 +SF
      SL21(J,I)=SLL2(J,I)-ALF*WZ2 +SF
      ALF = 10.**FCTION(J,THR2)
      SF = 10.*ALOG10(THR2/THR)
      SL12(J,I)=SLL1(J,I)-ALF*WZ1 +SF
      SL22(J,I)=SLL2(J,I)-ALF*WZ2 +SF
      ALF = 10.**FCTION(J,THR3)
      SF = 10.*ALOG10(THR3/THR)
      SL13(J,I)=SLL1(J,I)-ALF*WZ1 +SF
      SL23(J,I)=SLL2(J,I)-ALF*WZ2 +SF
      ALF = 10.**FCTION(J,THR4)
      SF = 10.*ALOG10(THR4/THR)
      SL14(J,I)=SLL1(J,I)-ALF*WZ1 +SF
      SL24(J,I)=SLL2(J,I)-ALF*WZ2 +SF
      SS11=SS11+10.0**(SL11(J,I)*0.1)
      SS12=SS12+10.0**(SL12(J,I)*0.1)
      SS13=SS13+10.0**(SL13(J,I)*0.1)
      SS14=SS14+10.0**(SL14(J,I)*0.1)
      SS21=SS21+10.0**(SL21(J,I)*0.1)
      SS22=SS22+10.0**(SL22(J,I)*0.1)
      SS23=SS23+10.0**(SL23(J,I)*0.1)
      SS24=SS24+10.0**(SL24(J,I)*0.1)
      ALF = 10.**FCTION(J,THR)
```

```
      SLL1(J,I) = SLL1(J,I) - ALF*WZ1
      SLL2(J,I) = SLL2(J,I) - ALF*WZ2
    2 CONTINUE
      SL11(1,I)=ALOG10(SS11) *10.
      SL12(1,I)=ALOG10(SS12) *10.
      SL13(1,I)=ALOG10(SS13) *10.
      SL14(1,I)=ALOG10(SS14) *10.
      SL21(1,I)=ALOG10(SS21) *10.
      SL22(1,I)=ALOG10(SS22) *10.
      SL23(1,I)=ALOG10(SS23) *10.
      SL24(1,I)=ALOG10(SS24) *10.
    3 CONTINUE
      CALL OLLER (F,THR,THR1,SL11,PN11)
      CALL OLLER (F,THR,THR2,SL12,PN12)
      CALL OLLER (F,THR,THR3,SL13,PN13)
      CALL OLLER (F,THR,THR4,SL14,PN14)
      CALL OLLER (F,THR,THR1,SL21,PN21)
      CALL OLLER (F,THR,THR2,SL22,PN22)
      CALL OLLER (F,THR,THR3,SL23,PN23)
      CALL OLLER (F,THR,THR4,SL24,PN24)
      CALL HEAD (THR,THR1,SL11,PN11,AL1)
      CALL HEAD (THR,THR2,SL12,PN12,AL1)
      CALL HEAD (THR,THR3,SL13,PN13,AL1)
      CALL HEAD (THR,THR4,SL14,PN14,AL1)
      CALL HEAD (THR,THR1,SL21,PN21,AL2)
      CALL HEAD (THR,THR2,SL22,PN22,AL2)
      CALL HEAD (THR,THR3,SL23,PN23,AL2)
      CALL HEAD (THR,THR4,SL24,PN24,AL2)
      CALL PLOT2(AL2,PN21,PN22,PN23,PN24,RV)
      RETURN
      END
```

```
      SUBROUTINE OLLER (F,THR,THRI,SL,PN)
      REAL M1,M2,L1,L2,LC,LCC
      COMMON/DAT1/ FF(24),M1(24),L1(24),LC(24),M2(24),L2(24)
      DIMENSION F(1),SL(15,1),PN(1)
      DO 5 I=1,21
      DO 100 J=2,15
      IF(SL(J,I).GT.136.0) 101,100
  101 PN(I)=777.7
      GO TO 5
  100 CONTINUE
      XMAX=SMAX=0.0
      DO 4 J=2,15
      FREQ=F(J-1)*SQRT(THR/THRI)
      IF(FREQ.GE.10000.0)4,26
   26 IF(FREQ.LT.50.0)27,6
    2 AW=AM*(SL(J,I)-ALO)
      AW=10.0**AW
      SMAX=SMAX+AW
      IF(AW.GT.XMAX) 3,14
    3 XMAX=AW
   14 IF(J.EQ.11) 30,31
   30 AW=XMAX+0.3*(SMAX-XMAX)
      SL(2,I)=40.0+33.3*ALOG10(AW)
   31 CONTINUE
    4 CONTINUE
      AW=XMAX+0.3*(SMAX-XMAX)
      PN(I)=40.0+33.3*ALOG10(AW)
    5 CONTINUE
      RETURN
   27 FREQ=52.0
    6 DO 7 K=1,24
      IF (FREQ.GT.FF(K)) 7,8
    7 CONTINUE
      STOP
    8 K1=K-1
      K2=K
      F1=FF(K1)
      F2=FF(K2)
      Y1=LC(K1)
      Y2=LC(K2)
      LCC=Y1+(Y2-Y1)*(FREQ-F1)/(F2-F1)
      IF (SL(J,I).GE.LCC) 9,10
    9 AM=M2(K1)+(M2(K2)-M2(K1))*(FREQ-F1)/(F2-F1)
      ALO=L2(K1)+(L2(K2)-L2(K1))*(FREQ-F1)/(F2-F1)
      GO TO 2
   10 AM=M1(K1)+(M1(K2)-M1(K1))*(FREQ-F1)/(F2-F1)
      ALO=L1(K1)+(L1(K2)-L1(K1))*(FREQ-F1)/(F2-F1)
      GO TO 2
      END
```

```
      SUBROUTINE HEAD (THR,THRI,SL,PN,AL)
      DIMENSION AL(1),PN(1),SL(15,1),FM(14)
      REAL M1,M2,L1,L2,LC
      COMMON/DAT3/ RN
      COMMON/DAT4/ RC,R,VM,DT,TH(21),XR1,XR2,THR1,THR2,THR3,THR4,F(14)
      DO 10 J=1,14
      FM(J)=F(J)*SQRT(THR/THRI)
   10 CONTINUE
      WRITE (61,1) RN,THR,THRI
    1 FORMAT (6(/) 1H1, 10X 10HRUN NUMBER,  F10.0,  4(/)
     * 10X 15HMODEL THRUST =        , F10.3, 5X              20HFULL SCALE T
     1HRUST = , F10.3,///  5X 2HL., 7X 5HPWD3., 5X,5HOASPL,12X 45HOCTAVE
     2    BAND    SOUND    PRESSURE    LEVELS  )
      WRITE(61,7) (FM(I),I=4,14)
    7 FORMAT (29X,11(F8.1)/)
      DO 2 I=1,21
      WRITE (61,6) AL(I),PN(I),SL(2,I),SL(1,I),(SL(J,I),J=5,15)
    2 CONTINUE
    6 FORMAT (1X,F7.1,F7.1,1H(,F5.1,1H),F7.1,11(F8.2))
      RETURN
      END
```

```
      FUNCTION FCTION(J,THRI)
      REAL M1,M2,L1,L2,LC
      COMMON/DAT2/ ICH,PI,AB0,AB1,AB2
      COMMON/DAT3/ RN,AP,TT1,TT2,PR,AR,VR,V1,RMM,EM1,THR,T,P,H,CF,TB
      COMMON/DAT4/ RC,R,VM,DT,TH(21),XR1,XR2,THR1,THR2,THR3,THR4,F(14)
      FREQ = F(J-1)*SQRT(THR/THRI)*.001
      XZ=ALOG10(FREQ)
      FCTION = AB0+XZ*(AB1+AB2*XZ)
      RETURN
      END
```

```
      SUBROUTINE PLOT2 (X, Y1, Y2, Y3, Y4, RN)
      DIMENSION X(21), Y1(21), Y2(21), Y3(21), Y4(21), ICHAR(4)
      ICHAR(1)=4H 10K$   ICHAR(2)=4H 20K $   ICHAR(3)=4H 40K
      ICHAR(4)=4H 80K
      DO 75 I=1,21
      X(I)=SQRT(X(I)**2 - 2250000.0)
   75 CONTINUE
      DO 76 I=17,21
      X(I)=-X(I)
   76 CONTINUE
      CALL PLOT(7.0, 0.0, 2)
      XD=7.0
      DO 1 I=1,7
      CALL PLOT(XD,0.0, 3)
      CALL PLOT(XD,0.05, 2)
      XD=XD-1.0
    1 CONTINUE
      CALL PLOT(0.0, 0.0, 3)
      CALL PLOT(0.0, 8.0, 2)
      YD=8.0
      DO 2 I=1,8
      CALL PLOT(0.0, YD, 3)
      CALL PLOT(0.05, YD, 2)
      YD=YD-1.0
    2 CONTINUE
      XP=.001*X(1)+1.0
      YP=0.1*Y1(1)-5.0
      CALL PLOT(XP+.05,YP,3)
      CALL PLOT(XP+.35,YP-.39,2)
      CALL SYMBOL(XP+.32, YP-.47, .16, ICHAR(1), 0, 4)
      CALL PLOT(XP, YP, 3)
      DO 3 I=2,21
      XP=.001*X(I)+1.0
      YP=0.1*Y1(I)-5.0
      CALL PLOT(XP, YP, 2)
    3 CONTINUE
      XP=.001*X(1)+1.0
      YP=0.1*Y2(1)-5.0
      CALL PLOT(XP+.05,YP,3)
      CALL PLOT(XP+.35,YP-.13,2)
      CALL SYMBOL(XP+.32, YP-.21, .16, ICHAR(2), 0, 4)
      CALL PLOT(XP, YP, 3)
      DO 4 I=2,21
      XP=.001*X(I)+1.0
      YP=0.1*Y2(I)-5.0
      CALL PLOT(XP, YP, 2)
    4 CONTINUE
      XP=.001*X(1)+1.0
      YP=0.1*Y3(1)-5.0
      CALL PLOT(XP+.05,YP,3)
      CALL PLOT(XP+.35,YP+.13,2)
      CALL SYMBOL(XP+.32, YP+.05, .16, ICHAR(3), 0, 4)
      CALL PLOT(XP, YP, 3)
      DO 50 I=2,21
      XP=.001*X(I)+1.0
      YP=0.1*Y3(I)-5.0
      CALL PLOT(XP, YP, 2)
```

```
50 CONTINUE
   XP=.001*X(1)+1.0
   YP=0.1*Y4(1)-5.0
   CALL PLOT(XP+.05,YP,3)
   CALL PLOT(XP+.35,YP+.39,2)
   CALL SYMBOL(XP+.32, YP+.31, .16, ICHAR(4), 0, 4)
   CALL PLOT(XP, YP, 3)
   DO 60 I=2,21
   XP=.001*X(I)+1.0
   YP=0.1*Y4(I)-5.0
   CALL PLOT(XP, YP, 2)
60 CONTINUE
   ICHAR(1)= 4HRUN    $   ICHAR(2)= 4HNO.
   CALL SYMBOL(.25, 8.5, .15, ICHAR(1), 0, 4)
   CALL SYMBOL(999., 999., .16, ICHAR(2), 0, 4)
   CALL NUMBER(999., 999., .16, RN, 0, -1)
   CALL PLOT(10.0,0.0,-3)
   RETURN
   END
```

APPENDIX D

SUMMARY OF OVERALL SOUND POWER LEVEL DATA

This appendix contains a set of 28 graphs which present the overall sound power level data, scaled to a 20,000 pound thrust engine, as a function of the ratio of secondary mass flow to primary mass flow. Each graph corresponds to one of the principal groups of runs defined in Table A-1.

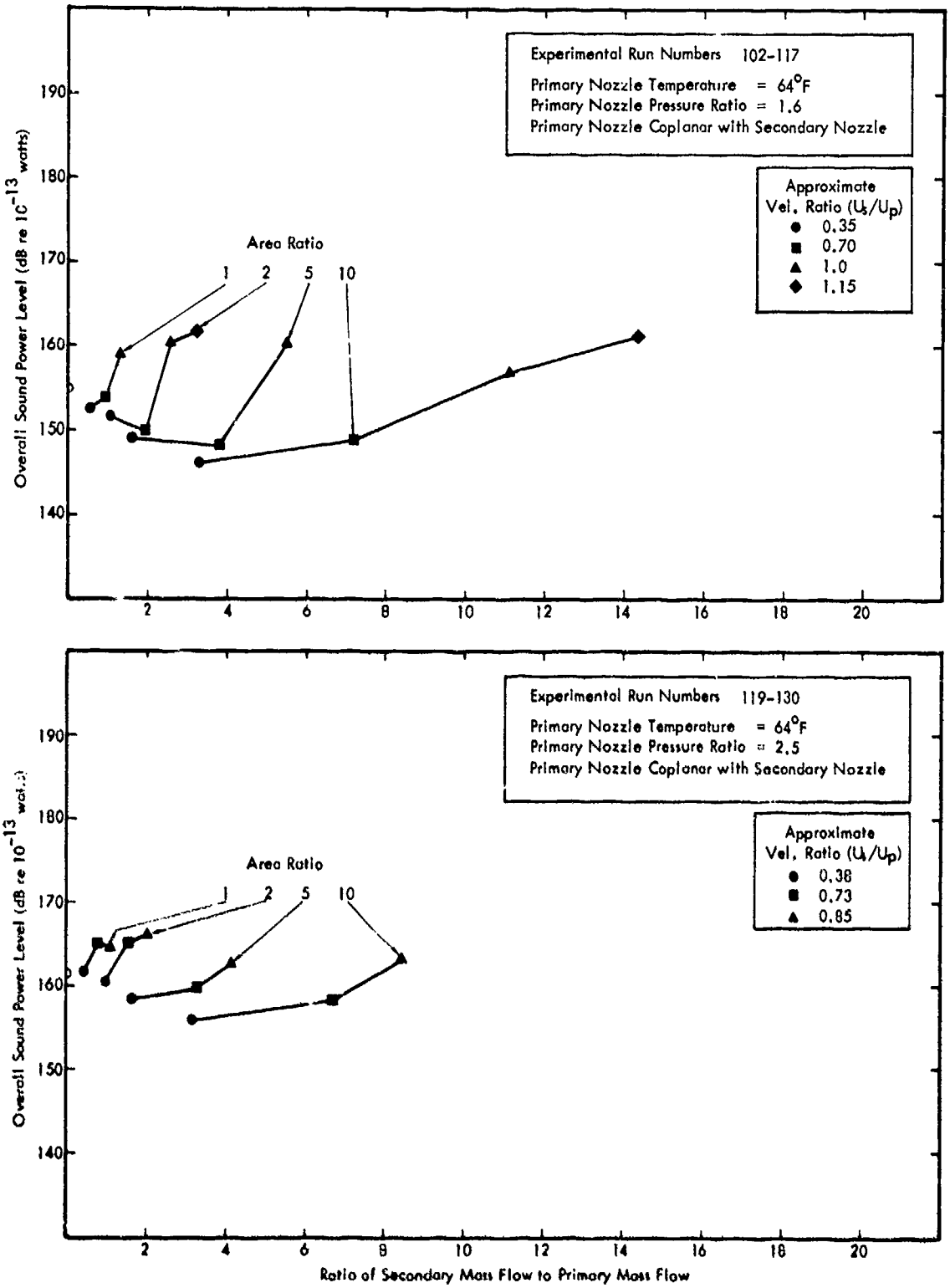

Figure D-1. Variation in Overall Sound Power with Bypass Ratio for Thrusts Scaled to 20,000 Lbs.

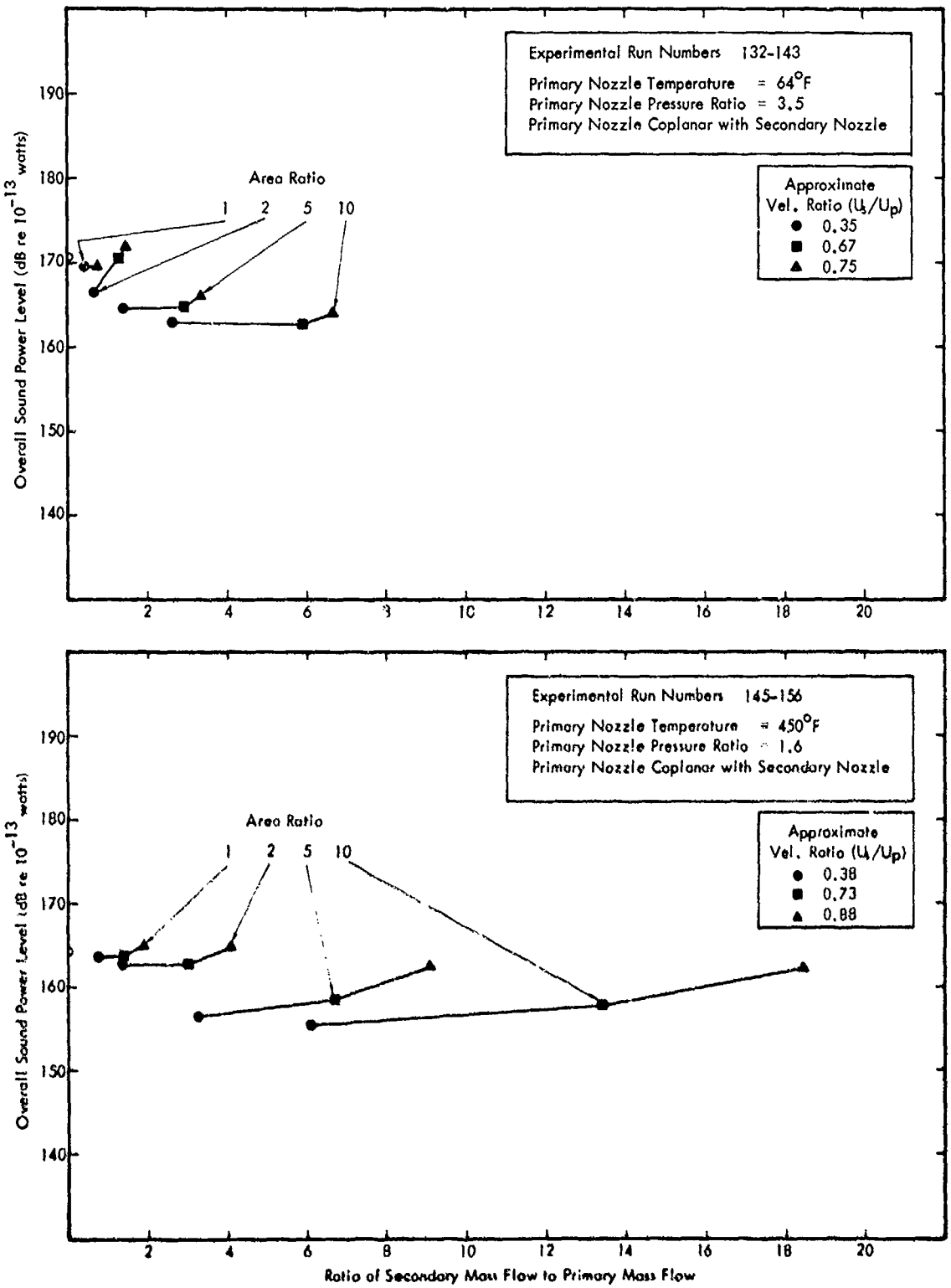

Figure D-1. continued ... Variation in Overall Sound Power with Bypass Ratio for Thrusts Scaled to 20,000 Lbs.

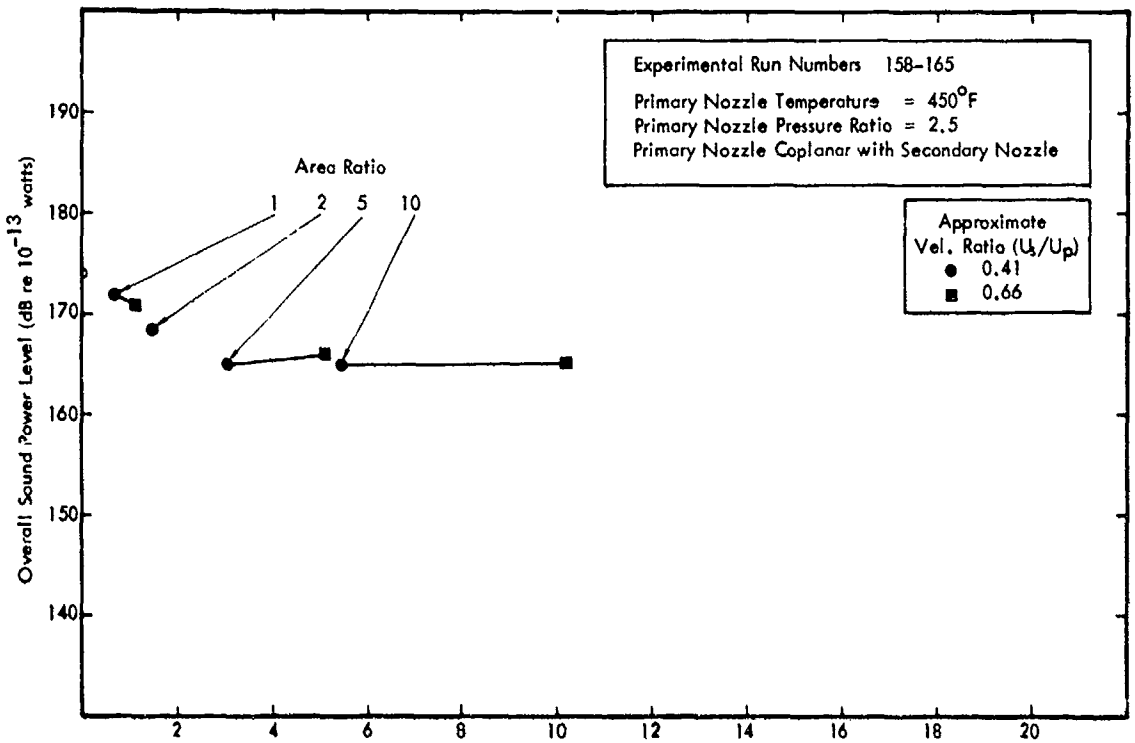

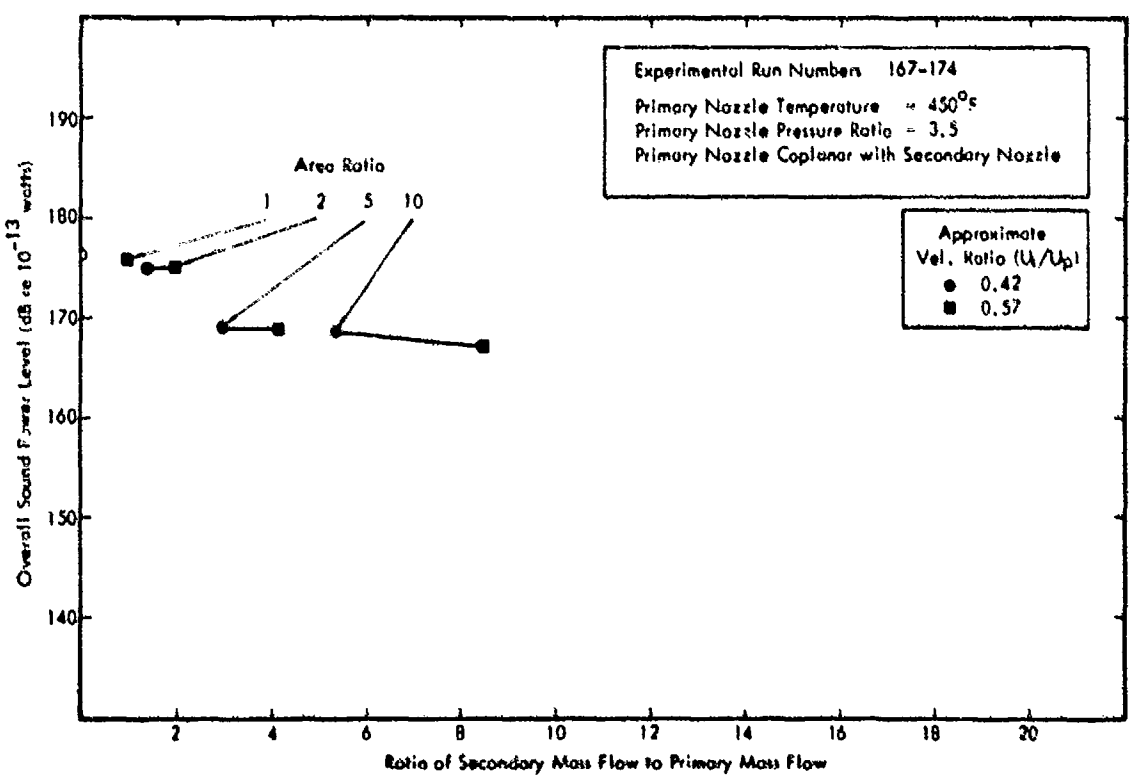

Figure D-1. continued ... Variation in Overall Sound Power with Bypass Ratio for Thrusts Scaled to 20,000 Lbs.

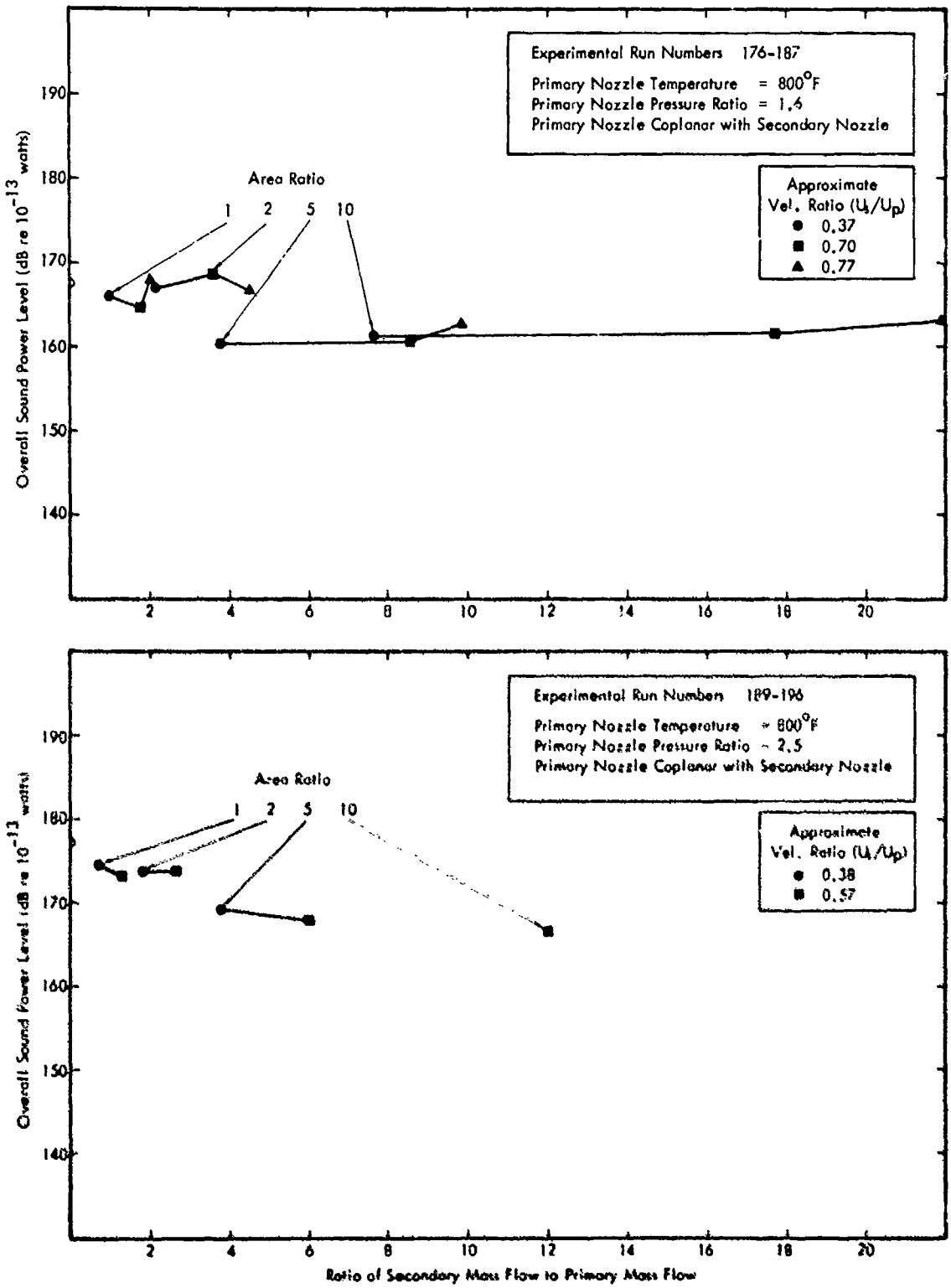

Figure D-1. continued ... Variation in Overall Sound Power with Bypass Ratio for Thrusts Scaled to 20,000 Lbs.

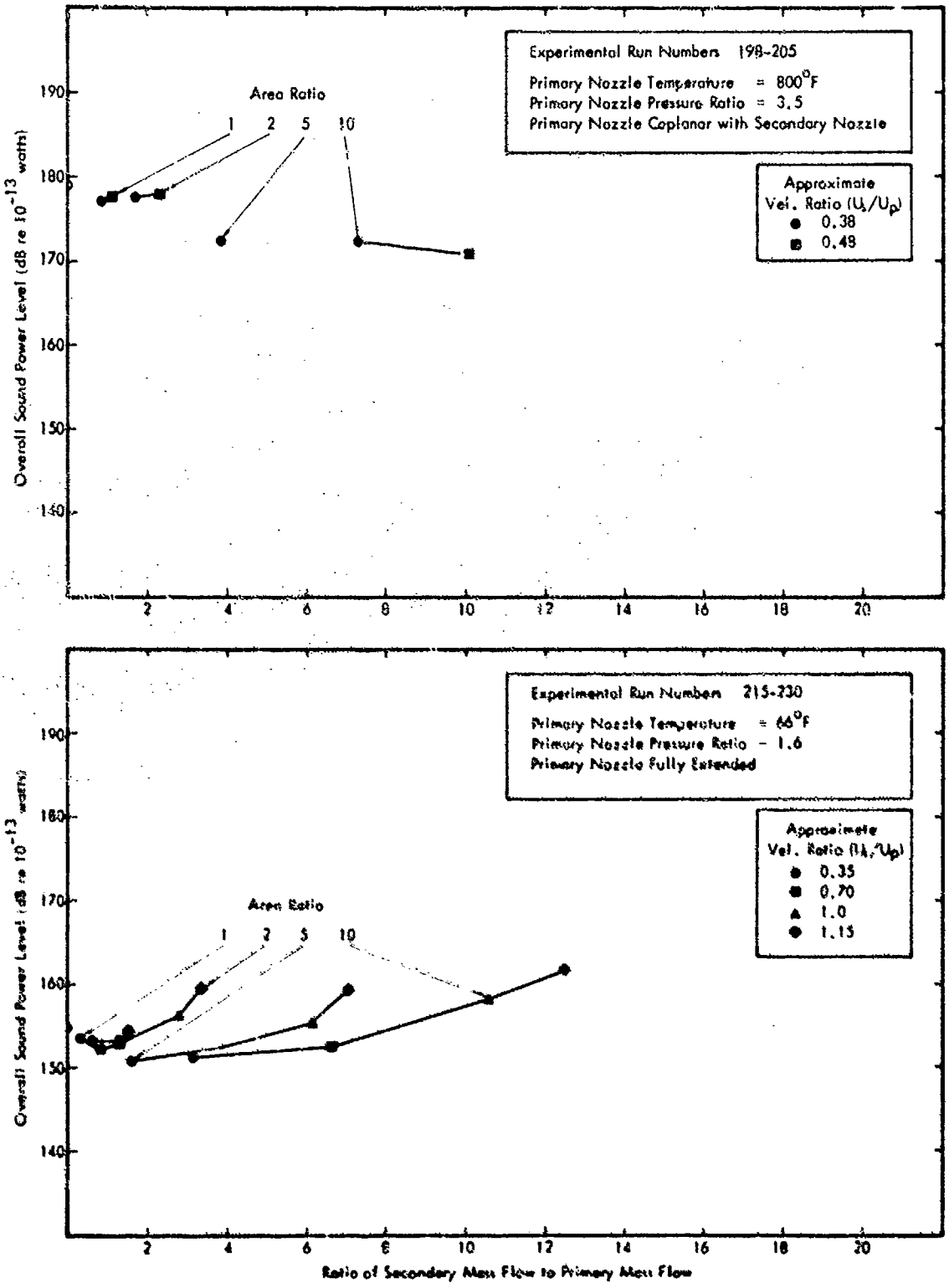

Figure D-1. continued . . . Variation in Overall Sound Power with Bypass Ratio for Thrusts Scaled to 20,000 Lbs.

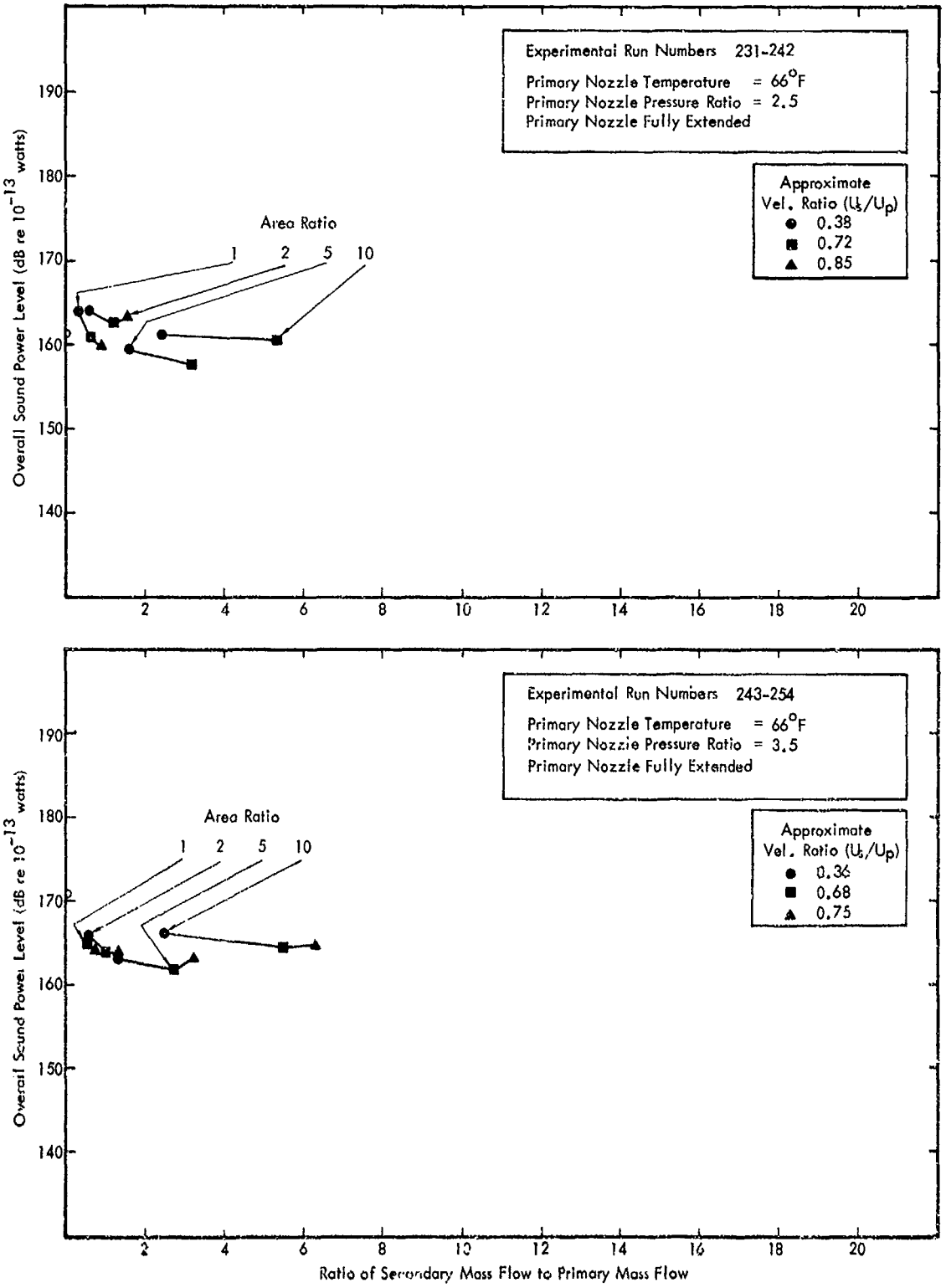

Figure D-1. continued ... Variation in Overall Sound Power with Bypass Ratio for Thrusts Scaled to 20,000 Lbs.

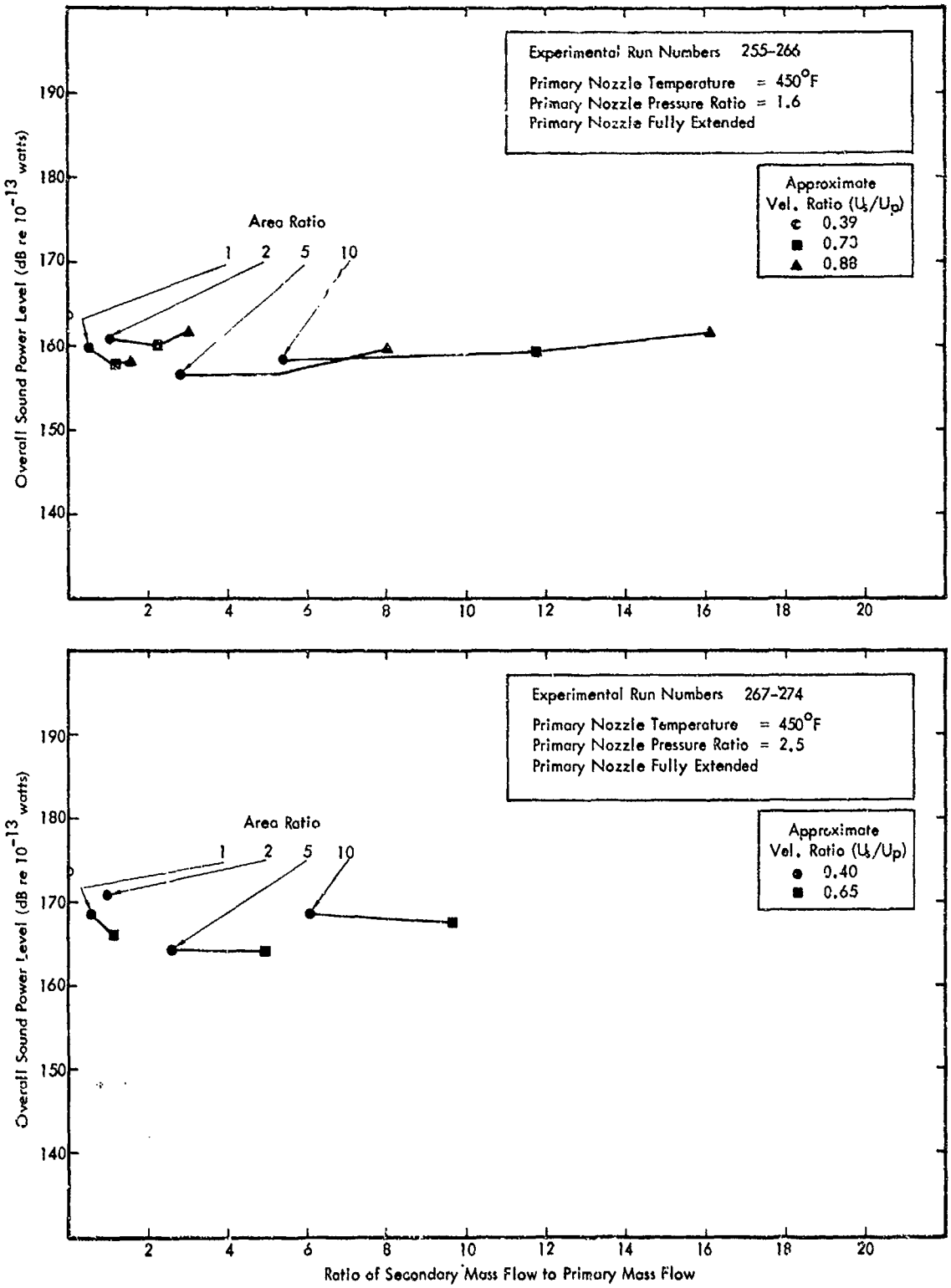

Figure D-1. continued ... Variation in Overall Sound Power with Bypass Ratio for Thrusts Scaled to 20,000 Lbs.

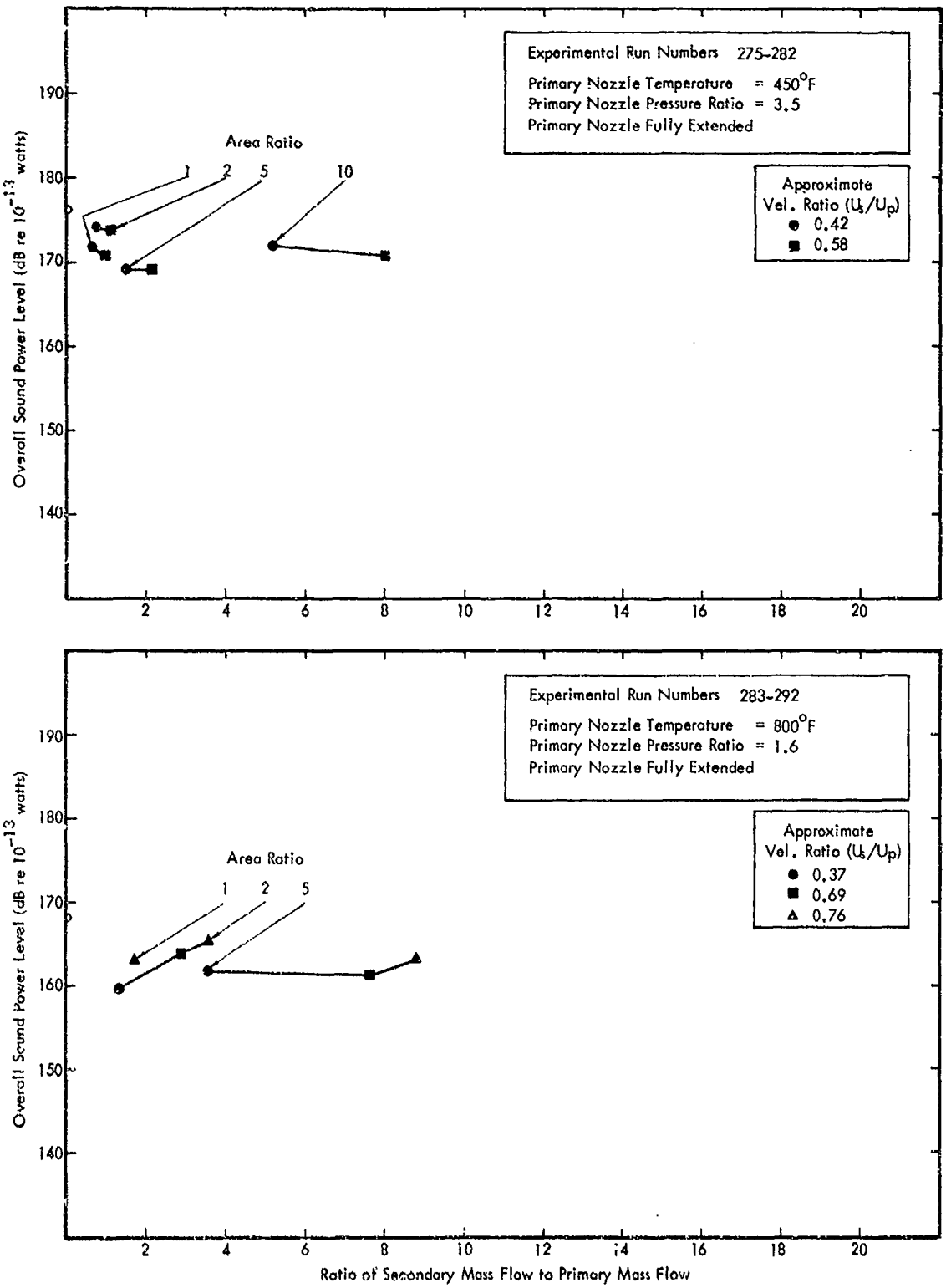

Figure D-1. continued ... Variation in Overall Sound Power with Bypass Ratio for Thrusts Scaled to 20,000 Lbs.

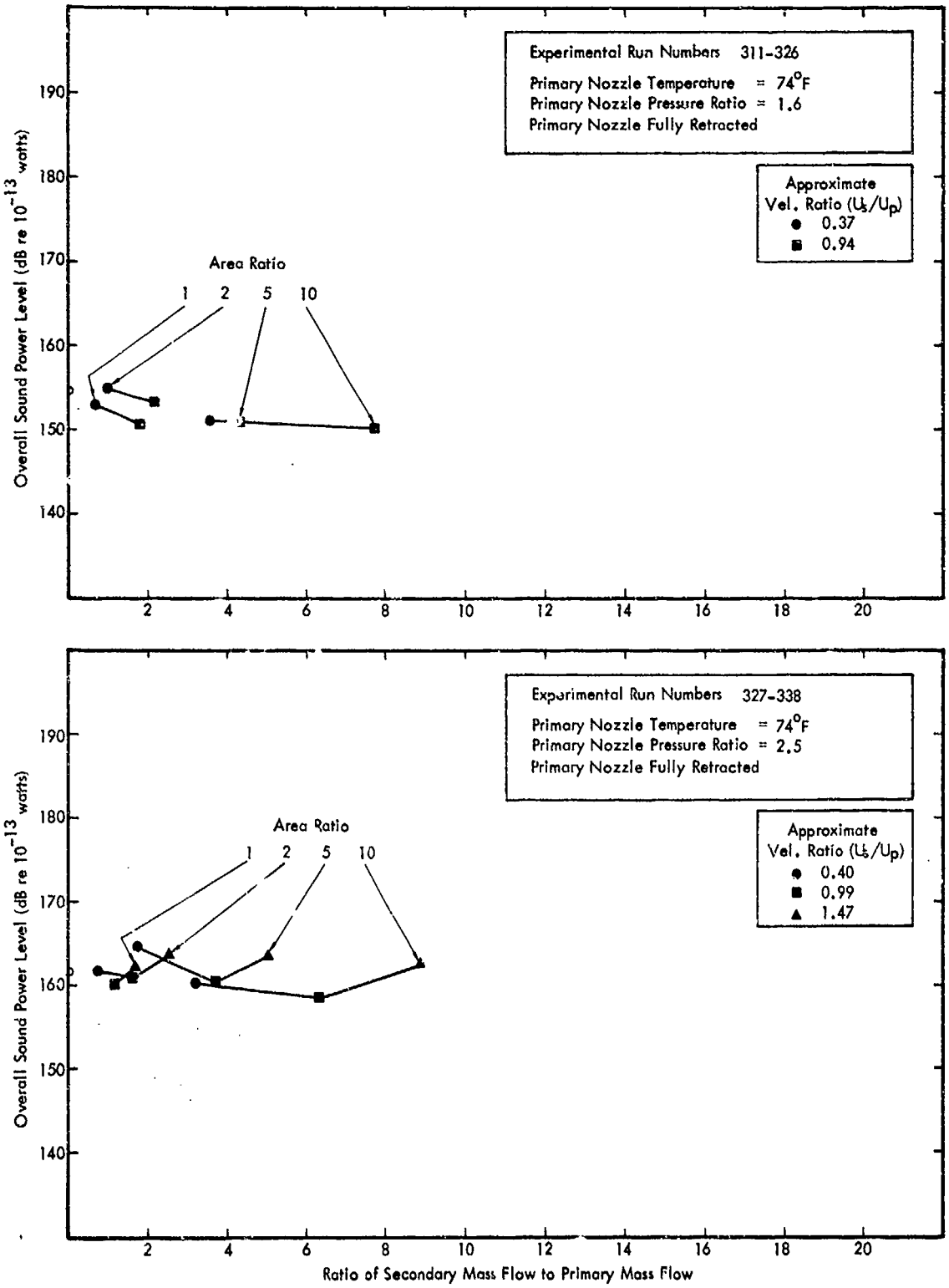

Figure D-1. continued ... Variation in Overall Sound Power with Bypass Ratio for Thrusts Scaled to 20,000 Lbs.

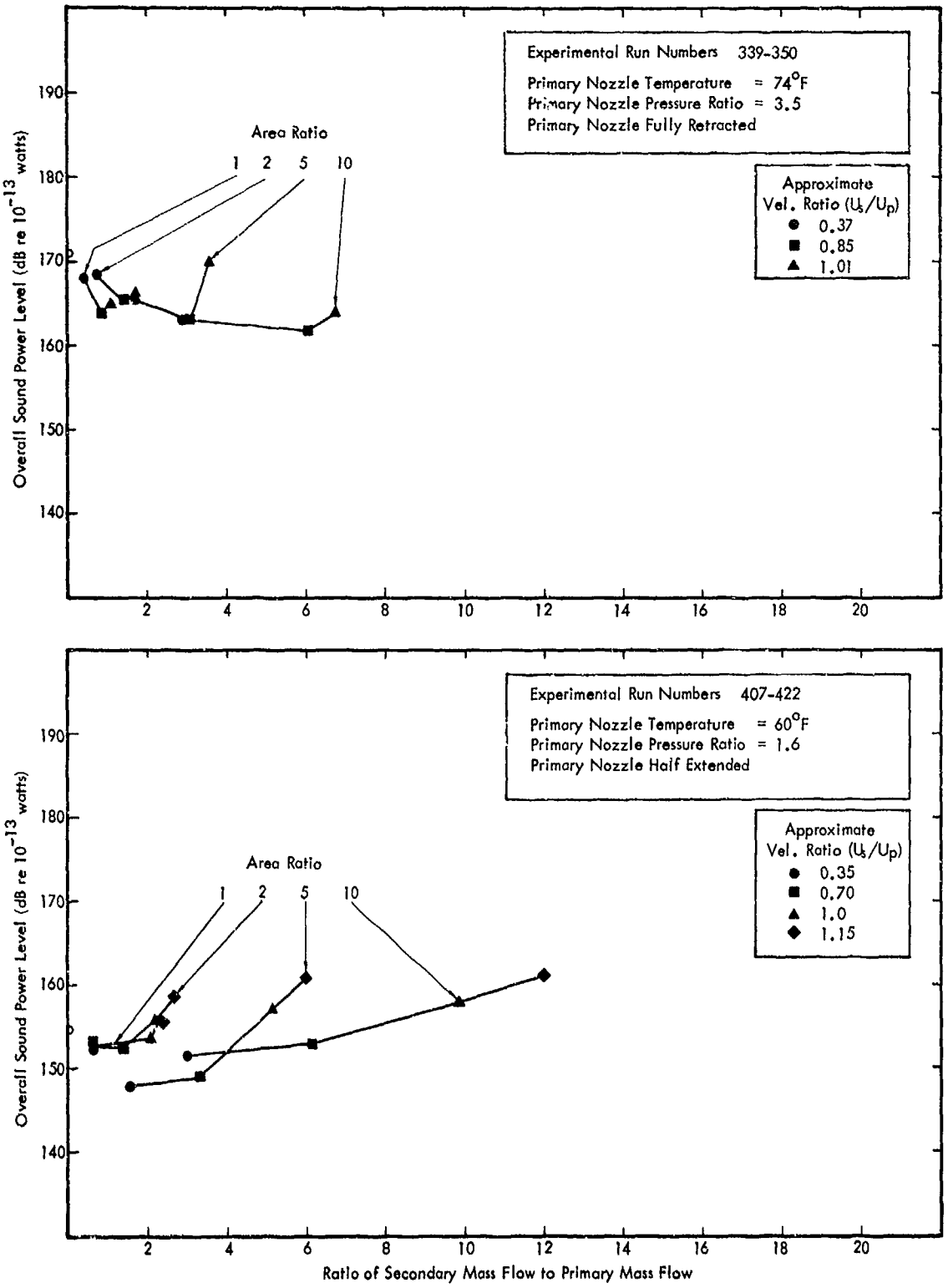

Figure D-1. continued ... Variation in Overall Sound Power with Bypass Ratio for Thrusts Scaled to 20,000 Lbs.

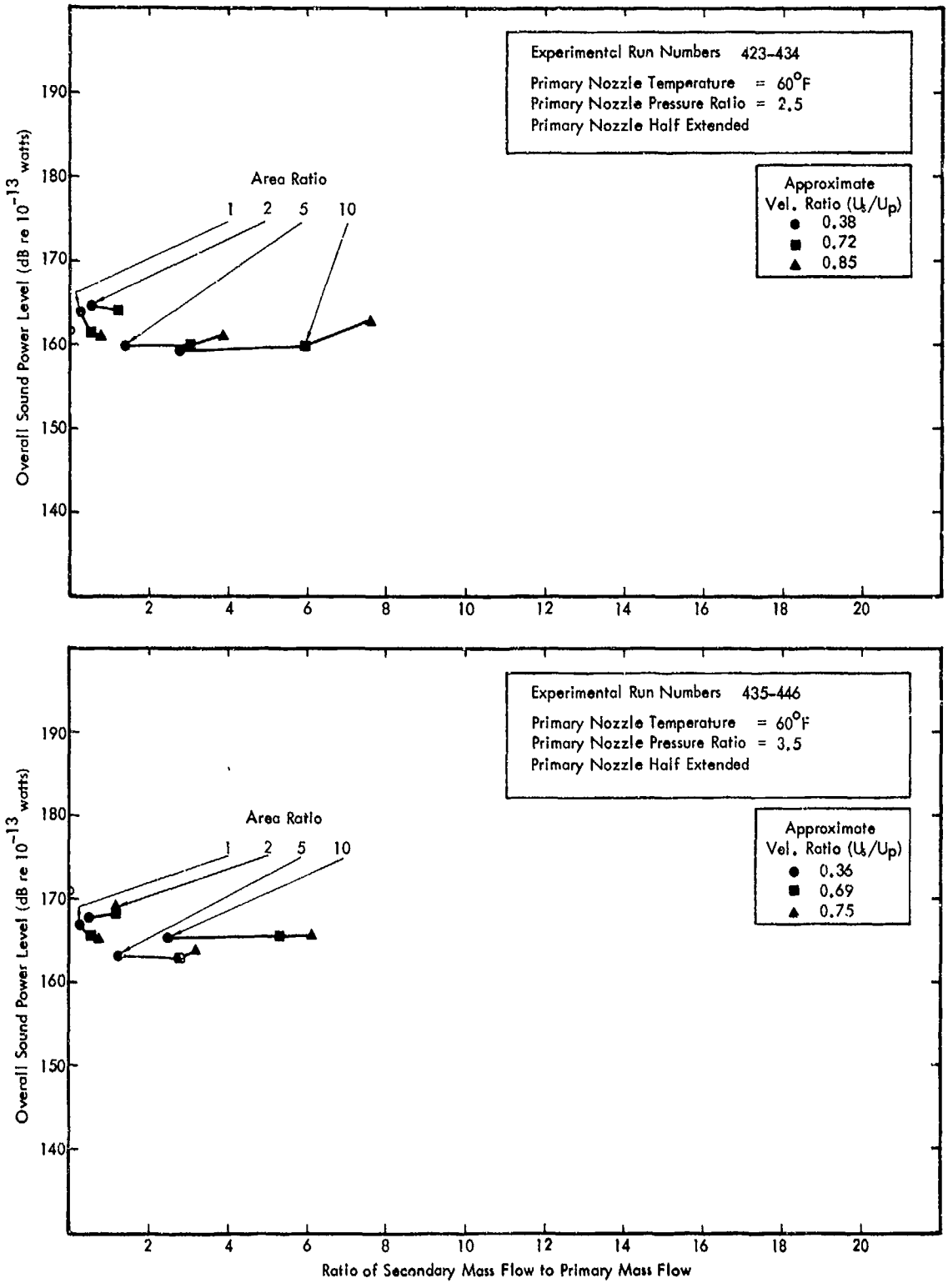

Figure D-1. continued ... Variation in Overall Sound Power with Bypass Ratio for Thrusts Scaled to 20,000 Lbs.

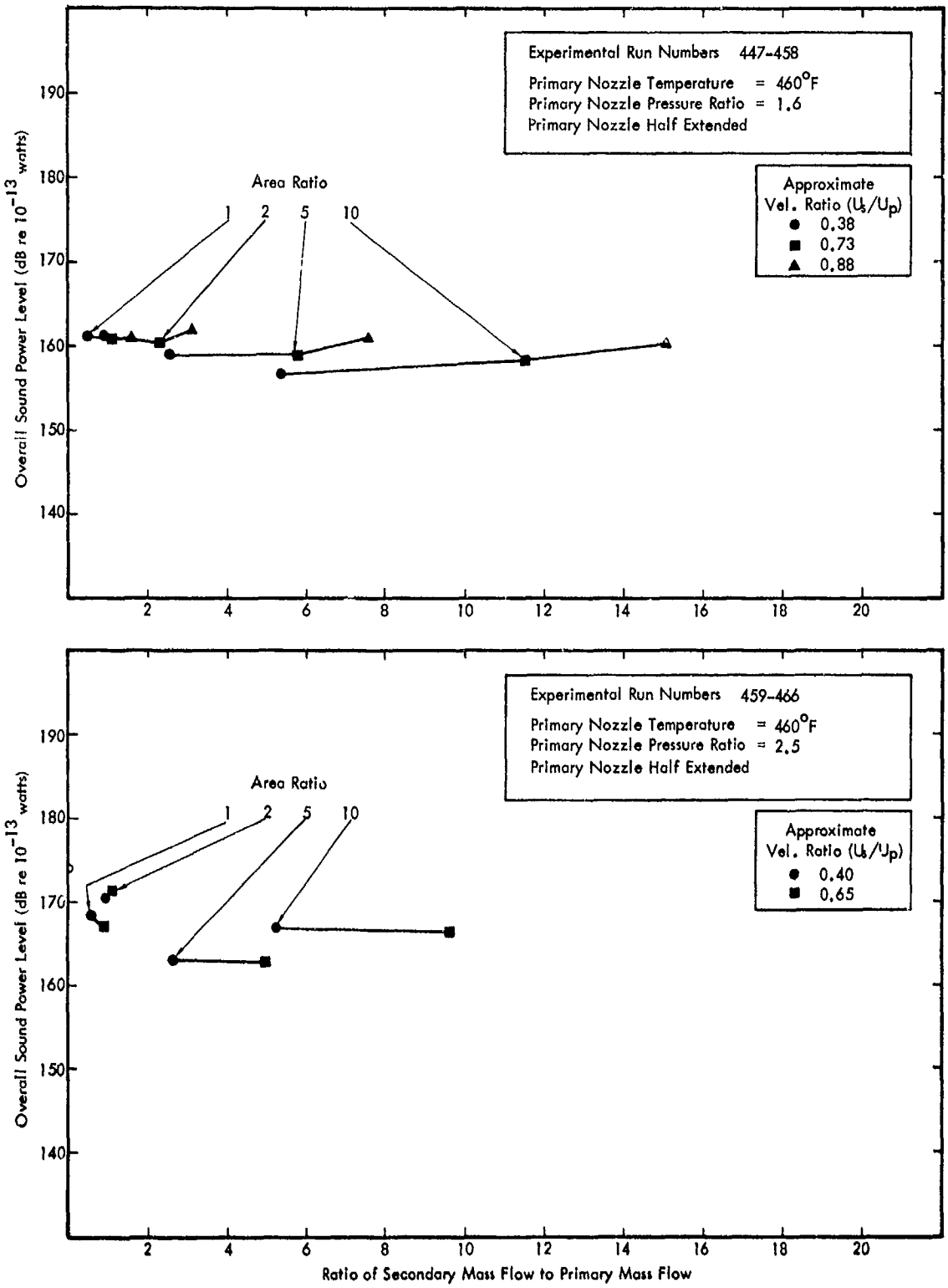

Figure D-1. continued ... Variation in Overall Sound Power with Bypass Ratio for Thrusts Scaled to 20,000 Lbs.

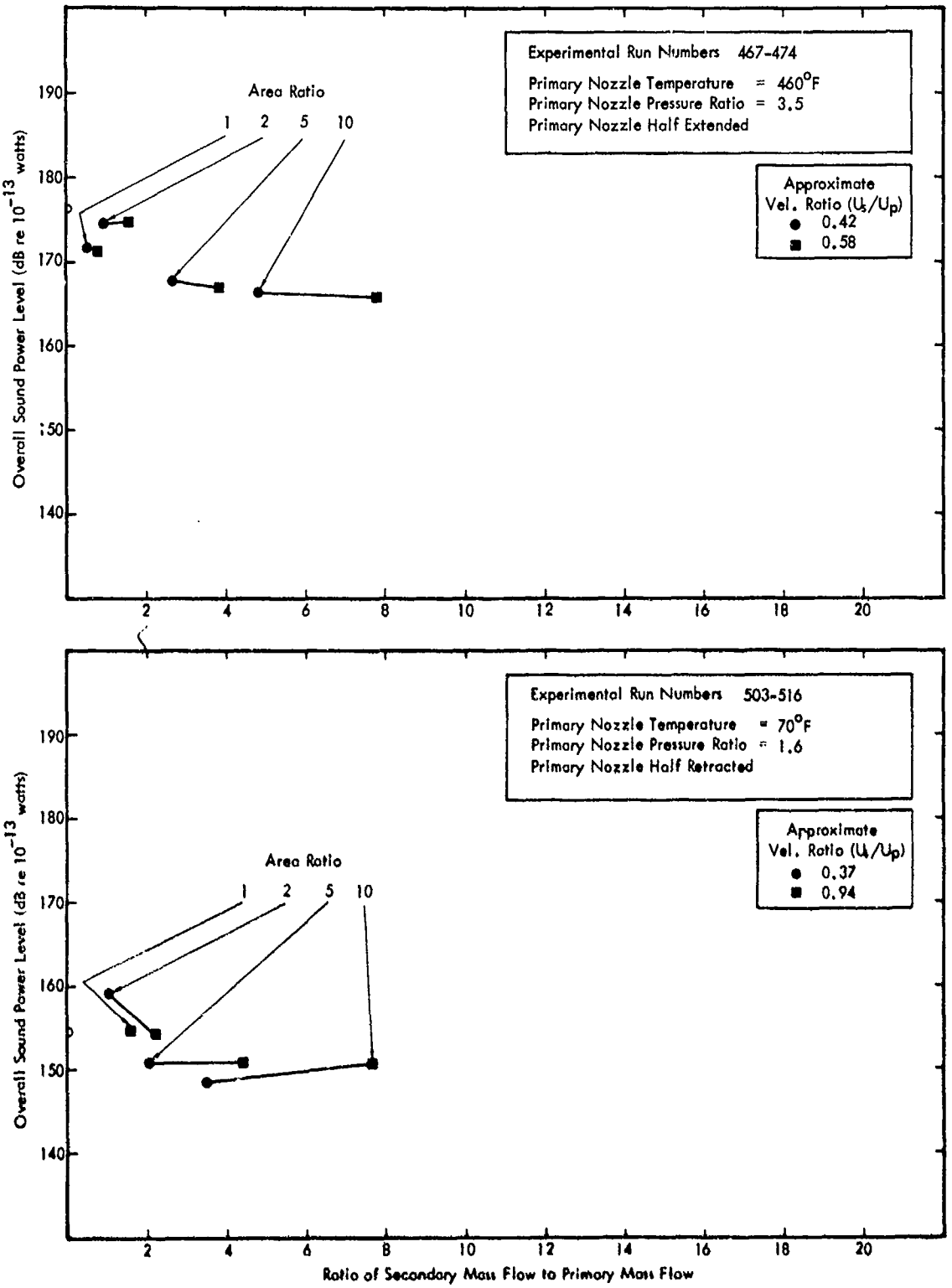

Figure D-1. continued ... Variation in Overall Sound Power with Bypass Ratio for Thrusts Scaled to 20,000 Lbs.

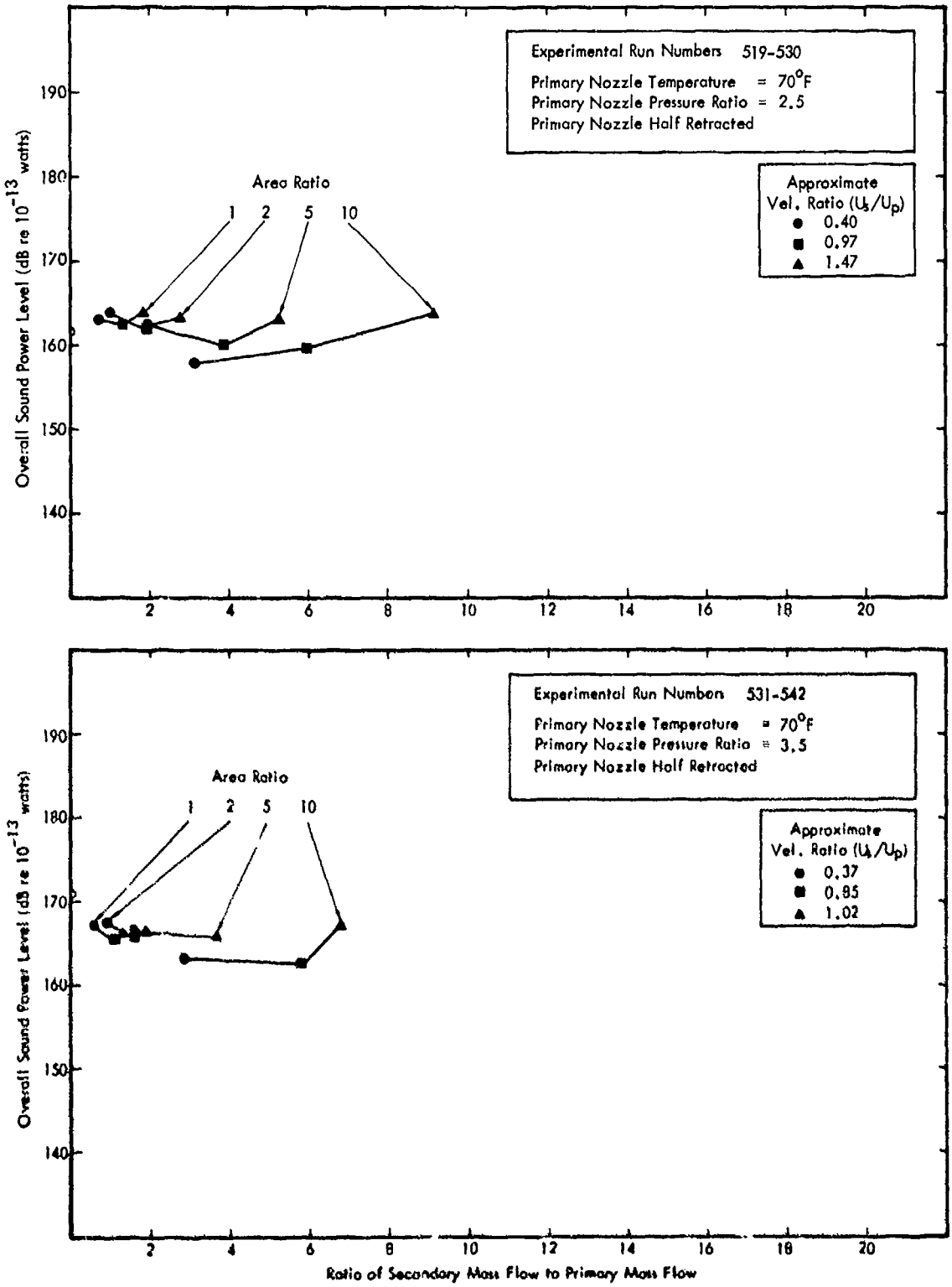

Figure D-1. concluded ... Variation in Overall Sound Power with Bypass Ratio for Thrusts Scaled to 20,000 Lbs.

Intentionally Left Blank

APPENDIX E

SUMMARY OF MAXIMUM PERCEIVED NOISE LEVEL DATA

This appendix contains a set of 28 graphs which present the maximum perceived noise level data on the 1500-foot sideline, scaled to a 20,000 pound thrust engine, as a function of the ratio of secondary mass flow to primary mass flow. Each graph corresponds to one of the principal groups of runs defined in Table A-1.

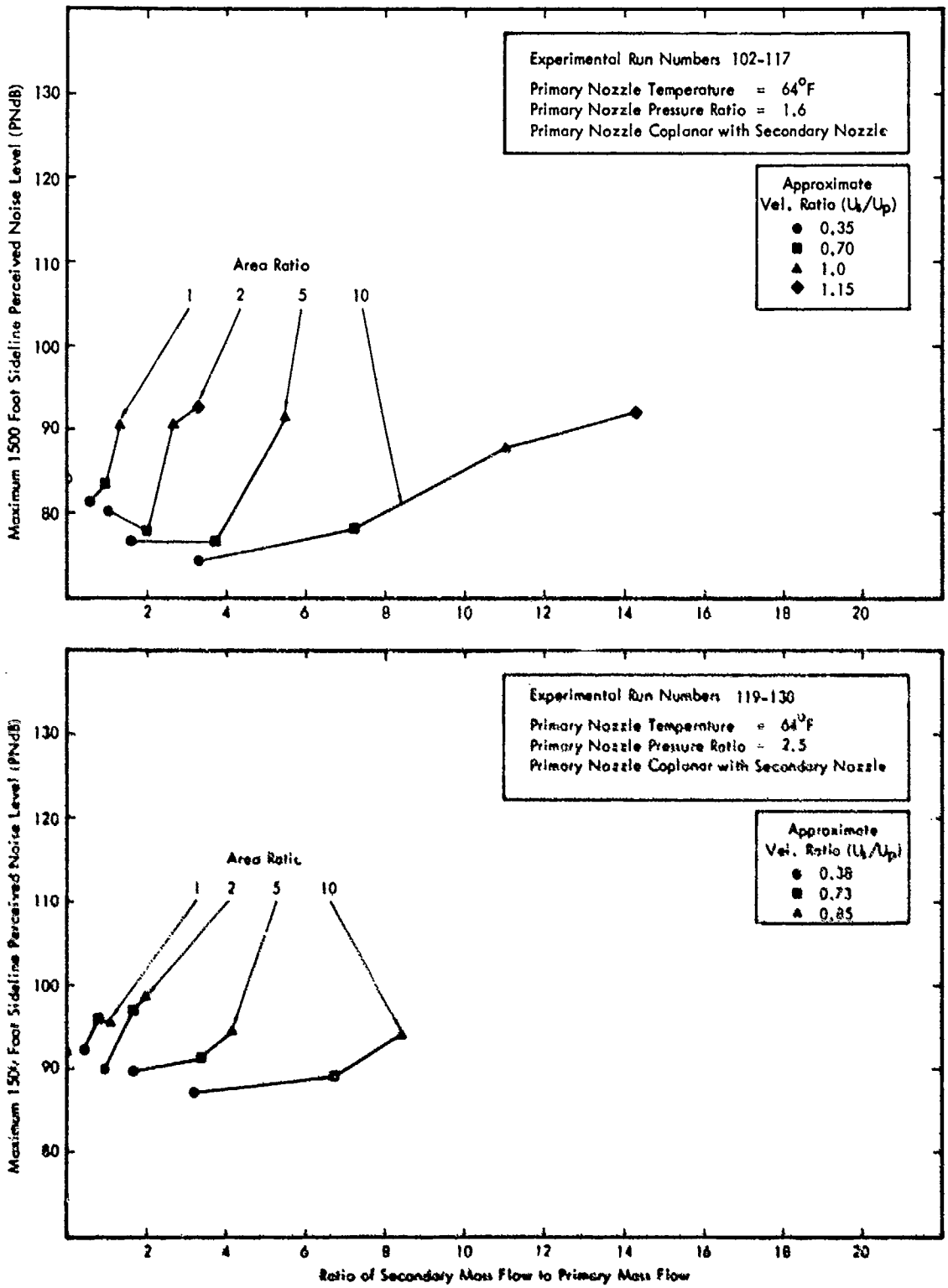

Figure E-1. Variation in Maximum Perceived Noise Level on a 1500-Foot Sideline with Bypass Ratio for Thrusts Scaled to 20,000 Lbs.

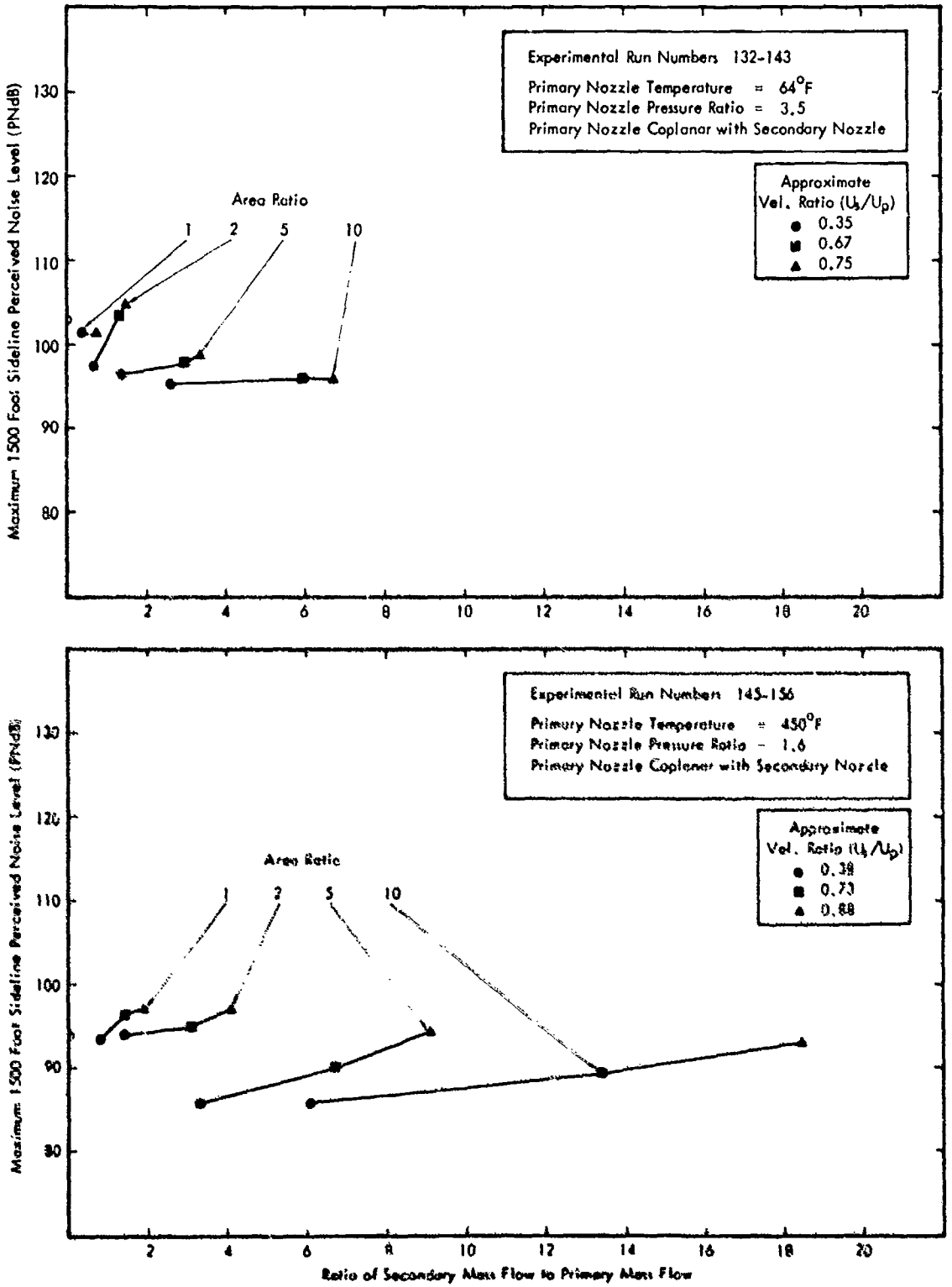

Figure E-1. continued ... Variation in Maximum Perceived Noise Level on a 1500-Foot Sideline with Bypass Ratio for Thrusts Scaled to 20,000 Lbs.

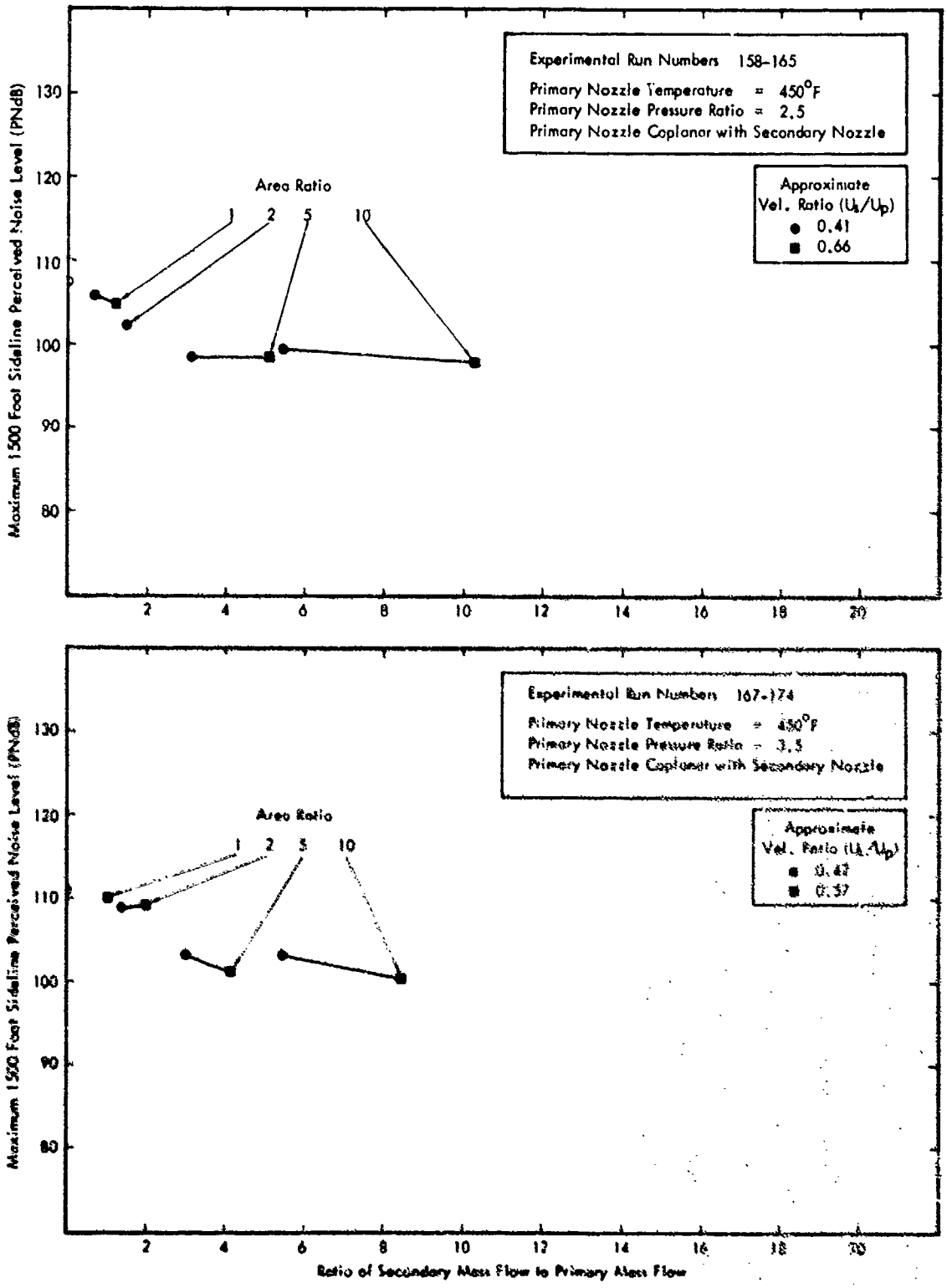

Figure E-1. continued ... Variation in Maximum Perceived Noise Level on a 1500-Foot Sideline with Bypass Ratio for Thrusts Scaled to 20,000 Lbs.

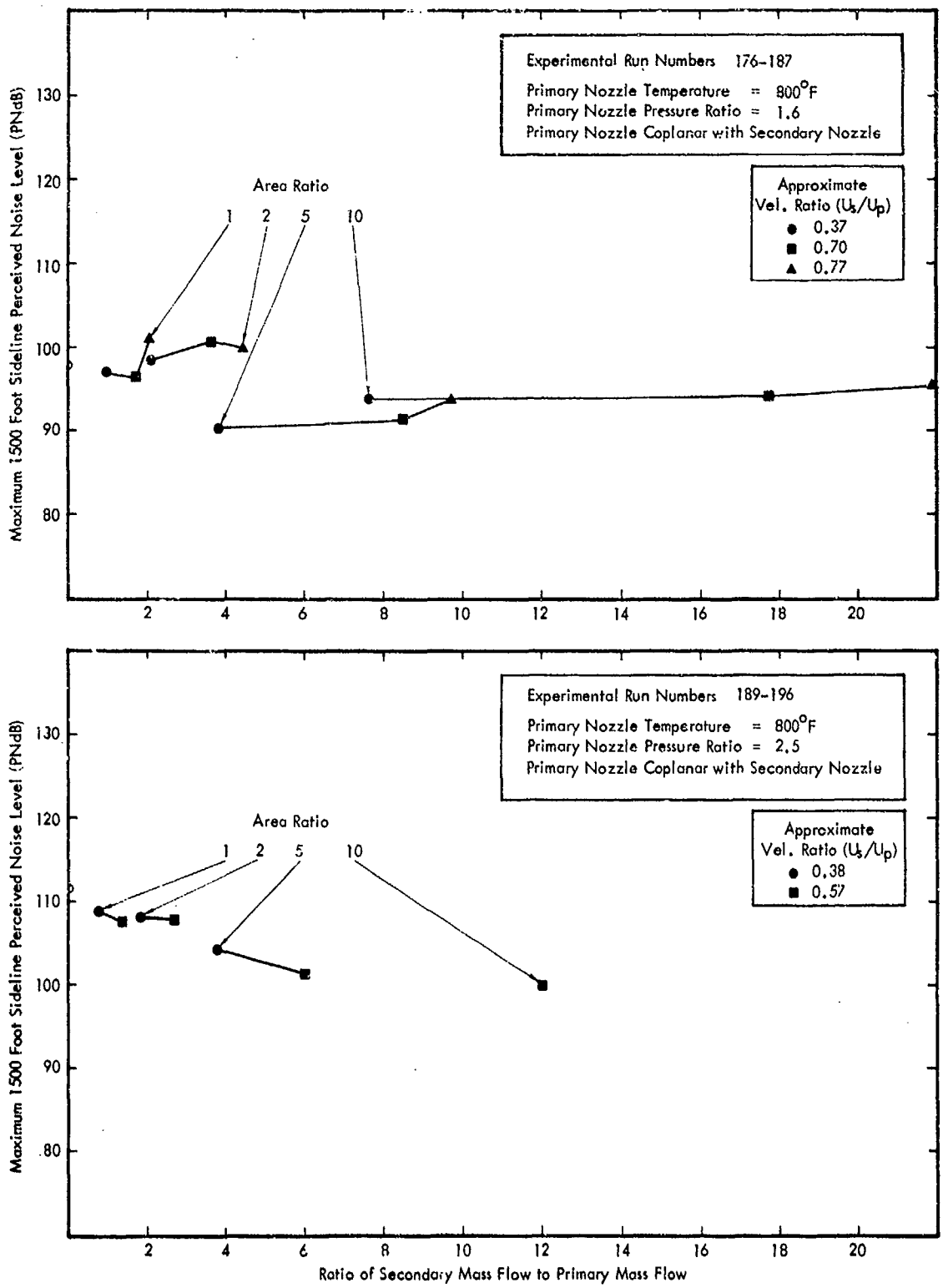

Figure E-1. continued ... Va ation in Maximum Perceived Noise Level on a 1500-Foot Sideline with Bypass Ratio for Thrusts Scaled to 20,000 Lbs.

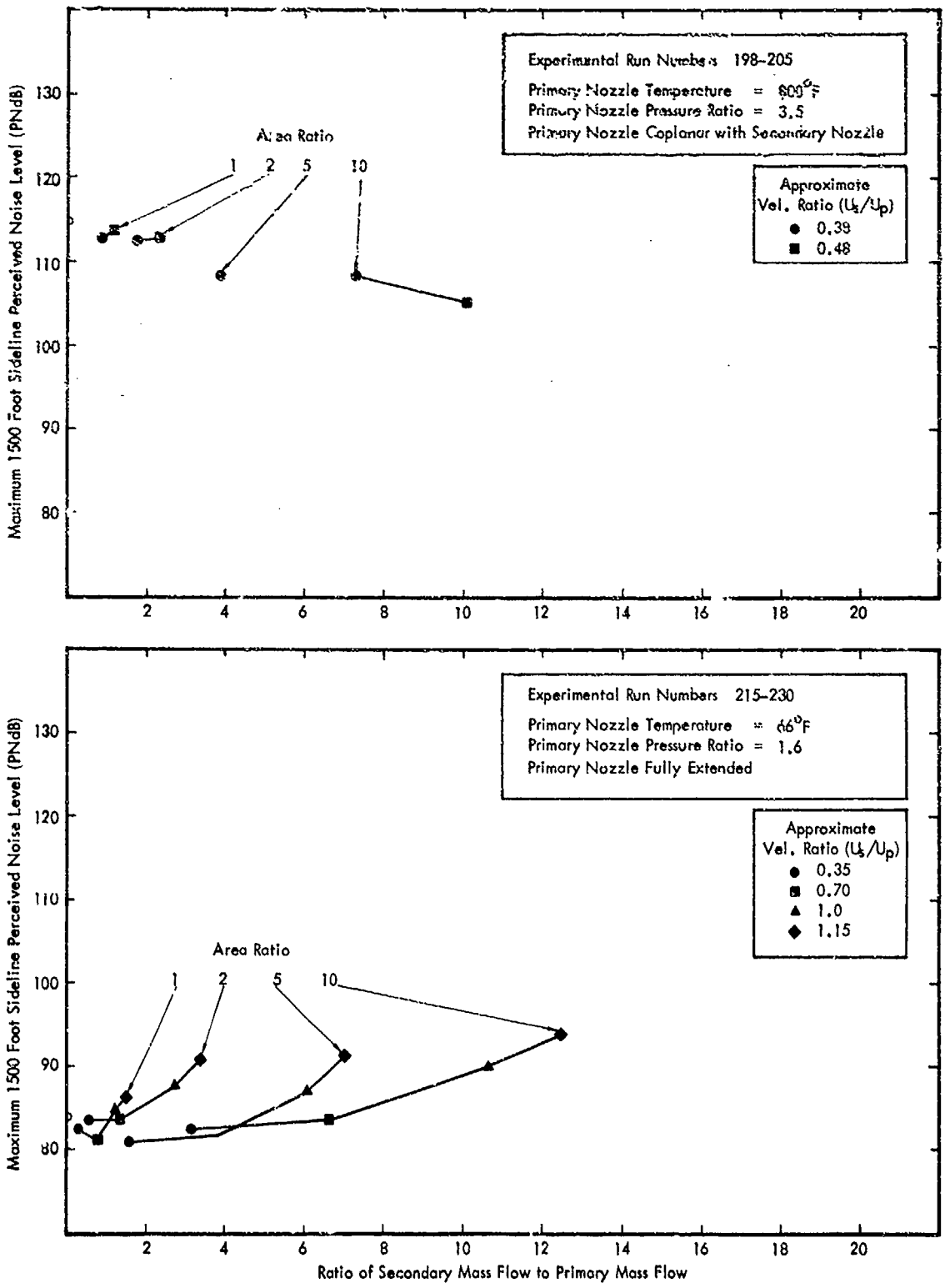

Figure E-1. continued ... Variation in Maximum Perceived Noise Level on a 1500-Foot Sideline with Bypass Ratio for Thrusts Scaled to 20,000 Lbs.

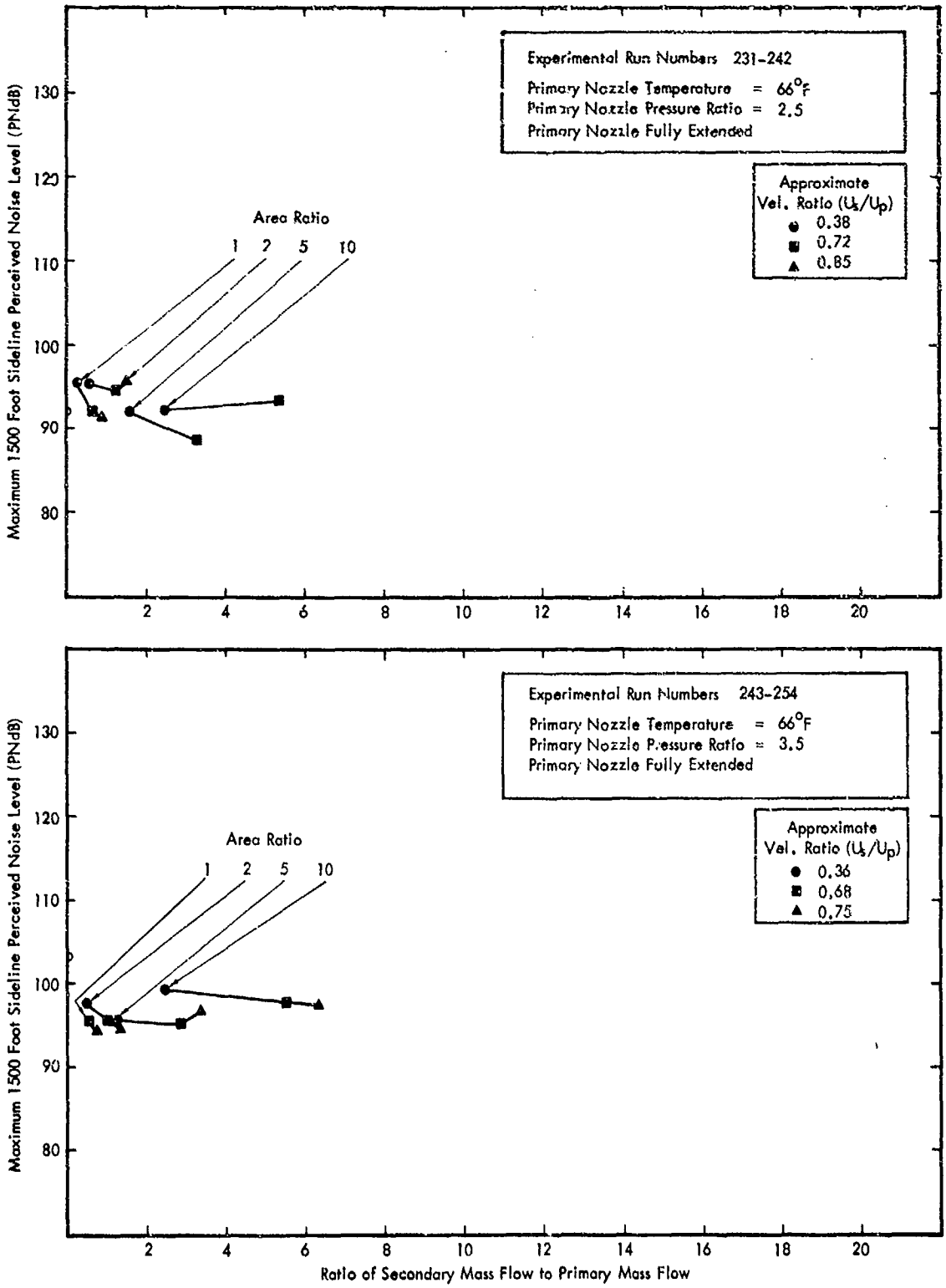

Figure E-1. continued ... Variation in Maximum Perceived Noise Level on a 1500-Foot Sideline with Bypass Ratio for Thrusts Scaled to 20,000 Lbs.

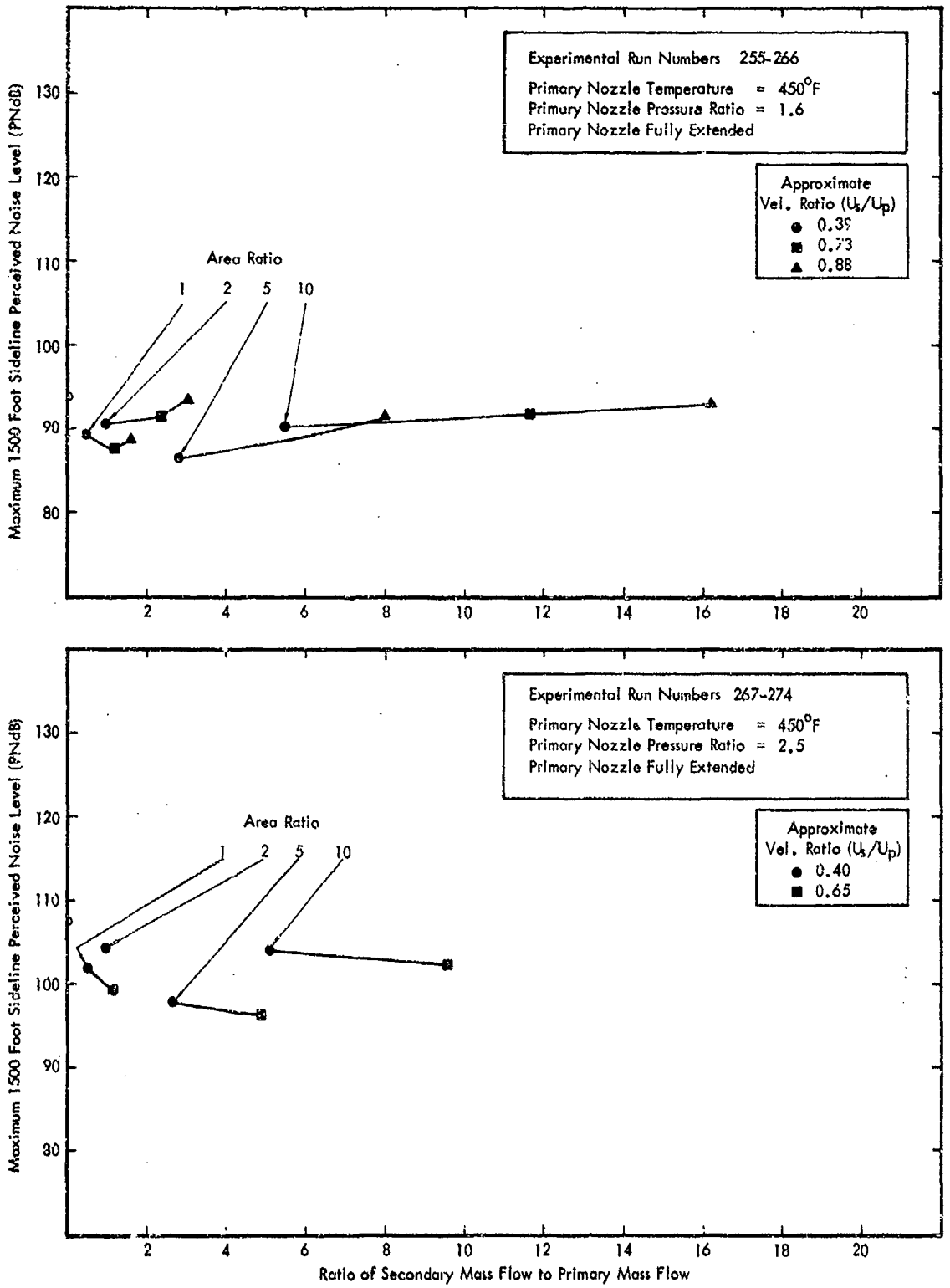

Figure E-1. continued ... Variation in Maximum Perceived Noise Level on a 1500-Foot Sideline with Bypass Ratio for Thrusts Scaled to 20,000 Lbs.

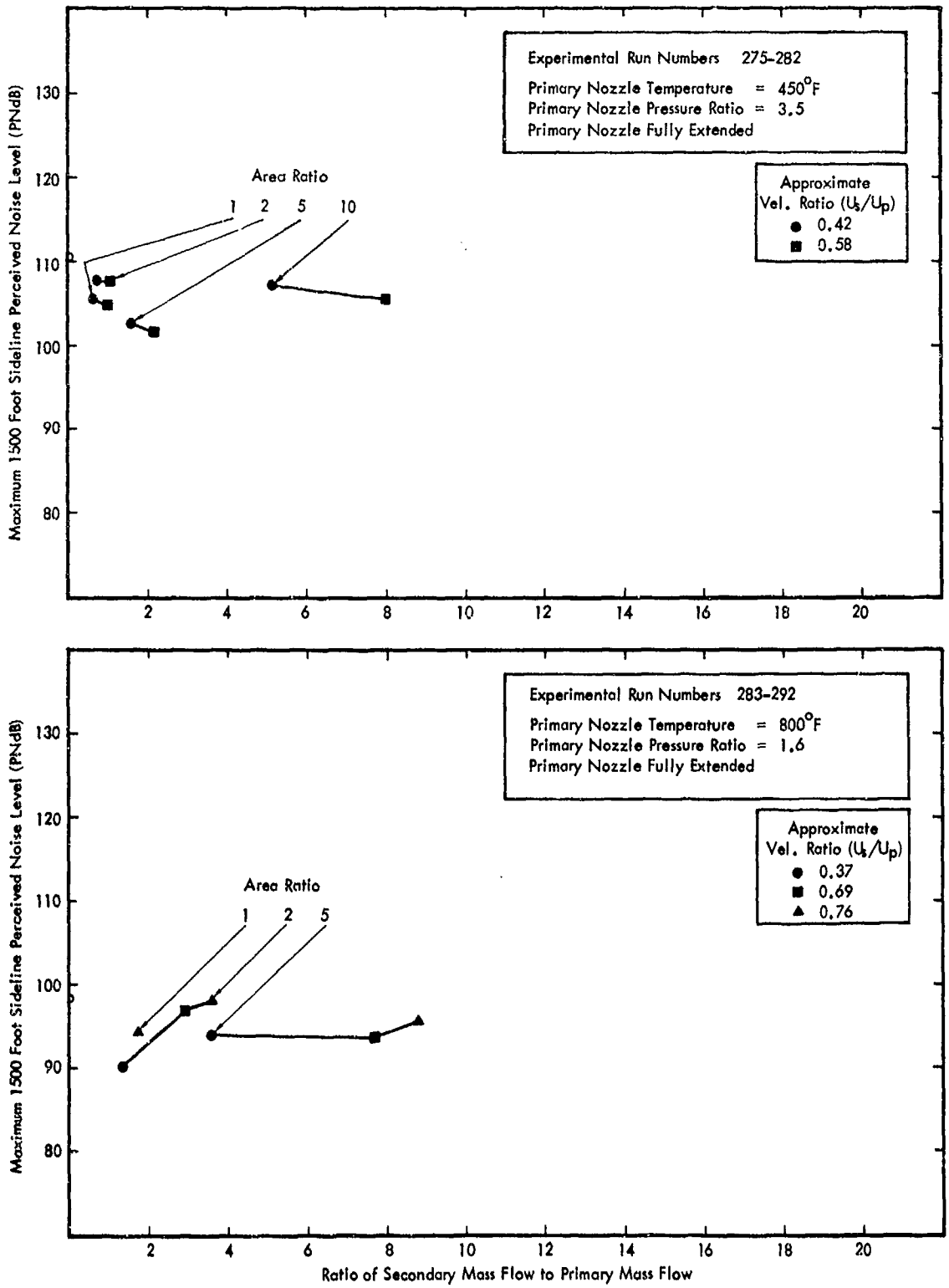

Figure E-1. continued ... Variation in Maximum Perceived Noise Level on a 1500-Foot Sideline with Bypass Ratio for Thrusts Scaled to 20,000 Lbs.

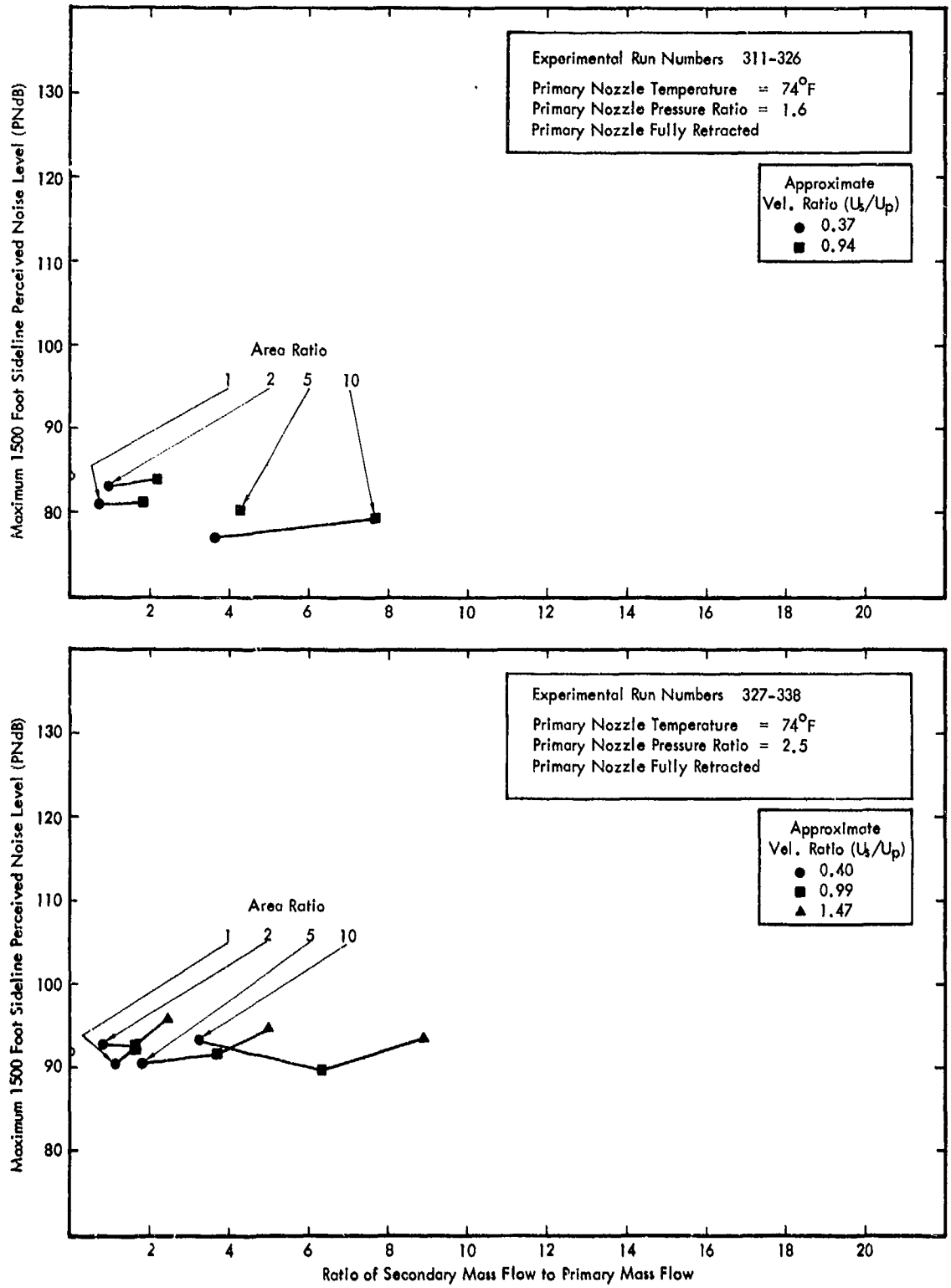

Figure E-1. continued ... Variation in Maximum Perceived Noise Level on a 1500-Foot Sideline with Bypass Ratio for Thrusts Scaled to 20,000 Lbs.

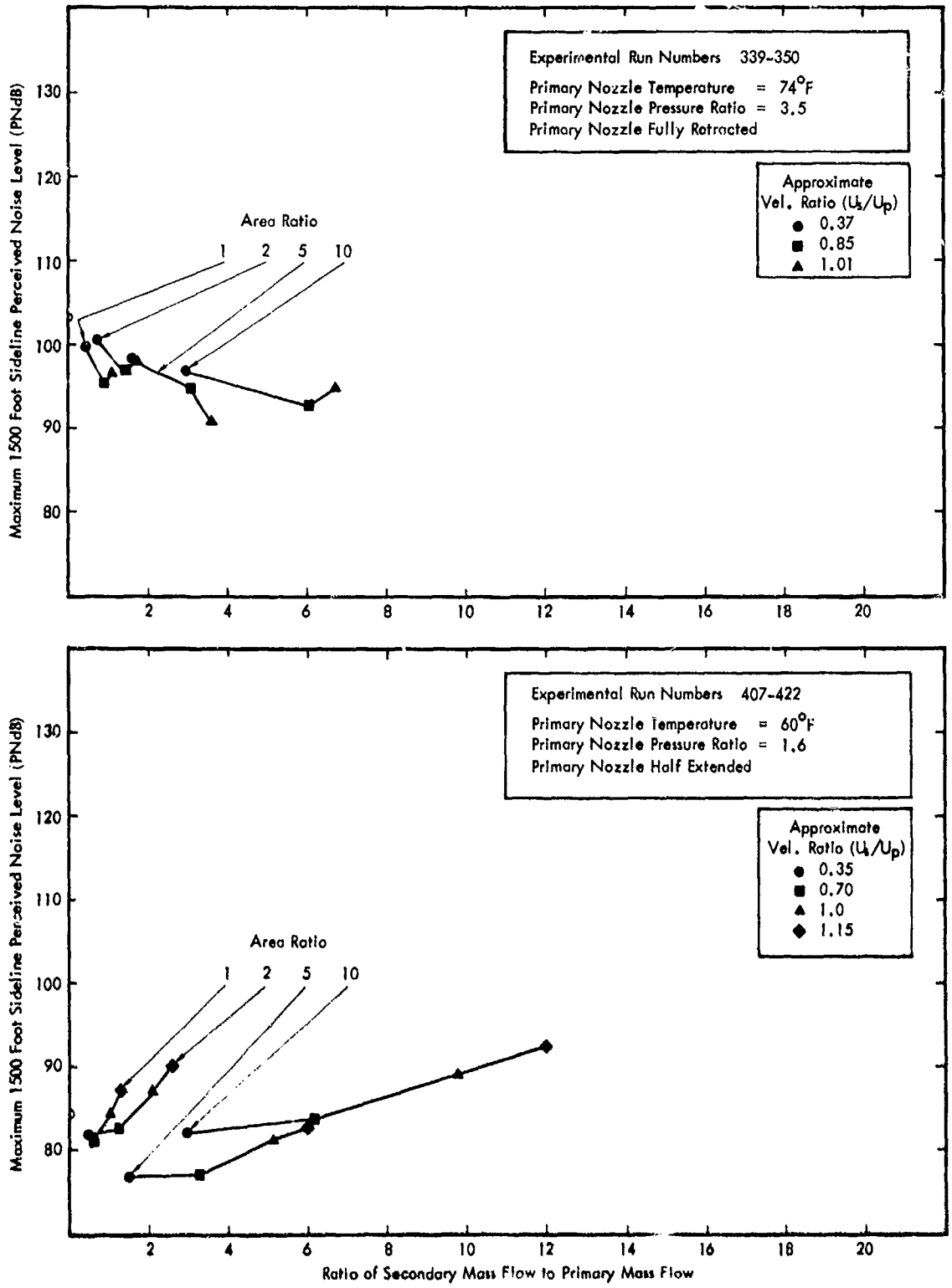

Figure E-1. continued ... Variation in Maximum Perceived Noise Level on a 1500-Foot Sideline with Bypass Ratio for Thrusts Scaled to 20,000 Lbs.

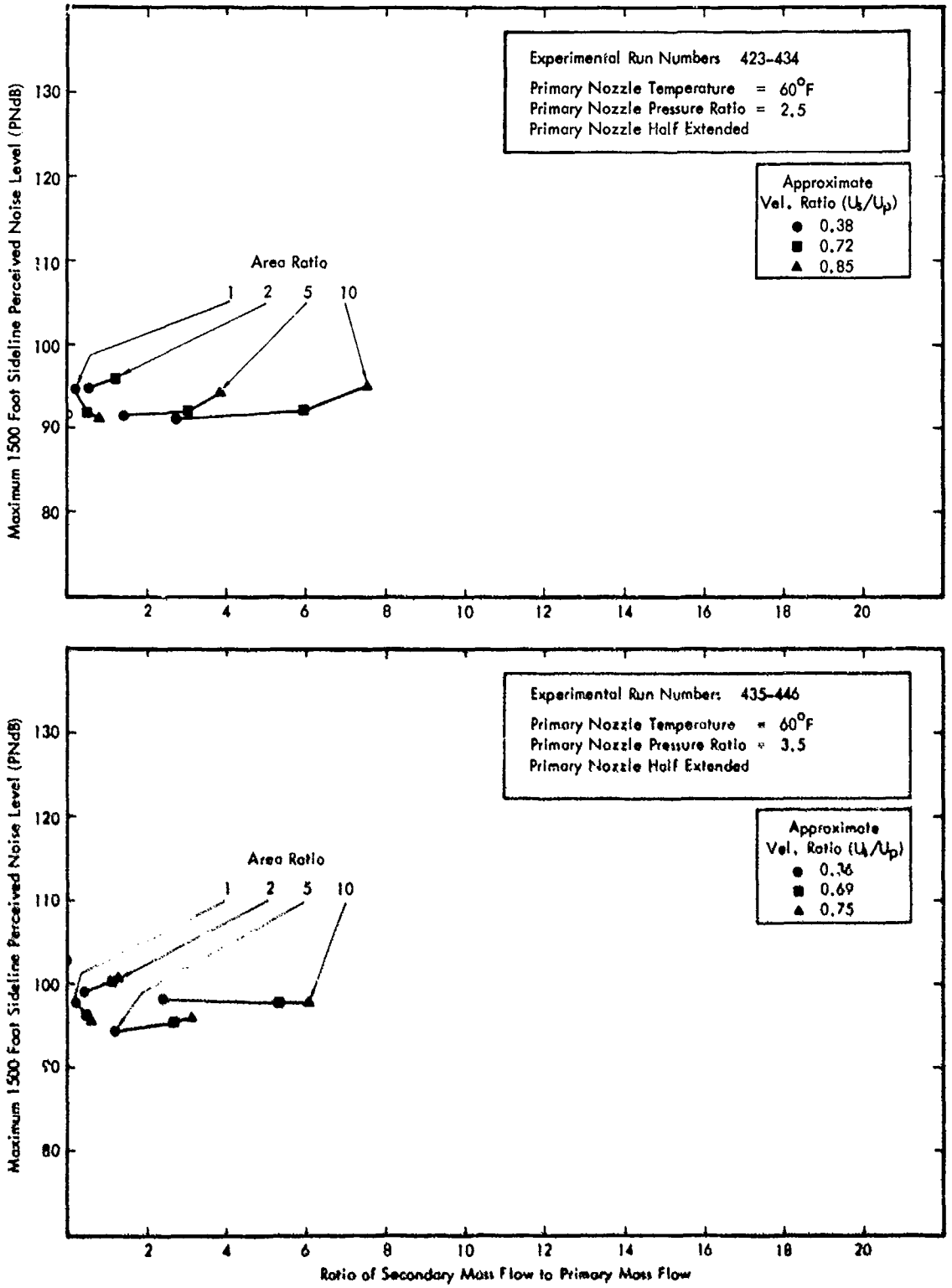

Figure E-1. continued ... Variation in Maximum Perceived Noise Level on a 1500-Foot Sideline with Bypass Ratio for Thrusts Scaled to 20,000 Lbs.

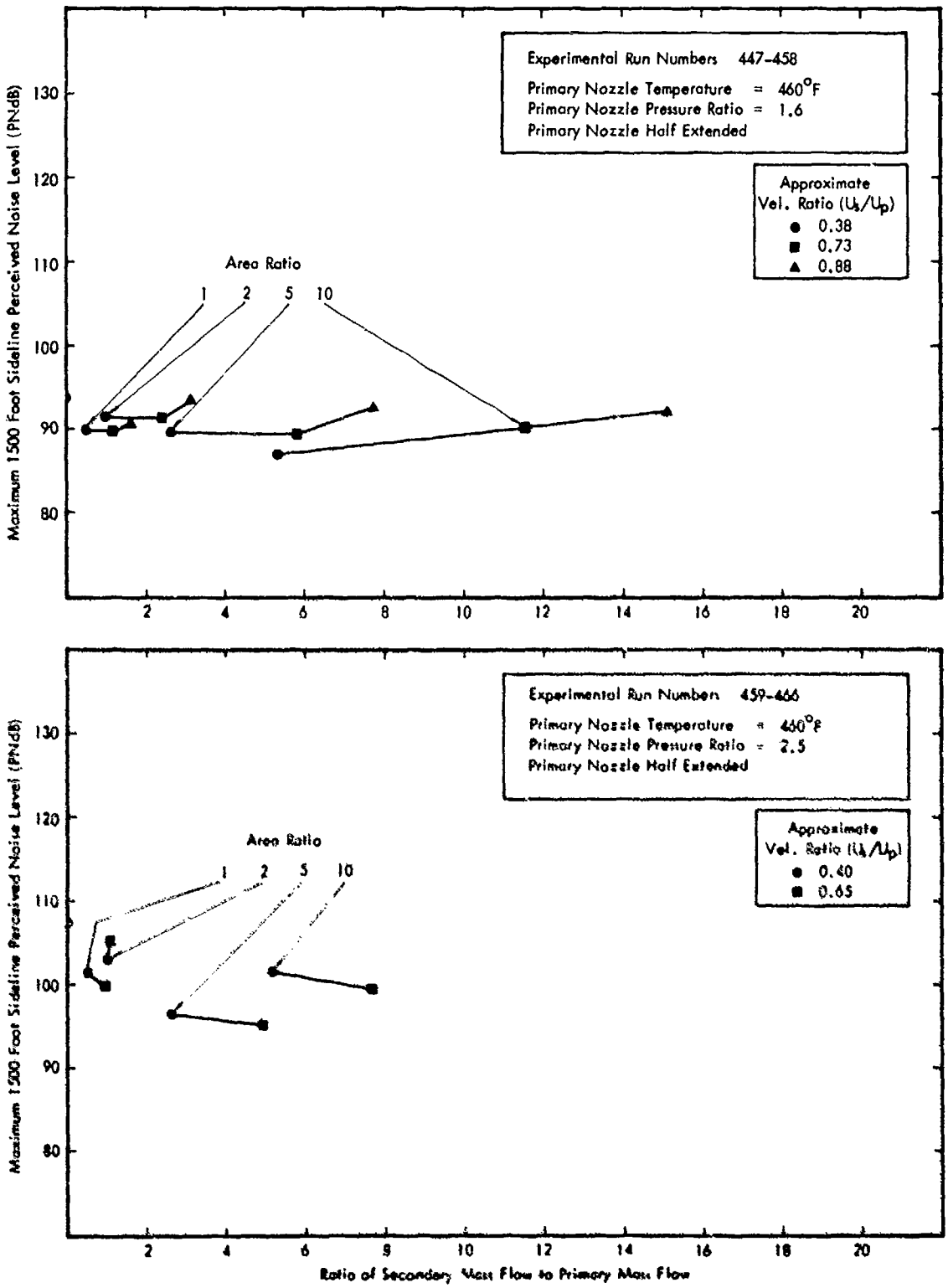

Figure E-1. continued ... Variation in Maximum Perceived Noise Level on a 1500-Foot Sideline with Bypass Ratio for Thrusts Scaled to 20,000 Lbs.

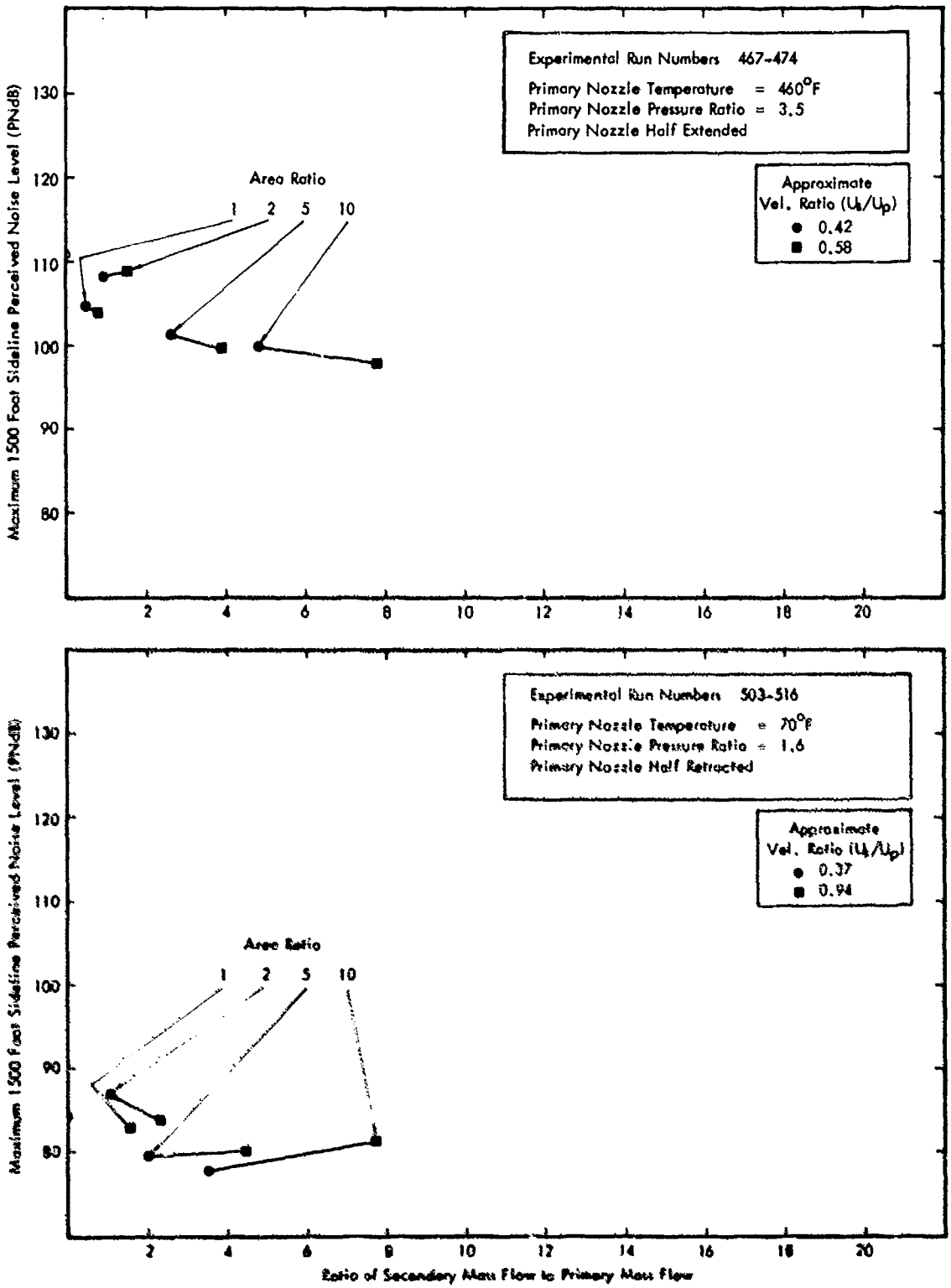

Figure E-1. continued ... Variation in Maximum Perceived Noise Level on a 1500-Foot Sideline with Bypass Ratio for Thrusts Scaled to 20,000 Lbs.

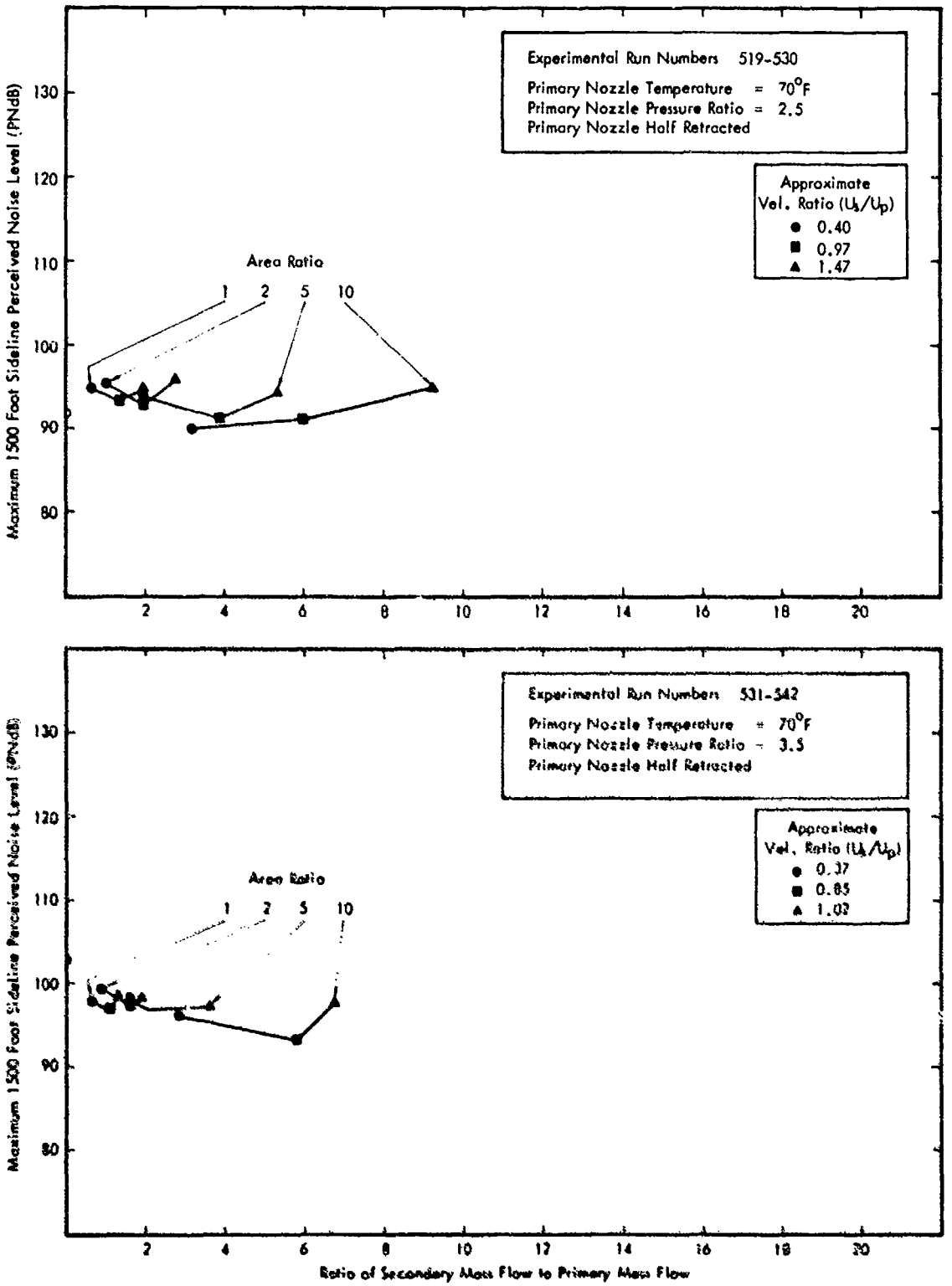

Figure E-1. concluded ... Variation in Maximum Perceived Noise Level on a 1500-Foot Sideline with Bypass Ratio for Thrusts Scaled to 20,000 Lbs.

Intentionally Left Blank

APPENDIX F

PRIMARY JET SOUND POWER SPECTRA AND DIRECTIVITY DATA

This appendix contains twelve (12) graphs which give the sound power spectra and directivity data measured for the three (3) primary nozzles. For each nozzle, the power spectra are given for three (3) temperatures, followed by three (3) graphs containing the associated octave band directivities for each temperature condition.

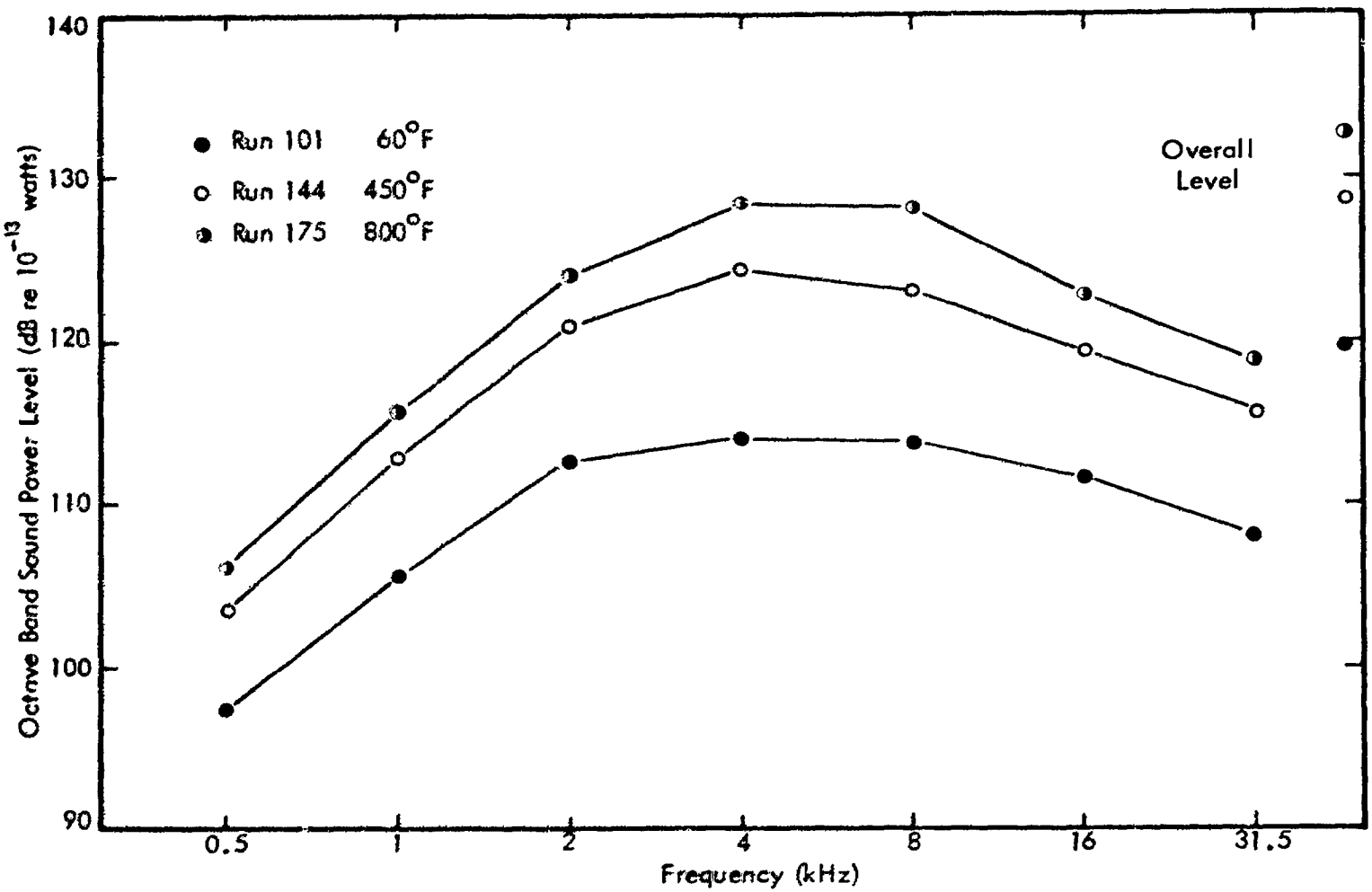

Figure F-1. Model Jet Sound Power Spectra for Primary Nozzles with Pressure Ratio 1.6.

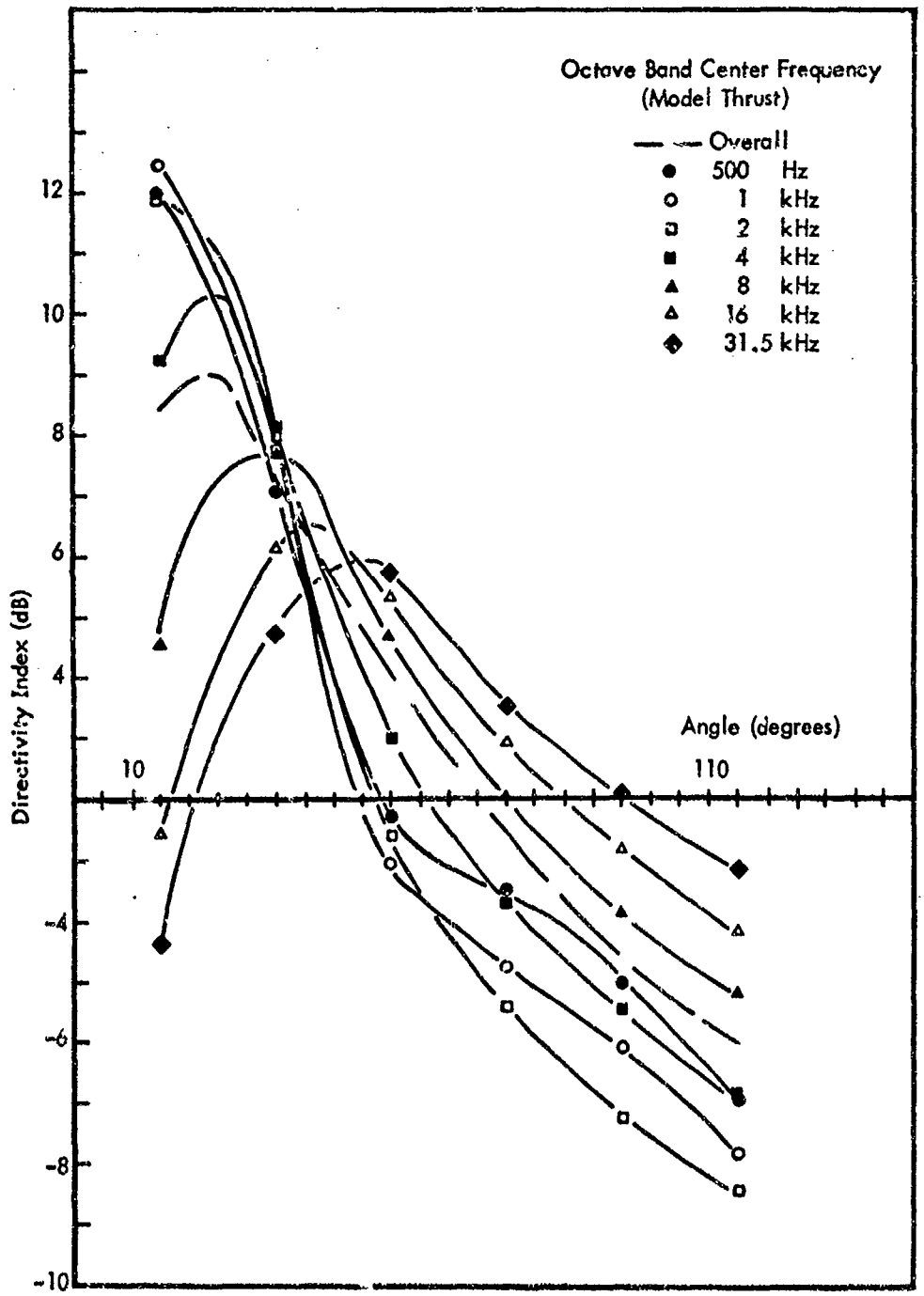

Figure F-2. Directivity Pattern for Run Number 101 (Pressure Ratio 1.6, Temperature 60°F).

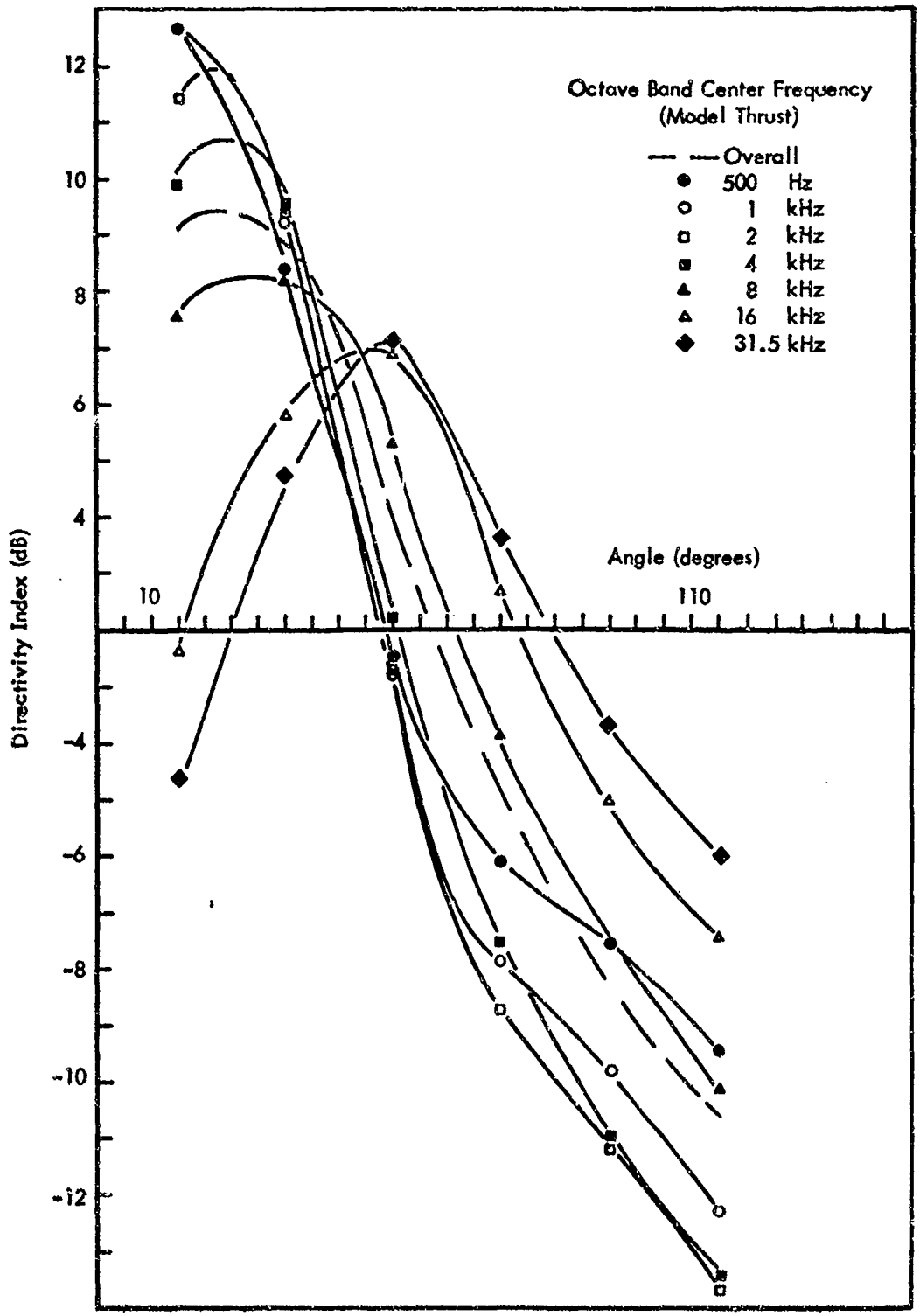

Figure F-3. Directivity Pattern for Run Number 144
(Pressure Ratio 1.6, Temperature 450°F).

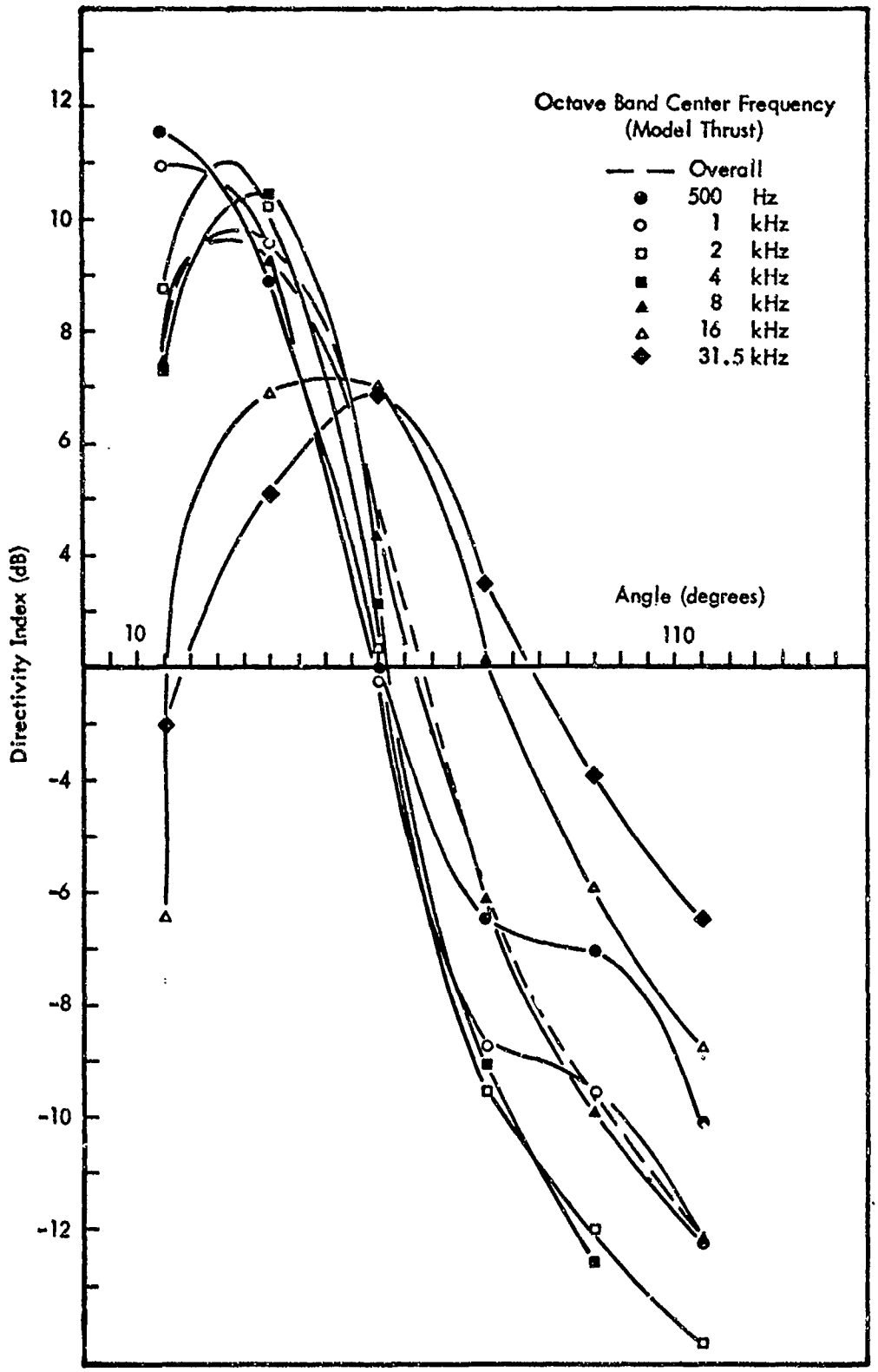

Figure F-4. Directivity Pattern for Run Number 175 (Pressure Ratio 1.6, Temperature 800°F).

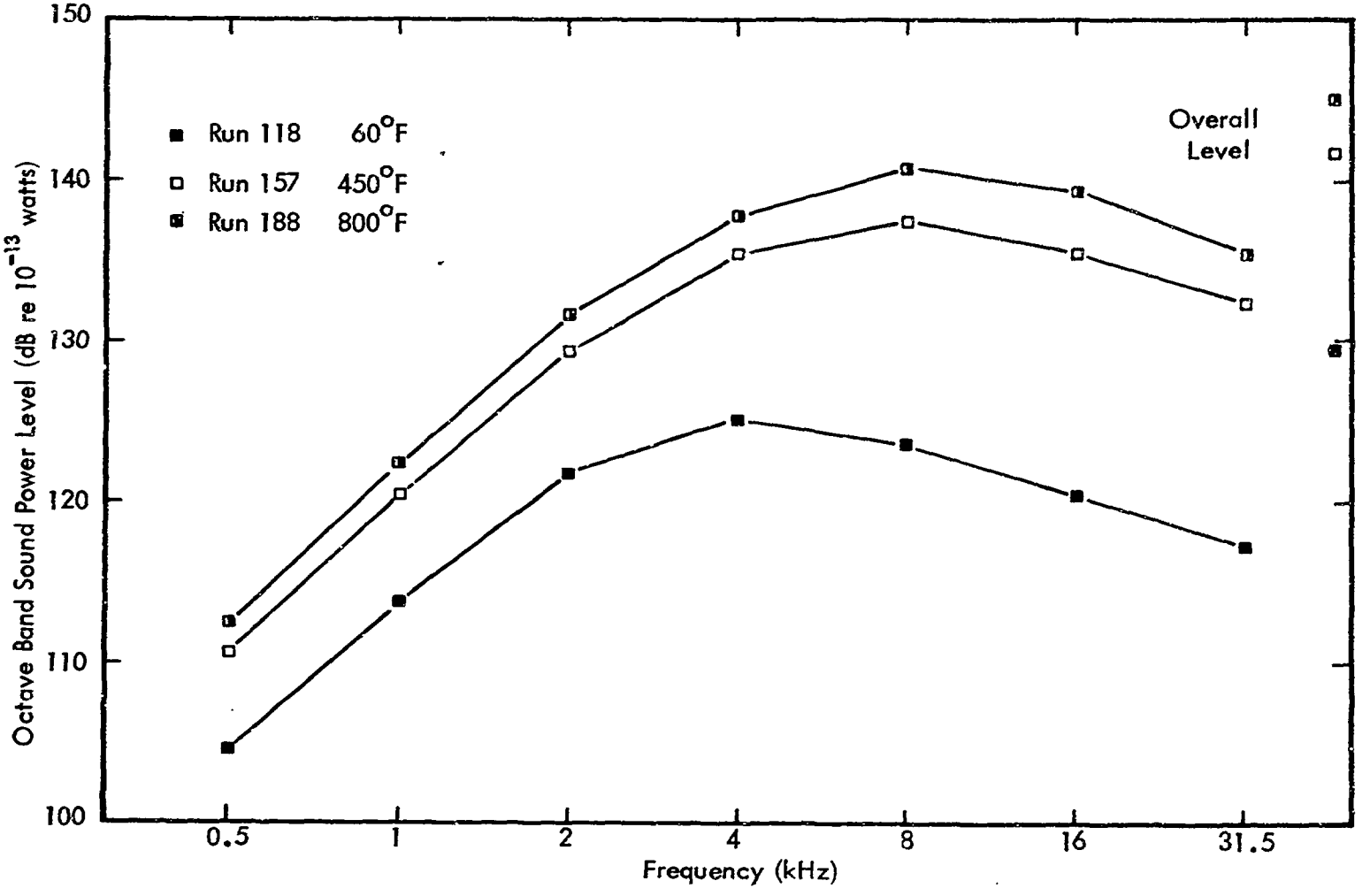

Figure F-5. Model Jet Sound Power Spectra for Primary Nozzles with Pressure Ratio 2.5.

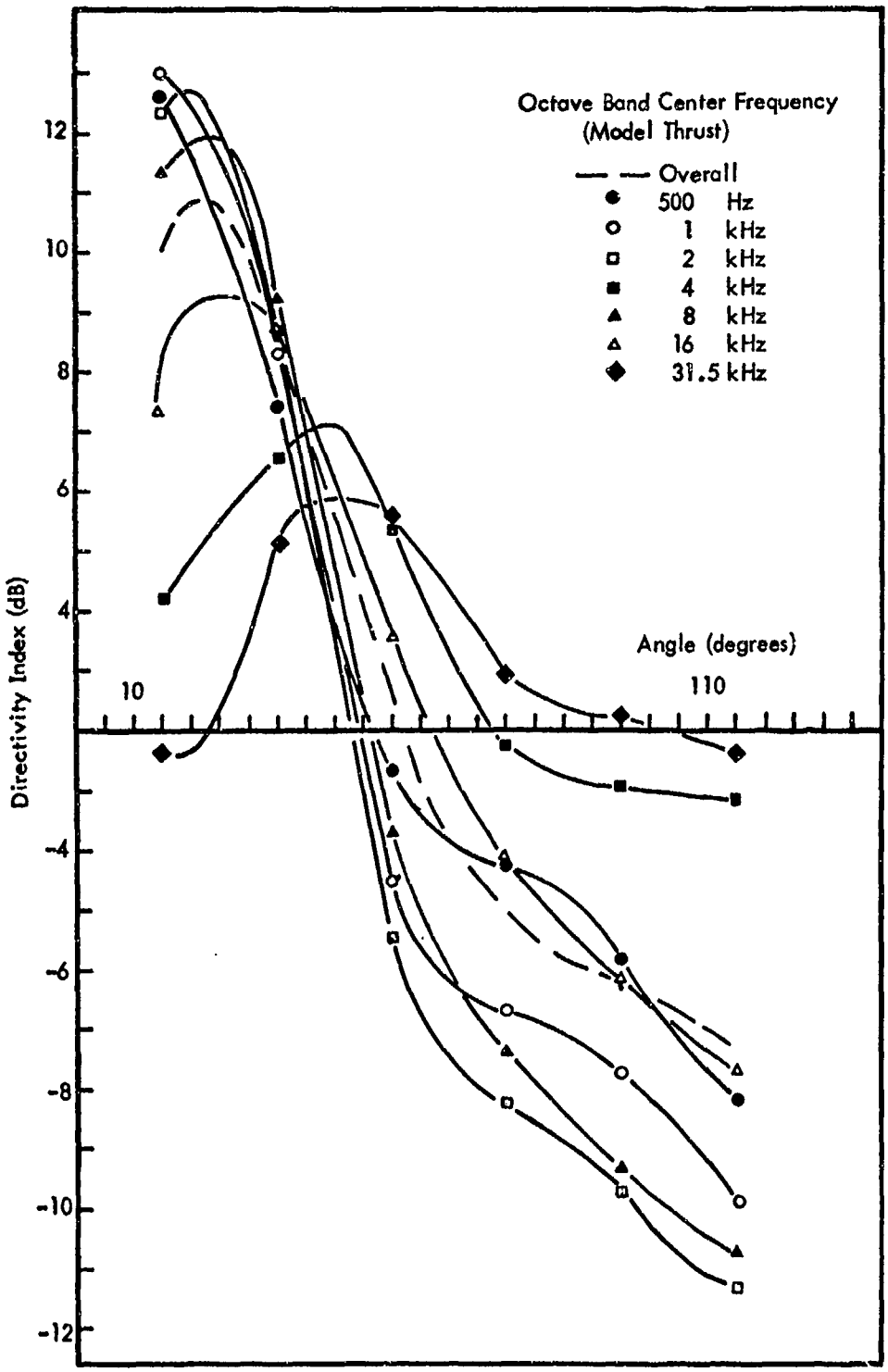

Figure F-6. Directivity Pattern for Run Number 118 (Pressure Ratio 2.5, Temperature 60°F).

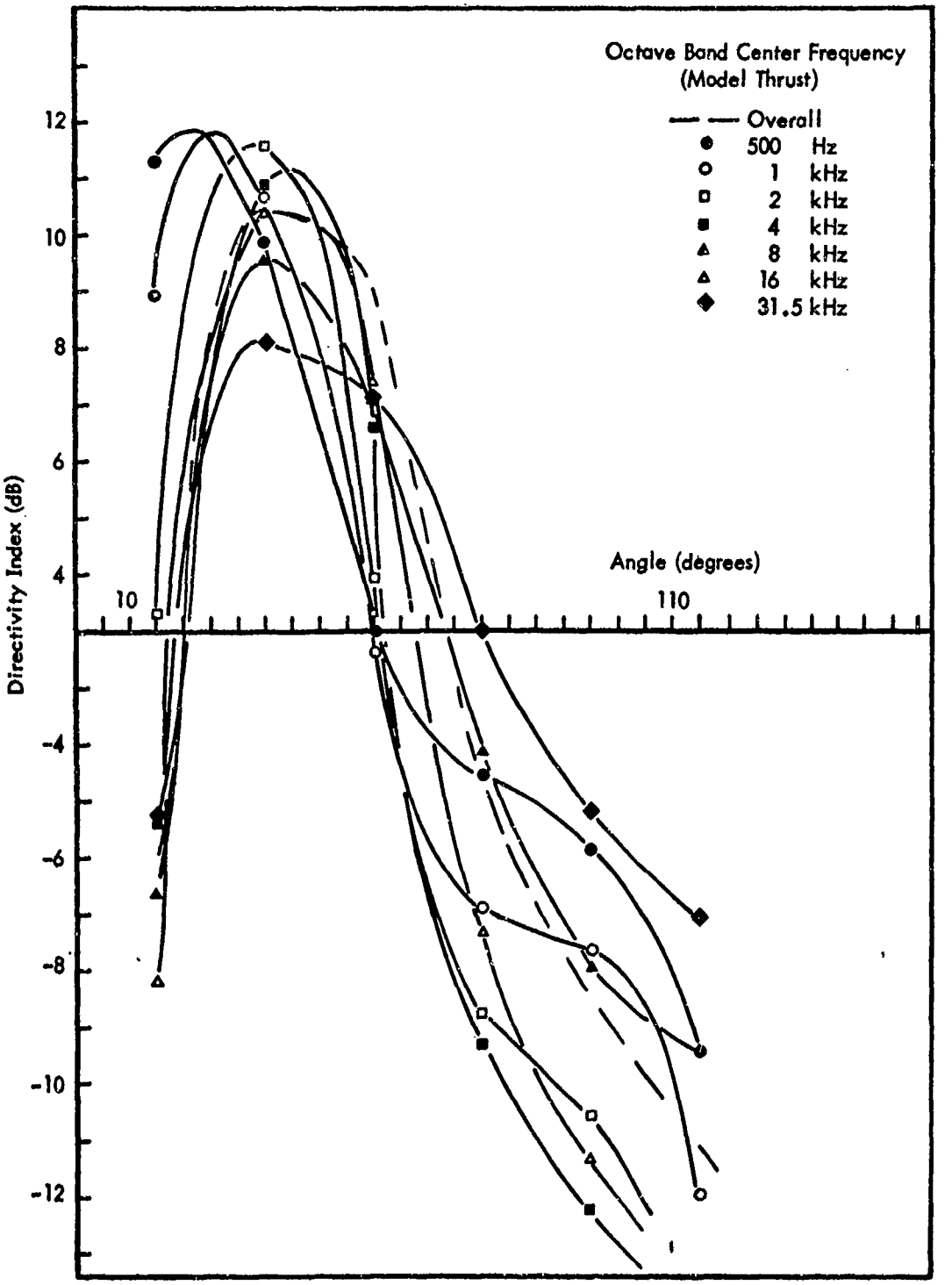

Figure F-7. Directivity Pattern for Run Number 157
(Pressure Ratio 2.5, Temperature 450°F).

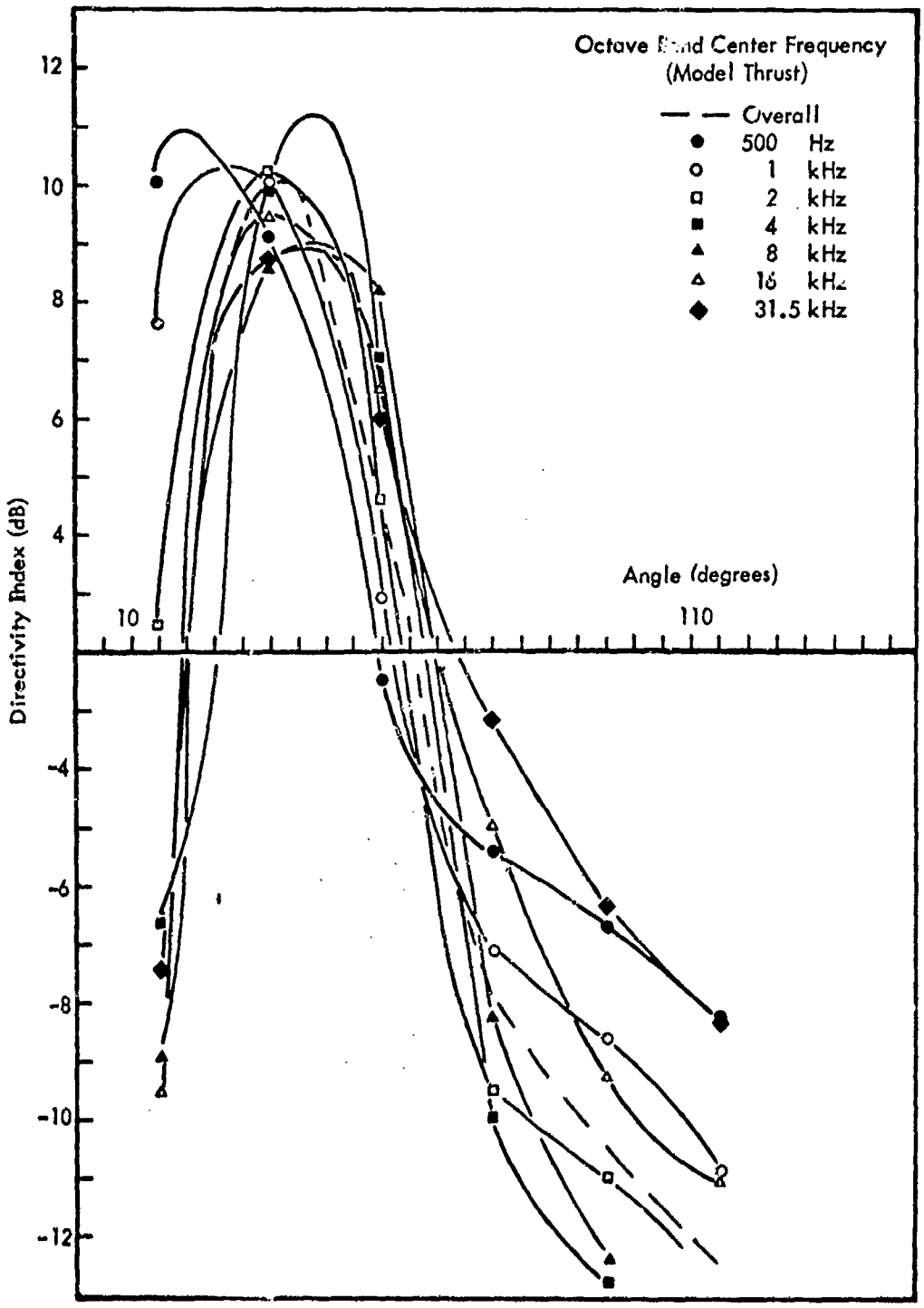

Figure F-8. Directivity Pattern for Run Number 188
(Pressure Ratio 2.5, Temperature 800°F).

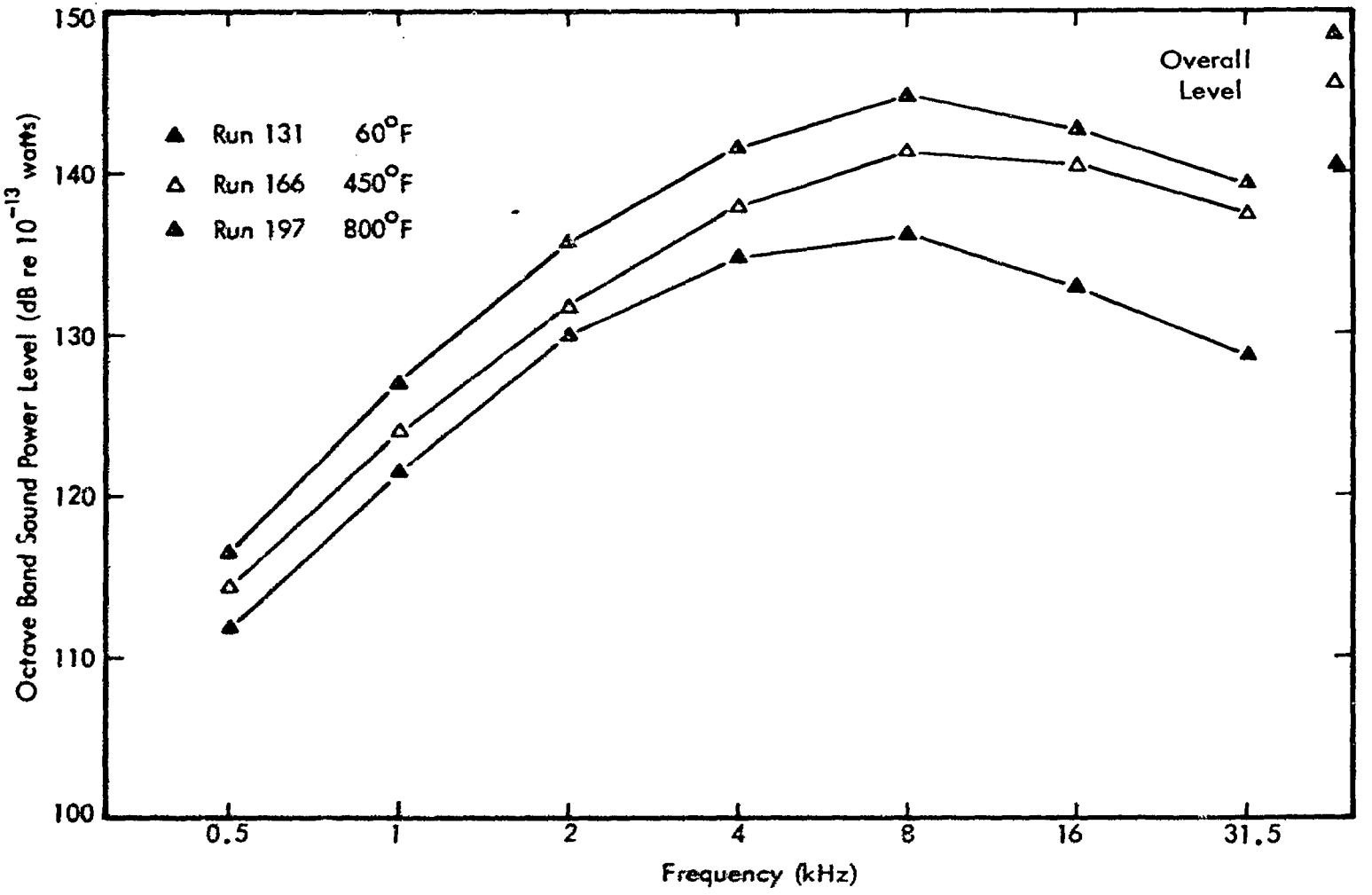

Figure F-9. Model Jet Sound Power Spectra for Primary Nozzles with Pressure Ratio 3.5.

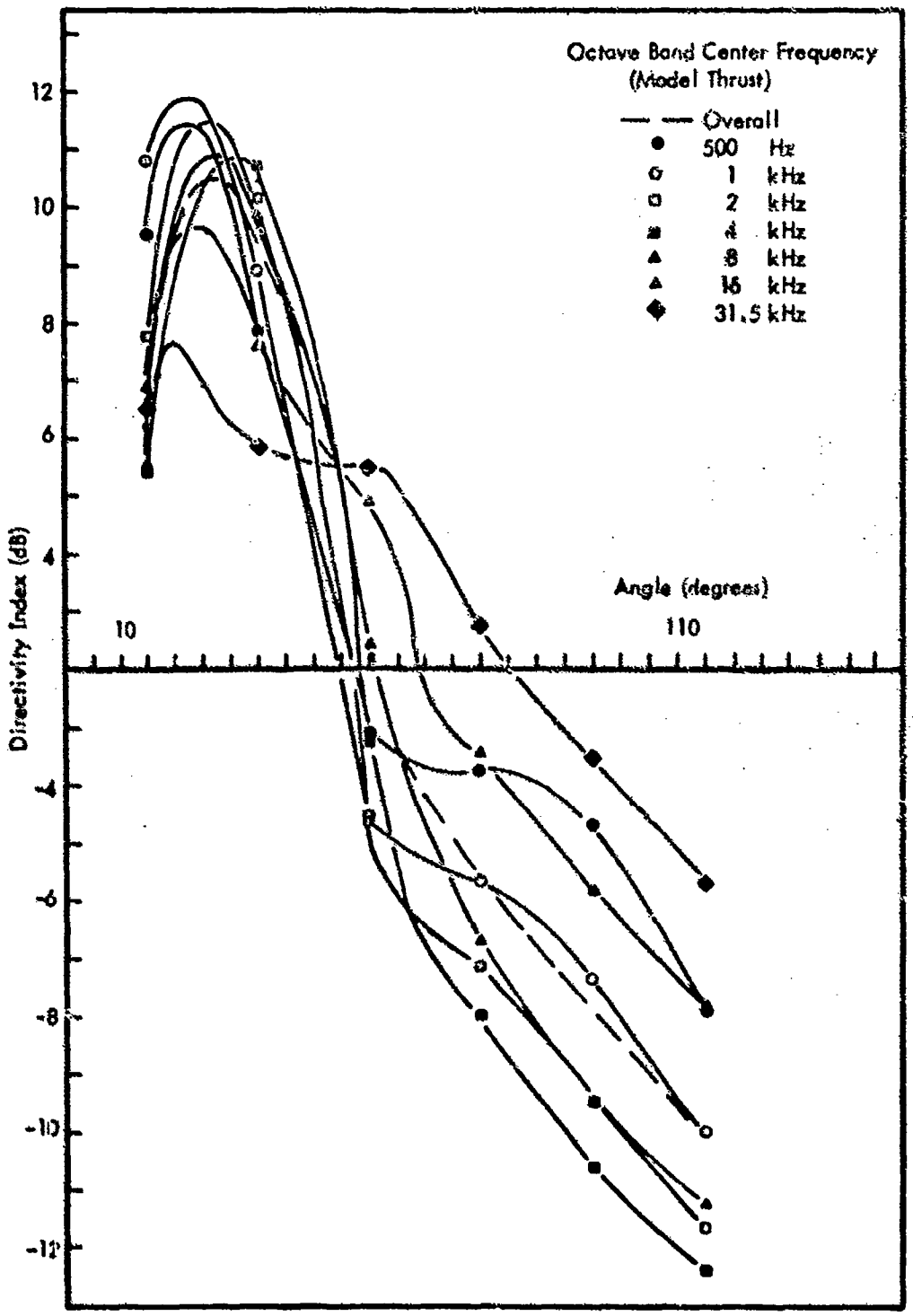

Figure F-10. Directivity Pattern for Run Number 131 (Pressure Ratio 3.5, Temperature 60°F).

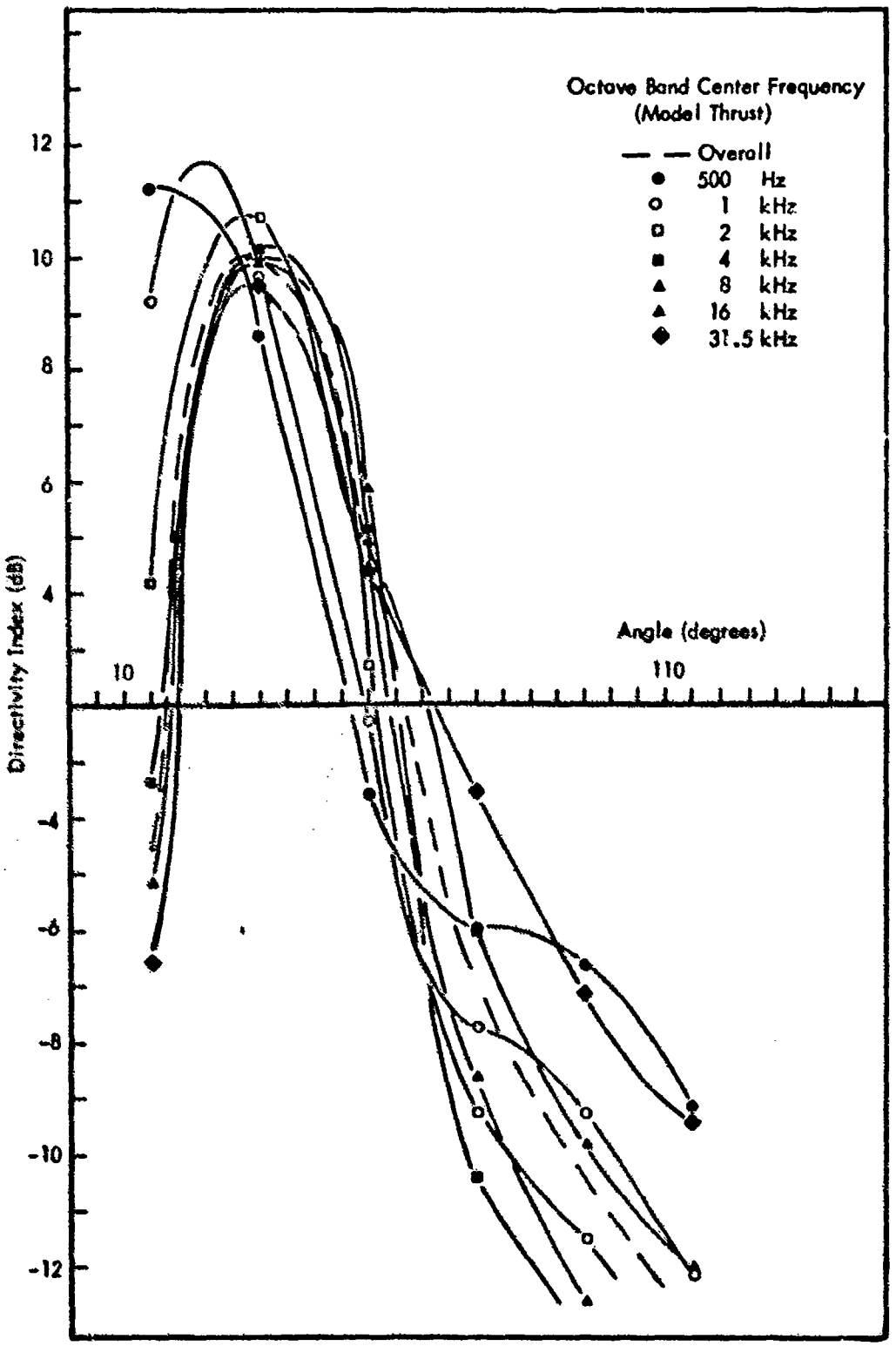

Figure F-11. Directivity Pattern for Run Number 166
(Pressure Ratio 3.5, Temperature 450°F)

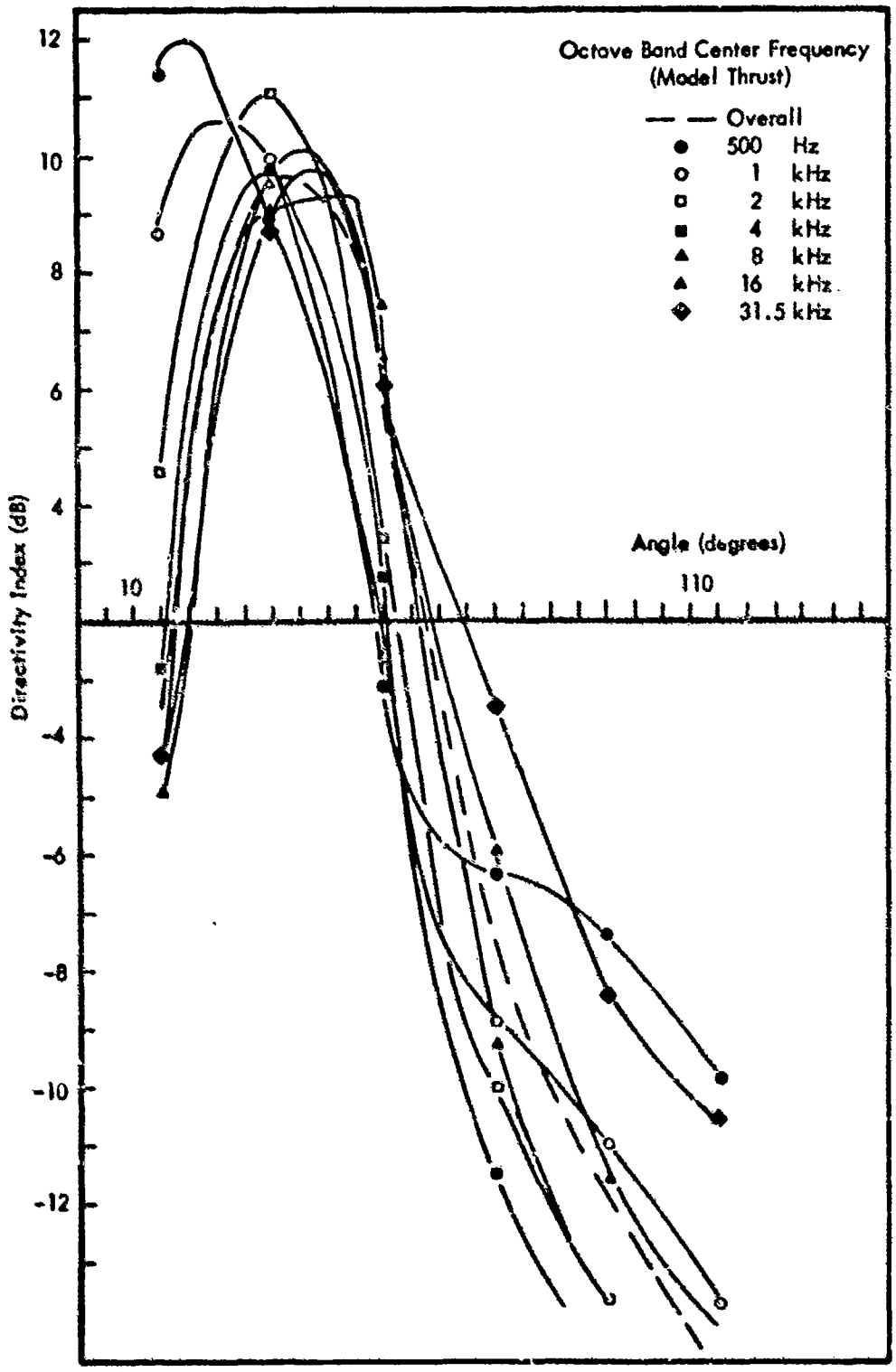

Figure F-12. Directivity Pattern for Run Number 197 (Pressure Ratio 3.5, Temperature 800°F).

Intentionally Left Blank

APPENDIX G

NOISE OF A SUPERSONIC NOZZLE OPERATING AT OFF-DESIGN PRESSURE RATIOS

It is to be expected that supersonic nozzles of jet engines, if designed for high-speed cruise at high altitude, may be operating at off-design pressure ratios at takeoff. Therefore, it was of interest to explore the noise generated during off-design operation to determine whether any anomalies may be present. A small number of exploratory runs were conducted for this purpose.

It was felt that if any anomalies (such as discrete tones) existed, they would certainly be apparent in a cold flow (i.e., 60°F). Therefore, the exploratory runs were made with a cold flow, using a supersonic nozzle designed for pressure ratio 3.5. When discrete tones occur in a test, even if they are not detectable by ear, they are very apparent from spikes in the directivity pattern for the octave band in which they occur. The computer printout data from these runs was reviewed and no pure tone anomalies were found.

Seven (7) runs were performed within a one-hour period, using operating pressure ratios ranging from 2.0 to 7.8, and repeating the on-design pressure ratio condition. Since the computer printout of the data lists the design pressure ratio but not the operating pressure ratio, that information is given in the table below. (For all other runs in the project, operating pressure ratio and design pressure ratio were nominally the same.)

Run Number	Primary Supply Pressure, psig	Operating Pressure Ratio
600	14.6	2.0
601	21.9	2.5
602	29.2	3.0
603	36.5	3.5
604	43.8	4.0
605	63.0	5.4
606	99.5	7.8

Run 131 provides another data point of on-design operation for the same nozzle. However, it was run at a different time, with a lower supply temperature, and had a slightly higher mass flow and a 2.1 dB higher acoustic power when compared to Run 603 in this series. Therefore, it is not used for comparison with these sequential results.

The directivity index values are shown for alternate runs in Figure G-1. There is a general trend to a sharper directionality (without shift in angle) as the operating pressure ratio is increased, but there are no apparent anomalies or disagreements with normal jet noise data. In terms of the octave band spectra at $\theta = 45^{\circ}$, Figure G-2, there is no significant change in spectrum shape for off-design operation.

Figure G-3 shows the effect of off-design operation on the model scale sound power generation with the U^8 slope mean data line for the primary nozzles for reference. Figure G-4 shows similar data for the 1500-foot sideline maximum perceived noise level. Here, the U^8 slope data curve for the other primary nozzles almost fits, indicating that the off-design conditions affect the power level more than they affect the perceived noise level. The reason may be that the sharper directivities for the nozzle, when operated above design velocity, tend to reduce the relative amount of noise radiated to the sideline.

It should be mentioned that in all runs except Run 600, the original data showed broadband noise in the 16 kHz and 31.5 kHz bands, which was removed in the same way as in the production runs for on-design cases (see Section 4.2). It is known that over-pressure operation of a convergent nozzle can produce what is called "shock cell noise," Reference G-1, and has even done so on full-scale engines operating at altitude, Reference G-2. Such noise is characterized by discrete tones of a highly directional nature, whose fundamental frequency (for a stationary jet) can be predicted from:

$$f_1 = \frac{a}{3d\,(R - R_c)^{1/2}} \qquad \text{(G-1)}$$

where

- f_1 = fundamental frequency, Hz
- R = operating pressure ratio
- R_c = critical pressure ratio, normally 1.89 (but should be design for a convergent divergent nozzle)
- a = ambient speed of sound, ft/sec
- d = jet exit diameter, ft

The original data (before correction) was reviewed. Anomalies were noted in most of the runs for the upper two octave bands of data (and sometimes in the upper three octave bands: 8 kHz, 16 kHz and 31.5 kHz) at θ = 100 - 110 degrees.

The results for 110 degrees and the upper three octave bands are given in Figure G-5. No anomalies in the directivities were observed at the two lower pressure ratios.

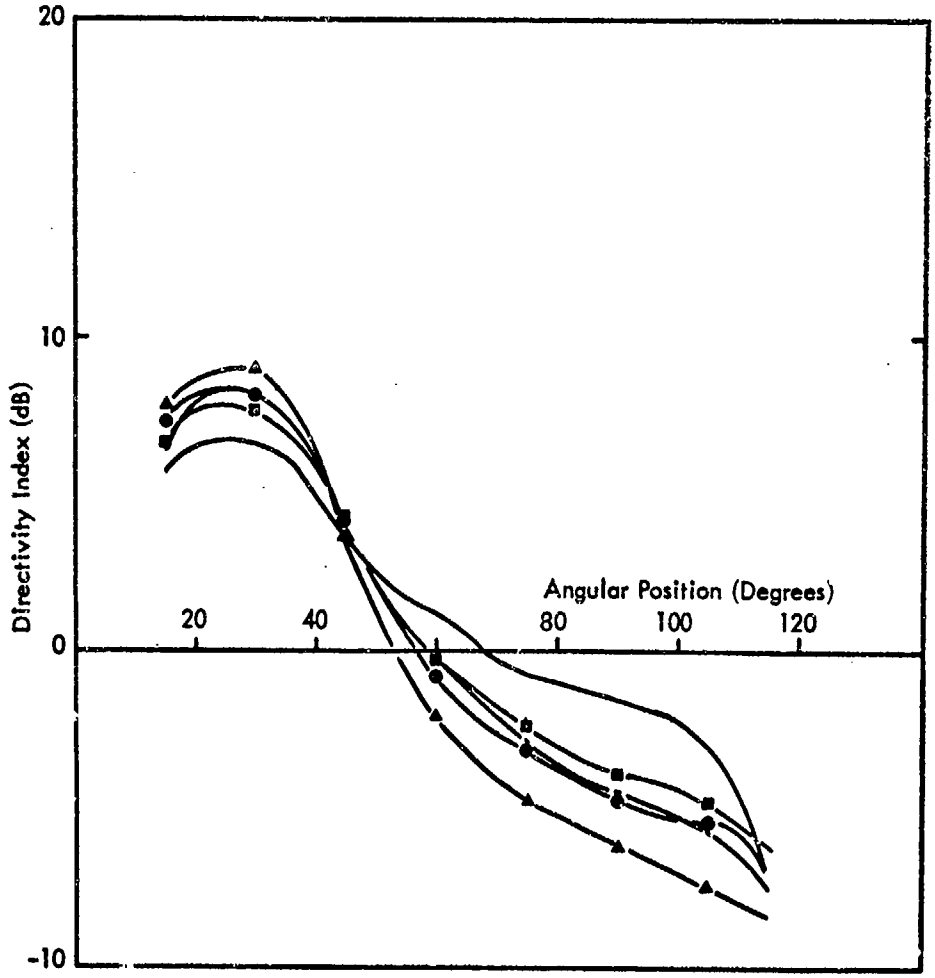

	Run No.	Operating Pressure Ratio
———	600	2.0
—·—·—	602	3.0
●—●	603	3.5 (design point)
■—■	604	4.0
▲—▲	606	7.8

Figure G-1. Directivity Index for Overall Sound Pressure Level for a Supersonic Nozzle Operating at Off-Design Pressure Ratios.

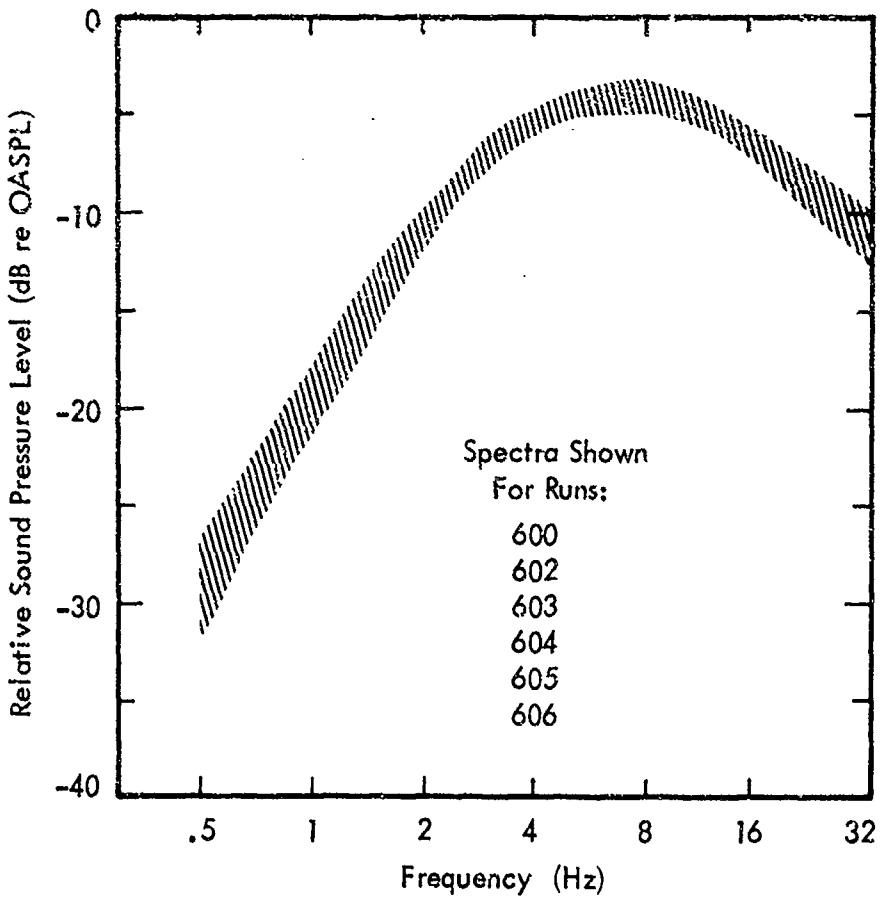

Figure G-2. Octave Band Sound Pressure Spectra at 45 Degrees to Jet Axis for Supersonic Nozzle Operating at Off-Design Pressure Ratios.

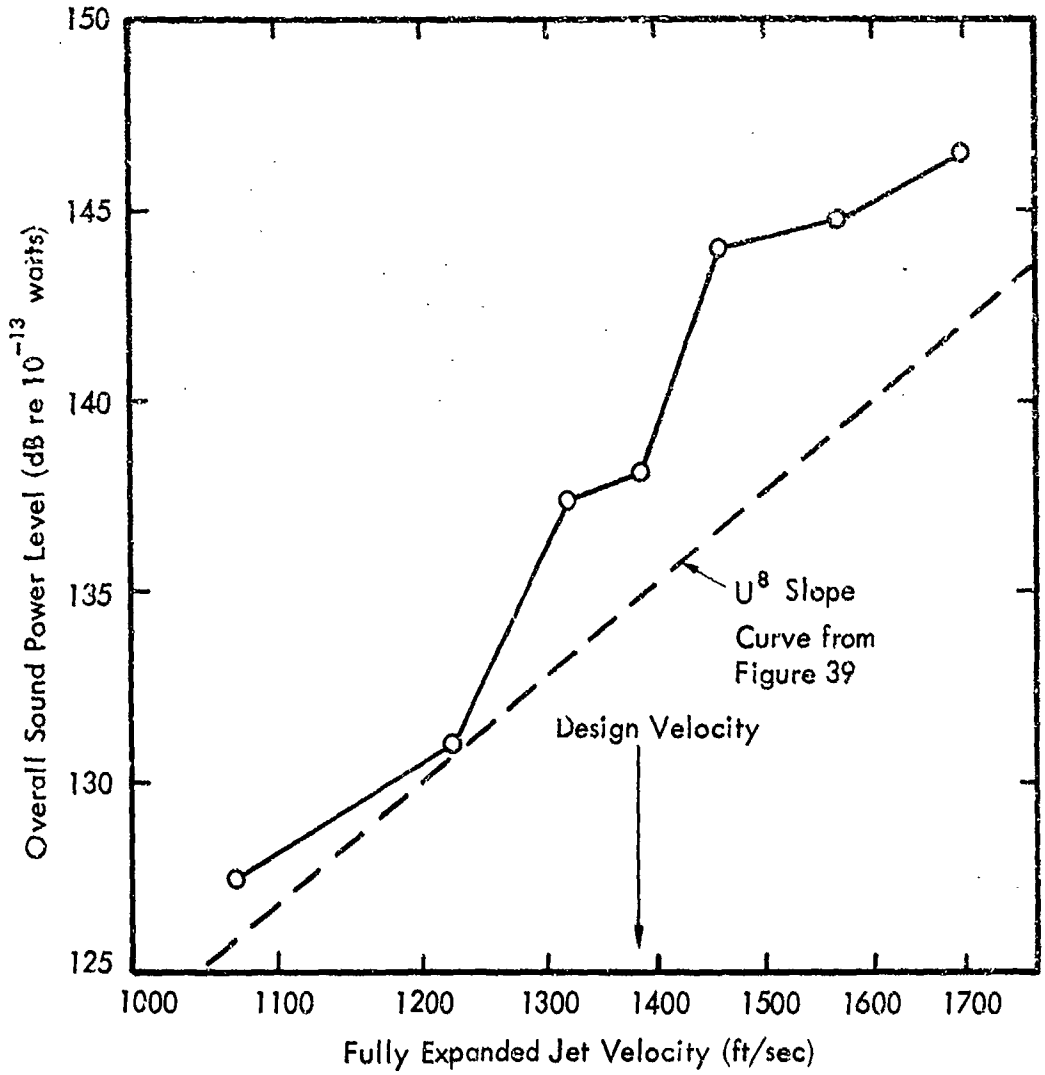

Figure G-3. Effect of Off-Design Operation of the Sound Power Generation by a Supersonic Jet Nozzle.

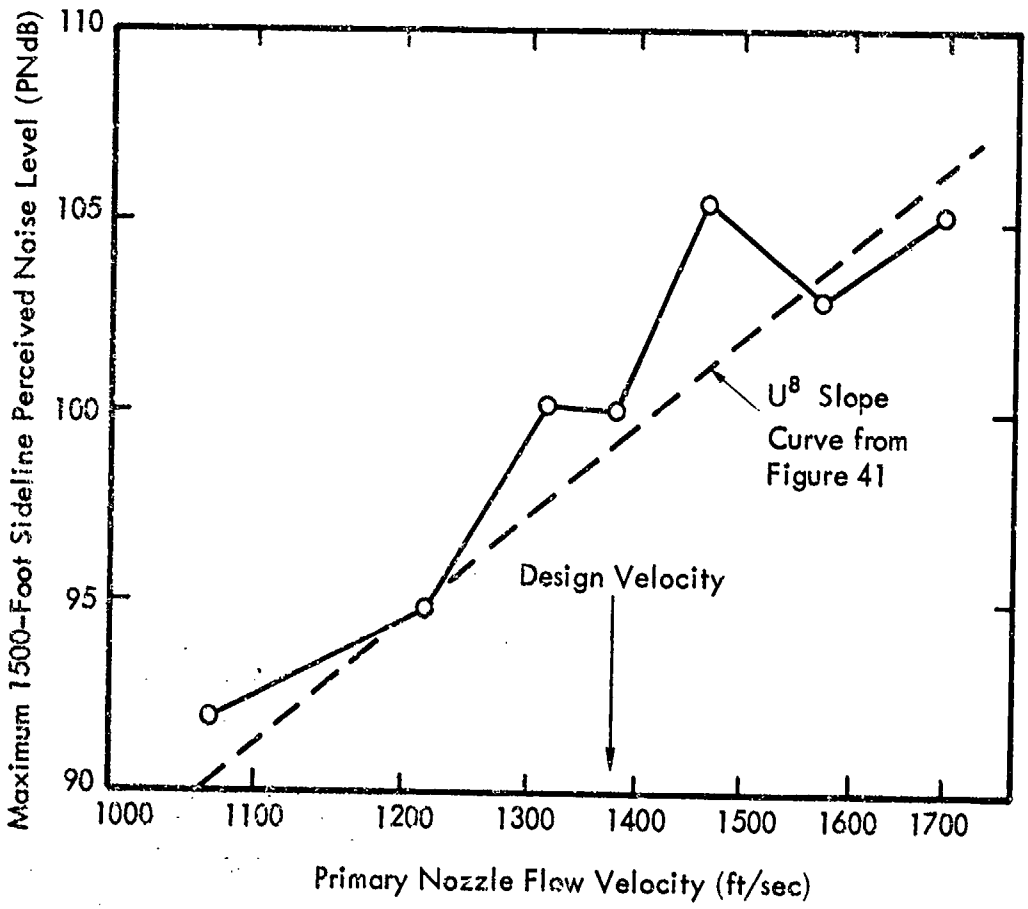

Figure G-4. Effect of Off-Design Operation on the Maximum Perceived Noise Level on a 1500-Foot Sideline. Scaled to 20,000 Lbs Thrust.

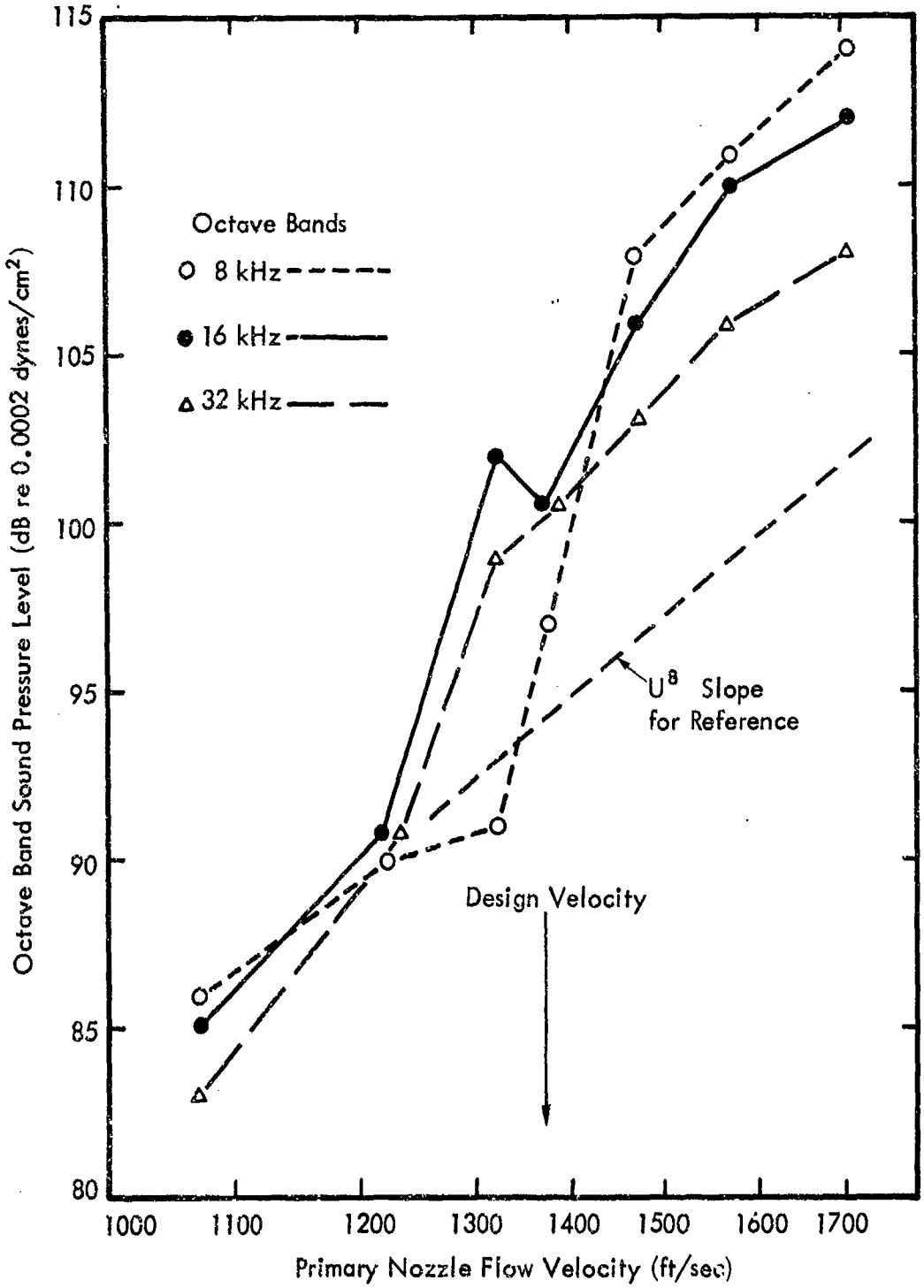

Figure G-5. Octave Band Sound Pressure Level at 110 Degrees, Showing Onset of the Third Anomaly Above 1200-ft/sec from Measured Raw Data.

Therefore, the U^8 slope reference line has been fitted through these points. Between the pressure ratios of 2.5 and 3.0, the anomaly just appears in the top two octave bands, with an increase of about 10 dB. At the design pressure ratio of 3.5, the 8 kHz octave band begins to increase; by a pressure ratio of 4.0, it is approximately 12 dB higher than might have been expected. Above the pressure ratio of 4.0, all three bands appear to be increasing with increasing pressure ratio more slowly – on the order of U^8 or less.

These data clearly show that this anomaly is a function of pressure ratio and begins in the vicinity of the design pressure ratio. The two higher frequency bands were affected at a slightly lower pressure ratio than the 8 kHz band – roughly in accordance with the expectations of Equation (G-1). However, the $1/10^{th}$ octave analysis shown in Section 4.2 did not indicate that pure tones are present, but that the phenomenon is at least an octave wide.

Although the actual optimum pressure ratio for the nozzle is probably slightly different than 3.5 because of boundary layer effects, it is considered that it could not be below 3.0 since the nozzle thrust coefficient was about .94, indicating a relatively thin boundary layer.

To obtain better insight on the problem requires additional runs using noise, schlieren photography and pressure probes as investigative tools.

REFERENCES

G-1. Powell, A., "On the Mechanics of Choked Jet Noise," Proc. Physical Society, B, Vol. LXVI, pp 1039-1056, 1953.

G-2. Hay, J.A., and Rose, E.G., "In-Flight Shock Cell Noise," J. Sound Vib., Vol. II, Part 4, pp 411-420, 1970.